Ministère de L'enseignement Supérieur et de la Recherche Scientifique

Université Hassiba Benbouali de Chlef

Faculté de Génie Civil et d'Architecture

Département de Génie Civil

THÈSE

Présentée pour l'obtention du diplôme de

DOCTORAT

Filière : Génie Civil

Spécialité : Géotechnique et Structures

Par

Houssem MESSAOUD

Thème :

STRENGTH AND DUCTILITY OF CIRCULAR CONCRETE COLUMNS CONFINED WITH GFRP WRAPS

Soutenue le 07 Juillet 2021, devant le jury composé de :

Ahmed DJAFAR HENNI	Professeur	Université HB Chlef	Président
Amar KASSOUL	Professeur	Université HB Chlef	Rapporteur
Abdelkader BOUGARA	Professeur	Université HB Chlef	Co-Rapporteur
Riad BENZAID	Professeur	Université MSB Jijel	Examinateur
Karim EZZIANE	Professeur	Université HB Chlef	Examinateur
Sidi Mohammed El-Amine BOURDIM	MCA	Université AIB Mostaganem	Examinateur

Ministry of High Education and Scientific Research

Hassiba Benbouali University of Chlef

Faculty of Civil Engineering and Architecture

Department of Civil Engineering

A THESIS

Submitted in partial fulfillment of the requirements for the degree of

DOCTOR

in Civil Engineering

Option: Geotechnics and Structures

by

Houssem MESSAOUD

Title:

STRENGTH AND DUCTILITY OF CIRCULAR CONCRETE COLUMNS CONFINED WITH GFRP WRAPS

Defended on July 07, 2021, in front of:

Ahmed DJAFAR HENNI	Professor	University HB Chlef	President
Amar KASSOUL	Professor	University HB Chlef	Supervisor
Abdelkader BOUGARA	Professor	University HB Chlef	Co-Supervisor
Riad BENZAID	Professor	University MSB Jijel	Examiner
Karim EZZIANE	Professor	University HB Chlef	Examiner
Sidi Mohammed El-Amine BOURDIM	MCA	University AIB Mostaganem	Examiner

Acknowledgment

As a first step, I would like to thank Allah, for giving me the ability and the power to finish this journey despite all the difficulties I have experienced.

I would like to thank my supervisor Prof. Amar KASSOUL for guiding me through the different stages of this research and always supporting me from the very beginning to the very end.

I also would like to express my gratitude to my co-supervisor Prof. Abdelkader BOUGARA for his consultation and advice through a number of stages of this research. I would like to extend my thanks to the members of the examination committee, Prof. Ahmed DJAFAR HENNI, Prof. Riad BENZAID, Prof. Karim EZZIANE and Dr. Sidi Mohammed El-Amine BOURDIM for taking the time and effort to review this thesis and providing positive feedback.

Finally, I would like to thank all who have been a source of constant encouragement, help, and support.

Thanks to all.

Dedication

To all who have contributed in this work. They do know who they are.

Abstract

Fiber-reinforced polymer (FRP) has been widely used in structural rehabilitation for over three decades as external confinement material for its significant enhancement in concrete strength and ductility, especially in the seismic retrofit of reinforced concrete structures. Numerous experimental studies were used to model the axial behavior of concrete columns confined with various types of FRP and many strength and strain models were suggested. However, few models were dedicated to Glass-FRP (GFRP) confinement. In this work, old and recent existing design-oriented models of FRP-confined concrete columns subjected to axial compression are reviewed and analyzed. The models were evaluated using a database of 163 compression test results of GFRP-wrapped normal and high-strength concrete columns collected from the literature to predict the ultimate strength and ultimate strain. New design-oriented strength and strain models for circular concrete columns confined with GFRP-wraps are proposed using a regression analysis. The obtained results show that the proposed models exhibit better performance and provide accurate predictions over the existing models. In addition, a review of the available literature on modeling the complete axial stress-strain relationship of FRP-confined concrete columns is performed. The performance of the existing stress-strain models in predicting the axial stress-strain behavior of GFRP-wrapped concrete columns has been evaluated using test results from the literature. Based on this evaluation, a new stress-strain model for GFRP-wrapped circular concrete columns has been proposed. The model applicable for concrete with compressive strength up to 128 MPa shows a good agreement with the experimental results, and provides much better predictions than the existing models. This study is ended by a parametric study investigating the influencing parameters on the behavior of axially loaded GFRP-wrapped concrete columns, such as concrete strength, specimen diameter and mechanical properties of the GFRP composites.

Keywords

Glass fiber-reinforced polymer (GFRP), circular column, confined concrete, strength model, strain model, stress-strain relationship, regression analysis.

Résumé

Les polymères renforcés de fibres (PRF) ont été largement utilisé dans la réhabilitation structurale pendant plus de trois décennies comme matériau de confinement externe pour leur amélioration significative de la résistance et de la ductilité du béton, en particulier dans la rénovation sismique des structures en béton armé. De nombreuses études expérimentales ont été utilisées pour modéliser le comportement axial des poteaux circulaires en béton confiné avec divers types de PRF, et de nombreux modèles de résistance et de déformation ont été suggérés. Cependant, peu de modèles ont été dédiés au confinement avec PRF-Verre (PRFV). Dans le cadre de ce travail, les anciens et les récents modèles des poteaux circulaires en béton confiné en FRP soumis à une compression axiale sont examinés et analysés. Les modèles ont été évalués à l'aide d'une base de données de 163 résultats d'essais de compression de poteaux circulaires en béton de normale et haute résistance enveloppés de PRFV recueillis à partir de la documentation, afin de prédire la résistance ultime et la déformation ultime. De nouveaux modèles de résistance et de déformation orientés vers la conception pour des poteaux circulaires en béton confiné avec des enveloppes de PRFV sont proposés à l'aide d'une analyse de régression. Les résultats obtenus montrent que les modèles proposés présentent une meilleure performance et fournissent des prévisions précises par rapport aux modèles existants. De plus, une revue de la documentation disponible sur la modélisation de la relation complète de contrainte-déformation axiale des poteaux circulaires en béton confiné avec des matériaux PRF est effectuée. Les performances des modèles contrainte-déformation existants prédit le comportement contrainte-déformation axiale de poteaux circulaires en béton enveloppés avec PRFV ont été évaluées à l'aide des résultats d'essais existants dans la littérature. Sur la base de cette évaluation, un nouveau modèle de contrainte-déformation pour les poteaux circulaires en béton enveloppé de PRFV a été proposé. Le modèle applicable pour le béton ayant une résistance à la compression allant jusqu'à 128 MPa montre un bon accord avec les résultats expérimentaux et fournit de meilleures prévisions par rapport aux modèles existants. Cette étude se termine par une étude paramétrique sur les paramètres influençant le comportement des poteaux circulaires en béton enveloppé PRFV soumis au chargement axiale, tels que la résistance du béton, le diamètre de l'échantillon et les propriétés mécaniques des composites PRFV.

Mots clés

Polymères renforcés de fibres de verre (PRFV), poteau circulaire, béton confiné, modèle de résistance, modèle de déformation, loi contrainte-déformation, analyse de régression.

ملخــص

تم استخدام البوليمرات المسلحة بالألياف (FRP) على نطاق واسع في إعادة هيكلة المنشآت الخرسانية لأكثر من ثلاثة عقود كمواد تقوية خارجية لدورها الكبير في تعزيز قوة و ليونة الخرسانة خاصة في أعمال التحديث الزلزالي للأعمدة الخرسانية المسلحة. تعتبر البوليمرات المسلحة بالألياف الزجاجية (GFRP) من بين البوليمرات الأكثر استخداما بسبب ميزتها الأفضل من حيث التكلفة والأداء. كمية معتبرة من الأبحاث تمت حول دراسة سلوك الأعمدة الدائرية الخرسانية المحصورة بالـ (FRP) تحت قوى الضغط المحوري المركز. على إثر ذلك، تم إجراء عدد كبير من الدراسات التجريبية لنمذجة سلوك الأعمدة الدائرية الخرسانية المحصورة بأنواع مختلفة من الـ (FRP)، وقد تم اقتراح العديد من النماذج للتنبؤ بالقوة و التشوه المحوري لهذه الأعمدة من قبل الباحثين. بالرغم من ذلك، عدد قليل من النماذج خُصِّصَ الأعمدة الدائرية الخرسانية المحصورة بالـ (GFRP). في هذه الأطروحة، النماذج القديمة و الحديثة الموجهة نحو التصميم والتي تم تطويرها للتنبؤ بالقوة القصوى و التشوه الأقصى للأعمدة الدائرية الخرسانية المحصورة بالـ (FRP) المختبرة تحت الضغط المحوري قد تم جمعها، و تقييم دقة نتائجها في التنبؤ بالقوة القصوى و التشوه الأقصى. تم تقييم هذة النماذج بالاعتماد على قاعدة بيانات تم تجميعها من البحوث المنشورة و التي تحتوي على 163 من نتائج اختبارات مقاومة الضغط لأعمدة دائرية خرسانية محصورة بلفائف الـ (GFRP)، ومن ثم مقارنة نتائجها بالقيم الفعلية للاختبارات. بالاعتماد على شكل و نتائج أداء النماذج السابقة و باستخدام قاعدة البيانات المجموعة، تم اقتراح نماذج جديدة موجهة نحو التصميم للتنبؤ بالقوة القصوى و التشوه الأقصى خصيصا الأعمدة الدائرية الخرسانية المدعمة بلفائف الـ (GFRP) و ذلك باستعمال تقنية تحليل الانحدار. أظهرت النتائج أن النماذج المقترحة تعطي أداءاً أفضل وتوفر تنبؤات دقيقة مقارنة بالنماذج المتوفرة. بالإضافة إلى ذلك، تم إجراء مراجعة للبحوث المتاحة حول نمذجة العلاقة بين الإجهاد والتشوه للأعمدة الدائرية الخرسانية المحصورة بالـ (FRP) ، و قد تم تقييم أداء هذه النماذج فيما يتعلق بنمذجة سلوك الإجهاد و التشوه المحوري بالاعتماد على نتائج عدة اختبارات من دراسات تجريبية مختلفة. واستناداً إلى هذا التقييم و بالاعتماد على نتائج مجموعة من الاختبارات، تم اقتراح نموذج جديد لسلوك الإجهاد و التشوه المحوري للأعمدة الدائرية الخرسانية المدعمة بلفائف الـ (GFRP). يظهر هذا النموذج و الموجه لخرسانة تصل مقاومة الضغط فيها إلى 128 ميجا باسكال اتفاقا جيدا مع النتائج التجريبية ويوفر تنبؤات أفضل مقارنة بالنماذج المختارة. تختم هذه الأطروحة بدراسة تأثير بعض المعاملات على القوة القصوى، التشوه الأقصى، و سلوك الإجهاد و التشوه للخرسانة المدعمة بلفائف الـ (GFRP) مثل قوة الخرسانة وقطر العينة والخواص الميكانيكية لمركبات الـ (GFRP) .

الكلمات المفتاحية :

البوليمرات المسلحة بالألياف الزجاجية (GFRP)، أعمدة دائرية، خرسانة محصورة، نموذج قوة ضغط، نموذج تشوه، نموذج الإجهاد و التشوه، تحليل الإنحدار.

Table of contents

List of tables

List of figures

List of symbols, abbreviations

E_c	Elastic modulus of unconfined concrete (MPa)
E_f	Elasticity modulus of the FRP composite (GPa)
E_l	Lateral stiffness of the FRP composite (MPa)
f'_{cc}	Peak strength of FRP-confined concrete (MPa)
f'_{co}	Compressive strength of unconfined concrete (MPa)
f_f	Tensile strength of FRP composite (MPa)
$f_{l,rup}$	Lateral confining pressure at rupture of FRP composite (MPa)
f_l	Ultimate lateral confining pressure of FRP composite (MPa)
k_ε	Strain efficiency factor of the FRP composite
n_{ply}	Number of plies in FRP wrapping
t_f	Thickness of FRP composite (mm)
$\overline{x}$	Average of experimental values
$\overline{y}$	Average of predicted values
$\varepsilon_{h,rup}$	Hoop rupture strain of FRP composite
ε_{cc}	Ultimate axial strain of FRP-confined concrete
ε_{co}	Axial strain of unconfined concrete at peak strength
ε_f	Ultimate strain of FRP composite
ε_l	Lateral strain of concrete
ν_c	Poisson's ratio of unconfined concrete
ρ_K	Stiffness ratio of FRP composite $\left(\rho_K = 2E_f t_f/\left((f'_{co}/\varepsilon_{co})d\right)\right)$
ρ_f	FRP volumetric ratio $\left(\rho_f = \pi d t_f/(\pi d^2/4) = 4t_f/d\right)$
ρ_ε	Strain ratio of the FRP composite $\left(\rho_\varepsilon = \varepsilon_{h,rup}/\varepsilon_{co}\right)$
h	Height of concrete cylinder (mm)
AAE	Average absolute error
R^2	Coefficient of determination

$RMSE$	Root mean square error
d	Diameter of the concrete cylinder (mm)
n	Number of data points
x	Experimental value
y	Predicted value

Chapter 1

Introduction

1.1 Research background

Aging, deterioration, and reduction in the service life of reinforced concrete (RC) structures is a serious concern worldwide, raising a major challenge to the civil engineering and research community. This phenomenon is attributed to several causes such as corrosion of internal steel reinforcement, the increase of loads due to change in the use of structure, lack of maintenance, construction errors, and in the cases of old structures, the lack of appropriate design provisions by the old seismic codes (e.g., spaced transverse reinforcement, short lap splice length at the column-footing interface) resulting in substandard and vulnerable structures (Fakharifar, 2016).

RC columns are often the most critical elements that affect the performance and stability of the structures. Besides carrying gravity loads, they provide the structures with sufficient ductility to withstand the lateral loads, such as those generated by earthquakes. Even failure of one column at a critical location can lead to a progressive collapse of the entire structure (Kharal, 2016).

It is clear that the destruction and rebuilding of all deficient structures are costly, time-consuming, and even impractical. Therefore, extensive studies on rehabilitation and retrofitting of existing vulnerable buildings and bridges have been undertaken by researchers to restore and improve their performance, especially against seismic actions (e.g., Saadatmanesh et al., 1994; Seible et al., 1997; Demers & Neale, 1999; Pantelides et al., 1999, 2001; Pessiki et al., 2001; Matthys et al., 2005; Ozbakkaloglu & Saatcioglu, 2006, 2007; Ozbakkaloglu & Akin, 2012; Parghi & Alam, 2017). This retrofitting was possible mainly through lateral confinement of the columns, which induces a tri-axial state of stress in the concrete, proving its efficiency in improving the strength, ductility, and energy absorption capacity of the columns (Rocca, 2007).

Steel and concrete jackets were the first and most widely-used retrofitting techniques. However, durability problems (corrosion of steel), the difficulty of application, need for equipment, and time and cost constraints of these techniques have encouraged to search for alternatives (Cui, 2009). In the past three decades, fiber-reinforced polymer (FRP) composites have been introduced as innovative and highly promising strengthening materials due to their outstanding combination of properties such as low weight (making them much easier to transport and handle on the site), excellent mechanical properties, good corrosion resistance, and ease and speed of application for any desired shape (Ghanem, 2016). In addition, the total rehabilitation project costs by using FRP are about 20% lower than steel due to the savings in construction expenses, even though their higher cost compared to steel (Chen, 2005). As a result, their external application on RC deficient structural members such as columns, beams, and slabs has seen a worldwide increase. Providing significant improvement in both strength and ductility to concrete columns is the essential advantage.

Common FRP materials are made based on high-performance fibers that can be either carbon fibers (CFRP), glass fibers (GFRP), or aramid fibers (AFRP). CFRP have the highest tensile strength and modulus of elasticity regarding the other types; however, they have the highest price as they tend to be 10 to 30 times more expensive than GFRP (Sonnenschein et al., 2016). Although GFRP materials provide lower strength and ductility compared to CFRP and AFRP, they are the most used in the industry due to their best cost-efficiency ratio.

Numerous studies have attempted to explore the feasibility of the FRP technique by applying it as external confinement for the retrofit of RC columns (Saadatmanesh et al., 1996, 1997; Xiao & Ma, 1997; Chang et al., 2004; Haroun & Elsanadedy, 2005; Ozcan et al., 2010; Han et al., 2014; Zeng et al., 2018; Farrokh Ghatte et al., 2019; Anagnostou et al., 2019 among others). The results of these studies have shown that the retrofitted columns have gained a significant improvement in both the strength and ductility.

1.2 Problem Statement

Numerous experimental and analytical studies have been carried out to understand the behavior of concrete confined with FRP under concentric loading. In the beginning, Fardis & Khalili (1981, 1982) and Saadatmanesh et al. (1994) suggested the use of steel-confined concrete and actively-confined concrete models of Richart et al. (1928), Newman & Newman (1971), and Mander et al. (1988) to describe the behavior of the FRP-confined concrete.

Later, due to the difference between the behavior of steel-confined concrete and that of FRP-confined concrete, a considerable number of experimental studies were carried out to understand the behavior of concrete confined with various types of FRP. This has led to extensive experimental data (e.g., Lam & Teng, 2004; Jiang & Teng, 2007; Vincent & Ozbakkaloglu, 2013; Hou et al., 2015; Guo et al., 2016; Oliveira et al., 2019; Narule & Bambole, 2021 for CFRP; Almusallam, 2007; Youssef et al., 2007; Kumutha et al., 2007; Cui & Sheikh, 2010; Elwan & Omar,

2014; Sun et al., 2017; Tu et al., 2019; Kissman & Sundar, 2020; Khaloo et al., 2020; for GFRP; Wu & Wang, 2010; Wang & Wu, 2011; Ozbakkaloglu & Akin, 2012; Vincent & Ozbakkaloglu, 2013; Lim & Ozbakkaloglu, 2015 for AFRP).

After that, numerous confinement stress and strain models calibrated from the test results were suggested by researchers. The large part of the models was devoted to diverse-use models that group all the FRP types (e.g., Lam & Teng, 2003; Ilki et al., 2004; Fahmy & Wu, 2010; Realfonzo & Napoli, 2011; Al Abadi et al., 2016; Lim et al., 2016; Cascardi et al., 2017; Jiang et al., 2020; Raza et al., 2020).

Furthermore, since the FRP composites exhibit different characteristics according to the type of fiber used in their constitution, and in order to reach more accuracy in modeling and limit the variability in the studies, researchers have attempted to dedicate for each type of FRP confinement a specific and independent predictive model (e.g., Xiao & Wu, 2000; Wu et al., 2006; Mesbah & Benzaid, 2017; Ahmad & Raza, 2020 for CFRP-confined concrete; Wu et al., 2009; Wu & Wang, 2010; Djafar-Henni & Kassoul, 2018; Arabshahi et al., 2020 for AFRP-confined concrete).

However, despite the wide use of GFRP composites in concrete retrofitting due to its best cost-effectiveness, few models were dedicated to GFRP confinement, such as that of Huang et al. (2016) for concrete confined with GFRP wraps and tubes and that of Touhari and Mitiche-Kettab (2016) developed for concrete confined with GFRP wraps which was based on a limited database. From the literature reported, it seems that no researcher has proposed confinement models for GFRP-wrapped concrete except Touhari and Mitiche-Kettab (2016).

1.3 Research Scope and objectives

In practice, it is known that the appropriate and reliable design of FRP confinement for concrete strengthening and retrofitting purposes is only feasible if the stress-strain behavior of FRP-confined concrete is well understood and accurately modeled.

Since most of the research work available in the literature regarding the modeling of the axial behavior of FRP-confined concrete has concentrated on concrete confined with diverse types of FRP, and given that GFRP wraps are the most used FRP materials in concrete retrofitting and rehabilitation projects, and considering the lack of reliable and accurate equations describing the behavior of GFRP-wrapped concrete under compression, a contribution in this area is of great interest.

This research is directed mainly towards understanding the axial behavior of concrete confined with GFRP wraps. The specific objectives of the present research can be summarized in the following points:

- Collect a reliable test database of axially loaded GFRP-wrapped concrete cylindrical specimens to use as a reference and verification tool for further analytical studies on FRP-confined concrete.
- Review and evaluate the performance of several popular and recent previous models predicting the ultimate stress and the ultimate axial strain of FRP-confined concrete.
- Develop new confinement models for predicting the ultimate stress and ultimate axial strain of GFRP-wrapped concrete.
- Review and evaluate the performance of some previous models predicting the axial stress-strain behavior of FRP-confined concrete.
- Develop a new stress-strain model describing the axial behavior of GFRP-wrapped concrete.
- Evaluate the influence of the concrete strength, the GFRP properties, and the specimen diameter on the axial behavior of GFRP-wrapped concrete.

1.4 Thesis outline

The thesis is structured in seven chapters covering the overall objectives of the research. In the present chapter, a brief introduction, objectives, scope of the undertaken research, and thesis methodology are presented. The content of the dissertation is organized into the following chapters:

Chapter 2 deals with the rehabilitation and retrofit of RC columns using FRP composites materials. It starts with an overview of the common deficiencies of RC columns and their causes. Then, it presents some conventional methods for the retrofit of concrete columns, such as concrete and steel jacketing, pointing out their advantages and weaknesses. The constitution, the properties, and the techniques of application of the FRP materials in confining concrete columns are also presented.

Chapter 3 treats the FRP-confinement mechanism and reviews the relevant literature regarding the experimental research conducted on the axial compression behavior of GFRP-wrapped concrete cylinders. In this chapter, the experimental results with detailed information are compiled and summarized in a comprehensive database of 163 test results.

Chapter 4 provides a literature review and a description of several published confinement models to predict the ultimate stress and ultimate strain of GFRP-confined concrete subjected to axial compression.

Chapter 5 presents a review and performance assessment of 20 well-known and recent design-oriented stress and strain confinement models devoted to GFRP-wrapped concrete. The assessment is performed by comparing the predictions of the models with the experimental database reported in Chapter 3. Statistical indices, namely the coefficient of the determination (R^2), the root-mean-square error ($RMSE$), and the average absolute error (AAE) are used in the evaluation. The chapter concludes with the development of new strength and strain design-

oriented models for GFRP-wrapped concrete. The proposed models are calibrated using regression analysis and compared with the selected models.

In Chapter 6, a review of the available literature on modeling the axial stress-strain behavior of FRP-confined concrete is presented. Details on the different existing equations are summarized. The performance of several published models is evaluated with the existing experimental curves of GFRP-wrapped concrete. A new stress-strain model composed is developed in this chapter and validated with several experimental data.

A parametric study is conducted in Chapter 7 to investigate the influence of various parameters such as concrete strength, specimen diameter, and mechanical properties of the FRP composites on the axial behavior of GFRP-wrapped concrete specimens. The relevant analytical results are discussed.

Finally, this thesis is ended with a conclusion highlighting the major findings of this work and some recommendations for future works.

Chapter 2

Fiber-reinforced polymers in the rehabilitation of RC columns

2.1 Introduction

This chapter presents an overview of the common deficiencies and damages of RC columns, pointing out their primary causes. Also, it provides a brief background on the conventional methods for the retrofit and rehabilitation of RC columns, focusing on FRP confinement as regards the traditional methods. The last section summarizes the constitution, the properties, and the techniques of application of the FRP materials in the retrofit RC columns.

2.2 Deficiencies in reinforced concrete columns

RC structures are susceptible to degradation due to a variety of factors. Columns in these structures are of crucial importance, as they are the principal load-carrying elements and the main influencing components on the overall performance, stability, and safety of the structures. Any severe damage to these elements may lead to total collapse, as demonstrated by the previous earthquakes worldwide (Figs. 2.1-2.3).

Figure 2.1 Building collapsed due to soft story (Van, Turkey 2011)

The causes of RC columns' vulnerability and deterioration can start from the early stages (design and construction phases). Construction errors, use of inferior materials, poor execution, and deviation from structural drawings and specifications in the construction phase; the design of weak stories (tall story with large openings for doors and windows), strong-beam weak-column joints, inconsideration of seismic actions by old design codes resulting in insufficient transverse reinforcement (small diameters with large spacing resulting insufficient confinement) (Fakharifar, 2016), poor anchorage of transverse reinforcement (90-degree anchorage bends with short extensions), inadequate lap splice length at spliced joints in old structures are among other factors (Walkup, 1998). In addition, the change of the structure use (increase of the load, removal of internal walls in buildings creating soft-stories), the lack of maintenance, the use of deicing salts, and the heavy traffic load in bridges are other factors contributing to the progressive degradation of RC structures (Wu & Eamon, 2017).

Figure 2.2 Cypress street viaduct failure (San Francisco, USA 1989)

Figure 2.3 Fukae viaduct expressway failure, Kobe, Japan 1995

2.3 Necessity for reinforcement

The construction works are in a rapid increase worldwide, and the vulnerable and deteriorating existing buildings and bridges are increasing concurrently even after recent updates in seismic codes to consider the earthquake actions (Nanni & Bradford, 1995; Teng & Lam, 2004). The replacement of all the deficient and substandard concrete structures is an impractical and time and budget-consuming solution. Therefore, cost-effective and durable retrofitting and rehabilitation technologies are a necessary option.

For that reason, repair and rehabilitation of existing damaged concrete structures have emerged as one of the primary construction activities globally. The money spent on retrofitting works has exceeded the money spent on building new constructions (Apandi et al., 2017). Several techniques have been developed to

retrofit concrete structures, primarily concrete columns, such that concrete jacketing, steel jacketing, and fiber-reinforced polymers (FRP) jacketing.

2.4 Methods of retrofitting of RC columns

2.4.1 General

In general, the retrofitting strategies of concrete structures can be classified into two major categories; global and local methods. The global methods concentrate at the structure level to obtain a better overall behavior of the entire structure. They include the addition of masonry walls, concrete shear walls, steel braces, energy dissipation devices. On the other side, the local methods focus on improving the performance in the element level (e.g., column, beam, column-beam joint) essentially through external confinement. (Chandrakar & Singh, 2017). The selection of the rehabilitation method depends on a large variety of criteria such as type, characteristics, and importance of the structure; the nature and severity of the damage, ease of the technology, total time and cost, as well as considerations related to the use and occupancy of the structure (Baciu et al., 2015). The use of both methods is also possible.

Over the years, various local methods have been developed for strengthening RC structures (e.g., Täljsten, 1997; Ghobarah & Said, 2001; Karayannis et al., 2008; Martinola et al., 2010; Ruano et al., 2014; Dubey & Kumar, 2016). Several forms of confining systems of different materials such that concrete jackets, hollow steel tubes, steel plates, steel prestressing strands, FRP jackets, FRP tubes, shape memory alloy (SMA) spirals, and hybrid FRP jackets-SMA spirals have been used.

The external confinement approaches can be divided into two types, namely, active and passive confinement. In the active confinement, the confining pressure is applied to prestress the concrete prior to concrete damage progression (Priestley et al., 1996; Buckle et al., 2006) (e.g., prestressing steel strands). Several researchers focused on exploring the feasibility of this technique for seismic retrofitting of concrete elements (e.g., Coffman et al., 1993; Saatcioglu & Yalcin, 2003; Shin & Andrawes, 2010; Fakharifar et al., 2016). The main advantage of this technique is the early application of the confining pressure that delays damages sustained by the concrete. However, its application is limited due to the in-site difficulty in applying the confining pressure (excessive mechanical hardware, labor, and time) (Saatcioglu & Yalcin, 2003; Nesheli & Meguro, 2006).

On the other side, in the passive confinement, the pressure is exerted only as a direct result of the lateral dilation of concrete due to the application of the load. This technique is popular and widely used compared to active confinement (Parghi, 2016). Steel plates, concrete jackets, and FRP jackets are the most common passive confinement methods of concrete columns.

In the scope of rehabilitation of concrete structures, the terms repair, strengthening, and retrofit are often used interchangeably, but, in fact, they refer to three different structural conditions. In repairing, the repairs are performed on

damaged structures to restore the initial structural performance after a disaster (e.g., reconstruction of non-structural walls, chimneys, boundary walls, repair of a crack). However, strengthening aims at enhancing the designed performance level of the structure. Whereas the term retrofit is usually related to the upgrade of existing structures to make them more resistant to seismic activity (e.g., adding diagonal braces, shear walls, external confinement of columns) (Hollaway, 2001).

2.4.2 External prestressing steel strands

This technique consists of prestressing steel strands with specially designed anchors placed externally on the concrete column as individual hoops (Fig. 2.4). The external prestressing strands provide hoop confining stress to the concrete, improving the strength and ductility of the column, as well as the shear resistance.

The installation process is quick and easy (it does not require any heavy equipment), and it is less intrusive to building occupants and roadway traffic. (Saatcioglu et al., 2002)

Different studies showed the advantage of using prestressing steel strands on the external confinement of concrete columns.

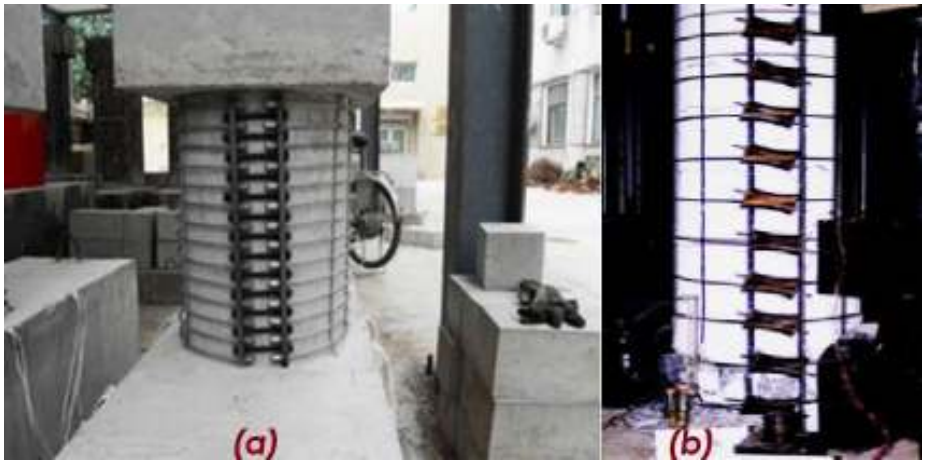

Figure 2.4 Concrete specimens confined with prestressing steel strands. (a) Daud and Hui (2014), (b) Saatcioglu and Yalcin (2003)

Gamble et al. (1996) constructed full-scale RC circular columns to examine the spliced regions at the base of the columns. They confined the RC columns using externally tensioned steel strands. The results showed that the performance of the RC columns was improved with the prestressing strands.

Saaticoglu and Yalcin (2003) tested full-scale RC columns under lateral cyclic loadings with a constant compression loading. The columns were retrofitted with externally prestressed hoops in the transverse direction. The results showed that the flexural behavior was improved, and the shear failure was prevented.

However, further tests proved that retrofitted columns with prestressed steel strands under cyclic loading experienced strength deterioration due to the high losses of the prestressing forces of the confining strands caused by spalling of the

concrete cover and penetration of the prestressed strands into the concrete (Fakharifar, 2016).

2.4.3 Shape memory alloys (SMAs) spirals

SMAs are a class of metallic alloys that have a unique capability of recovering their original shape after being excessively deformed (superelasticity 6-8% of strain). The shape recovery could be attained by heating the alloy to a temperature above the transformation temperature, which is a material property predetermined by the manufacturer (Shin, 2012).

These two properties (i.e., recoverability and superelasticity) have been discovered in various alloys such as the Au-Cu (Gold-Copper) alloy in the 1930s, the In-Ti (Indium-Titanium) alloy in the 1950s, and the Ni-Ti (Nickel-Titanium) alloy in 1963 (Tadaki et al., 1988; Otsuka & Wayman, 1999).

The recovery stress highly depends on the material composition, the manufacturing procedure, and the deformation level experienced before shape recovery (Otsuak & Wayman, 1999).

Due to their advantageous properties, SMAs have been proposed as an innovative material in seismic retrofits and strengthening of bridges and buildings, especially for columns. Various types of SMAs can be considered in the construction industry, but the most widely used SMAs are Ni-Ti alloy-based since they provide good mechanical properties, excellent shape memory effect, and good corrosion and fatigue resistance (DesRoches et al., 2004).

After the SMAs are elongated and wrapped around the concrete column, they will be heated, and thus they will attempt to shrink to their original length. And since the concrete column they are wrapped around is essentially incompressible, the induced shrinkage causes the SMA spirals to squeeze the concrete column and hence provides an active confinement pressure to the column that could reach up to 800 MPa (Otsuka & Wayman, 1999) (Fig. 2.5).

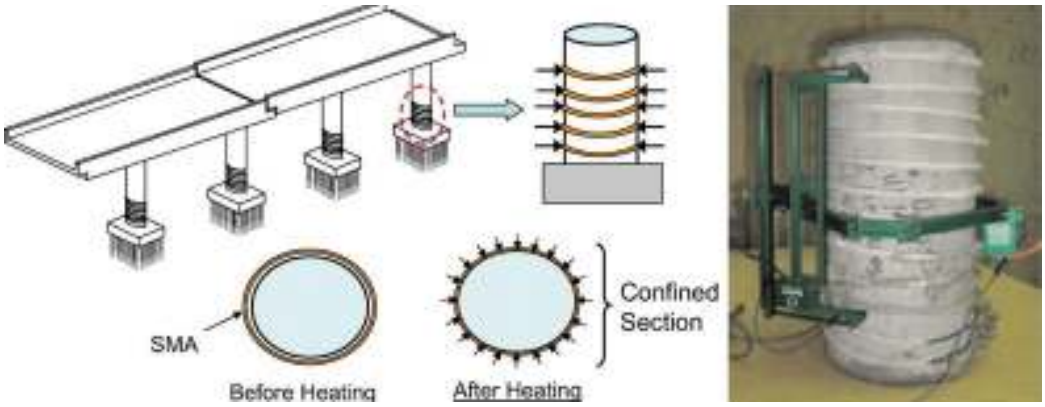

Figure 2.5 Schematic illustration of active confinement of concrete bridge piers using shape memory alloys (Andrawes et al., 2010)

This technique is advantageous since it requires limited labor and time for installation and prestressing (no need for excessive use of mechanical devices) (Shin, 2012).

Different experimental studies have treated the use of SMAs spirals on concrete confinement. For instance, Shin and Andrawes (2011) conducted an experimental investigation on actively confined RC piers with shape memory alloy (SMA) spiral wires. The pier was tested under lateral cyclic load along with a constant axial load. The results showed that the retrofitted piers using SMA had gained more strength, stiffness, and ductility compared to the as-built pier.

2.5 Passive confinement techniques

2.5.1 Steel jacketing

Confinement with steel jackets is one of the most common methods for retrofitting and strengthening concrete columns. This method usually involves installing steel jackets around the column, followed by field welding of parts along the length of the jacket (Fig. 2.6). The gap between the jacket and the concrete is usually filled with cement-based non-shrink grout (Itani, 2003; He et al., 2015). A gap of approximately 50 mm is typically provided between the end of the jacket and any supporting member (e.g., footing, beam, cap beam) in order to avoid the jacket to act as a compression member. In the case of rectangular columns, the cross-section is often modified into an oval/elliptical shape before applying the steel jacket to increase the effectiveness of the confining jacket (Chai et al., 1990; Priestley et al., 1996).

Extensive research studies had been performed on concrete confined with steel jackets (Aboutaha et al., 1996; Ghobarah et al., 1997; Li et al., 2005; Xiao & Wu, 2003; Xiao et al., 2011 among others). All the studies have shown that steel jacketing is an effective retrofit technique for seismically-deficient concrete columns.

Figure 2.6 Strengthening of RC columns with steel jackets; Left: Illinois, USA (Tobias et al., 2008), Right: Oita, Japan (Yoshimura et al., 2004)

For instance, Kawashima (1990) conducted a series of experimental investigations to retrofit 50 bridge piers with steel plates. Some of them were implemented in actual bridge piers, which were tested under real ground shaking during the 1995 Kobe earthquake. None of the retrofitted piers has suffered any major damage.

Priestly et al. (1994) studied theoretically and experimentally the retrofit of bridge columns using steel jackets. Circular and rectangular columns were prepared and tested in as-built and retrofitted conditions. The results showed that the columns retrofitted with steel jackets performed better than the as-built columns in flexural ductility and energy absorption capacity, while the as-built columns failed in a brittle manner.

Wu et al. (2003) used steel plates as confining jackets to rectangular RC columns and found that this method can significantly increase the ductility of concrete columns. Li et al. (2005) obtained stress-strain relationships of concrete confined with steel jackets with various thicknesses in addition to different types of internal reinforcement, including spirals, hoops, and steel wires. The authors concluded that steel jackets improved the strength and the ductility of concrete cylinders.

However, this technique revealed many disadvantages that restrict its recent usage, such as corrosion of the steel plates, the high cost, the need for specialized heavy equipment at the workplace with intensive labor, the difficulty in manipulating the heavy steel plates in tight construction sites, the limitation in available plate lengths. (Parghi, 2016; Raza et al., 2019)

2.5.2 Concrete jackets

Concrete jacketing is one of the most common and popular traditional methods for strengthening and repairing deficient and damaged RC columns. It was considered as the most economical of the retrofitting techniques and the most suitable method for retrofitting bridge piers in the water (Parghi, 2016).

Typically, this method involves constructing a thick layer of concrete with longitudinal and transverse reinforcement around the existing RC column (Fig. 2.7). The effectiveness of concrete jacketing is directly attributed to the monolithic behavior of the composite element (i.e., old and new concrete). To that end, the treatment of the interface, roughening of the concrete surface, and the use of epoxy resin are essential to increase the bonding between the new and the concrete. Higher-strength concrete might be used to reduce the thickness of the jacket. Moreover, as the compaction of the new concrete layer is difficult to be performed, self-compacting concrete (SCC) is more suitable than conventional concrete (Ma et al., 2017).

Concrete jackets increase the stiffness, and flexural and shear strengths as well as the deformation capacity of the column. Also, the additional cross-section area helps the column transfers more load while providing additional confinement (Parghi, 2016).

A vast number of research studies have been conducted on RC jacketing of concrete columns. Bett et al. (1988) conducted a repair and retrofit of three square

RC columns with RC jackets using identical geometry and reinforcement. One of the column specimens was tested and sustained severe damage, then repaired with a concrete jacket and re-tested under the same loading protocol, while the remaining two columns were retrofitted by jacketing before testing. The columns were tested under a constant axial load and a single lateral displacement history up to failure. Test results indicated that the repaired column and the two retrofitted columns had almost similar performance and outperformed the original column.

Figure 2.7 Concrete column retrofitted with concrete jackets (Constrofacilitator.com)

Rodriguez and Park (1994) studied the performance of four RC columns (damaged and undamaged RC columns) to evaluate the effect of RC jackets on the strength, stiffness, and ductility of the columns. The columns were tested under a constant axial load with a lateral cyclic loading until failure. Two of the columns were tested in the as-built condition, and they demonstrated poor performance. The two damaged columns and the other two undamaged columns were retrofitted with RC jackets. Test results indicated a very satisfactory performance of the retrofitted columns in terms of strength and stiffness up to three times than the original columns. Recent research on concrete jacketing focuses on using other materials, such as self-compacting concrete (SCC) (e.g., Dubey & Kumar, 2016), engineered cementitious composite (ECC) (e.g., Deng & Zhang, 2018), reactive powder concrete (RPC) and high ductile fiber reinforced concrete (HDC) (Deng & Zhang, 2017).

This technique has some drawbacks such as time and labor consumption, the possibility of shrinkage and bonding problems with substrate concrete, reduction of available floor-space area in the case of buildings, increase in additional seismic mass and stiffness, and the absorbed seismic actions (modification of the dynamic characteristics of the entire structure) (Parghi, 2016).

2.5.3 FRP composites

Early applications of fiber-reinforced polymers have mainly been limited to aerospace, chemical, and shipbuilding due to the cost and research limitations (Emmons, 1998). However, recent developments in the manufacturing of FRP materials have made them available for a wide range of applications, including civil engineering. The FRP-wrapping technology was first applied on concrete chimneys in Japan (Wu & Fahmy, 2020).

In the last three decades, FRP have attracted the attention of researchers as alternative materials for seismic retrofit and strengthening of RC structural members like columns and beams.

FRP materials are available in a variety of forms of interest, such as bars and grids, which are primarily used in the place of steel reinforcement in new constructions, and in the form of sheets (Fig. 2.8) in rehabilitation applications of beams to improve the flexural and shear capacity, and in columns to enhance the strength and deformation capacity (Wu & Eamon, 2017) (Fig. 2.9).

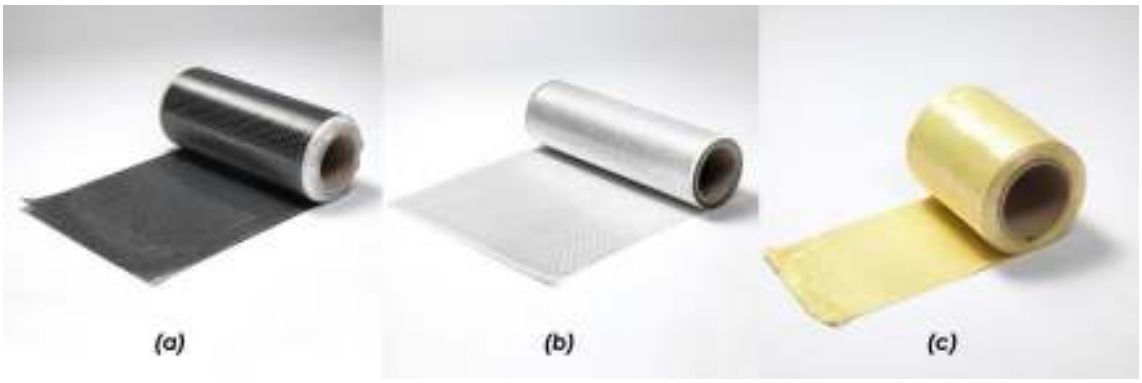

Figure 2.8 FRP material sheets. (a) CFRP, (b) GFRP, (c) AFRP (strongtie.com)

Figure 2.9 Retrofitting of RC columns with CFRP sheets (horseen.com)

Numerous investigations have been conducted to study the effectiveness of FRP in strengthening circular, square, and rectangular RC columns (Lavergne & Labossiere, 1997; Mirmiran & Shahawy, 1997; Seible et al., 1999; Fukuyama et al., 1999; Pantelides et al., 2000b; Bousias et al., 2004; Harajli et al., 2006; Siddiqui et al., 2014; Ouyang et al., 2017; Eid & Paultre, 2017; Del Zoppo et al., 2017; Anagnostou et al., 2019; Dadvar et al., 2020 among others).

For instance, Xiao and Wu (2000) reported their experimental results on axial compression tests of 27 concrete cylinders confined with CFRP jackets. The results showed that confining concrete using CFRP increases both the compressive strength and axial ductility.

Haralji et al. (2006) reported that confining rectangular columns with FRP results in significant improvement in axial strength and ductility. For square column sections without longitudinal reinforcement (plain concrete), the increase in axial strength was found to be 154, 213, and 230% for one, two, or three layers of CFRP wraps, respectively.

Siddiqui et al. (2014) tested short and slender RC columns wrapped with CFRP sheets under eccentric axial loading. The results showed that CFRP-strengthening improves the strength and ductility of the columns substantially.

FRP confinement is more efficient in circular than in rectangular columns as the circular sections are entirely confined with the FRP in contrast with rectangular sections where the confinement action is mainly located at corners (Cozmanciuc et al., 2009).

The FRP materials have many advantages (Fakharifar, 2016; Wu & Eamon, 2017; Wu et al., 2020), such as:

- High strength, which makes possible generating high confining pressures where only layers are needed to strengthening beams and columns without altering the original dimensions of the members.
- Lightweight. FRP materials possess 20% to 25% the density of steel and 70%-80% of the density of conventional plain concrete, which decreases the transportation and labor cost, adds minimum dead load to the structure, and reduces disturbance of the use and occupancy of the structures during installation.
- Excellent corrosion resistance, which is a principal advantage.
- Ease and speed of installation, especially following earthquakes (require no formwork and less or no scaffolding to install).
- Excellent fatigue characteristics (Higher fatigue stress steel reinforcement), which make them preferable for dynamic load-bearing structural components.
- Remarkable durability.

Moreover, FRP confinement can improve column ductility without considerable stiffness amplification, thereby maintaining the structure's dynamic properties (Haroun et al., 2005). It also prevents premature compression failure of the

concrete cover and buckling of the longitudinal steel bars leading to improved performance under seismic loading (Sarker et al., 2011).

2.5.3.1 FRP strengthening methods

2.5.3.1.1 Wet lay-up process

This technique is widely used in both buildings and bridges in which FRP sheets are impregnated in resins and wrapped around the concrete element (Fig. 2.10). Installation of the FRP fabric on the concrete surface requires saturating resin, usually after a primer has been applied. The FRP can be applied with two methods: whether applying the resin uniformly on the concrete surface and then wrapping the element with the FRP jacket or impregnating the FRP in the resin using a saturator machine and then wrapping the element (Cozmanciuc et al., 2009).

Figure 2.10 Bridge pier confinement using FRP wet-layup technique (informedinfrastructure.com)

This technique is straightforward and very fast. However, because it is completely carried out by hands, it is more difficult to control the quality of resin mix, attainment of good wet-out of the FRP jacket with uniform resin impregnation without excessive voids and wrinkling (Wu et al., 2020).

2.5.3.1.2 Prefabricated shells

In this technique, the column is wrapped with prefabricated FRP shells (prepreg: FRP sheets pre-impregnated with a saturated resin at the manufacturer's facility (Fig. 2.11). The FRP shells can be either circular or rectangular, depending on the cross-sectional shape of the column. The technique is simple for site applications and can ensure a high level of material quality control due to the controlled factory-based fabrication of shells. However, the shells must be fabricated with strict tolerance with respect to column dimensions. The confining action of shells is less efficient in rectangular sections, so it is usually better to change the cross-

sectional shape of the column. For multiple layers, the shells must be appropriately positioned to ensure the desired jacketing effect (Wu et al. 2020).

Figure 2.11 RC column confined using prefabricated FRP shells (Kabeyasawa, 2005)

2.5.3.1.3 Automated winding

The automated winding consists of using a wrapping machine to automatically wind the fibers around the column (Fig. 2.12). The machine, which was developed for the first time in Japan, was created to enhance bridge piers, but it can also be used to reinforce building columns. The fibers are wound on reels, then inserted into the fiber winding head, impregnated with resin, and wound around the column. After the winding is over, a curing cover is applied. The machine also allows winding the fibers while pre-tensioning them to obtain an active confining system. Computers monitor the winding angle, fiber volume fraction, and thickness (Wu et al., 2020). A key advantage of the technique, apart from good quality control, is the rapid installation (Cozmanciuc et al., 2009). While the disadvantage is that preliminary calibration operations are required for non-leveled soils, which logically slows down its use (Wu et al., 2020).

Figure 2.12 Bridge pier retrofitted using FRP automated winding technique (Cozmanciuc et al., 2009)

2.6 FRP materials

In the following subsections, the composition, properties, as well as fabrication procedures of FRP materials are discussed.

2.6.1 Constituents

The FRP materials primarily consist of a resin (polymer matrix material) reinforced with fibers (reinforcing material, typically, carbon, glass, or aramid) to produce a combination of properties that cannot be achieved with either of the constituents acting alone (synergistic material). (Mallick, 2007; Wu et al., 2020). To provide unique performance attributes, FRP can also include other materials such as coupling agents, coatings, and fillers. To strengthen bonding across the fiber-matrix interface and facilitate load transfer between the fibers and the matrix, coupling agents and coatings are added to the fibers. To reduce shrinkage and cost some of polymeric matrices fillers are added (Mallick, 2007; Abbood et al., 2020). Combinations of these constituent materials allow for a diverse range of strengths, cost, durability, and other attributes such as resistance to fire (ACMA, 2016).

2.6.1.1 Fibers

Fibers are the principal load-carrying element and strength and stiffness provider to the FRP composite. They are typically made of glass, carbon, and aramid. The typical volume fraction of fibers in different FRP composites ranges from 25% to 35% for wet lay-up FRP sheets and 50% to 65% for pre-cured FRP plates or bars. (Wu et al., 2020). The fiber volume fraction is an important parameter in designing FRP products, in which an optimal quantity of fiber is required for the achievement of strength and stiffness requirements (ACMA, 2016).

- Carbon fibers

Carbon fibers are widely used in industry in a variety of applications in view of their mechanical characteristics, including high stiffness, high tensile strength, low density, low conductivity, high-temperature resistance, and chemical stability. However, they are the most expensive compared to the other fibers. Carbon fibers can be divided based on their performance into high-strength fibers (HS) and high-modulus fibers (HM) (Wu et al., 2020).

- Glass fibers

Of all the FRP reinforcing fibers, glass fibers are the most common. Their principal advantages are low cost, high tensile strength, and high chemical resistance. However, they have relatively low tensile modulus, high density among the other fibers, relatively low fatigue resistance, sensitivity to abrasion during handling (which frequently decreases its tensile strength), and high hardness (Mallick, 2007).

Two types of glass fibers are commonly used in the FRP industry: E-glass and S-glass. E-glass (electrical glass) has the lowest cost of all commercially available

reinforcing fibers, which is the reason for its widespread use in the FRP industry (more than 50% of the glass fibers used for reinforcements are of this type) (Wu et al., 2020). However, its mechanical properties are lower than other grades of glass fibers.

S-glass (structural glass), developed firstly for aircraft components and missile casings, has higher strength than E-glass (about 30% higher), but they are more expensive due to manufacturing cost and the difference in the composition compared to E-glass (Mallick, 2007; Wu et al., 2020).

- Aramid fibers

Aramid fibers are a class of synthetic fibers, which also have the trade name of Kevlar®. They have approximately half the density of glass fibers, with good mechanical properties between glass and carbon fibers, such as very high strength, tensile modulus, and shock and abrasion resistance (Gibson, 1994). Aramid fibers have good resistance to fire and chemical attacks (can work well in high temperatures (250 ℃)). However, they are sensitive to UV radiation and suffer from severe stress relaxation. Moreover, their cost is almost the same as that of carbon fibers which limits their applications (Wu et al., 2020).

A summary of the mechanical properties of the typical fibers used in civil engineering applications is shown in Table 2.1.

Table 2.1 Typical reinforcing fiber material properties (Wu et al. 2020)

Fiber type	Diameter (μm)	Tensile strength (MPa)	Elasticity modulus (GPa)	Density (kg/m^3)	Failure strain (%)
HS Carbon	5-8	3000-6000	230-300	1500-1800	2-2.5
HM Carbon	5-8	2500-4500	350-500	1800-2000	0.4-1.5
E-Glass	3.3-4.8	3400-3700	72-77	2500-2600	4.8
S-Glass	4.2-5.4	4300-4900	75-88	2500-2600	5.2-7
Aramid	12	2750-3040	70-113	1390-1450	2.3-4.4

2.6.1.2 Matrix

Although the properties of FRP materials highly depend on the properties of the reinforcing fibers, the fibers by themselves cannot be beneficial. Instead, when the fibers are embedded in a matrix, the resulting composite material becomes with distinct advantageous features.

The matrix can play various roles in FRP materials, such as holding and bonding the fibers in the appropriate location and orientation, transferring the stresses through the fiber-matrix interface to the fibers, and protecting fibers from mechanical degradation (e.g., by abrasion), and from direct exposure to the environment (elevated temperatures, moisture, and chemical attacks) (Barbero, 2011).

In general, matrix materials can be made of polymers (resins), metals, or ceramics. Because of the ease of fabricating complex components and the relatively low cost of tooling, the polymer matrix is the most widely used matrix material. (Barbero, 2011). Resins or polymers are classified into thermosetting and thermoplastic matrices.

- Thermoset polymers

Thermoset polymers, such as epoxies, polyesters, and vinyl esters, are more commonly used as FRP matrix materials, mainly because of the ease of processing (require low processing temperatures and short processing time) due to their low viscosity.

Thermosets are formed into a polymer matrix through an irreversible chemical process and cannot be melted by the application of heat. Thermosets are commonly brittle; however, they offer high rigidity, thermal stability, high resistance to electrical and chemical effects (Abbood et al., 2020). They also cost less than thermoplastic resins (Hyer, 1998).

Polyester- and vinyl esters-based matrices are often used in FRP due to their low cost compared to epoxies. However, epoxies have better mechanical properties, higher temperature resistance, and better durability than vinyl esters and polyesters (Górski et al., 2016; Wu et al., 2020).

- Thermoplastic polymers

On the other side, the thermoplastic polymer can be heat-softened, melted as many times as desired (reversible process). FRP made of these resins are easy to repair by heating, reshaping, and then cooling them off. However, their high cost (compared to thermosetting resins) and manufacturing conditions limit their applications (Hyer, 1998; Wu et al., 2020). Table 2.2 gives mechanical properties of typical polymer matrices used in FRP materials.

Table 2.2 Typical polymer matrices properties (Hyer (1998))

Matrix		Tensile strength (MPa)	Elasticity modulus (GPa)	Density (kg/m^3)	Failure strain (%)
Thermosetting	Epoxy	35-130	2-6	1100-1400	1-8.5
	Polyester	40-90	1.2-4.5	1100-1500	2-5
	Vinyl ester	65-90	3-4	1150	1-5
Thermoplastic		25-185	1-5	900-1400	3-300

2.6.2 Fabrication

The manufacturing processes of FRP materials require significantly less energy than the manufacturing processes of metals. The processes start from the formation of a lamina (a ply, usually with 0.1–1 mm of thickness) which consists of a large number of fibers incorporated into a thin layer of matrix. A lamina can be made from continuous (long) or discontinuous (short) fibers. Stacking and consolidation of several laminas in a specified sequence form a laminate (Fig. 2.13).

For continuous fiber-based laminas, a laminate is formed by stacking several laminas in a specified sequence and then consolidating them. Various laminas in a laminate may contain fibers either all in one direction or different directions.

The fibers may be arranged either in a unidirectional orientation (i.e., all fibers arranged in one direction Fig. 2.13(a)), in a bidirectional orientation (i.e., fibers arranged in two directions, usually normal to each other, Fig. 2.13(b)), or in a multidirectional orientation (i.e., fibers arranged in more than two directions, Fig. 2.13(c)). The bi- or multidirectional orientation of fibers is obtained by weaving or other processes used in the textile industry.

For a lamina containing unidirectional fibers, the strength and ductility have their highest values in the longitudinal fibers' direction and the lowest values in the transverse direction. While, for a lamina containing bidirectional fibers, the strength and modulus depend on the amounts of fibers in the longitudinal and transverse directions, and they are the same in both directions in a balanced lamina.

In discontinuous fiber-based lamina, the discontinuous fibers can be arranged either in unidirectional orientation (Fig. 2.13(d)) or in random orientation (Fig. 2.13(e)).

Different kinds of fibers can be used in a laminate to form either an interplay hybrid laminate, where different laminas of different kinds of fibers are used or an

intraply hybrid laminate in which different kinds of fibers combined in the same lamina to form the laminate. In hybrid laminates, the same matrix is generally used throughout the laminate in order to form a coherent bond between the laminas.

With different fiber orientations and different staking sequences of layers, a wide range of mechanical properties for the composite laminate can be generated (Mallick, 2007).

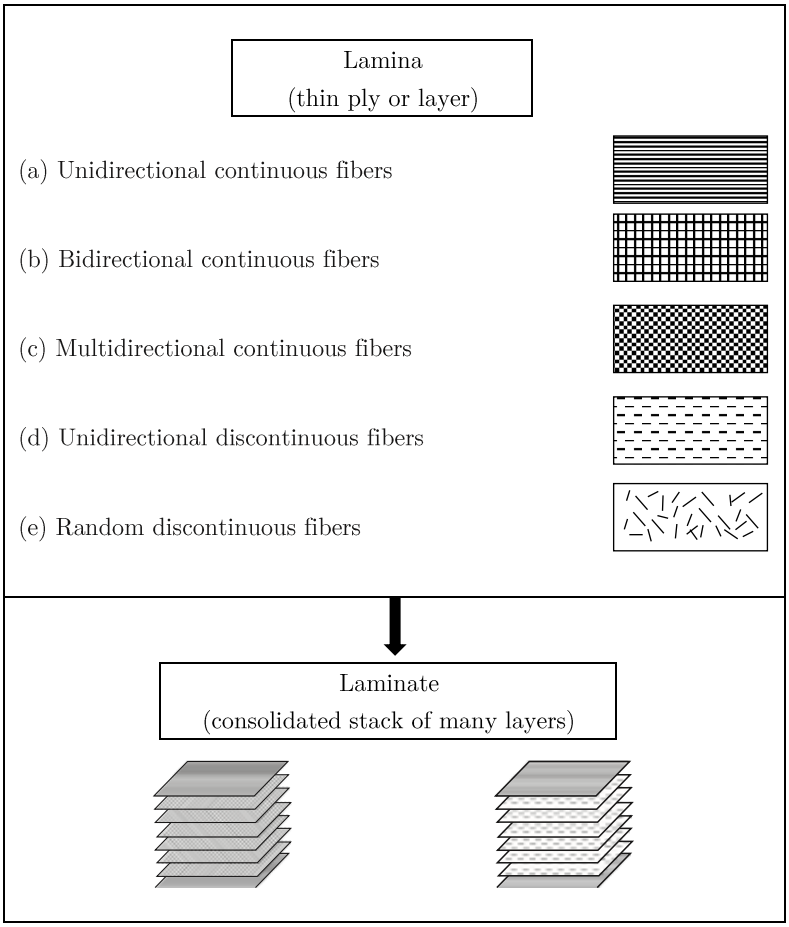

Figure 2.13 Composition blocs of FRP material (Mallick, 2007)

2.6.3 Properties of FRP composites

The finished characteristics of FRP composites depend on the type and ratio of matrix and reinforcing fibers, the fibers' orientation relative to the loads, the fabrication method utilized, the manufacturer's expertise, and many other factors (ACMA, 2016). In the following subsections, the principal mechanical properties of FRP composites are discussed.

2.6.3.1 Tensile strength and elasticity modulus

FRP materials provide stiffness and strength along the fiber direction in tension and behave linearly elastic along that direction up to brittle failure (Fig. 2.14). The tensile strength and elasticity modulus of FRP materials are typically governed by different factors such as fiber type, fiber tensile properties, fiber volume, orientation, and layer arrangement sequence (Rasheed, 2016; ACMA, 2016).

The tensile properties of the common FRP sheets are reported in Table 2.3. It can be seen from the values of this table that CFRP typically have the highest modulus and tensile strength, followed by AFRP and GFRP, and lower ultimate strain than GFRP. Despite the lower mechanical properties of GFRP, it is preferable for many civil engineering applications due to its lower cost (Xiao et al., 2003). In general, the tensile strength of FRP is significantly higher than that of ordinary steel (which only ranges from 400 to 500 MPa). However, they have a lower elasticity modulus than steel except for the CFRP materials (Abbood et al., 2020).

Table 2.3 Mechanical properties of typical FRP sheets (Wu et al. 2020)

FRP type	Tensile strength (MPa)	Elasticity modulus (GPa)	Failure strain (%)
HS CFRP	3500	230	1.5
HM CFRP	1900	540	0.35
E-GFRP	1500	73	2.1
AFRP	2060	118	1.7

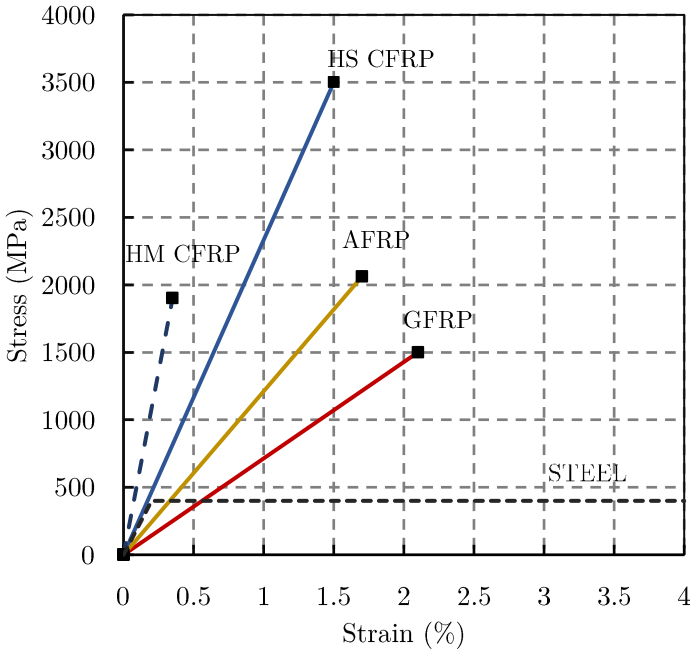

Figure 2.14 Stress-strain curves of typical FRP sheets (Wu et al. 2020)

2.6.3.2 Fiber volume fraction

The fiber volume fraction (V_f) typically describes the volumetric percentage of the fiber reinforcement in the total volume of the composite material. The (V_f) is an essential parameter in designing FRP products, in which optimal quantity of fiber is required for the achievement of strength and stiffness requirements. An alternative to (V_f) is the fiber weight ratio (W_f). It specifies the weight percentage of reinforcement in the composite (ACMA, 2016).

2.6.3.3 Fatigue and Creep

The importance of fatigue and creep behavior of the FRP composites becomes significant when structures strengthened with FRP are under dominant cyclic loads or a high level of sustained load. The evaluation of FRP under different levels of cyclic and sustained stresses and the prediction of corresponding fatigue strength and allowable stress are the key for FRP applications (Wu et al., 2020).

- Fatigue

The fatigue failure is the failure of a structure, component, or material under cyclic stress or strain, which is usually less than the ultimate load strength or strain (Wu et al., 2020). The fatigue properties of FRP composites are much better than the properties of metals. FRP undergo gradual degradation along with rupture and delamination of single fiber and micro damages of the matrix, and complete damage takes place after significant development of such micro damages; however, steel is usually destroyed by the propagation of a single crack (Górski et al., 2016).

In most of the applications, the cyclic stresses on the FRP are not high enough to cause a fracture of the fibers directly in the composites (Wu et al., 2020).

- Creep

Creep rupture stress denotes the stress-causing failure after a specified period from the initiation of a sustained load. It can occur in long-term, axially-loaded columns and beams at significantly high applied load levels (Zureick & Scott, 1998; Sa et al., 2011). Creep stress determines the upper limit of the design stress. The creep rupture stresses of several FRP types are listed in Table 2.4.

Table 2.4 Creep rupture stresses of typical FRP (Wu et al. 2020)

FRP	CFRP	GFRP	AFRP
Creep rupture stress	0.70 f_f	0.29 f_f	0.55 f_f

f_f: Tensile strength of FRP

CFRP possesses the highest creep rupture stress value among the other FRP types, while the GFRP has the lowest value. Creep studies of FRP composites indicate that these properties are largely controlled by the matrix material, where thermoset-based composites are less susceptible to performance degradation due to long-term loads compared to thermoplastic FRP materials (ACMA, 2016; Wu et al., 2020).

2.7 Conclusion

In this chapter, methods for the retrofit and rehabilitation of RC columns such as concrete jackets, steel jackets have been briefly reviewed after pointing out the main causes of damage. Various aspects regarding the employment of FRP composites as strengthening materials in the construction industry have been presented. This review has mainly focused on delivering information about the composition of FRP materials and the characteristics of their constituents, their advantages. It can be concluded that owing to the advantageous properties of FRP materials, FRP jacketing offers an excellent replacement for traditional methods for improving the strength and ductility of RC columns.

Chapter 3

Previous experimental research on axially loaded FRP-confined concrete

3.1 Introduction

This chapter treats the confinement mechanism of concrete columns using FRP materials and reviews some of the existing experimental studies conducted on the axial behavior of FRP-wrapped concrete columns. An experimental database of concrete cylinders confined with GFRP wraps tested under axial compression is collected, which will be the essential experimental framework for the analytical work.

3.2 Mechanism of FRP confinement

A clear understanding of the interaction between the concrete and the FRP confining material is needed to analyze the behavior of FRP-confined concrete (Benzaid et al., 2010).

When a circular concrete column confined with FRP is subjected to axial loading, the column experiences lateral expansion. At low levels of axial strain, the lateral dilation of the concrete is minimal, and the concrete behaves elastically and follows the behavior as the unconfined concrete. At this level, the FRP is barely stressed, and it has practically no effect. However, with the increase in the axial load, the lateral expansion increases, and the concrete starts to push on the FRP (Lam & Teng, 2003). The FRP develops confining stresses to restrain the gradual dilation of the concrete. In this condition, the concrete is subjected to a triaxial state of stress (Fig. 3.1). The confining stresses keep increasing with the expansion of the concrete until the rupture of the FRP.

Based on the equilibrium of the forces of the free-body diagram of the confined concrete section, and the compatibility of the strain (the lateral strain of the

concrete is equal to the strain in the FRP), the maximum confining stress (fl) generated by the FRP is expressed as shown in Eq. (3.1).

$$f = \frac{2t_f f_f}{d} = \frac{\rho_f f_f}{2} = E_l \varepsilon_f \tag{3.1}$$

Where,

t_f = thickness of the FRP (mm);

f_f = FRP ultimate tensile strength (MPa);

d = diameter of the concrete cylinder (mm);

ρ_f = volumetric ratio of the FRP expressed in (Eq. (3.2));

E_l = lateral stiffness of the FRP in (MPa) expressed in (Eq. (3.3));

ε_f = ultimate strain of the FRP.

$$\rho_f = \frac{4t_f}{d} \tag{3.2}$$

$$E_l = \frac{2t_f E_f}{d} \tag{3.3}$$

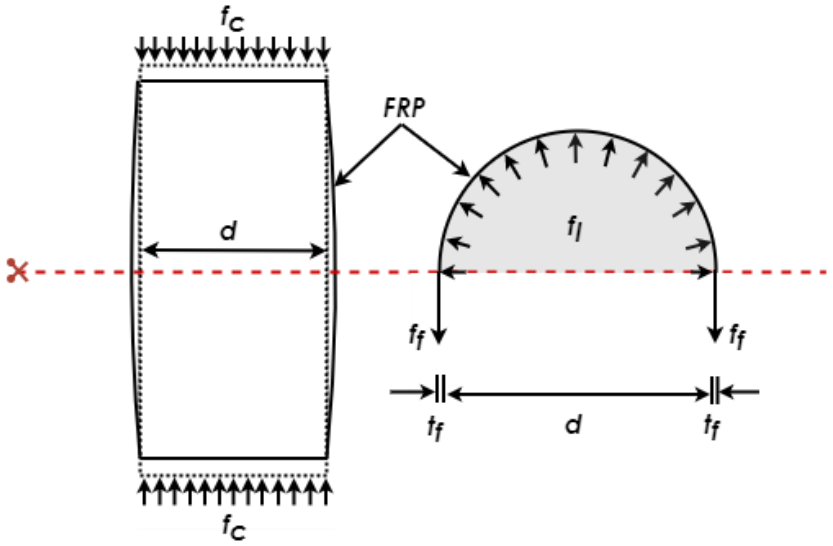

Figure 3.1 Stress state and deformation shape of concrete cylinder confined with FRP under uniaxial compression

In square and rectangular sections, as opposed to circular sections in which the confining pressure is uniform around the concrete's entire circumference (Fig. 3.1), the confining pressure of the FRP is pointed at the corners and less outside (Harries and Carey, 2003).

Failure of the FRP-confine concrete occurs when the FRP reaches its ultimate tensile capacity corresponding to its ultimate strain (ε_f). However, it has been observed that the FRP ruptures at a strain ($\varepsilon_{h,rup}$) lower than its ultimate strain (ε_f) (Spoelstra & Monti, 1999; Xiao & Wu, 2000; Shahawy et al., 2000; Pessiki et al., 2001; De Lorenzis & Tepfers, 2003; Lam & Teng, 2003). For this reason, Pessiki et al. (2001) has proposed a strain reduction factor (k_ε) to account for this reduction. Therefore, the confinement stress at rupture ($f_{l,rup}$) becomes (Eq. (3.4)):

$$f_{l,rup} = \frac{2t_f E_f \varepsilon_{h,rup}}{d} = \frac{2t_f E_f k_\varepsilon \varepsilon_f}{d} = \rho_K \rho_\varepsilon f'_{co} \tag{3.4}$$

Where,

E_f = elasticity modulus of the FRP (MPa);

ρ_K = stiffness ratio of the FRP relative to that of the concrete (Eq. (3.5));

ρ_ε = strain ratio of the FRP relative to that of the concrete (Eq. (3.6));

f'_{co} = unconfined concrete strength (MPa).

$$\rho_K = \frac{2t_f E_f}{d(f'_{co}/\varepsilon_{co})} \tag{3.5}$$

$$\rho_\varepsilon = \frac{\varepsilon_{h,rup}}{\varepsilon_{co}} \tag{3.6}$$

Where,

ε_{co} = axial strain of unconfined concrete.

3.3 Previous experimental work on FRP-confined concrete under axial compression

The first works regarding the beneficial effects of lateral confinement on the strength and deformation of concrete were conducted by Considère (1903) and Richart et al. (1928). Their research was based on a series of circular mortar (Considère, 1903) and concrete (Richart et al., 1928) specimens confined through fluid pressures in three perpendicular directions and plain and spirally reinforced concrete specimens tested under axial compression. They found that the laterally confined specimens show improved strength and deformation compared to plain specimens. Thereafter, extensive research studies have been carried out on confined concrete columns.

For FRP-confined concrete, the first studies conducted by Fardis and Khalili (1981, 1982) and Saadatmanesh et al. (1994) have suggested to model FRP-confined concrete by the models developed for steel-confined concrete developed by Richart et al. (1928), Newman and Newman (1972), and Mander et al. (1988).

However, numerous experimental studies have shown the difference in the stress-strain behavior of FRP-confined concrete and steel confined concrete (Mirmiran

et al., 1996; Miyauchi et al., 1997; Samaan et al., 1998; Spoelstra & Monti, 1999; Saafi et al., 1999).

Consequently, researchers have carried out extensive experimental studies to model the behavior of FRP-confined concrete under compression leading to extensive experimental data of concrete cylinders confined with the various types of FRP (e.g., Lam & Teng, 2004; Vincent & Ozbakkaloglu, 2013; Guo et al., 2016; Narule & Bambole, 2021 for CFRP; Youssef et al., 2007; Kumutha et al., 2007; Cui & Sheikh, 2010; Elwan & Omar, 2014; Sun et al., 2017; Tu et al., 2019; Kissman & Sundar, 2020; Khaloo et al., 2020; for GFRP; Wu & Wang, 2010; Wang & Wu, 2011; Ozbakkaloglu & Akin, 2012; Vincent & Ozbakkaloglu, 2013; Lim & Ozbakkaloglu, 2015 for AFRP).

In the following, some of the experimental research programs performed on FRP-confined concrete specimens are presented. A brief description of objectives, test program, research parameters, and findings are summarized for each study.

3.3.1 Lin and Chen (2001)

- Objectives:

The authors aimed in this study to investigate the strength of concrete cylinders confined by FRP composites in different stacking sequences.

- Experimental work:

Lin and Chen (2001) performed three sets of experimental tests on concrete cylinders of (100 mm × 200 mm × 25.1 MPa) and (120 mm × 240 mm × 32.7 MPa) in (diameter × height × unconfined concrete strength) confined with FRP under axial compression. In the first set, the concrete cylinders of (120 mm × 240 mm) were wrapped with one or two layers of either GFRP or CFRP composites. In the second set, the concrete cylinders of (100 mm × 200 mm) were confined with both GFRP and CFRP together in six stacking sequences (G/C/C, C/G/C, C/C/G, G/G/C, G/C/G and C/G/G). While in the third set, the concrete cylinders of (100 mm × 200 mm) were partially wrapped with GFRP and CFRP composites in six reinforcing patterns. The concrete strengths used were 25.1 and 32.7 MPa. The tensile strength, the elasticity modulus, and the thickness per layer of GFRP and CFRP composites were 743.9 MPa, 32.9 GPa, 0.9 mm and 770 MPa, 157.54 GPa, 0.5 mm, respectively.

- Findings:

The authors reported that the strength of the confined specimens increases proportionally with the number of layers of the FRP. They found that the stacking sequence of the FRP affects the strength of the specimens, and recommended wrapping the concrete first with more ductile FRP. The authors also observed that the strength of the specimens wrapped with different FRP in distinct regions is lesser than that of specimens confined with one type of FRP.

The authors developed a model for the prediction of the ultimate strength of FRP-confined concrete. They found that the results of this model are in close agreement with the experiments than the existing models.

3.3.2 Thériault et al. (2004)

- Objectives:

This study aimed to investigate experimentally the influence of slenderness ratio and specimen size on axially loaded FRP-confined concrete columns.

- Experimental work:

In this study, 42 concrete cylinders were tested under axial compression. Twenty-four cylinders were confined with either GFRP or CFRP sheets with (1, 2, 3, and 4 layers), and the 18 remainings (unconfined) were kept as a reference. Two slenderness ratios (h/d = 2 and 6) were used with 3 diameters (51, 152, 304 mm). The GFRP and CFRP used have tensile strength and modulus of elasticity of 552 MPa, 27.6 GPa, and 3481 MPa, 230 GPa, respectively. The unconfined concrete strength varied from 18 to 39 MPa.

- Findings:

The authors concluded that there are no significant variations in the compressive strength between medium and long FRP-confined concrete specimens. In addition, they found that the effect of the confining pressure of the FRP is independent of the slenderness ratio. The authors reported that the conventional FRP-confined concrete cylinders could be effectively used to model the axial behavior of short columns.

3.3.3 Lin and Liao (2004)

- Objectives:

The aim of this study was to develop a model to predict the compressive strength of concrete columns confined by composite materials.

- Experimental work:

Lin and Liao (2004) tested nine sets of concrete cylinders of 100 mm diameter and 200 mm long under axial compression. The cylinders were plain, axially reinforced, and axially and transversely reinforced with steel reinforcement, where one or two layers were applied in each type of cylinders. The average tensile strength and elasticity modulus of the GFRP were 248 MPa and 23 GPa. The properties of reinforcing steel of axially reinforced cylinders and axially and transversely reinforced specimens were 423, 616 MPa yield strength and 212, 206 GPa elasticity modulus of 3.5 mm diameter.

- Findings:

The experimental results showed that the strength of the concrete is proportional to the number of layers of GFRP. In addition, the effect of the steel reinforcement

was found to be associative to that of the GFRP (the combined confinement of steel and FRP is the sum of the confinement of steel and the confinement of the FRP). The authors developed a strength model for FRP-confined concrete. They reported that the predictions of the proposed model are in close agreement with experimental results compared to the other models.

3.3.4 Berthet et al. (2005)

- Objectives:

The main objective of this study was to identify the main parameters affecting the mechanical behavior of short concrete columns externally confined by CFRP and GFRP jackets.

- Experimental work:

The authors tested 63 concrete cylinders of (160 mm × 320 mm) and (70 mm × 140 mm) (diameter × height) under axial compression. Five concrete strengths were used (20, 40, 50, 100, and 200 MPa). Fifteen cylinders were kept as control specimens, 33 were wrapped with (2, 3, 5) plies of GFRP jackets, and 15 were wrapped with (1, 1.5, 2, 4, 5, 6, 9, 12) plies of CFRP jackets. The concrete was designed to have five strengths (20, 40, 50, 100, and 200 MPa). The tensile strength and the elasticity modulus of the GFRP and CFRP jackets were 2500 MPa, 74 GPa, and 3200 MPa, 230 GPa, respectively.

- Findings:

Berthet et al. (2005) found that the ultimate strength and ultimate strain increase with the number of FRP layers and confinement level and decrease with the concrete strength. Also, they found that the transition zone and the slope of the second branch of the stress-strain curve depend on the FRP jacket stiffness.

3.3.5 Almusallam (2007)

- Objectives:

Study the effectiveness of GFRP confinement on concrete cylinders subjected to uniaxial compression loads.

- Experimental work:

Almusallam (2007) tested 54 concrete cylinders of 150 × 300 mm under uniaxial compression. The cylinders were divided into six groups according to the concrete strength and the amount of GFRP. The concrete is designed to have six compressive strengths varied from normal to high strength (i.e., 40, 45, 55, 75, 85, and 100 MPa). Each group includes three cylinders confined with one layer of GFRP, three cylinders confined with three layers of GFRP, and three cylinders left unconfined to quantify the amount of gain obtained using the GFRP. The thickness of the GFRP was 1.3mm, and the tensile strength and modulus of elasticity of GFRP laminates were 540 MPa and 27 GPa, respectively.

- Findings:

Almusallam (2007) reported that GFRP confinement substantially increases the compressive strength and ductility of concrete cylinders. He found that confinement is more effective on normal strength concrete than on high-strength concrete (for a given confinement, strength and ductility are higher for normal strength concrete than high strength concrete). Also, he observed that the strength and ductility increase with the number of layers used for confinement.

Almusallam (2007) developed a theoretical model to predict the stress-strain relationship of GFRP confined concrete cylinders in the axial and lateral directions. The model shows excellent agreement with the experimental values.

3.3.6 Sheikh et al. (2007)

- Objectives:

In this study, the authors aimed to study the behavior of full-scale concrete-filled GFRP shells under concentric compression.

- Experimental work:

The authors tested seventeen large-scale circular concrete columns of 356 mm in diameter and 1524 mm long under axial compression. Three groups of specimens were performed. The first group included plain concrete specimens (with no steel reinforcement). The second group included specimens reinforced with longitudinal steel and steel hoops with 320 mm spacing, whereas in the last group, the specimens were reinforced with longitudinal steel and steel spirals at 75 mm pitch. The specimens of all the groups were confined with GFRP shells of a different number of layers with different directions and orientations. The concrete strength of all specimens was 30 MPa, and the yield strength for longitudinal and transverse steel was 402 and 500 MPa, respectively.

- Findings:

The authors concluded that the FRP shells could be used for stay-in-place formwork and effective confinement reinforcement for concrete columns by significantly increasing their compressive strength, ductility, and energy capacity. The authors also observed that a specimen confined with a GFRP shell composed of one transverse layer of GFRP performs better than a similar specimen reinforced with 320 mm spacing lateral steel. Similarly, a specimen confined with a GFRP shell composed of two transverse layers of GFRP performs better than a similar specimen reinforced with steel spirals with a 75 mm pitch. In addition, the authors found that a GFRP shell composed of 45° inclined fibers is more effective in achieving more ductile behavior of concrete columns than a similar GFRP shell with fibers oriented in the longitudinal and transverse directions.

The authors reported that GFRP shells improve the effect of steel reinforcement by delaying buckling of the longitudinal bars and preventing spalling of the concrete cover.

3.3.7 Wu et al. (2008)

- Objectives:

The purpose of the study of Wu et al. (2008) was to understand the performance of concrete columns confined with hybrid FRP composites.

- Experimental work:

Wu et al. (2008) tested 35 cylindrical specimens with dimensions of 150 × 300 mm in uniaxial compression. The specimens included 12 cylinders confined with a single type of FRP (i.e., high strength CFRP, high modulus CFRP, AFRP, GFRP, and Polypara-phenyleneBenzo-bis-Oxazole PBO FRP), 20 cylinders confined with hybrid FRP sheets (i.e., CFRP-PBO, CFRP-AFRP, CFRP-GFRP), and three cylinders left as control specimens. The experimental parameters include the type of FRP, the number of layers, and the different FRP hybridizations. The concrete used in this study had a compressive strength of 23 MPa.

- Findings:

Wu et al. (2008) reported that confinement with FRP effectively increases the strength, ductility, and energy absorption capacity of concrete cylinders. In addition, they observed that the hybrid ratio of the FRP has great importance. For instance, they observed that the ultimate strength of FRP-confined concrete could be improved using a high strength FRP to a high stiffness FRP, whereas the strain remains the same as for the counterpart specimen confined only with the high stiffness FRP sheet.

Wu et al. (2008) proposed analytical models for predicting the ultimate strength and strain as well as the stress-strain relationship of concrete cylinders confined with hybrid FRP composites. The models have been found to show good agreement with the experimental results.

3.3.8 Benzaid et al. (2009)

- Objectives:

The purpose of the study was to evaluate the effectiveness of strengthening circular and square high-strength concrete columns with GFRP.

- Experimental work:

Benzaid et al. (2009) tested under uniaxial compression circular and square prismatic high strength concrete specimens strengthened with E-glass FRP until failure. Thirteen experiments divided into two groups were performed. The first group consisted of six cylindrical specimens of 160 mm × 320 mm wrapped with 1, 2, and 4 layers of GFRP, where two of them were reinforced with steel reinforcement. The second group included seven square plain concrete specimens of 100 mm × 100 mm × 300 mm wrapped with 1 and 2 layers of GFRP. This group was divided according to the corner radius of the specimen into three subgroups: sharp corner, 8 mm corner radius, and 16 mm corner radius. The GFRP

used had a tensile strength of 383 MPa and an elasticity modulus of 23.8 GPa. The parameters considered are the number of layers, the corner radius for square specimens, and the GFRP confinement relationship with steel reinforcement.

- Findings:

Benzaid et al. (2009) reported that the GFRP confinement enhances the strength and strain of the confined specimens, and it is more effective on circular specimens than on square specimens. They found that square specimens with high corner radius perform better than small radius specimens, and they have attributed that to the intensification of the stresses at the corners.

The authors found that the models of Samaan et al. (1998), Saafi et al. (1999), Shehata et al. (2002), and Kumutha et al. (2007) can predict the ultimate strength of FRP-confined concrete with good accuracy.

3.3.9 Comert et al. (2010)

- Objectives:

Comert et al. (2010) aimed at developing a stress-strain model for GFRP-confined low-strength concrete.

- Experimental work:

Ten concrete cylinder specimens of 150 mm in diameter and 300 mm in height were tested under concentric compression. Two cylinders were confined with two plies of GFRP sheets, six cylinders were wrapped with two plies of GFRP sheets after applying a layer of 25mm thick of cement-based low-strength mortar over the concrete surface, and the two remaining cylinders were remained unwrapped as a reference. Different compressive strengths were used. The concrete is designed to have 9.3 MPa compressive strength, and the mortar 2, 7.6, and 7.8 MPa. The GFRP sheets have 0.28 mm per ply and 1700 MPa and 65 GPa of tensile strength and elasticity modulus. The authors have applied the mortar before the GFRP wraps to obtain different slopes for the second branch of the stress-strain curves of GFRP-confined concrete.

- Findings:

Comert et al. (2010) reported that GFRP confinement improved the performance of the concrete cylinders in terms of strength and deformability.

They found that comparing the confined specimens, adding a mortar layer improves the deformability of the specimens. However, it decreases the strength. They have attributed the increase to the extra lateral strain absorbed by the mortar layer and the decrease of the strength to that increase in the cross-sectional area, which reduces the effectiveness of the GFRP confinement.

Comert et al. (2010) reported that the behavior of these specimens might be preferable when higher deformability is required without a remarkable increase in strength.

The authors showed that the slope of the second branch of the stress-strain curve decreased with the use of an extra mortar layer due to the damage and cracks of the mortar layer between the concrete and the GFRP confinement.

3.3.10 Cui and Sheikh (2010)

- Objectives:

This study aimed to investigate the behavior of concrete confined with FRP.

- Experimental work:

Cui and Sheikh (2010) conducted an experimental study on 112 cylindrical concrete specimens, each 152 mm in diameter and 305 mm in height, 88 FRP wrapped, and 24 unwrapped. The specimens were tested under monotonic uniaxial compression. Test variables included FRP type (i.e., GFRP and CFRP wraps), amount of FRP, concrete strength (45 to 112 MPa), and the concrete condition before strengthening (the concrete was pre-cracked under a load of approximately 80% of its unconfined strength before they were wrapped).

- Findings:

Cui and Sheikh (2010) found that the strength, deformability, and energy absorption capacity of confined concrete improve with the number of FRP layers, with the deformability showing larger improvement. They also found that strength enhancement is independent of the FRP amount when a high modulus FRP is applied. However, when low modulus FRP is applied, a minimum amount of FRP is required to achieve strength enhancement.

The authors reported that the increase of the unconfined concrete strength had a negative effect on the strength enhancement, ductility, and energy absorption capacity of the specimens. While, for the pre-cracking condition, the authors observed that the stress-strain response of FRP confined NSC was unaffected by a pre-cracking load of up to 77% of unconfined concrete strength before wrapping.

3.3.11 Micelli and Modarelli (2013)

- Objectives:

The purpose of this study of Micelli and Modarelli (2013) was to examine the effect of various experimental parameters on the confinement effectiveness of FRP jackets on both circular and rectangular concrete columns with a solid or hollow core.

- Experimental program:

Micelli and Modarelli (2013) prepared and tested 128 concrete specimens in uniaxial compression until failure, 89 of them were strengthened with CFRP and GFRP, and the remaining were kept as a reference.

The specimens were divided according to the parameters studied. Two concrete strength (i.e., 28 and 38 MPa); three types of specimens (cylinders of 150 $\times$ 300

mm and 250 × 500 mm; square and rectangular prisms of 150 × 150 × 300 mm and 150 × 200 × 400 mm, hollow cylinders with a hollow core of 50 and 150 mm in diameter, and prismatic specimens with a hollow core of 50 × 50 mm, 100 × 50 mm and 200 × 50 mm, respectively). Corner radius (10 mm and 25 mm) for prismatic specimens. Four FRP thicknesses (i.e., one, two, three, and five layers of CFRP and GFRP).

- Findings:

The experimental results showed that the FRP confinement enhances the compressive strength, ductility of the confined specimens.

The effect of FRP confinement decreased with the increase of the concrete strength and from passing from circular to square to rectangular sections, and it is more pronounced for hollow specimens. In addition, they showed that the confinement effect in terms of strength and displacement decreases in specimens without rounded corners due to high stress-concentration in the FRP close to the sharp corners. The increase in the FRP amount did not significantly affect the slope of the second branch of the stress-strain curve.

The authors reported that the models of Samaan et al. (1998), Spoelstra and Monti (1999), Lam and Teng (2002), and CNR DT-200 show good predictions of the compressive strength. However, they provide lower accuracy for the prediction of the ultimate strain of the confined specimens.

3.3.12 Touhari and Mitiche-Kettab (2016)

- Objectives:

The work aimed to investigate the behavior of FRP-confined concrete cylinders subjected to axial compressive loading.

- Experimental work:

Touhari and Mitiche-Kettab (2016) tested 54 FRP concrete cylinders of 160 mm × 320 mm confined with GFRP and CFRP wraps under axial compression. Three concrete mixtures were used (26, 40, and 60 MPa), and three thicknesses of FRP were applied for each group (one, two, and three layers). The effects of several parameters such as unconfined concrete strength, type, and amount of FRP were investigated.

- Findings:

The results showed that the confinement with FRP materials improves the strength and ductility of the concrete cylinders, where a more pronounced effect is obtained using CFRP. In addition, it was found that the effectiveness of the FRP increased with the number of layers and decreased with the unconfined concrete strength.

The authors developed a new model to predict the compressive strength and its corresponding strain of FRP-confined concrete cylinders basing on their

experimental results. They reported that the predictions of the model are in good agreement with the experimental results.

3.3.13 Guo et al. (2016)

- Objectives:

The study intended to investigate the axial compressive behavior of CFRP-confined damaged NSC and HSC concrete.

- Experimental work:

Guo et al. (2016) tested 60 cylindrical concrete specimens of 150 mm × 300 mm (diameter × height) under axial compression. The specimens were divided into two groups (30 NSC and 30 HSC). In the first group (NSC), three cylinders were kept as control specimens, nine intact (undamaged) specimens were wrapped with one, two, or three layers of CFRP sheets, nine damaged specimens with 80% residual strength were wrapped with one, two, or three layers of CFRP sheets, and nine damaged specimens with 75% residual strength were wrapped with one, two, or three layers of CFRP sheets. For the second group (HSC), the specimens were divided equally as the first group, except the damaged specimens (nine damaged specimens with 85% of residual strength and nine damaged specimens with 78% of residual strength). The concrete was designed to have 45.6 MPa (NSC) and 70.2 MPa (HSC). The CFRP sheet has a tensile strength and elasticity modulus of 4354.7 MPa and 219 GPa, respectively.

- Findings:

The authors found that the CFRP confinement improved the ultimate strength and strain of intact and damaged concrete greatly. For NSC wrapped with a small amount of CFRP, the effect of pre-existing damage is significant. However, for HSC wrapped with the same CFRP amount, this effect is relatively small.

The results also showed that the CFRP began to carry loads at low stresses (before reaching the unconfined concrete strength) for damaged specimens compared to the intact specimens. In addition, the effect of the pre-existing damage was eliminated with the use of a great amount of CFRP.

The authors reported that the models of (Bisby et al. (2005), Teng et al. (2007), Youssef et al. (2007), Xiao et al. (2010), Pham and Hadi (2014), Tamzus et al. (2006), and Albanesi et al. (2007))are not able to provide accurate predictions for the damage CFRP confined concrete whether they overestimate of the ultimate strength and strain of CFRP-confined HSC or they significantly underestimate that of CFRP-confined damaged NSC.

3.3.14 Oliveira et al. (2019)

- Objectives:

Experimental analysis of the effect of CFRP and GFRP confinement on normal-, high-, and ultra-high strength concrete (NSC, HSC, and UHSC) cylinders.

- Experimental work:

Oliveira et al. (2019) tested 102 FRP-confined concrete cylinders under axial compression. NSC with or without silica fume (SF), HSC with or without SF, and UHSC with or without thermal curing (TC). The specimens had (50 × 100) mm, (100 × 200), and (150 × 300) mm in (diameter × height). The unconfined concrete strength ranged from 38 to 200 MPa. The specimens of each group were wrapped with one, two, and four layers of GFRP or CFRP sheets. GFRP and CFRP properties were a tensile strength of 1,670 MPa and 3420 MPa, and an elastic modulus of 78.2 GPa and 244 GPa, respectively.

- Findings:

The authors have developed a new equation to predict the strain efficiency factor and verified it with the existing literature. The authors confirmed with the reported literature their results on the shape of the stress-strain curve of FRP-NSC (parabolic branch followed by a linear ascending or descending branch depending on the confinement level). For HSC and UHSC, the authors identified three types of stress-strain behavior depending on the confinement level (full strain softening, softening followed by strength recovering, or full hardening) and proposed expressions to predict key points defining the stress-strain behavior of FRP-confined HSC and UHSC. In addition, the authors found that for a high confinement ratio, strength enhancement is higher on NSC than on HSC. The results also revealed that silica fume slightly improved the strength and strain enhancement of confined specimens.

3.3.15 Khaloo et al. (2020)

- Objectives:

The purpose of this study was to investigate the axial and lateral behavior of low-strength concrete confined by GFRP wraps.

- Experimental work:

A total of 48 cylindrical concrete specimens having 150 mm × 300 mm (diameter × height) have been tested by the authors under axial compression. Twelve cylinders were kept as reference, and the remaining 36 cylinders were wrapped with 3, 5, and 7 layers of GFRP. The concrete was designed to achieve the target strengths of 5, 10, 15, and 20 MPa. The GFRP wraps had a tensile strength of 2500 MPa and an elasticity modulus of 115 GPa.

- Findings:

The results of the study showed that the GFRP confinement improves the strength and ductility of the confined concrete; however, it is less effective when higher-strength concrete. It was found that the compressive strength is a more effective criterion on the ultimate strength, ultimate strain, and the strain factor than the amount of GFRP. In addition, the lateral confining pressure and the unconfined concrete strength were found to be the influencing factors on the lateral strain-axial strain relationship. The authors also reported that most of the models

developed for NSC provide accurate predictions for predicting the strength and strain improvement for LSC.

3.4 Experimental database

3.4.1 Existing databases

Several databases of FRP-confined concrete specimens tested under axial compression have been collected by researchers (e.g., Lam & Teng, 2002; De Lorenzis & Tepfers, 2003; Realfonzo & Napoli, 2011; Lim & Ozbakkaloglu, 2014; Huang et al., 2016). Table 3.1 summarizes details of some existing available databases.

Table 3.1 Summary of some existing databases

Source	Number of studies	Number of datasets	FRP type	f'_{co} (MPa)	d (mm)	h (mm)
Lam and Teng (2002)	9	83	CFRP, GFRP, and AFRP wraps	18-55.2	100-152	200-610
Lam and Teng (2003)	14	76	CFRP, HM-CFRP, GFRP, and AFRP wraps and tubes	26.2-55.2	100-200	200-610
De Lorenzis and Tepfers (2003)	17	180	CFRP, GFRP, and AFRP wraps and tubes	19.4-82.1	51-219	102-438
Bisby et al. (2005)	23	197	CFRP, GFRP, and AFRP wraps	15-103	500-300	
Turgay et al. (2009)	20	127	CFRP wraps and tubes	17.4-171.0	51-200	102-610
Realfonzo and Napoli (2011)	63	465	CFRP and GFRP wraps	15.2-169.7	51-406	102-1824
Ozbakkaloglu and Lim (2013)	99	832	CFRP, GFRP, AFRP, HM CFRP, and UHM CFRP wraps and tubes	6.2-55.2	47-600	100-1200

Lim and Ozbakkaloglu (2014)	23	231	CFRP, GFRP, AFRP, HM CFRP, and UHM CFRP wraps and tubes	56.7-169.7	51-298	102-610
Huang et al. (2016)	37	212	GFRP wraps and tubes	15-188	51-406	102-812.8
Raza et al. (2020)	47	520	FRP	12.41-188.2	51-406	102-812

3.4.2 Selection of the new database

A new experimental database of short concrete columns confined with GFRP wraps tested under axial compression is collected through an extensive review of the literature. Due to the variability of the available experimental data, a set of criteria listed below is used in the selection of the test data in order to ensure reliable and consistent results. This resulted in 163 test data from 27 experimental studies (Table 3.2), making it by far the most comprehensive database reported in the literature of axially loaded circular GFRP-wrapped concrete columns.

- Specimens that had considerably different results from other datasets were excluded.
- Specimens reported with insufficient details were excluded.
- Specimens with a height-to-diameter ratio greater than three were excluded to eliminate any possible effect of specimen slenderness.
- Specimens with negligible strength or strain improvement were excluded.
- Specimens with internal steel reinforcement were excluded.
- Only specimens confined with GFRP sheets were included (i.e., concrete-filled GFRP tubes were excluded).
- Only specimens fully wrapped GFRP sheets were included (i.e., partially GFRP-wrapped specimens were excluded).
- Only specimens wrapped with GFRP sheets having fibers primarily oriented in the hoop direction were included.
- Only specimens that failed due to the rupture of the GFRP sheet were included

For each specimen, the following information is reported: the specimen dimensions (height h (mm), diameter d (mm), and the ratio h/d); the properties of unconfined concrete (unconfined concrete strength f'_{co} (MPa) and its corresponding strain ε_{co} (%)); the properties of GFRP (tensile strength f_f (MPa), elastic modulus E_f (GPa), total thickness t_f (mm), and the ultimate tensile strain ε_f (%)); the confined concrete properties (ultimate strength f'_{cc} (MPa), ultimate axial strain ε_{cc} (%), rupture strain of the GFRP $\varepsilon_{h,rup}$ (%),strain efficiency factor k_ε, and confinement effectiveness strength and strain ratios (f'_{cc} /f'_{co}) and ($\varepsilon_{cc}/\varepsilon_{co}$), respectively). It is noted that when a dataset includes both fiber properties and FRP properties, FRP

properties are used, unlike some previous studies (e.g., Ozbakkaloglu & Lim, 2013; Lim et al., 2016) that have used fiber properties or those who did not differentiate between the properties of fiber and those of the FRP.

Table 3.2 Summary of the test results

No.	Source	Specimen dimensions			Unconfined concrete properties		GFRP properties				Experimental results					
		d (mm)	h (mm)	h/d	f'_{co} (MPa)	ε_{co} (%)	E_f (GPa)	f_f (MPa)	t_f (mm)	ε_f (%)	f'_{cc} (MPa)	ε_{cc} (%)	$\varepsilon_{h,rup}$ (%)	k_ε	f'_{cc}/f'_{co}	$\varepsilon_{cc}/\varepsilon_{co}$
1	Ahmad et al. (1991)	101.6	203.2	2.00	38.99	0.20	48.3	2070	0.8	4.286	115.3	1.130			2.96	5.65
2		101.6	203.2	2.00	50.51	0.24	48.3	2070	0.8	4.286	135.1	1.240			2.67	5.17
3		101.6	203.2	2.00	64.2	0.27	48.3	2070	0.8	4.286	145.59	1.230			2.27	4.56
4	Nanni and Bradford (1995)	150	300	2.00	36.3	0.28	52	175	0.3	0.337	46	2.292			1.27	8.19
5		150	300	2.00	36.3	0.28	52	175	0.6	0.337	60.52	3.079			1.67	11.00
6		150	300	2.00	36.3	0.28	52	175	0.6	0.337	59.23	3.405			1.63	12.16
7		150	300	2.00	36.3	0.28	52	175	0.6	0.337	59.77	2.744			1.65	9.80
8		150	300	2.00	36.3	0.28	52	175	0.6	0.337	60.16	2.887			1.66	10.31
9		150	300	2.00	36.3	0.28	52	175	0.6	0.337	69.02	3.100			1.90	11.07
10		150	300	2.00	36.3	0.28	52	175	0.6	0.337	55.75	2.489			1.54	8.89

11		150	300	2.00	36.3	0.28	52	175	0.6	0.337	56.41	2.968			1.55	10.60
12		150	300	2.00	36.3	0.28	52	175	1.2	0.337	84.88	3.145			2.34	11.23
13		150	300	2.00	36.3	0.28	52	175	1.2	0.337	84.33	4.150			2.32	14.82
14		150	300	2.00	36.3	0.28	52	175	1.2	0.337	79.64	4.100			2.19	14.64
15		150	300	2.00	36.3	0.28	52	175	2.4	0.337	106.87	5.242			2.94	18.72
16		150	300	2.00	36.3	0.28	52	175	2.4	0.337	104.94	5.453			2.89	19.48
17		150	300	2.00	36.3	0.28	52	175	2.4	0.337	107.91	4.509			2.97	16.10
18	Karbhari and Gao (1997)	152	305	2.01	18.01		35.856	513.1	5.31	1.431	82.25	2.400			4.57	
19	Mastrapa (1997)	152.5	305	2.00	31.2		11.703	345	3	2.948	64.67	2.950	2.223	0.770	2.07	
20		152.5	305	2.00	31.2		11.703	345	3	2.948	64.7	3.150	1.972	0.680	2.07	
21		152.5	305	2.00	31.2		11.703	345	5	2.948	91	3.800	1.798	0.620	2.92	
22		152.5	305	2.00	31.2		11.703	345	5	2.948	96.9	6.200	1.769	0.610	3.11	
23		152.5	305	2.00	31.2		11.703	345	3	2.948	63.1	2.650	2.204	0.760	2.02	

24		152.5	305	2.00	31.2		11.703	345	3	2.948	65.4	2.800	2.175	0.750	2.10	
25		152.5	305	2.00	31.2		11.703	345	5	2.948	91.9	4.200	1.943	0.670	2.95	
26		152.5	305	2.00	31.2		11.703	345	5	2.948	89	4.800	1.711	0.590	2.85	
27	Lin and Chen (2001)	120	240	2.00	32.7	0.20	32.9	743.9	0.9	2.261	62.2				1.90	
28		120	240	2.00	32.7	0.20	32.9	743.9	0.9	2.261	61.4				1.88	
29		120	240	2.00	32.7	0.20	32.9	743.9	0.9	2.261	66.3				2.03	
30		120	240	2.00	32.7	0.20	32.9	743.9	1.8	2.261	101.3				3.10	
31		120	240	2.00	32.7	0.20	32.9	743.9	1.8	2.261	88				2.69	
32		120	240	2.00	32.7	0.20	32.9	743.9	1.8	2.261	104.5				3.20	
33	Harries and Kharel (2002)	152	305	2.01	32.1	0.28	4.9*	75*	9*	1.531	46.7	0.680	1.110	0.725	1.45	2.43
34		152	305	2.01	32.1	0.28	4.9*	75*	12*	1.531	50.2	0.820	1.090	0.712	1.56	2.93
35		152	305	2.01	32.1	0.28	4.9*	75*	15*	1.531	60	0.870	1.110	0.725	1.87	3.11
36		152	305	2.01	32.1	0.39	4.9*	75*	9*	1.600	53.2	0.950	1.438	0.900	1.66	2.44

37	Harries and Carey (2003)	152	305	2.01	32.1	0.39	4.9*	75*	9*	1.600	46.7	0.680	1.132	0.900	1.45	1.74
38	Lin and Liao (2004)	100	200	2.00	26.987		23.8253	445.437	1.84	1.870	62.422				2.31	
39		100	200	2.00	20.888		23.8253	445.437	1.84	1.870	62.056				2.97	
40		100	200	2.00	23.846		23.8253	445.437	1.84	1.870	61.446				2.58	
41		100	200	2.00	26.987		22.4579	403.141	3.89	1.795	93.557				3.47	
42		100	200	2.00	20.888		22.4579	403.141	3.89	1.795	90.69				4.34	
43		100	200	2.00	23.846		22.4579	403.141	3.89	1.795	88.983				3.73	
44	Lam and Teng (2004)	152	305	2.01	38.5		22.455	490	1.27	2.325	56.2		1.849	0.744	1.46	
45		152	305	2.01	38.5		22.455	490	1.27	2.325	51.9	1.315	1.442	0.744	1.35	
46		152	305	2.01	38.5		22.455	490	1.27	2.325	58.3	1.459	1.885	0.744	1.51	
47		152	305	2.01	38.5		22.455	490	2.54	2.325	75.7	2.457	1.762	0.744	1.97	
48		152	305	2.01	38.5		22.455	490	2.54	2.325	77.3	2.188	1.674	0.744	2.01	
49		152	305	2.01	38.5		22.455	490	2.54	2.325	75.2		1.772	0.744	1.95	

50	Faella *et al.* (2005)	150	300	2.00	35		80.7	2560	0.48	3.500	60	0.943	1.200	0.343	1.71	
51		150	300	2.00	35		80.7	2560	0.48	3.500	59.4	1.637	1.683	0.481	1.70	
52		150	300	2.00	35		80.7	2560	0.48	3.500	61.2	0.930	1.371	0.392	1.75	
53		150	300	2.00	35		80.7	2560	0.48	3.500	61.7				1.76	
54		150	300	2.00	35		80.7	2560	0.96	3.500	76.3	1.190	1.061	0.303	2.18	
55		150	300	2.00	35		80.7	2560	0.96	3.500	86.1	1.056	1.047	0.299	2.46	
56		150	300	2.00	35		80.7	2560	0.96	3.500	78.6				2.25	
57		150	300	2.00	35		80.7	2560	0.96	3.500	84.6				2.42	
58	Mandal *et al.* (2005)	100	200	2.00	30.7	0.27	26.1	575	1.3	2.200	54.5	1.540			1.78	5.70
59		100	200	2.00	30.7	0.27	26.1	575	2.6	2.200	79.3	2.750			2.58	10.19
60		100	200	2.00	46.3	0.23	26.1	575	1.3	2.200	58.5	0.900			1.26	3.91
61		100	200	2.00	46.3	0.23	26.1	575	2.6	2.200	83.8	1.480			1.81	6.43
62		100	200	2.00	54.5	0.24	26.1	575	2.6	2.200	84.1	0.800			1.54	3.33

63		100	200	2.00	67.1	0.22	26.1	575	1.3	2.200	86.8	0.320			1.29	1.45
64		100	200	2.00	67.1	0.22	26.1	575	2.6	2.200	95	0.380			1.42	1.73
65		100	200	2.00	80.6	0.22	26.1	575	1.3	2.200	102.7	0.370			1.27	1.68
66		100	200	2.00	80.6	0.22	26.1	575	2.6	2.200	98.3	0.350			1.22	1.59
67	Au and Buyukozturk (2005)	150	375	2.50	24.2	0.36	26.1	575	1.2	2.200	43.8	1.630	1.480	0.672	1.81	4.53
68	Li *et al.* (2006)	152.4	304.8	2.00	45.6	0.80	15.1	320.2	1.476	2.320	54.62	2.200			1.20	2.75
69	Green *et al.* (2006)	152	305	2.01	59		33.8*	748*	2*	2.200	73				1.24	
70	Shao *et al.* (2006)	152	305	2.01	40.2	0.22	26.13	610	1.02	2.500	49.6	0.730	1.340		1.23	3.32
71		152	305	2.01	40.2	0.22	26.13	610	2.03	2.500	71.4	0.850	1.320		1.78	3.86
72	Silva and Rodrigues (2006)	150	300	2.00	31.1	0.21	21.3	575	2.54	2.700	91.6	2.610	2.180		2.95	12.43
73		150	300	2.00	29.6	0.19	21.3	575	2.54	2.700	89.4	2.720	2.180		3.02	14.32
74		150	300	2.00	31.1	0.20	21.3	575	2.54	2.700	87.5	2.280	2.180		2.81	11.40

75		150	450	3.00	31.1		21.3	575	2.54	2.700	91.9	2.340	2.180	2.95	
76		150	450	3.00	29.6		21.3	575	2.54	2.700	89.8	2.320	2.180	3.03	
77		150	450	3.00	31.2		21.3	575	2.54	2.700	91.9	2.310	2.180	2.95	
78		250	750	3.00	31.2	0.24	21.3	575	2.54	2.700	55.8	1.090	2.180	1.79	4.54
79	Youssef *et al.* (2007)	406.4	812.8	2.00	29.4	0.24	18.5	425	7.267	2.160	70.77	1.527		2.41	6.36
80		406.4	812.8	2.00	29.4	0.24	18.5	425	7.267	2.160	71.78	1.445		2.44	6.02
81		406.4	812.8	2.00	29.4	0.24	18.5	425	7.267	2.160	76.78	1.387		2.61	5.78
82	Youssef *et al.* (2007)	406.4	812.8	2.00	29.4	0.24	18.5	425	4.472	2.160	49.53	1.345		1.68	5.60
83		406.4	812.8	2.00	29.4	0.24	18.5	425	4.472	2.160	54.9	1.003		1.87	4.18
84		406.4	812.8	2.00	29.4	0.24	18.5	425	4.472	2.160	61.19	1.189		2.08	4.95
85		406.4	812.8	2.00	29.4	0.24	18.5	425	3.354	2.160	49.3	0.971		1.68	4.05
86		406.4	812.8	2.00	29.4	0.24	18.5	425	3.354	2.160	51.19	0.897		1.74	3.74
87		406.4	812.8	2.00	29.4	0.24	18.5	425	3.354	2.160	47.88	0.912		1.63	3.80

88		406.4	812.8	2.00	29.4	0.24	18.5	425	1.677	2.160	44.14	0.781		1.50	3.25
89		406.4	812.8	2.00	29.4	0.24	18.5	425	1.677	2.160	42.96	0.695		1.46	2.90
90		406.4	812.8	2.00	29.4	0.24	18.5	425	1.677	2.160	45.11	0.715		1.53	2.98
91		152.4	304.8	2.00	44.1	0.24	18.5	425	3.354	2.160	94.1	2.013		2.13	8.39
92		152.4	304.8	2.00	44.1	0.24	18.5	425	3.354	2.160	91.87	2.014		2.08	8.39
93		152.4	304.8	2.00	44.1	0.24	18.5	425	3.354	2.160	89.29	2.011		2.02	8.38
94		152.4	304.8	2.00	44.1	0.24	18.5	425	2.236	2.160	80.39	1.518		1.82	6.33
95		152.4	304.8	2.00	44.1	0.24	18.5	425	2.236	2.160	80.04	1.488		1.81	6.20
96		152.4	304.8	2.00	44.1	0.24	18.5	425	2.236	2.160	81.13	1.530		1.84	6.38
97		152.4	304.8	2.00	44.1	0.24	18.5	425	1.677	2.160	66.2	1.298		1.50	5.41
98		152.4	304.8	2.00	44.1	0.24	18.5	425	1.677	2.160	66.6	1.357		1.51	5.65
99		152.4	304.8	2.00	44.1	0.24	18.5	425	1.677	2.160	63.62	1.295		1.44	5.40
100		150	300	2.00	47.72	0.31	27	540	3.9	2.000	100.11	2.723	0.800	2.10	8.83

101	Almusallam (2007)	150	300	2.00	50.57	0.29	27	540	3.9	2.000	89.88	1.968	0.802		1.78	6.68
102		150	300	2.00	60.52	0.30	27	540	3.9	2.000	99.6	1.597	0.698		1.65	5.37
103		150	300	2.00	80.82	0.27	27	540	3.9	2.000	101.43	0.694	0.869		1.26	2.62
104		150	300	2.00	90.29	0.32	27	540	3.9	2.000	110	0.900	0.825		1.22	2.81
105	Bakhshi *et al.* (2007)	150	300	2.00	14.8	0.24	26.49	537	0.508	2.027	30	1.850			2.03	7.71
106		150	300	2.00	25.1	0.23	26.49	537	0.508	2.027	34.2	1.400			1.36	6.09
107		150	300	2.00	41.7	0.28	26.49	537	0.508	2.027	51.9	0.430			1.24	1.54
108		150	300	2.00	25.1	0.23	26.49	537	1.016	2.027	55.5	1.960			2.21	8.52
109		150	300	2.00	25.1	0.23	26.49	537	2.032	2.027	83.3	2.770			3.32	12.04
110	Wu *et al.* (2008)	150	300	2.00	23.1	0.27	73	1500	0.354	2.055	46.4	2.490			2.01	9.22
111		150	300	2.00	22.7	0.31	73	1500	0.354	2.055	45	2.360			1.98	7.61
112	Benzaid *et al.* (2009)	160	320	2.00	56.7	0.24	23.8	383	0.44	2.120	74	1.120	1.140	0.708	1.31	4.67
113		160	320	2.00	56.7	0.24	23.8	383	0.88	2.120	84	1.280	1.150	0.715	1.48	5.33

114		160	320	2.00	56.7	0.24	23.8	383	1.76	2.120	95.5	1.880	1.260	0.783	1.68	7.83
115	Comert *et al.* (2010)	150	300	2.00	9.3	0.20	65	1700	0.56	2.800	41	5.500			4.41	27.50
116		150	300	2.00	9.3	0.20	65	1700	0.56	2.800	43.2	5.100			4.65	25.50
117	Cui and Sheikh (2010)	152	305	2.01	47.76	0.22	26.84	620	1.25	2.310	59.1	1.350	2.020	0.874	1.24	6.08
118		152	305	2.01	47.76	0.22	26.84	620	1.25	2.310	59.8	1.150	2.143		1.25	5.18
119		152	305	2.01	47.76	0.22	26.84	620	2.5	2.310	88.9	2.210	2.032	0.880	1.86	9.95
120		152	305	2.01	47.76	0.22	26.84	620	2.5	2.310	88	2.210	2.114		1.84	9.95
121		152	305	2.01	47.76	0.22	26.84	620	3.75	2.310	113.2	2.850	2.112		2.37	12.84
122		152	305	2.01	47.76	0.22	26.84	620	3.75	2.310	112.5	2.800	2.110		2.36	12.61
123		152	305	2.01	47.76	0.22	26.84	620	1.25	2.310	63.4	1.150	2.179		1.33	5.18
124		152	305	2.01	47.76	0.22	26.84	620	1.25	2.310	62.4	1.350	2.116		1.31	6.08
125		152	305	2.01	47.76	0.22	26.84	620	2.5	2.310	89.7	2.140	2.074	0.898	1.88	9.64
126		152	305	2.01	47.76	0.22	26.84	620	2.5	2.310	88.3	2.050	2.049	0.887	1.85	9.23

127		152	305	2.01	47.76	0.22	26.84	620	3.75	2.310	108	2.620	1.893	0.819	2.26	11.80
128		152	305	2.01	79.9	0.24	26.84	620	3.75	2.310	120.8	1.260	2.008	0.869	1.51	5.23
129		152	305	2.01	79.9	0.24	26.84	620	3.75	2.310	126.1	1.180	1.916	0.829	1.58	4.90
130		152	305	2.01	110.6	0.26	26.84	620	5	2.310	174.6	0.950	1.398	0.605	1.58	3.63
131		152	305	2.01	110.6	0.26	26.84	620	5	2.310	172.9	1.280	1.538	0.666	1.56	4.89
132	Micelli and Modarelli (2013)	150	300	2.00	28.35	0.49	65	1700	0.23	2.600	53.27	1.900	4.980		1.88	3.88
133	Li *et al.* (2013)	150	300	2.00	31.72	0.30	69.45	1079	0.222	2.230	47.63	1.081	1.225	0.600	1.50	3.58
134	Lim and Ozbakkaloglu (2015)	63	126	2.00	51.6	0.25	95.3	3055	0.2	3.210	101.2	3.030	2.350	0.733	1.96	12.37
135		63	126	2.00	51.6	0.25	95.3	3055	0.4	3.210	153.7	4.310	2.190	0.683	2.98	17.59
136		63	126	2.00	51.6	0.25	95.3	3055	0.4	3.210	152.9	4.500	2.250	0.702	2.96	18.37
137		63	126	2.00	51.6	0.25	95.3	3055	0.4	3.210	174.7	5.180	2.440	0.761	3.39	21.14
138		63	126	2.00	128	0.32	95.3	3055	0.4	3.210	161.8	2.150	2.340	0.730	1.26	6.83
139		63	126	2.00	128	0.32	95.3	3055	0.4	3.210	166.3	2.250	2.360	0.736	1.30	7.14

140	Touhari and Mitiche -Kettab (2016)	160	320	2.00	26.2	0.27	26	325	1	1.900	38.3	1.500	1.480	0.780	1.46	5.62
141		160	320	2.00	26.2	0.27	26	325	1	1.900	34.6	1.260	1.450	0.760	1.32	4.72
142		160	320	2.00	26.2	0.27	26	325	1	1.900	38	1.390	1.500	0.790	1.45	5.21
143		160	320	2.00	26.2	0.27	26	325	2	1.900	49.4	2.410	1.450	0.760	1.89	9.03
144		160	320	2.00	26.2	0.27	26	325	2	1.900	52.5	2.550	1.500	0.790	2.00	9.55
145		160	320	2.00	26.2	0.27	26	325	3	1.900	62.8	3.390	1.400	0.740	2.40	12.70
146		160	320	2.00	26.2	0.27	26	325	3	1.900	56.4	2.980	1.300	0.680	2.15	11.16
147		160	320	2.00	26.2	0.27	26	325	3	1.900	54.7	2.890	1.290	0.680	2.09	10.82
148		160	320	2.00	42.6	0.29	26	325	1	1.900	56.5	1.100	1.430	0.750	1.33	3.81
149		160	320	2.00	42.6	0.29	26	325	1	1.900	55.5	1.040	1.400	0.730	1.30	3.60
150		160	320	2.00	42.6	0.29	26	325	1	1.900	59.8	1.230	1.630	0.860	1.40	4.26
151		160	320	2.00	42.6	0.29	26	325	2	1.900	68.5	1.650	1.460	0.770	1.61	5.71
152		160	320	2.00	42.6	0.29	26	325	2	1.900	70	1.720	1.470	0.770	1.64	5.95

153	160	320	2.00	42.6	0.29	26	325	2	1.900	71.7	1.810	1.500	0.790	1.68	6.26
154	160	320	2.00	42.6	0.29	26	325	3	1.900	75.5	2.100	1.400	0.730	1.77	7.27
155	160	320	2.00	42.6	0.29	26	325	3	1.900	78.8	2.490	1.500	0.780	1.85	8.62
156	160	320	2.00	42.6	0.29	26	325	3	1.900	77.5	2.240	1.430	0.750	1.82	7.75
157	160	320	2.00	61.7	0.31	26	325	1	1.900	77.5	1.110	1.600	0.840	1.26	3.57
158	160	320	2.00	61.7	0.31	26	325	2	1.900	80.8	1.490	1.500	0.790	1.31	4.79
159	160	320	2.00	61.7	0.31	26	325	2	1.900	76.7	1.350	1.420	0.740	1.24	4.34
160	160	320	2.00	61.7	0.31	26	325	2	1.900	78	1.440	1.480	0.780	1.26	4.63
161	160	320	2.00	61.7	0.31	26	325	3	1.900	90.1	1.710	1.350	0.710	1.46	5.50
162	160	320	2.00	61.7	0.31	26	325	3	1.900	92.1	1.880	1.420	0.740	1.49	6.05
163	160	320	2.00	61.7	0.31	26	325	3	1.900	94.4	1.950	1.500	0.790	1.53	6.27

*E_f: elasticity modulus is given in KN/mm-ply; *f_f: tensile strength is given in N/mm-ply; *t_f: thickness is given in ply.

3.5 Conclusion

This chapter has described the mechanics of FRP confinement of FRP confined concrete and examined some previous experimental studies investigating the axial behavior of FRP-confined concrete. An experimental database of GFRP-wrapped concrete columns with details collected from the available literature basing on selection criteria was also reported.

Chapter 4

Previous research on modeling the ultimate conditions FRP-confined concrete under compression

4.1 Introduction

This chapter provides a review of the current state of the art on modeling the ultimate conditions of axially loaded FRP-confined concrete. Previous design-oriented models for ultimate stress and ultimate axial strain of FRP-confined concrete are presented.

4.2 Modeling of FRP-confined concrete under axial compression

The constitutive relationship of confined concrete is a long historical topic in concrete research since reliable design and retrofit of concrete members necessitates clear understanding and accurate modeling of the stress-strain behavior (Hui, 2007).

After the immerge of the FRP composites in the civil engineering industry as promising materials for the structural strengthening of concrete structures, extensive analytical studies have been carried out to model the behavior of FRP-confined concrete under compression since the early models of steel-confined concrete were not applicable and provided inaccurate and often unconservative results for FRP-confined concrete (Mirmiran & Shahawy, 1996; Spoelstra & Monti, 1999).

A large number and a wide variety of models have been proposed for predicting the stress-strain relationship and the ultimate conditions (i.e., ultimate stress and ultimate strain) of FRP-confined concrete, ranged from diverse-use models which

devoted to any type of FRP (e.g., Lam & Teng, 2003; Ilki et al., 2004; Fahmy & Wu, 2010; Lim et al., 2016; Cascardi et al., 2017; Fallah Pour et al., 2018; Jiang et al., 2020) to models specific for one type of FRP (e.g., CFRP: Wu et al., 2006; Gandomi et al., 2010; Benzaid et al., 2010; AFRP: Lobo et al., 2018; GFRP: Huang et al., 2016).

The majority of models can be classified into two main categories: design-oriented models (DOMs) and analysis-oriented models (AOMs) (Lam & Teng, 2003). DOMs are closed-form equations calibrated empirically from experimental results on FRP-confined concrete. Its simplicity makes them convenient for design purposes (e.g., Karbhari & Gao, 1997; Lam & Teng, 2003; Berthet et al., 2006; Fahmy & Wu, 2010; Keshtegar et al., 2017; Raza et al., 2020). Whereas, AOMs are developed using an incremental-iterative procedure basing on the dilation relationship (i.e., lateral strain-to-axial strain relationship) of FRP-confined concrete, the stress-strain curves, and the peak stress and peak strain equations of actively confined concrete for different active confinement levels (Ozbakkaloglu & Lim, 2013) (e.g., Mirmiran & Shahawy, 1997; Spoelstra & Monti, 1999; Fam & Rizkalla, 2001; Marques et al., 2004; Jiang & Teng, 2007; Xiao et al., 2010; Pan et al., 2017; Yang & Feng, 2020).

In addition, other models in the literature were based on other approaches (e.g., plasticity approach: Karabinis & Rousakis, 2002; Eid & Paultre, 2007; Rousakis et al., 2008; Ozbakkaloglu et al., 2016; Farahmandpour et al., 2017; Damage-based model: Moran & Pantelides, 2005; finite element: Mirmiran et al., 2000; Yu et al., 2010; Youssf et al., 2014; Rasouli & Broujerdian, 2019).

In the following, a review of some existing design-oriented models of FRP-confined concrete circular columns is presented.

4.3 Review of some design-oriented ultimate stress and ultimate strain models for FRP-confined concrete

The ultimate conditions and stress-strain model of FRP-confined concrete are essential to structural design and prediction of the structural response of retrofitted structures. (Jiang et al., 2020). Conventionally, in modeling FRP-confined concrete, the ultimate stress and strain are firstly determined. The majority of the models have adopted the general form of the expressions proposed by Richart et al. (1929) for the ultimate strength and the ultimate strain (Eqs. (4.1) and (4.2)) for concrete confined by hydrostatic fluid pressure (Ozbakkaloglu & Lim, 2013).

$$\frac{f'_{cc}}{f'_{co}} = c_1 + k_1 \frac{f_l}{f'_{co}} \tag{4.1}$$

$$\frac{\varepsilon_{cc}}{\varepsilon_{co}} = c_2 + k_2 \frac{f_l}{f'_{co}} \tag{4.2}$$

Where,

f'_{cc} = compressive strength of FRP-confined concrete (MPa);

f'_{co} = compressive strength of unconfined concrete (MPa);

f_l = ultimate lateral confining pressure of FRP (MPa);

ε_{cc} = axial strain corresponding to (f'_{cc});

ε_{co} = axial strain corresponding to (f'_{co});

c_1, c_1 = calibration constants;

k_1, k_2 = strength and strain enhancement coefficients for FRP-confined concrete.

4.3.1 Fardis and Khalili (1982)

The of Fardis and Khalili (1982) was the first model developed for FRP-confined concrete. The authors studied the behavior of concrete-encased GFRP tubes. They performed axial compression tests on 46 concrete cylinders of (75 mm × 150 mm) (diameter × height) of 34.5 MPa and (100 mm × 200 mm) of 31 MPa encased in GFRP tubes made with 1 to 5 layers of GFRP. Based on their experimental results, they reported that both the model of Richart et al. (1929) (Eq. (4.3)) and the model proposed by Newman and Newman (1971) (Eq. (4.4)) can both provide satisfactory estimates for predicting the ultimate strength of FRP-confined concrete.

$$\frac{f'_{cc}}{f'_{co}} = 1 + 4.1\left(\frac{f_l}{f'_{co}}\right) \tag{4.3}$$

$$\frac{f'_{cc}}{f'_{co}} = 1 + 3.7\left(\frac{f_l}{f'_{co}}\right)^{0.86} \tag{4.4}$$

For the prediction of the ultimate axial strain, the authors proposed the expression shown in (Eq. (4.5)):

$$\varepsilon_{cc} = 0.002 + 0.001\left(\frac{E_f t_f}{d f'_{co}}\right) \tag{4.5}$$

Where,

E_f = FRP elasticity modulus (GPa);

t_f = thickness of the FRP (mm);

d = diameter of the concrete cylinder (mm).

The models were developed on limited test data of small-scale specimens of normal-strength concrete and used the steel-confined concrete models to predict the ultimate strength of FRP-confined concrete.

4.3.2 Karbhari and Gao (1997)

The strength and strain models suggested by Karbhari and Gao (1997) are among the early models developed for FRP-confined concrete cylinders under compression.

Karbhari and Gao (1997) proposed design strength and strain models (Eqs. (4.6) and (4.7)) based on their experimental data on concrete cylinders confined with a variety of FRP types (CFRP, GFRP, AFRP), orientations (0°, 45°, 90°) and thickness.

$$\frac{f'_{cc}}{f'_{co}} = 1 + 2.1\left(\frac{f_l}{f'_{co}}\right)^{0.87} \tag{4.6}$$

$$\frac{\varepsilon_{cc}}{\varepsilon_{co}} = 1 + \frac{0.01}{\varepsilon_{co}}\left(\frac{f_l}{f'_{co}}\right) \tag{4.7}$$

The model implemented a power function of the confinement ratio as the model of Newman and Newman (1971) for the strength model and a simple function for the strain model.

4.3.3 De Lorenzis and Tepfers (2003)

De lorenzis and Tepfers (2003) collected a database of 180 datasets of concrete cylinders confined with CFRP, GFRP, and AFRP wraps and tubes and performed a performance analysis of some strength and strain models of FRP-confined concrete. On the basis of the database and the performance of the existing models, the authors developed a new model for the prediction of the ultimate strain. The model predicts the strain ratio as a power function of the ultimate confinement pressure and the confinement stiffness (E_l) (Eqs. (4.8) and (4.9)).

For FRP-wrapped concrete:

$$\frac{\varepsilon_{cc}}{\varepsilon_{co}} = 1 + 26.2\left(\frac{f_l}{f'_{co}}\right)^{0.8} {E_l}^{-0.148} \tag{4.8}$$

For concrete-filled FRP tubes:

$$\frac{\varepsilon_{cc}}{\varepsilon_{co}} = 1 + 26.2\left(\frac{f_l}{f'_{co}}\right)^{0.68} {E_l}^{-0.127} \tag{4.9}$$

4.3.4 Lam and Teng (2003)

The strength and strain models proposed by Lam and Teng (2003) are expressed in Eqs. (4.10) and (4.11) respectively. The models were developed for confined concrete with FRP wraps based on 76 datasets of CFRP, GFRP, and AFRP confined concrete cylinders assembled from the literature. In these models, the authors considered the hoop rupture strain of the FRP ($\varepsilon_{h,rup}$) instead of the strain obtained from FRP tensile coupon tests. Based on the evaluation of the test

results, the authors suggested strain efficiency factors to account for the reduction of FRP rupture strain.

$$\frac{f'_{cc}}{f'_{co}} = 1 + 3.3\left(\frac{f_{l,rup}}{f'_{co}}\right) \tag{4.10}$$

$$\frac{\varepsilon_{cc}}{\varepsilon_{co}} = 1.75 + 12\left(\frac{f_{l,rup}}{f'_{co}}\right)\left(\frac{\varepsilon_{h,rup}}{\varepsilon_{co}}\right)^{0.45} \tag{4.11}$$

Where,

$f_{l,rup}$ = Lateral confining pressure at rupture of FRP (MPa).

$\varepsilon_{h,rup}$ = hoop rupture strain of FRP.

The models of Lam and Tang (2003) were adopted by the ACI 440.2R-08 design guideline for FRP-confined concrete with some modifications.

4.3.5 Wu et al. (2009)

Wu et al. (2009) investigated the properties of HSC circular columns confined by AFRP sheets under axial compression. They performed 60 experiments on high-strength concrete (HSC) circular columns confined with continuous and discontinuous AFRP wrapping. Based on their experimental results, the authors developed ultimate strength and ultimate strain models using regression analysis (Eqs. (4.12) and (4.13)). The models relate the ultimate strength and ultimate strain ratios with the confinement ratio with simple linear equations.

$$\frac{f'_{cc}}{f'_{co}} = 1 + 3.2\left(\frac{f_l}{f'_{co}}\right) \tag{4.12}$$

$$\frac{\varepsilon_{cc}}{\varepsilon_{co}} = 1 + 9.5\left(\frac{f_l}{f'_{co}}\right) \tag{4.13}$$

4.3.6 Benzaid et al. (2010)

Benzaid et al. (2010) conducted an experimental and analytical study on the axial behavior of plain-and RC cylinders strengthened with CFRP wraps. The authors tested 30 concrete cylinders of 26, 50, and 62 MPa compressive strength under axial compression wrapped with CFRP to investigate the effect of several parameters such as the number of CFRP layers, unconfined concrete strength on the effectiveness of CFRP strengthening of plain and RC cylinders. Basing on the regression of their experimental results, the authors proposed simple equations (Eqs. (4.14) and (4.15)) for the prediction of the ultimate strength and ultimate strain for FRP-confined concrete basing on the model of Richart et al. (1929).

$$\frac{f'_{cc}}{f'_{co}} = 1 + 1.6\left(\frac{f_l}{f'_{co}}\right) \tag{4.14}$$

$$\frac{\varepsilon_{cc}}{\varepsilon_{co}} = 2 + 5.55\left(\frac{f_l}{f'_{co}}\right) \tag{4.15}$$

4.3.7 Pellegrino and Modena (2010)

Pellegrino and Modena (2010) studied the effect of interaction between external FRP confinement and internal steel reinforcement on the stress-strain response of RC columns. The authors proposed analytical models (Eqs. (4.16) and (4.17)) to predict strength and ductility for FRP-confined axially loaded circular columns basing on a database of 219 axial compression tests of plain FRP-confined circular concrete columns.

$$\frac{f'_{cc}}{f'_{co}} = 1 + 3.55\left(\frac{f_{l,rup}}{f'_{co}}\right)^{0.85} \tag{4.16}$$

$$\frac{\varepsilon_{cc}}{\varepsilon_{co}} = 2 + 23\left(\frac{f_{l,rup}}{f'_{co}}\right) \tag{4.17}$$

4.3.8 Rousakis et al. (2012)

Rousakis et al. (2012) conducted an analytical study to evaluate 20 existing models for predicting the compressive strength of FRP-confined concrete basing on a database of 471 experiments on cylindrical concrete columns confined with CFRP, GFRP, and AFRP wraps and tubes. On the basis of the collected data, the authors proposed a strength model for FRP-wrapped and tube-encased concrete.

For FRP-wrapped concrete:

$$\frac{f'_{cc}}{f'_{co}} = 1 + \left(\frac{\rho_f E_f}{f'_{co}}\right)\left(-0.336E_f \times 10^{-7} + 0.0223\right) \tag{4.18}$$

For concrete-filled FRP tubes:

$$\frac{f'_{cc}}{f'_{co}} = 1 + \left(\frac{\rho_f E_f}{f'_{co}}\right)\left(-0.23E_f \times 10^{-7} + 0.0195\right) \tag{4.19}$$

Where,

ρ_f = volumetric ratio of the FRP.

4.3.9 Elsanadedy et al. (2012)

Elsanadedy et al. (2012) conducted an analytical study on FRP-confined concrete models. The authors developed regression models (Eqs. (4.20) and (4.21)) and neural network models to predict the compressive strength and the ultimate strain of FRP-confined concrete based on a database of compression test results of 272 cylindrical specimens of normal and high strength concrete (up to 169 MPa) confined with varying types of FRP (CFRP, GFRP, AFRP). Various parameters found affecting the compressive strength and the ultimate strain, such as the volumetric ratio of the FRP, the (E_f/f'_{co}) ratio, and the (f_f/f'_{co}) ratio, were considered.

$$\frac{f'_{cc}}{f'_{co}} = 1 + 0.038{\rho_f}^{1.32}\sqrt{\frac{f_f}{f'_{co}}}\left(\frac{E_f}{f'_{co}}\right)^{0.8}\left(\frac{42}{f'_{co}}\right)^{0.6} \tag{4.20}$$

$$\frac{\varepsilon_{cc}}{\varepsilon_{co}} = \frac{0.002}{\varepsilon_{co}} + 0.035\left(\frac{{\rho_f}^{0.7}}{\varepsilon_{co}}\right)\left(\frac{f_f}{f'_{co}}\right)\left(\frac{E_f}{f'_{co}}\right)^{0.02}\left(\frac{42}{f'_{co}}\right)^{1.3} \tag{4.21}$$

4.3.10 Ozbakkaloglu and Lim (2013)

Ozbakkloglu and Lim (2013) assembled a database of axial compression tests on 832 circular concrete specimens confined with CFRP, GFRP, and AFRP wraps and tubes. The authors examined the test results to investigate the influence of parameters on the behavior of FRP-confined concrete. Basing on this investigation, new design-oriented models developed to quantify the compressive strength and the ultimate axial strain of FRP-confined concrete were developed by the authors (Eqs. (4.22) and (4.23)). The results showed improved predictions of the proposed models compared to the existing models. The models were applicable to specimens that achieve strength enhancement after the first peak stress (strain-hardening response) (Eq. (4.30)).

$$f'_{cc} = c_1 f'_{co} + k_1\left(f_{l,rup} - f_{lo}\right) \tag{4.22}$$

$$\varepsilon_{cc} = c_2\varepsilon_{co} + k_2\left(\frac{E_l}{f'_{co}}\right)^{0.9}{\varepsilon_{h,rup}}^{1.35} \tag{4.23}$$

Where,

$$c_1 = 1 + 0.0058\frac{E_l}{f'_{co}} \tag{4.24}$$

$$c_2 = 2 - \frac{f'_{co} - 20}{100} \geq 1 \tag{4.25}$$

$$k_1 = 3.2 \tag{4.26}$$

$$k_2 = 0.27 \tag{4.27}$$

$$f_{lo} = \left(0.43E_l + 0.009\frac{{E_l}^2}{f'_{co}}\right)\varepsilon_{co} \tag{4.28}$$

$$\varepsilon_{co} = (-0.067{f'_{co}}^2 + 29.9f'_{co} + 1053) \times 10^{-6} \tag{4.29}$$

$$E_l \geq {f'_{co}}^{1.65} \tag{4.30}$$

Equations ((4.22)-(4.29)) can be simplified as:

$$\frac{f'_{cc}}{f'_{co}} = 1 + 3.2\left(\frac{f_{l,rup}}{f'_{co}}\right) + (0.0058 - 1.376\varepsilon_{co})\left(\frac{E_l}{f'_{co}}\right) - (0.0288\varepsilon_{co})\left(\frac{E_l}{f'_{co}}\right)^2 \tag{4.31}$$

$$\frac{\varepsilon_{cc}}{\varepsilon_{co}} = 2.2 - \frac{f'_{co}}{100} + 0.27\left(\frac{E_l}{f'_{co}}\right)^{0.9}\frac{{\varepsilon_{h,rup}}^{1.35}}{\varepsilon_{co}} \tag{4.32}$$

4.3.11 Lim and Ozbakkaloglu (2014)

Lim and Ozbakkaloglu (2014) investigated the influence of the shape factors on the compressive behavior of FRP-confined concrete in square and rectangular sections. The authors collected a database of 1547 circular, square, and rectangular concrete specimens with unconfined concrete strengths ranging from 6.2 to 169.7 MPa. Existing theoretical models were reviewed and assessed to predict the ultimate conditions of the FRP-confined concrete in square and rectangular sections. Based on the collected database, the authors developed a unified model for FRP-confined concrete in circular, square, and rectangular sections with unconfined concrete strengths up to 120 MPa. For circular sections, the models are expressed in Eqs. (4.33) and (4.34):

$$\frac{f'_{cc}}{f'_{co}} = 1 + 4.1\left(E_l - 73.7e^{0.027f'_{co}}\right)\frac{\varepsilon_{h,rup}}{f'_{co}} \tag{4.33}$$

$$\frac{\varepsilon_{cc}}{\varepsilon_{co}} = 2.2 - \frac{f'_{co}}{100} + 0.27\left(\frac{E_l}{f'_{co}}\right)^{0.9}\frac{{\varepsilon_{h,rup}}^{1.35}}{\varepsilon_{co}} \tag{4.34}$$

Where,

$$E_l - 73.7e^{0.027f'_{co}} \geq 0 \tag{4.35}$$

$$2.2 - \frac{f'_{co}}{100} \geq 1 \tag{4.36}$$

$$\varepsilon_{co} = \left(-0.067{f'_{co}}^2 + 29.9f'_{co} + 1053\right) \times 10^{-6} \tag{4.37}$$

4.3.12 Al abadi et al. (2016)

In this research, the authors aimed to investigate the influence of the confinement parameters, including the concrete strength and the confining pressure, on the strength enhancement of FRP-confined concrete specimens. A database of 927 compression test results on FRP-confined concrete cylinders was used in the performance evaluation of 15 existing strength models. Basing on the two-dimensional Gauss function and using nonlinear surface fit process, a new strength enhancement model was proposed (Eq. (4.38)).

$$\frac{f'_{cc}}{f'_{co}} = 1.06 + 5.54e^{-0.00042\left(f'_{co}+25.6\right)^2 - 0.0083(f_l - 18.67)^2} \tag{4.38}$$

The results showed that predictions from the proposed model provided better estimations in comparison with the existing evaluated models.

4.3.13 Cascardi et al. (2017)

Cascardi et al. (2017) aimed to develop a new model to predict the strength of FRP-confined concrete basing on artificial neural networks (AAN) approach. The authors used an extensive database of 465 compression tests on circular concrete specimens confined with FRP to define the variables of the model. The accuracy of the model was tested versus the experimental results and with some existing models and international codes such as ACI 440.2R-02, CSA-S806, CNR-DT 200

R1/2013, TR 55 (2012), and its validity is verified through a parametric study. The model adopted the general equation of Richart et al. (1929) (Eq. (4.39)).

$$\frac{f'_{cc}}{f'_{co}} = 1 + k\left(\frac{f_l^{0.5}}{f'_{co}}\right) \tag{4.39}$$

Using (ANN), the authors determined the formula of the coefficient (k) corresponding to minimum errors between the theoretical and the experimental values as the following (Eqs. (4.40)-(4.48)):

$$k = \frac{4.58}{1 + e^{-y_6}} \tag{4.40}$$

Where,

$$y_6 = 0.73y_5 + 0.72y_5y_3 - 0.87{y_5}^2 + 0.16 \tag{4.41}$$

$$y_5 = 0.69y_4 - 0.18{y_4}^2 \tag{4.42}$$

$$y_4 = -0.60\alpha + 1.66\beta - 0.20\alpha\beta + 0.88\alpha^2 - 2.12 \tag{4.43}$$

$$y_3 = 0.88y_1y_2 + 0.33{y_2}^2 - 1.10{y_1}^2 \tag{4.44}$$

$$y_2 = 0.19\alpha - 1.58 \tag{4.45}$$

$$y_1 = 0.48\alpha + 1.05\beta - 1.88 \tag{4.46}$$

$$\alpha = \frac{f'_{co}}{E_f} \times 1000 \tag{4.47}$$

$$\beta = \frac{t_f}{d} \tag{4.48}$$

The results showed that the proposed model can be used for an accurate prediction of the compressive strength of FRP-confined concrete.

4.3.14 Raza et al. (2020)

Raza et al. (2020) conducted an analytical study on the ultimate axial strength of FRP-confined concrete. The authors evaluated 12 previous strength models predicting the compressive strength of FRP-confined concrete on the basis of a large database of 520 cylindrical concrete specimens of unconfined concrete strength up to 188 MPa collected from the literature. The strength models were assessed over this database using statistical indices such as coefficient of determination (R^2) and root mean square error (RMSE). Using curve fitting method in MATLAB and basing the experimental database, the authors developed a new strength model for FRP-confined concrete (Eq. (4.49)).

$$\frac{f'_{cc}}{f'_{co}} = 1 + 3\left(\frac{f_l}{f'_{co}}\right)^{\frac{3}{4}} \tag{4.49}$$

The authors validated the proposed model by performing an experimental work of 6 CFRP-confined concrete cylinders under compression, as well as a nonlinear finite element analysis (NLFEA) using ABAQUS software.

4.3.15 Arabshahi et al. (2020)

In this study, the authors conducted analytical research on the behavior of concrete specimens confined with AFRP. A new series of equations, including maximum confined stress (Eq. (4.50)) and strain (Eqs. (4.51) and (4.52)) as well as the stress-strain relationship, for fully and partially AFRP-confined circular and square concrete specimens were proposed. The authors collected an experimental database of 269 test results using a set of selection criteria to derive the models basing on multi-expression programming (MEP).

For fully FRP-confined circular concrete specimens:

$$\frac{f'_{cc}}{f'_{co}} = 1 + \frac{39}{\ln^2(f'_{co})}\left(\frac{f_l}{f'_{co}}\right) \tag{4.50}$$

$$\frac{\varepsilon_{cc}}{\varepsilon_{co}} = 1 + \frac{1}{\varepsilon_{co}} + \left(\frac{f_l \varepsilon_{h,rup}}{f_l \varepsilon_{h,rup} + f'_{co}}\right)^{0.77} \qquad with \quad (\varepsilon_{h,rup}) \tag{4.51}$$

$$\frac{\varepsilon_{cc}}{\varepsilon_{co}} = \frac{0.21 f_l^{0.68}}{(f'_{co} - \ln(\varepsilon_{co}))\varepsilon_{co}} \qquad without \quad (\varepsilon_{h,rup}) \tag{4.52}$$

Based on the experimental database, the models were evaluated compared to other available models and found to provide accurate predictions for AFRP-confined concrete.

In addition, the authors developed a new equation for the lateral hoop rupture strain of AFRP wraps and a confinement threshold equation to specify sufficiently AFRP-confined concrete.

4.3.16 Ahmad et al. (2020)

Ahmad et al. (2020) conducted an analytical study to investigate the predictions the ultimate conditions of FRP-confined concrete cylinders. Twelve previously proposed strength and strain models were evaluated based on a database of 708 specimens for strength and 572 specimens for strain of unconfined concrete ranging from 13 to 188 MPa collected from previous experiments. Based on the database, the authors proposed new models based on (ANN) and regression analysis technique for the prediction of the ultimate strength and strain of FRP-confined concrete. The accuracy of the proposed models was assessed using statistical indices such as the correlation coefficient (R) and mean square error (MSE) and compared to the previous models. The strength regression model (Eq. (4.53)) was based on the equation of Richart et al. (1929), and the strain model (Eq. (4.54)) was based on the general form of the model of Lam and Teng (2003).

$$\frac{f'_{cc}}{f'_{co}} = 1 + 3.1\left(\frac{f_{l,rup}}{f'_{co}}\right)^{0.83} \tag{4.53}$$

$$\frac{\varepsilon_{cc}}{\varepsilon_{co}} = 1.85 + 7.46{\rho_K}^{0.71}{\rho_\varepsilon}^{1.171} \tag{4.54}$$

The results showed that the performance of the proposed models was superior to any one of the examined models.

4.4 Conclusion

This chapter has provided a brief state of the art on modeling the axial ultimate conditions of FRP-confined concrete, pointing out some previous ultimate stress and ultimate strain design-oriented models available in the literature. The early models were developed basing on steel confinement models and proved to be inappropriate for FRP-confined concrete. Subsequently, models devoted to FRP confinement with various forms and parameters based on databases of different sizes were developed, where the majority were based on the general form of the equation of Richart et al. (1929).

Chapter 5

Evaluation and proposition of ultimate condition models for axially loaded GFRP-wrapped concrete

5.1 Introduction

In this chapter, a comprehensive review and performance assessment of 20 old and recent and existing FRP-confined concrete models predicting the ultimate stress and strain of axially loaded FRP-confined concrete with strain-hardening behavior are provided. The performance of the selected models is assessed using the collected database of GFRP wrapped concrete cylinders reported in Chapter 3.

In the final part of this chapter, design-oriented equations to determine the compressive strength and its corresponding strain for GFRP-wrapped concrete are proposed. The proposed models are verified with the experimental data and compared with the selected previous models.

5.2 Existing strength and strain models

Central to any stress-strain curve of FRP-confined concrete is its end point, which is essential for the design and use of FRP-confined concrete members in practice (Keshtegar et al., 2017). This point characterizes the rupture of the FRP confinement materials and corresponds in the case of sufficiently confined concrete (i.e., strain hardening behavior) to the ultimate strain and the ultimate stress of the FRP-confined concrete (Lam & Teng, 2003).

The majority of the models predicting the ultimate stress and ultimate strain of FRP-confined concrete are empirical equations categorized as design-oriented models (DOMs). These models are derived from experimental results (either small

or large experimental data) and influenced by the parameters ranges and the number of the datasets used in their calibration.

In the following, 20 of old and recent existing DOMs developed to predict the ultimate strength and ultimate axial strain of FRP-confined concrete circular columns exhibiting strain-hardening behavior are reviewed and evaluated based on the experimental database reported in Chapter 3, which includes 163 test results of GFRP-wrapped normal and high-strength concrete cylindrical specimens. The selected models are summarized in Table 5.1.

Table 5.1 Selected design-oriented strength and strain models

No.	Source	Strength equation	Strain equation	Type of confinement
1	Saadatmanesh et al. (1994)	$\frac{f'_{cc}}{f'_{co}} = -1.254 - 2\left(\frac{f_l}{f'_{co}}\right) + 2.254\sqrt{1 + 7.94\frac{f_l}{f'_{co}}}$	$\frac{\varepsilon_{cc}}{\varepsilon_{co}} = 1 + 5\left(\frac{f'_{cc}}{f'_{co}} - 1\right)$	GFRP and CFRP-confined concrete
2	Karbhari and Gao (1997)	$\frac{f'_{cc}}{f'_{co}} = 1 + 2.1\left(\frac{f_l}{f'_{co}}\right)^{0.87}$	$\frac{\varepsilon_{cc}}{\varepsilon_{co}} = 1 + \frac{0.01}{\varepsilon_{co}}\left(\frac{f_l}{f'_{co}}\right)$	FRP-wrapped concrete
3	Toutanji (1999)	$\frac{f'_{cc}}{f'_{co}} = 1 + 3.5\left(\frac{f_l}{f'_{co}}\right)^{0.85}$	$\frac{\varepsilon_{cc}}{\varepsilon_{co}} = 1 + (310.57\varepsilon_f + 1.9)\left(\frac{f'_{cc}}{f'_{co}} - 1\right)$	FRP-wrapped concrete
4	Moran and Pantelides (2002)	$\frac{f'_{cc}}{f'_{co}} = 1 + 4.14\left(\frac{f_l}{f'_{co}}\right)$	$\frac{\varepsilon_{cc}}{\varepsilon_{co}} = 1 + \frac{(f_l/f'_{co})}{9.27 \times 10^{-3}\left(\frac{E_l}{f'_{co}}\right)^{\frac{1}{3}}}$	FRP-confined concrete
5	Xiao and Wu (2003)	$\frac{f'_{cc}}{f'_{co}} = 1 + \left(4.1 - 0.45\left(\frac{E_l}{f'^{2}_{co}}\right)^{-1.4}\right)\left(\frac{f_{l,rup}}{f'_{co}}\right)$	$\frac{\varepsilon_{cc}}{\varepsilon_{co}} = \frac{\varepsilon_{h,rup} - 0.00047}{10\varepsilon_{co}} \times \left(\frac{E_l}{f'_{co}}\right)^{0.9}$	CFRP and GFRP-confined concrete
6	Bisby et al. (2005)	$\frac{f'_{cc}}{f'_{co}} = 1 + 3.587\left(\frac{f_l^{0.84}}{f'_{co}}\right)$	$\frac{\varepsilon_{cc}}{\varepsilon_{co}} = 1 + \frac{0.0137}{\varepsilon_{co}}\left(\frac{f_l}{f'_{co}}\right)$	CFRP, GFRP and AFRP-confined concrete
7	Matthys et al. (2005)	$\frac{f'_{cc}}{f'_{co}} = 1 + 3.5\left(\frac{f_{l,rup}}{f'_{co}}\right)^{0.85}$	$\frac{\varepsilon_{cc}}{\varepsilon_{co}} = 1 + (310.57\varepsilon_f + 1.9)\left(\frac{f'_{cc}}{f'_{co}} - 1\right)$	FRP-wrapped concrete

8	Berthet et al. (2006)	$\begin{cases} \frac{f'_{cc}}{f'_{co}} = 1 + 3.45\left(\frac{f_{l,rup}}{f'_{co}}\right) \\ for\ \ 20\ MPa \le f'_{co} \le 50\ MPa \\ \frac{f'_{cc}}{f'_{co}} = 1 + 9.5\left(\frac{f_{l,rup}}{f'^{1.25}_{co}}\right) \\ for\ \ 50\ MPa \le f'_{co} \le 200\ MPa \end{cases}$	$\frac{\varepsilon_{cc}}{\varepsilon_{co}} = 1 + \frac{\varepsilon_{h,rup} - \nu_c\varepsilon_{co}}{\frac{1}{\sqrt{2}}\varepsilon_{co}} \times \left(\frac{E_l}{f'^{2}_{co}}\right)^{\frac{2}{3}}$	CFRP and GFRP-wrapped concrete
9	Wu et al. (2006)	$\frac{f'_{cc}}{f'_{co}} = 0.408 + 6.157\left(\frac{f_l}{f'_{co}}\right) - 3.25\left(\frac{f_l}{f'_{co}}\right)^2$	$\frac{\varepsilon_{cc}}{\varepsilon_{co}} = \frac{\varepsilon_f}{0.56\varepsilon_{co}}\left(\frac{f_l}{f'_{co}}\right)^{0.66}$	FRP-wrapped concrete
10	Ciupala et al. (2007)	$\frac{f'_{cc}}{f'_{co}} = 1 + 3.4\left(\frac{f_l}{f'_{co}}\right)^{0.8}$	$\frac{\varepsilon_{cc}}{\varepsilon_{co}} = 1 + 6.7\left(\frac{f'_{cc}}{f'_{co}} - 1\right)^{\frac{2}{3}}$	CFRP and GFRP-confined concrete
11	Youssef et al. (2007)	$\frac{f'_{cc}}{f'_{co}} = 1 + 2.25\left(\frac{f_l}{f'_{co}}\right)^{1.25}$	$\frac{\varepsilon_{cc}}{\varepsilon_{co}} = \frac{0.003368}{\varepsilon_{co}} + \frac{0.2590}{\varepsilon_{co}}\left(\frac{f_f}{E_f}\right)^{\frac{1}{2}}\left(\frac{f_l}{f'_{co}}\right)$	CFRP and GFRP-confined concrete
12	Fahmy and Wu (2010)	$\begin{cases} \frac{f'_{cc}}{f'_{co}} = 1 + 4.5\left(\frac{f_l^{0.7}}{f'_{co}}\right) \\ \quad for\ f'_{co} \le 40MPa \\ \frac{f'_{cc}}{f'_{co}} = 1 + 3.75\left(\frac{f_l^{0.7}}{f'_{co}}\right) \\ \quad for\ f'_{co} > 40MPa \end{cases}$	$\frac{\varepsilon_{cc}}{\varepsilon_{co}} = \frac{f'_{cc} - f'_{co}}{E_2\varepsilon_{co}}$ $E_2 = m_2\left(245.61 f'^{m_1}_{co} + 0.6728E_l\right)$ $\begin{cases} m_1 = 0.5,\ \ m_2 = 0.83, & f'_{co} \le 40MPa \\ m_1 = 0.2,\ \ m_2 = 1.73, & f'_{co} > 40MPa \end{cases}$	FRP-wrapped concrete
13	Pham and Hadi (2014)	$\frac{f'_{cc}}{f'_{co}} = 0.91 + 1.88\left(\frac{f_{l,rup}}{f'_{co}}\right) + 7.6\left(\frac{t_f}{df'_{co}}\right)$	$\frac{\varepsilon_{cc}}{\varepsilon_{co}} = 1 + \frac{13.24\left(t_f f_f \frac{\varepsilon_{h,rup}}{\varepsilon_{co}}\right)}{\left(df'_{co} + 3.3 f_f t_f\right)}$	FRP-wrapped concrete
14	Sadeghian and Fam (2015)	$\frac{f'_{cc}}{f'_{co}} = 1 + (2.77\rho_K^{0.77} - 0.07)\rho_\varepsilon^{0.91}$	$\frac{\varepsilon_{cc}}{\varepsilon_{co}} = 1.5 + 6.78\rho_K^{0.63}\rho_\varepsilon^{1.08}$	FRP-confined concrete
15	Touhari and Mitiche-Kettab (2016)	$\frac{f'_{cc}}{f'_{co}} = 1 + 1.85\left(\frac{f_l}{f'_{co}}\right)$	$\frac{\varepsilon_{cc}}{\varepsilon_{co}} = 1.45 + 15\left(\frac{f_l}{f'_{co}}\right)$	GFRP-wrapped concrete
16	Huang et al. (2016)	$\frac{f'_{cc}}{f'_{co}} = 1 + 1.69\left(\frac{f_{l,rup}}{f'_{co}}\right)^{0.63}$	$\frac{\varepsilon_{cc}}{\varepsilon_{co}} = 1 + 13.2\left(\frac{f_{l,rup}}{f'_{co}}\right)^{0.6}$	GFRP-wrapped concrete and concrete-filled GFRP tube
17	Baji et al. (2016)	$\frac{f'_{cc}}{f'_{co}} = 1 + 3.29\left(\frac{f_{l,rup}}{f'_{co}}\right)$	$\frac{\varepsilon_{cc}}{\varepsilon_{co}} = 1 + 0.54\left[\left(\frac{1}{5.1}\right)\left(\frac{\varepsilon_{h,rup}}{\varepsilon_{co}}\right)\left(\frac{E_l}{f'_{co}}\right)^{0.56}\right]$	FRP-wrapped concrete

18	Lim et al. (2016)	$\frac{f'_{cc}}{f'_{co}} = \frac{1 + E_l\varepsilon_{h,rup} + {E_l}^{1.5}{\varepsilon_{h,rup}}^2 + a}{f'_{co}}$ $a = \sqrt{E_l - \frac{f'_{co}}{\sqrt{\varepsilon_{h,rup}}}} \geq 0$	$\frac{\varepsilon_{cc}}{\varepsilon_{co}} = \left(1 + \frac{b}{\varepsilon_{co}}\right)\left({\varepsilon_{co}}^c + \frac{E_l}{f'_{co}}(2\varepsilon_{co} + b)\right)$ $b = \varepsilon_{h,rup} - {\varepsilon_{h,rup}}^{\frac{E_l}{f'_{co}}}$ $c = {f'_{co}}(\varepsilon_{co} + \varepsilon_{h,rup} + e^{\varepsilon_{h,rup}})/E_l$ $\varepsilon_{h,rup} = \varepsilon_f / {f'_{co}}^{0.125}$ $\varepsilon_{co} = ({f'_{co}}^{0.225}/1000)k_s k_a$ $k_s = (152/d)^{0.1};\ k_a = (2d/h)^{0.13}$	FRP-wrapped concrete
19	Keshtegar et al. (2017)	$\frac{f'_{cc}}{f'_{co}} = 1 + (0.85 + 1.40\rho_\varepsilon){\rho_a}^{0.82}{\rho_E}^{0.91}$ $\rho_a = \frac{t_f}{d}\ ;\ \rho_E = \frac{2E_f}{f'_{co}/\varepsilon_{co}}$	$\frac{\varepsilon_{cc}}{\varepsilon_{co}} = 1.5 + (-0.09 + 3.27{\rho_a}^{0.4}){\rho_E}^{0.6}{\rho_\varepsilon}^{1.04}$ $\rho_a = \frac{t_f}{d}\ ;\ \rho_E = \frac{2E_f}{f'_{co}/\varepsilon_{co}}$	FRP-wrapped concrete
20	Fallah Pour et al. (2018)	$\frac{f'_{cc}}{f'_{co}} = 1 + \frac{(2.5 - 0.01f'_{co})E_l\varepsilon_f}{f'_{co}}$	$\frac{\varepsilon_{cc}}{\varepsilon_{co}} = 1.5 + (0.3 - 0.001f'_{co})\left(\frac{E_l}{f'_{co}}\right)^{0.75}\frac{{\varepsilon_f}^{1.35}}{\varepsilon_{co}}$	FRP-confined concrete

5.3 Study of the performance of the strength and strain models

The performance of the existing strength and strain models is evaluated by comparing their predictions with the experimental data reported in Chapter 3. Each model was assessed against all the test results included in the database unless specific limitations or specific equations for certain parameters are specified by the mode, such as unconfined concrete strength (f'_{co}) and strain at unconfined concrete strength (ε_{co}).

5.3.1 Statistical evaluation

The performance of the models has been evaluated statistically using three statistical indices, namely the coefficient of the determination (R^2), the root mean square error (RMSE), and the average absolute error (AAE) expressed in Eqs. ((5.1)-(5.3)) respectively.

$$R^2 = \left(\frac{\sum(x - \overline{x})(y - \overline{y})}{\sqrt{\sum(x - \overline{x})^2 \sum(y - \overline{y})^2}}\right)^2 \tag{5.1}$$

$$RMSE = \sqrt{\frac{\sum(x - y)^2}{n}} \tag{5.2}$$

$$AAE = \frac{\sum\left|\frac{x - y}{y}\right|}{n} \tag{5.3}$$

Where,

x = the experimental value;

y = the predicted value corresponding to x;

$\bar{x}$ = the average of the experimental values;

$\bar{y}$ = the average of the predicted values;

n = the total number of the datasets.

(R^2) is used to determine how the variations in the actual values can be described by the variations in the values predicted by the model. In other words, it shows how much the actual values are linearly correlated to the predicted values. (R^2) ranges from 0 (no correlation) to 1 (perfect correlation), where a higher value of (R^2) indicates a better prediction. However, a perfect correlation ($R^2 = 1$) does not necessarily imply a perfect prediction; it simply indicates the presence of a perfect linear correlation between the predicted and the actual values (Sadeghian & Fam, 2015), as demonstrated in Fig. 5.1. In this figure, although the two models (A) and (B) have the same ($R^2 = 0.97$), model (B) provides deviated predictions from the perfect line. Hence, the evaluation should not rely only on the (R^2).

To assess the overall accuracy of the models and indicate how close are the predicted values to the actual values, both the root mean square error (RMSE) and the average absolute error (AAE) are used in this study. Lower values of (RMSE) and (AAE) indicate an accurate fit (Fig. 5.1).

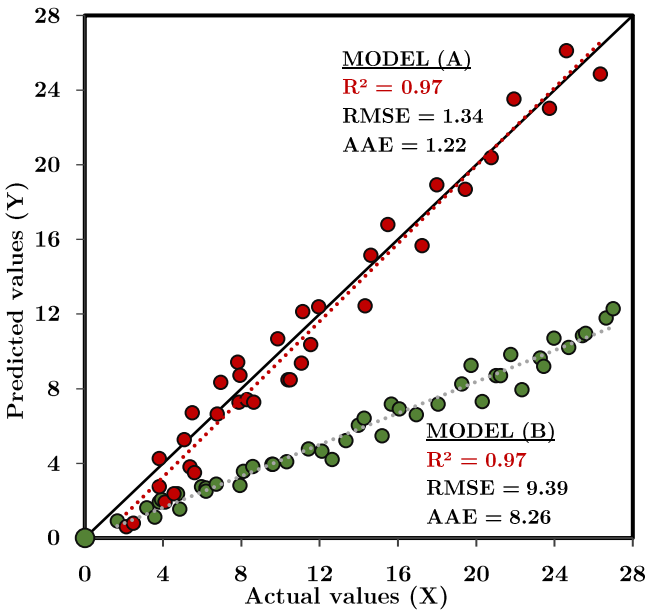

Figure 5.1 R^2, RMSE, and AAE for two cases of data

5.3.2 Strain efficiency factor

Since the values of the strain efficiency factor (k_ε) required by the majority of the reported models for the calculation of the rupture confinement stress ($f_{l,rup}$) and the strain ratio (ρ_ε) are often not provided in the available test results, prediction of the omitted values is performed in this study.

Analyzing the experimental results of (k_ε), it is observed that (k_ε) depends on the properties of the GFRP and the unconfined concrete strength. It was found that an increase in (f_f) results in a decrease in the strain reduction factor, whereas an increase in (f'_{co}) results in a decrease in (k_ε). Other studies such as that of Ozbakkaloglu and Akin (2012) for CFRP and AFRP-confined concrete, and that of Lim and Ozbakkaloglu (2014) for FRP-wrapped and tube-encased concrete showed that an increase in (f'_{co}) results in a decrease of (k_ε), which is the opposite of the observation reported above in this study. Using regression analysis, the influence of these two parameters resulted in the expression shown in Eq. (5.4) for the calculation of the strain reduction factor.

$$k_\varepsilon = 0.645 + 1.49\, f'_{co} \times 10^{-3} + 15.5/f_f - 15.13\, {f_f}^2 \times 10^{-8} \qquad (5.4)$$

where (f'_{co}) and (f_f) are in MPa.

The statistical evaluation shown in Fig. 5.2 demonstrates a strong correlation (R^2 = 0.85) with the experimental results and very low errors (RMSE = 0.05) and (AAE = 0.04) for this equation, which indicates an accurate fit between experimental and predicted values.

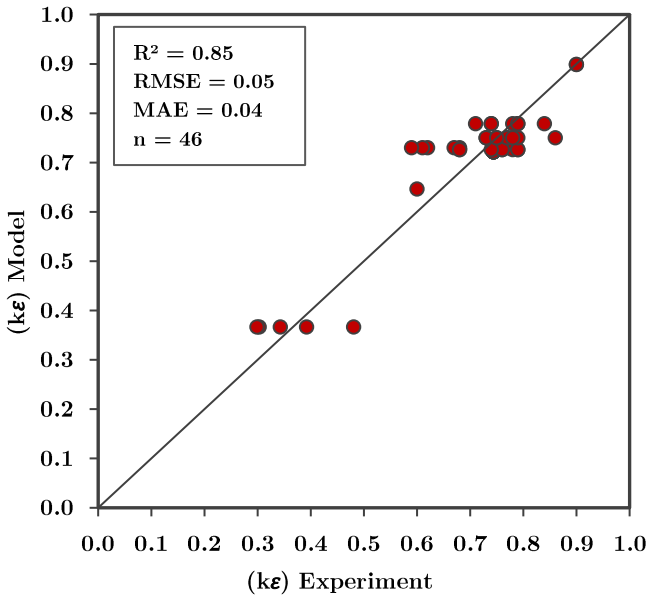

Figure 5.2 Performance of the proposed equation for the strain efficiency factor

5.3.3 Performance assessment of the models

The strength and strain models reported in Table 5.1 are examined basing on the collected database using the statistical indices described above. For each model, the obtained results are graphically represented by plotting the experimental versus the predicted values, where the 45° line corresponds to the perfect agreement between the predictions and experimental results. The points falling below the 45° line indicate conservative predictions, whereas points falling above indicate unconservative predictions (i.e., overestimation of the experimental results). A summary of the obtained results is reported in Table 5.2.

5.3.3.1 Saadatmanesh et al. (1994)

Saadatmanesh et al. (1994) adopted the model of Mander et al. (1988) developed for steel-confined concrete by replacing the confinement pressure of the steel with the ultimate pressure provided by the FRP (Eq. (5.5)). The model suggested a nonlinear relationship between the strength of the concrete and the confinement pressure.

$$\frac{f'_{cc}}{f'_{co}} = -1.254 - 2\left(\frac{f_l}{f'_{co}}\right) + 2.254\sqrt{1 + 7.94\left(\frac{f_l}{f'_{co}}\right)} \tag{5.5}$$

The authors expressed the ultimate strain with a linear relationship of the confinement effectiveness (Eq. (5.6)).

$$\frac{\varepsilon_{cc}}{\varepsilon_{co}} = 1 + 5\left(\frac{f'_{cc}}{f'_{co}} - 1\right) \tag{5.6}$$

Where,

f_l = the maximum confining pressure of the FRP;

ε_{co} = strain at unconfined concrete strength: $\varepsilon_{co} = 0.002$.

The performance of the strength model is shown in Fig. 5.2 with $R^2 = 0.52$, RMSE= 0.65, and AAE = 0.55. The indices and the figure demonstrate that the model overestimates (f'_{cc}) of most of the data points. On the other side, the strain model showed very poor performance with a low correlation $R^2 = 0.10$, and high errors (RMSE = 4.69, AAE = 3.33), and scattered data (Fig. 5.3).

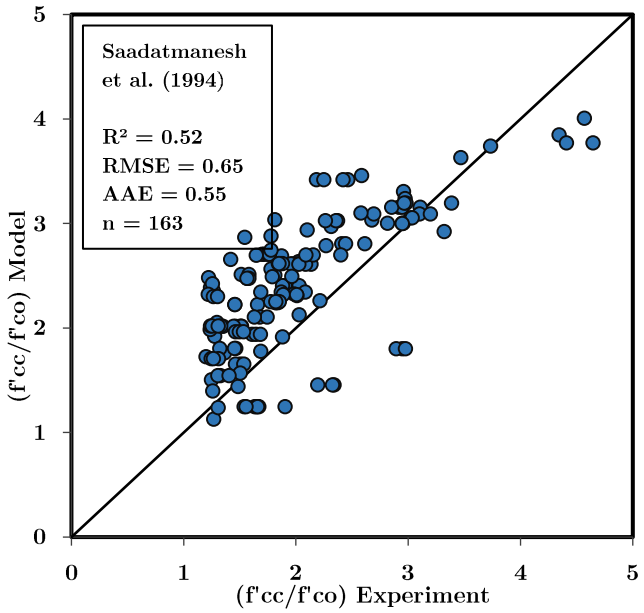

Figure 5.3 Performance of the strength model of Saadatmanesh et al. (1994)

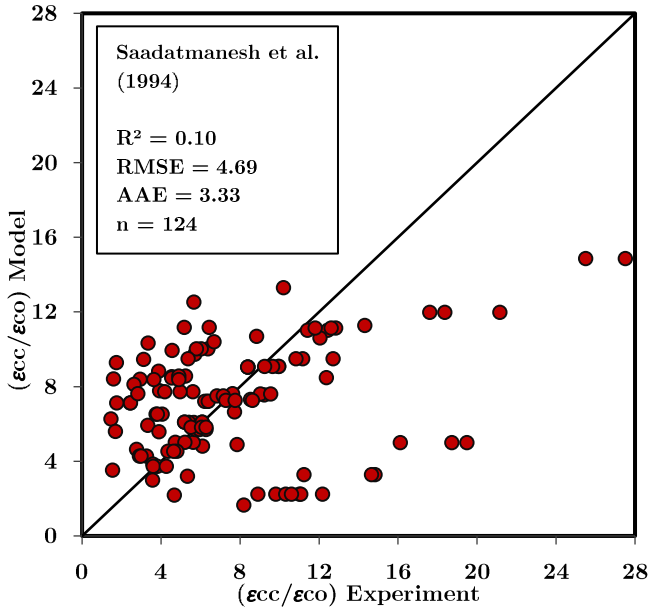

Figure 5.4 Performance of the strain model of Saadatmanesh et al. (1994)

5.3.3.2 Karbhari and Gao (1997)

The authors conducted an experimental and analytical study on concrete confined with FRP composites. They proposed a strength model and strain model based on their experimental data on concrete cylinders confined with a variety of FRP, in various orientations and thicknesses. The models of Karbhari and Gao (1997) are among the early models proposed for FRP-confined concrete under axial compression.

The authors have based on the general form of the equations of Richart et al. (1929) and calibrated the models using regression analysis based on the experimental data (Eqs. (5.7) and (5.8)). In these models, it was assumed that the FRP wrap could reach its full tensile strength in the hoop direction.

$$\frac{f'_{cc}}{f'_{co}} = 1 + 2.1\left(\frac{f_l}{f'_{co}}\right)^{0.87} \tag{5.7}$$

$$\frac{\varepsilon_{cc}}{\varepsilon_{co}} = 1 + \frac{0.01}{\varepsilon_{co}}\left(\frac{f_l}{f'_{co}}\right) \tag{5.8}$$

Using the collected database of 163 data points, the performance of the strength model is shown in Fig. 5.4 with $R^2 = 0.65$, RMSE = 0.42, and AAE = 0.31. The values and the figure show a moderate prediction with a good distribution of the data around the perfect line. This shows that using a linear relationship between the confinement effectiveness (f'_{cc}/f'_{co}) and the power of the confinement ratio (f_l/f'_{co}) may be appropriate for predicting the compressive strength.

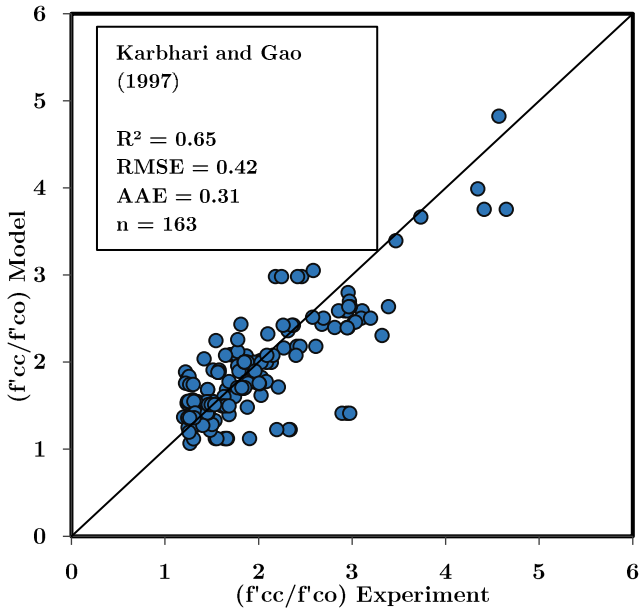

Figure 5.5 Performance of the strength model of Karbhari and Gao (1997)

The performance of the strain model is shown in Fig. 5.5 with $R^2 = 0.26$, RMSE = 6.68 and AAE = 5.20. The indices and the figure show a very low correlation, high errors, and very deviated data, demonstrating a high underestimation of the experimental values. It can be concluded that the unconfined concrete strain (ε_{co}) may not be a suitable parameter in the equation of Richart et al. (1929) for the prediction of the ultimate strain.

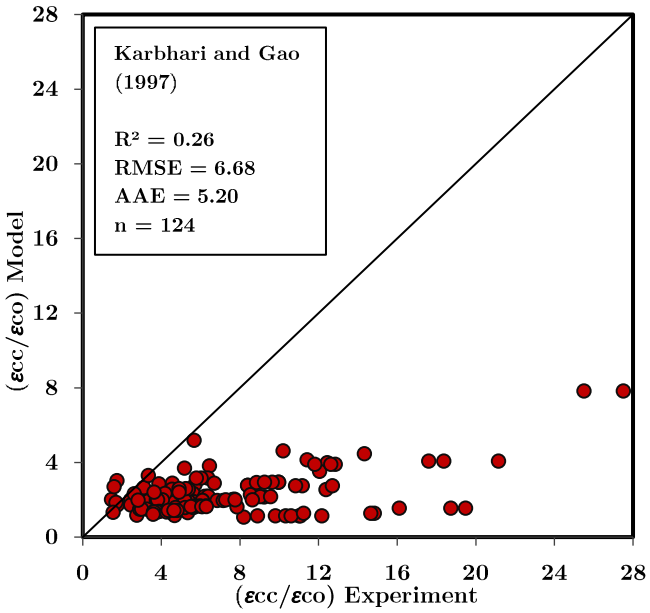

Figure 5.6 Performance of the strain model of Karbhari and Gao (1997)

5.3.3.3 Toutanji (1999)

Toutanji (1999) conducted an experimental and analytical study on the performance of concrete cylindrical specimens confined with FRP under compression. The specimens of 31 MPa concrete strength were wrapped CFRP and GFRP sheets. Based on the experimental results, equations for predicting the ultimate strength and the ultimate strain were proposed by the author based on the general form of the models of Richart et al. (1929), in which the compressive strength and the ultimate strain of the FRP were implemented in the strain model (Eq. (5.9) and (5.10)).

$$\frac{f'_{cc}}{f'_{co}} = 1 + 3.5\left(\frac{f_l}{f'_{co}}\right)^{0.85} \tag{5.9}$$

$$\frac{\varepsilon_{cc}}{\varepsilon_{co}} = 1 + (310.57\varepsilon_f + 1.9)\left(\frac{f'_{cc}}{f'_{co}} - 1\right) \tag{5.10}$$

Where,

ε_f = the lateral strain of the FRP composite.

Using the database, the performance of the strength model is shown in Fig. 5.6 with $R^2 = 0.65$, RMSE = 0.85, and AAE = 0.69. The model demonstrates similar predictions as the model of Karbhari and Gao (1997) but with higher errors and overestimated values.

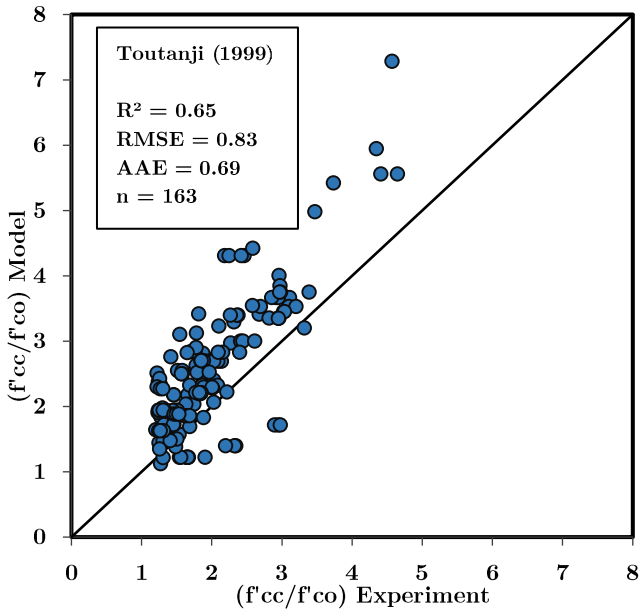

Figure 5.7 Performance of the strength model of Toutanji (1999)

The strain model shows high scattered and significantly overestimated data with ($R^2 = 0.18$) that depicts a very low correlation together with high indices of errors (RMSE = 10.10 and AAE = 7.85) (Fig. 5.7). Thus, having a separate term for (ε_f) maybe not reasonable for this prediction.

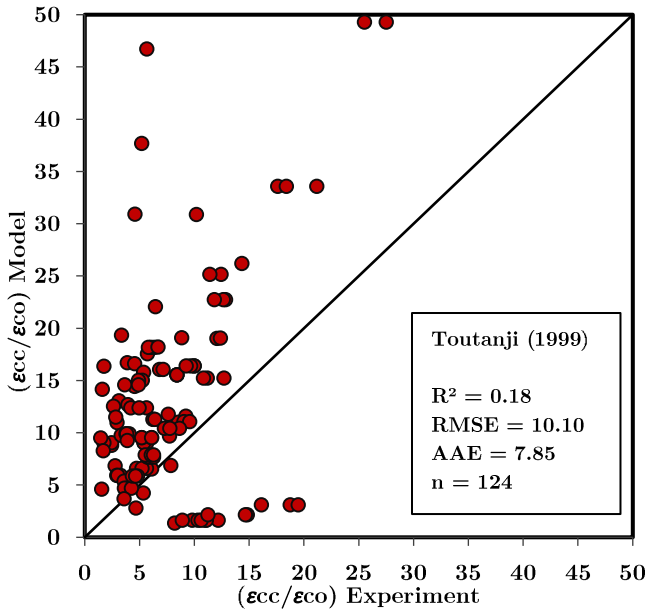

Figure 5.8 Performance of the strain model of Toutanji (1999)

5.3.3.4 Moran and Pantelides (2002)

Expressions for determining the compressive axial stress and its corresponding strain of FRP-confined concrete were developed by Moran and Pantelides (2002). The authors have calibrated the models using regression analysis of experimental data on CFRP-confined concrete cylinders based on the general form of the models of Richart et al. (1929). In the strength model, the strength ratio was related to the confinement ratio with a simple linear equation (Eq. (5.11)), while in the strain model, the strain enhancement coefficient has been expressed with the lateral stiffness to the unconfined concrete strength ratio (E_l/f'_{co}) (Eq. (5.12)).

$$\frac{f'_{cc}}{f'_{co}} = 1 + 4.14\left(\frac{f_l}{f'_{co}}\right) \tag{5.11}$$

$$\frac{\varepsilon_{cc}}{\varepsilon_{co}} = 1 + \frac{(f_l/f'_{co})}{9.27 \times 10^{-3}\left(\frac{E_l}{f'_{co}}\right)^{\frac{1}{3}}} \tag{5.12}$$

The strength model shows similar performance as the models of Karbhari and Gao (1997) and Toutanji (1999) but with higher errors ($R^2 = 0.66$, RMSE = 1.05, and AAE = 0.81) and high overestimation of the experimental data. This implies that the form with the power function of the confinement ratio (f_l/f'_{co}) could be more appropriate.

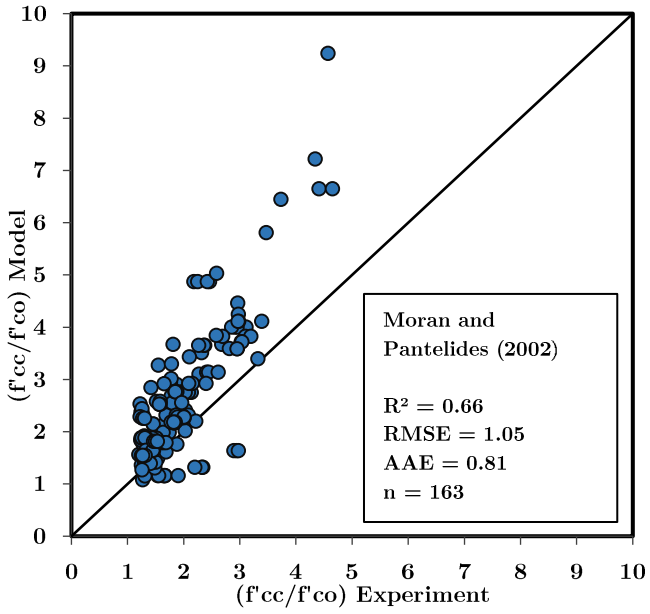

Figure 5.9 Performance of the strength model of Moran and Pantelides (2002)

Using the database, the performance of the strain model is shown in Fig. 5.9 with $R^2 = 0.12$, RMSE = 10.07 and AAE = 8.82. The statistical indices and the figure indicate low and unconservative predictions of (ε_{cc}) for most of the data points with a high scatter. This reduction is may be due to the inclusion of the (E_l/f'_{co}) ratio in the strain enhancement coefficient.

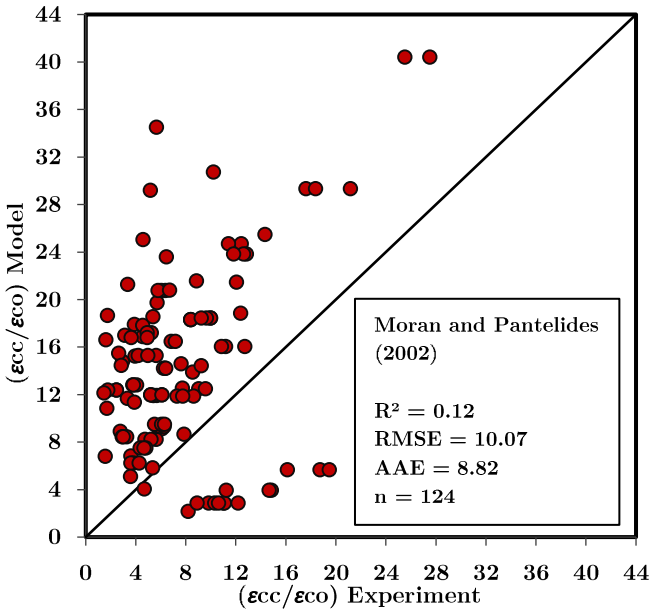

Figure 5.10 Performance of the strain model of Moran and Pantelides (2002)

5.3.3.5 Xiao and Wu (2003)

Xiao and Wu (2003) performed an experimental and analytical study on the behavior of FRP-confined concrete cylinders confined with CFRP and GFRP jackets under axial compression. The authors studied the impact of different design parameters, including unconfined concrete strength, types of FRP as well as jacket thickness, and developed confinement strength and strain models based on the experimental data using regression analysis (Eqs. (5.13) and (5.14)). They found that the lateral stiffness (E_l), the confinement strength of the FRP ($f_{l,rup}$), and the rupture strain of the FRP are the critical parameters in describing the system confinement effectiveness.

$$\frac{f'_{cc}}{f'_{co}} = 1 + \left(4.1 - 0.45\left(\frac{E_l}{f'^{\,2}_{co}}\right)^{-1.4}\right)\left(\frac{f_{l,rup}}{f'_{co}}\right) \tag{5.13}$$

$$\frac{\varepsilon_{cc}}{\varepsilon_{co}} = \frac{\varepsilon_{h,rup} - 0.00047}{10\varepsilon_{co}} \times \left(\frac{E_l}{f'_{co}}\right)^{0.9} \tag{5.14}$$

The performance of the strength model is shown in Fig. 5.10 with R^2 = 0.69, RMSE = 0.99 and AAE = 0.65. the indices and the figure show moderate and overestimated predictions of the experimental data. Comparing to the models of Karbhari and Gao (1997) and Toutanji (1999) that adopted the same general equation from Richart et al. (1929), no significant improvement has been achieved by the model of Xiao and Wu (2003). Therefore, simple equations may be more appropriate.

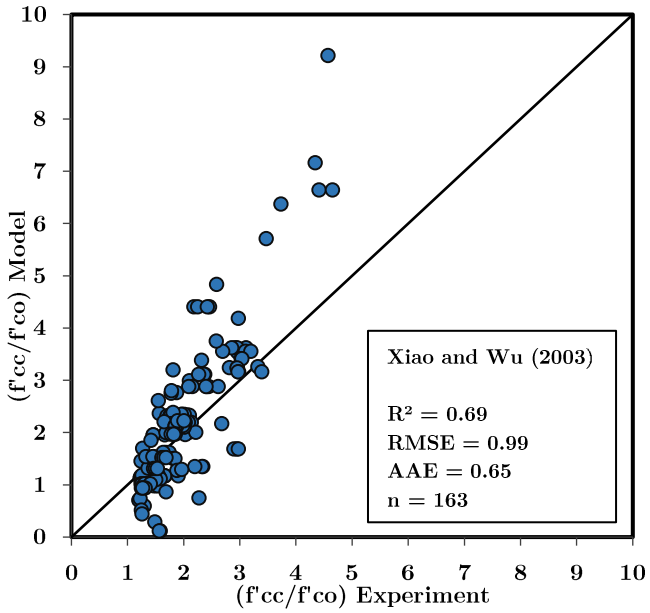

Figure 5.11 Performance of the strength model of Xiao and Wu (2003)

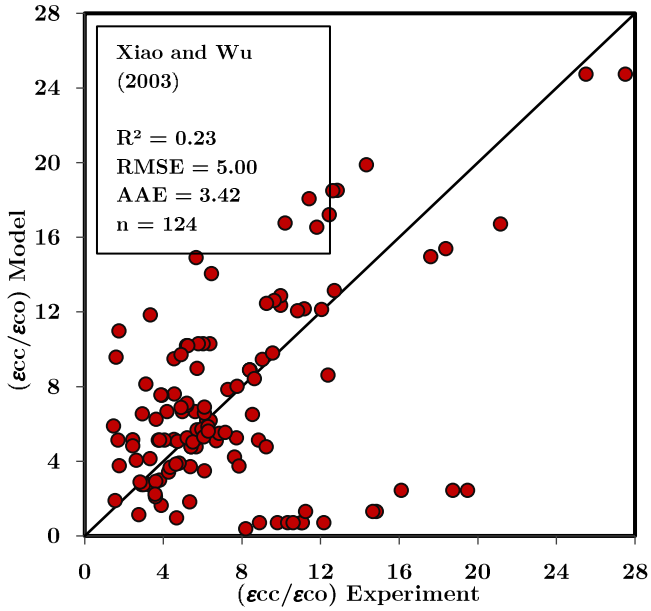

Figure 5.12 Performance of the strain model of Xiao and Wu (2003)

The performance of the strain model is shown in Fig. 5.11. The indices and the figure show low correlation and high errors (R^2 = 0.23, RMSE = 5.00, and AAE = 3.42), and the predicted points are scattered.

5.3.3.6 Bisby et al. (2005)

Bisby et al. (2005) evaluated various previous models predicting the ultimate stress and strain of FRP-confined concrete on the basis of an extensive database of

approximately 200 axially loaded CFRP, GFRP, and AFRP-wrapped concrete cylinders collected from the available literature. Based on the evaluation, the authors modified several existing models to achieve the best fit with the experimental data using regression analysis.

The strength model (Eq. (5.15)) was based on the general form of the model of Richart et al. (1929) and modified from the model of Samaan (1998). On the other side, the strain model (Eq. (5.16)) was modified on the model of Karbhari and Gao (1997) and adjusted based on the FRP type.

$$\frac{f'_{cc}}{f'_{co}} = 1 + 3.587\left(\frac{f_l^{0.84}}{f'_{co}}\right) \tag{5.15}$$

For GFRP confined concrete:

$$\frac{\varepsilon_{cc}}{\varepsilon_{co}} = 1 + \frac{0.0137}{\varepsilon_{co}}\left(\frac{f_l}{f'_{co}}\right) \tag{5.16}$$

The performance of the strength model is shown in Fig. 5.12 with $R^2 = 0.69$, RMSE = 0.40, and AAE = 0.28. The model shows moderate predictions of the experimental data with a small scatter around the perfect line. Slightly better performance is recorded compared to the other models, which may be due to the modified form of the model that adopts a power for only the FRP confining stress (f_l) instead of the confinement ratio (f_l/f'_{co}).

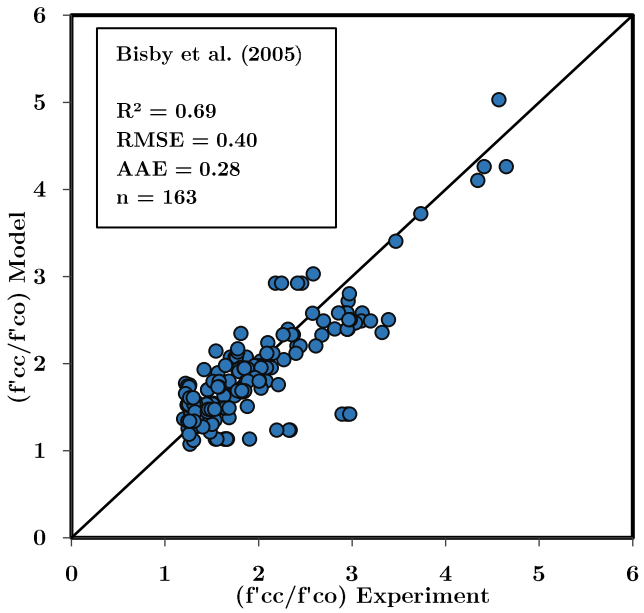

Figure 5.13 Performance of the strength model of Bisby et al. (2005)

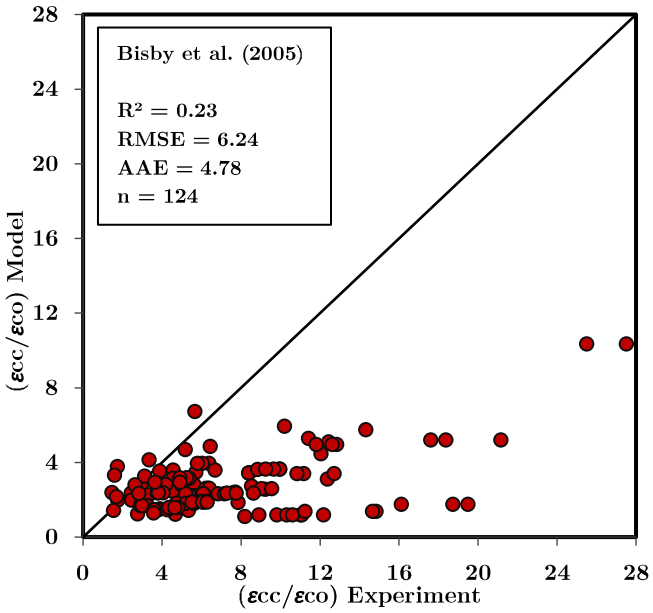

Figure 5.14 Performance of the strain model of Bisby et al. (2005)

Using the database, the performance of the strain model is shown in Fig. 5.13. The model shows a similar performance to the model of Karbhari and Gao (1997) with $R^2 = 0.23$, RMSE = 6.24, and AAE = 4.78. The indices and the figure demonstrate a high underestimation of the ultimate strain (ε_{cc}) for most of the data points. The inclusion of the unconfined concrete strain (ε_{co}) may be the cause of this poor prediction.

5.3.3.7 Matthys et al. (2006)

Matthys et al. (2005) conducted an experimental and analytical study on the behavior of axially loaded large-scale columns confined with FRP wrapping. The authors evaluated different models predicting the entire axial stress–axial and circumferential strain behavior of FRP-confined concrete in light of the experimental results. The authors modified the models proposed by Toutanji (1999) for the ultimate conditions of the stress-strain behavior (Eqs. (5.17) and (5.18)), where the strain at rupture of the FRP ($\varepsilon_{h,rup}$) is considered in the calculation of the ultimate confinement stress of the FRP.

$$\frac{f'_{cc}}{f'_{co}} = 1 + 3.5\left(\frac{f_{l,rup}}{f'_{co}}\right)^{0.85} \tag{5.17}$$

$$\frac{\varepsilon_{cc}}{\varepsilon_{co}} = 1 + (310.57\varepsilon_f + 1.9)\left(\frac{f'_{cc}}{f'_{co}} - 1\right) \tag{5.18}$$

Where,

$f_{l,rup}$ = the lateral confining pressure at failure of the FRP.

Comparing to the model of Toutanji (1999), the strength model of Matthys et al. (2005) shows lower performance with scattered data around the perfect line (lower

correlation (R^2 = 0.55) with better indices of errors RMSE = 0.50 and AAE = 0.38) (Fig. 5.14).

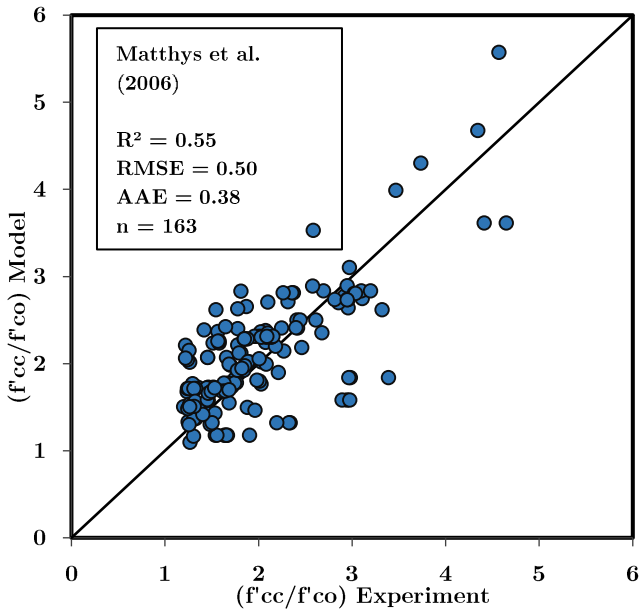

Figure 5.15 Performance of the strength model of Matthys et al. (2006)

Whereas the strain model shows poor predictions with R^2 =0.07, RMSE = 6.53, and AAE = 4.89 and highly scatted data compared to the model of Toutanji (1999) (Fig. 5.15). The indices and the figure show that the formula used is not appropriate for GFRP-wrapped concrete.

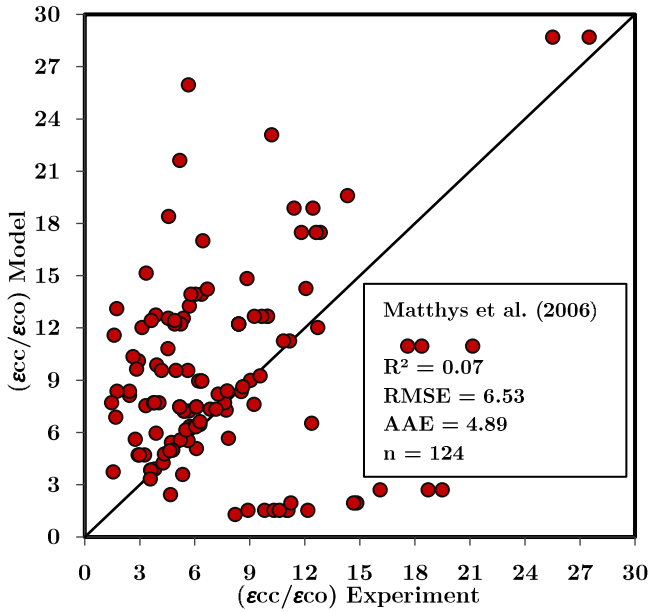

Figure 5.16 Performance of the strain model of Matthys et al. (2006)

5.3.3.8 Berthet et al. (2006)

Berthet et al. (2006) conducted an analytical study to model the ultimate behavior and the stress-strain response of concrete confined with FRP based on experimental data obtained in a previous paper (Berthet et al. 2005) on concrete cylinders confined with CFRP and GFRP jackets. The verification of the models has also been performed using other experimental data available in the literature.

The strength model was based on the general form of Richart et al. (1929) and fitted as a function of the unconfined concrete strength using regression analysis (Eq. (5.19) and (5.20)).

$$\frac{f'_{cc}}{f'_{co}} = 1 + 3.45\left(\frac{f_{l,rup}}{f'_{co}}\right) \qquad for\ 20 \leq f'_{co} \leq 50\ MPa \tag{5.19}$$

$$\frac{f'_{cc}}{f'_{co}} = 1 + 9.5\left(\frac{f_{l,rup}}{f'^{1.25}_{co}}\right) \qquad for\ 50 \leq f'_{co} \leq 200\ MPa \tag{5.20}$$

The authors proposed a model predicting the ultimate strain in a nonlinear equation in a function of the FRP rupture strain ($\varepsilon_{h,rup}$), the strain and Poisson's ratio of unconfined concrete (ε_{co} and ν_c), and the ratio of the lateral stiffness to the compressive strength of the concrete (E_l/f'_{co}), as shown in Eq. (5.21) below:

$$\frac{\varepsilon_{cc}}{\varepsilon_{co}} = 1 + \frac{\varepsilon_{h,rup} - \nu_c\varepsilon_{co}}{\frac{1}{\sqrt{2}}\varepsilon_{co}} \times \left(\frac{E_l}{f'^{2}_{co}}\right)^{\frac{2}{3}} \tag{5.21}$$

Using the database with 163 data points, the performance of the strength model is illustrated in Fig. 5.16 with $R^2 = 0.63$, RMSE = 0.53 and AAE = 0.35. According to the indices of performance and the figure, the model shows a similar performance to the previous strength models such as Karbhari and Gao (1997) and Toutanji (1999) that use the same equation form. Thus, it can be concluded that dividing the model in function of the unconfined concrete strength maybe not necessary.

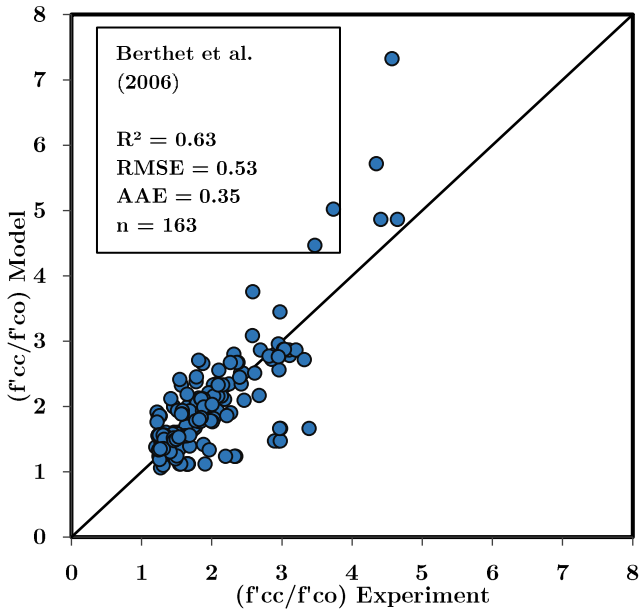

Figure 5.17 Performance of the strength model of Berthet et al. (2006)

The performance of the strain model is shown in Fig. 5.17. The model shows better performance than the model of Xiao and Wu (2003), which has a similar equation form with $R^2 = 0.31$, RMSE = 4.07, and AAE = 3.12. However, the indices of performance and the figure show poor and underestimated predictions of the ultimate strain.

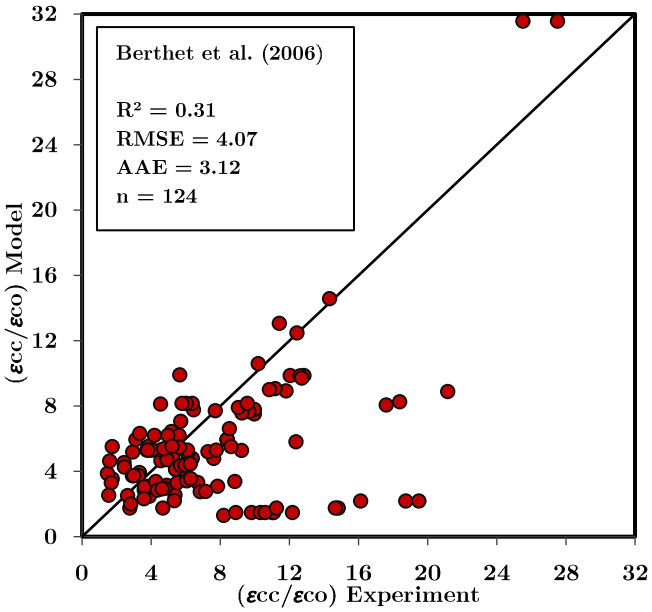

Figure 5.18 Performance of the strain model of Berthet et al. (2006)

5.3.3.9 Wu et al. (2006)

Wu et al. (2006) calibrated ultimate stress and strain models of FRP-confined concrete based on experimental results of more than 300 CFRP, GFRP, and AFRP-confined concrete collected from the literature. A second-order polynomial equation of the confinement ratio (f_l/f'_{co}) was proposed for predicting the ultimate strength using regression analysis (Eq. (5.22)).

$$\frac{f'_{cc}}{f'_{co}} = 0.408 + 6.157\left(\frac{f_l}{f'_{co}}\right) - 3.25\left(\frac{f_l}{f'_{co}}\right)^2 \tag{5.22}$$

The authors found that the ultimate strain was not related only to the confinement ratio (f_l/f'_{co}), but also to the ($\varepsilon_f/\varepsilon_{co}$) ratio (Eq. (5.23)).

$$\frac{\varepsilon_{cc}}{\varepsilon_{co}} = \frac{\varepsilon_f}{0.56\varepsilon_{co}}\left(\frac{f_l}{f'_{co}}\right)^{0.66} \tag{5.23}$$

The performance of the strength model using the database of 163 data points is shown in Fig. 5.18. A high scatter of the data is shown with very poor performance indices (R^2 = 0.26, RMSE = 0.75, and AAE = 0.52), which indicate that the polynomial equation of the confinement ratio may not be suitable for this prediction.

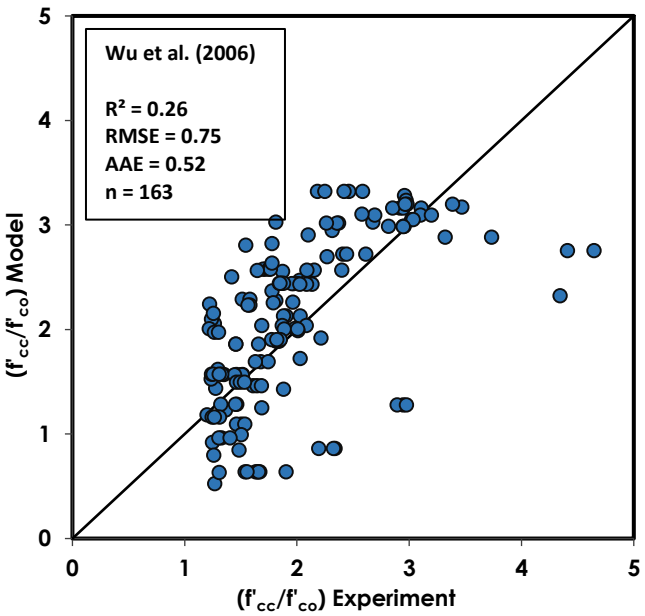

Figure 5.19 Performance of the strength model of Wu et al. (2006)

The performance of the strain model is illustrated in Fig. 5.19. Low correlation and high indices of errors are recorded for this model (R^2= 0.15, RMSE = 6.08, and AAE = 4.00) with scattered data points.

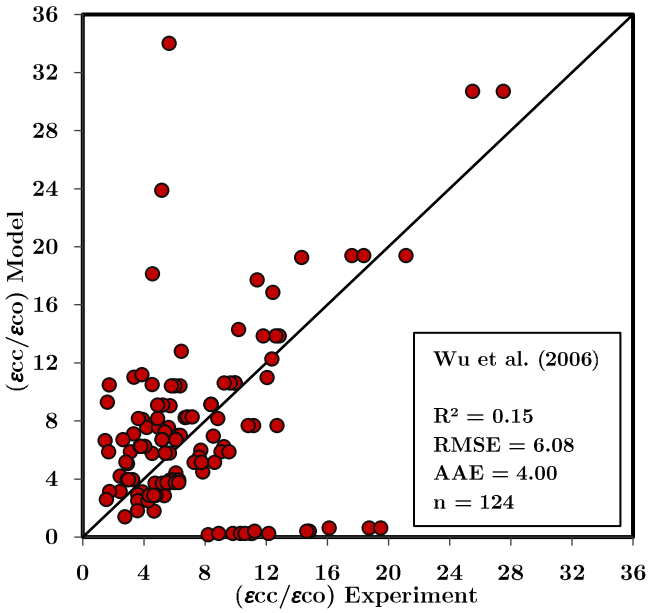

Figure 5.20 Performance of the strain model of Wu et al. (2006)

5.3.3.10 Ciupala et al. (2007)

Ciupala et al. (2007) developed strength and strain models for FRP-confined concrete basing on the general form of the equation of Richart et al. (1929). The calibrated constants of the strength model (Eq. (5.24)) are similar to those of the model of Toutanji (1999), whereas those of the strain model (Eq. (5.25)) are similar to the model of Saadatmanesh et al. (1994).

$$\frac{f'_{cc}}{f'_{co}} = 1 + 3.4\left(\frac{f_l}{f'_{co}}\right)^{0.8} \tag{5.24}$$

$$\frac{\varepsilon_{cc}}{\varepsilon_{co}} = 1 + 6.7\left(\frac{f'_{cc}}{f'_{co}} - 1\right)^{\frac{2}{3}} \tag{5.25}$$

As a result, the performance of the strength model is similar to that of Toutanji (1999) where $R^2 = 0.64$, RMSE = 0.81 and AAE = 0.69. The majority of the data points are overestimated, as shown in Fig. 5.20.

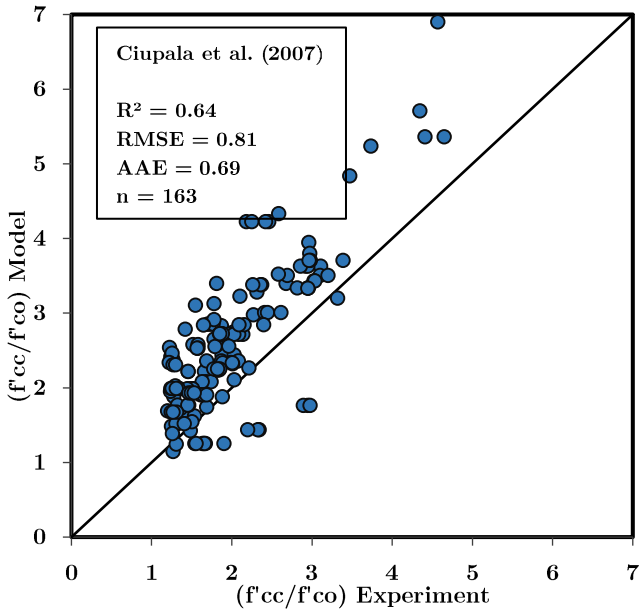

Figure 5.21 Performance of the strength model of Ciupala et al. (2007)

The performance of the strain model is illustrated in Fig. 5.21 with (R^2= 0.65, RMSE = 3.13 and AAE = 2.30). The indices of performance and the figure indicate very good predictions of the ultimate strain compared to all the assessed models. However, the data points are a little dispersed around the perfect line.

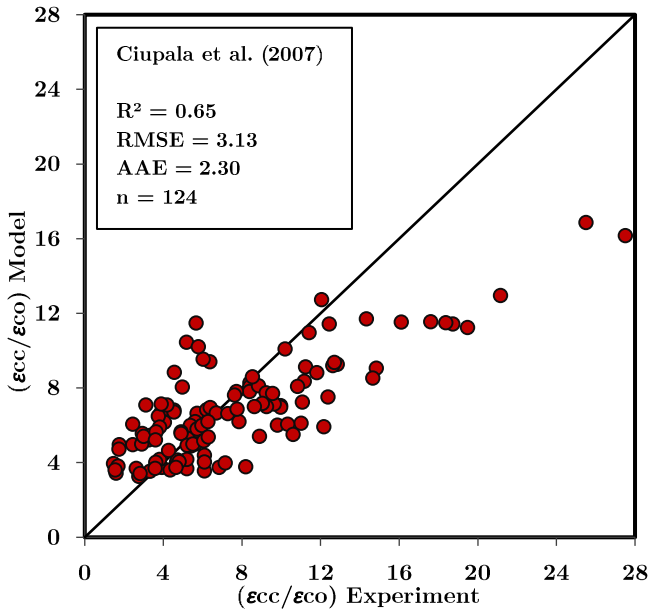

Figure 5.22 Performance of the strain model of Ciupala et al. (2007)

5.3.3.11 Youssef et al. (2007)

The authors conducted an experimental and analytical study on the axial behavior of FRP-confined concrete. Experimental compression tests on large-scale axially loaded circular, square and rectangular concrete specimens confined by CFRP and GFRP jackets were performed. Based on the experimental results, the authors developed confinement models to predict the ultimate stress and the ultimate strain and depict the entire stress-strain diagram for FRP-confined concrete specimens.

The strength model (Eq. (5.26)) was based on the general formula of Richart et al. (1929) and calibrated using regression analysis.

For circular sections:

$$\frac{f'_{cc}}{f'_{co}} = 1 + 2.25\left(\frac{f_l}{f'_{co}}\right)^{1.25} \tag{5.26}$$

The ultimate strain was expressed by a linear function of $(f_f/E_f)^{1/2}$ (f_l/f'_{co}) (Eq. (5.27)) using regression analysis.

For circular sections:

$$\frac{\varepsilon_{cc}}{\varepsilon_{co}} = \frac{0.003368}{\varepsilon_{co}} + \frac{0.2590}{\varepsilon_{co}}\left(\frac{f_f}{E_f}\right)^{\frac{1}{2}}\left(\frac{f_l}{f'_{co}}\right) \tag{5.27}$$

Where,

f_f = the ultimate tensile strength of the FRP;

E_f = the elastic modulus of the FRP.

The performance of the strength model is shown in Fig. 5.22 with $R^2 = 0.67$, RMSE = 0.49 and AAE = 0.37. The indices and the figure indicate moderate prediction and similar performance to the models of the same equation form as Karbhari and Gao (1997) and Toutanji (1999). However, the prediction of the strain model is very poor with $R^2 = 0.23$, RMSE = 5.12, and AAE = 3.57, indicating low correlation, high errors, and high scattered data (Fig. 5.23).

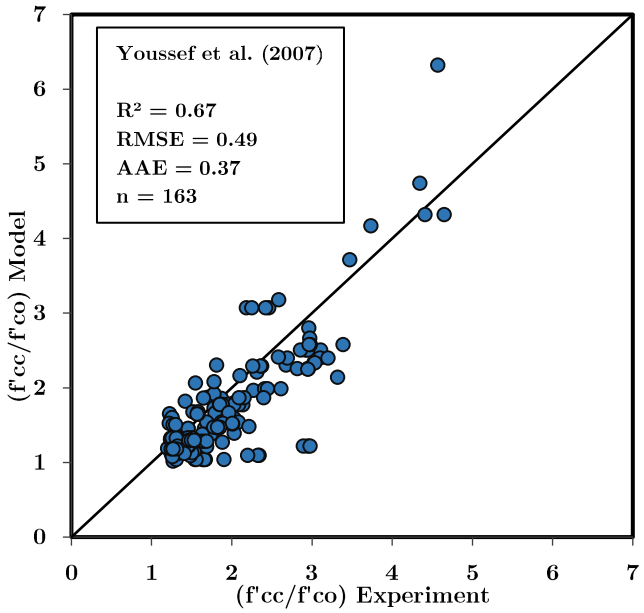

Figure 5.23 Performance of the strength model of Youssef et al. (2007)

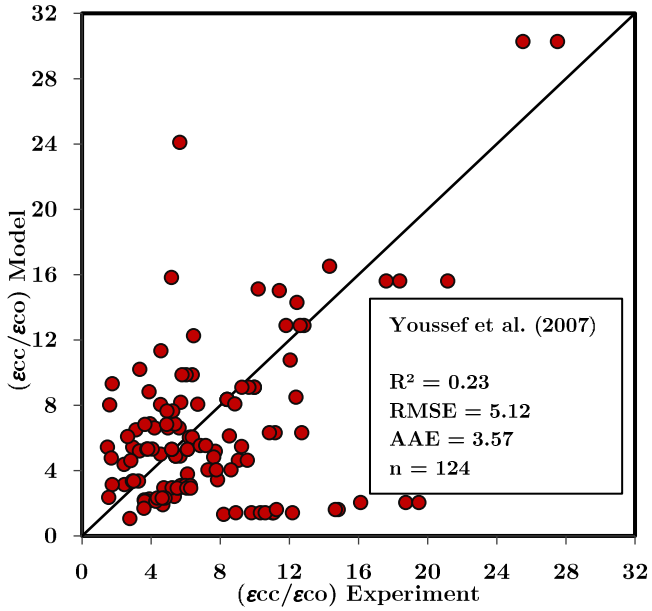

Figure 5.24 Performance of the strain model of Youssef et al. (2007)

5.3.3.12 Fahmy and Wu (2010)

Fahmy and Wu (2010) conducted an analytical study on the prediction of the stress-strain behavior of FRP-confined concrete. Five previous design-oriented models were evaluated in the light of a database of 257 test results of cylindrical CFRP, GFRP, and AFRP-confined concrete specimens collected from the literature. The authors calibrated a new stress-strain relationship based on the

collected database to model the axial FRP-confined concrete strain-hardening behavior (i.e., with a second ascending branch).

The ultimate strength of the confined concrete (Eqs. (5.28) and (5.29)) was calibrated with explicit consideration to the effect of unconfined concrete compressive strength basing on the general form of the equation of Richart et al. (1929).

$$\frac{f'_{cc}}{f'_{co}} = 1 + 4.5\left(\frac{f_l^{0.7}}{f'_{co}}\right) \quad for\ f'_{co} \leq 40MPa \tag{5.28}$$

$$\frac{f'_{cc}}{f'_{co}} = 1 + 3.75\left(\frac{f_l^{0.7}}{f'_{co}}\right) \quad for\ f'_{co} > 40MPa \tag{5.29}$$

The ultimate strain equation was expressed in function of the second stiffness (E_2) and considering the effect of the unconfined concrete strength (Eq. (5.30)).

$$\frac{\varepsilon_{cc}}{\varepsilon_{co}} = \frac{f'_{cc} - f'_{co}}{E_2 \varepsilon_{co}} \tag{5.30}$$

Where,

$$E_2 = m_2\left(245.61 {f'_{co}}^{m_1} + 0.6728E_l\right)$$

$$\begin{cases} m_1 = 0.5, \ m_2 = 0.83, & f'_{co} \leq 40MPa \\ m_1 = 0.2, \ m_2 = 1.73, & f'_{co} > 40MPa \end{cases}$$

The performance of the strength model using the database of 163 data points is shown in Fig. 5.24. High correlation with relatively low indices of errors are recorded of this model (R^2 = 0.72, RMSE = 0.47, and AAE = 0.34). Although conservativeness of the model (most of the data is underestimated), it shows significantly better predictions than the previous strength models.

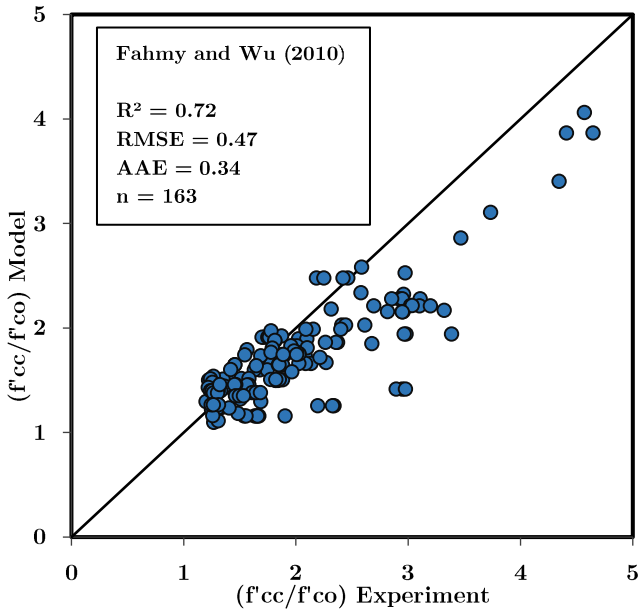

Figure 5.25 Performance of the strength model of Fahmy and Wu (2010)

The performance of the strain model is illustrated in Fig. 5.25 with $R^2 = 0.09$, RMSE = 5.12 and AAE = 3.65. The figure and the indices of performance show poor predictions with high errors and high scatter in the data.

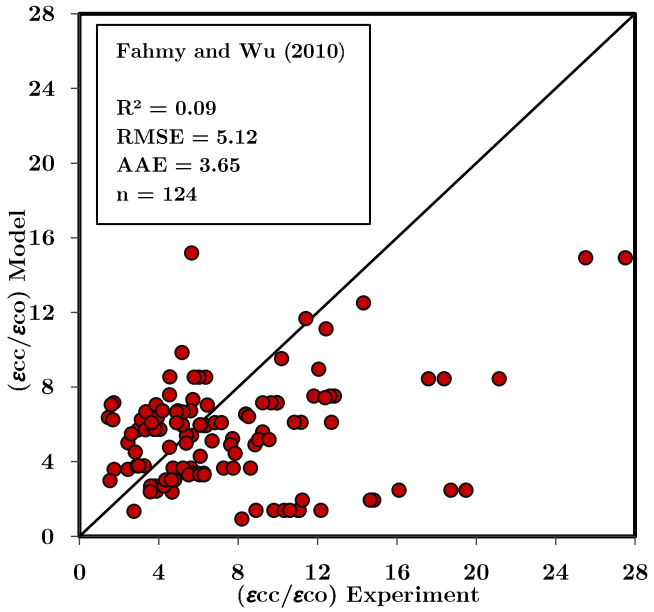

Figure 5.26 Performance of the strain model of Fahmy and Wu (2010)

5.3.3.13 Pham and Hadi (2014)

Pham and Hadi (2014) conducted an analytical study to model the behavior of FRP-confined concrete under compression. A database of 574 FRP circular normal- and high-strength concrete columns confined with different types of FRP

(CFRP, GFRP, and AFRP) was collected from the literature and used to calibrate new confinement models for the prediction of the ultimate conditions of FRP-confined concrete.

In the strength model, the unconfined concrete strength (f'_{co}), the confining pressure (f_l), and the ratio between the FRP thickness and the diameter of the cylinder (t/d) were considered in a linear equation (Eq. (5.31)).

$$\frac{f'_{cc}}{f'_{co}} = 0.91 + 1.88\left(\frac{f_{l,rup}}{f'_{co}}\right) + 7.6\left(\frac{t_f}{df'_{co}}\right) \tag{5.31}$$

Whereas, a database of 215 specimens extracted from the full database was used in the calibration of the strain model (Eq. (5.32)) basing on regression analysis.

$$\frac{\varepsilon_{cc}}{\varepsilon_{co}} = 1 + \frac{13.24\left(t_f f_f \rho_\varepsilon\right)}{\left(df'_{co} + 3.3 f_f t_f\right)} \tag{5.32}$$

The performance of the strength model is shown in Fig. 5.26. Moderate indices of performance are recorded of this model (R^2 = 0.58, RMSE = 0.78 and AAE = 0.63), and most of the data is underestimated. Compared to Moran and Pantelides (2002) model, the inclusion of the thickness per diameter ratio (t_f/d) in the strength model has not improved the performance. Thus, the simple equation is more appropriate.

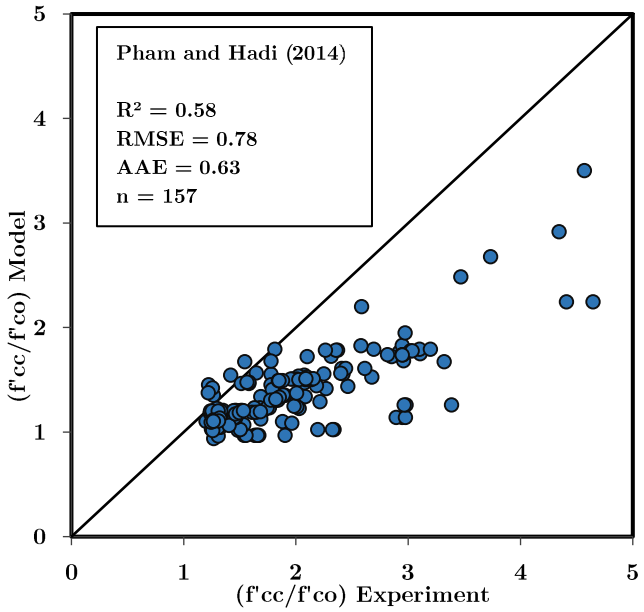

Figure 5.27 Performance of the strength model of Pham and Hadi (2014)

The performance of the strain model is shown in Fig. 5.27 with R^2 = 0.11, RMSE = 6.45 and AAE = 4.85. The indices and the figure show a very poor prediction with high errors and scattered data.

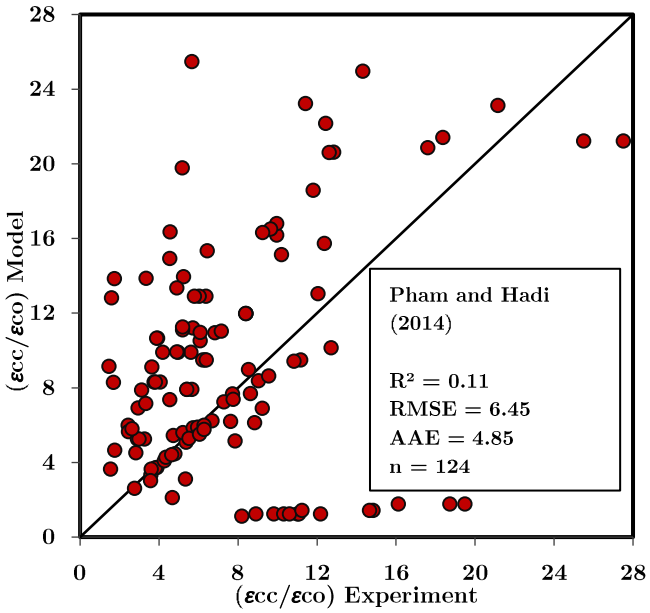

Figure 5.28 Performance of the strain model of Pham and Hadi (2014)

5.3.3.14 Sadeghian and Fam (2015)

Sadeghian and Fam (2015) evaluated the performance of nine major existing strength and strain models for the ultimate condition of FRP-confined concrete based on a large experimental database of 518 cylindrical concrete specimens wrapped with CFRP GFRP and AFRP. Using regression analysis, different forms of strength and strain models were developed by the authors to obtain the best fit with the experimental data. The best performing models (Eq. (5.33) and (5.34)) were selected based on two different statistical indices, the coefficient of determination (R^2) and the root mean square error (RMSE).

$$\frac{f'_{cc}}{f'_{co}} = 1 + (2.77{\rho_K}^{0.77} - 0.07){\rho_\varepsilon}^{0.91} \tag{5.33}$$

$$\frac{\varepsilon_{cc}}{\varepsilon_{co}} = 1.5 + 6.78{\rho_K}^{0.63}{\rho_\varepsilon}^{1.08} \tag{5.34}$$

Where,

ρ_K = the stiffness ratio of the FRP, defined in Eq. (5.35);

ρ_ε = the strain ratio of the FRP, defined in Eq. (5.36).

$$\rho_K = \frac{2E_f t_f}{(f'_{co}/\varepsilon_{co})d} \tag{5.35}$$

$$\rho_\varepsilon = \frac{\varepsilon_{h,rup}}{\varepsilon_{co}} \tag{5.36}$$

The performance of the strength model is shown in Fig. 5.28 with R^2= 0.47, RMSE = 0.47 and AAE = 0.37. The figure and the indices of performance demonstrate

low prediction with high errors and a large spread of the data around the perfect line.

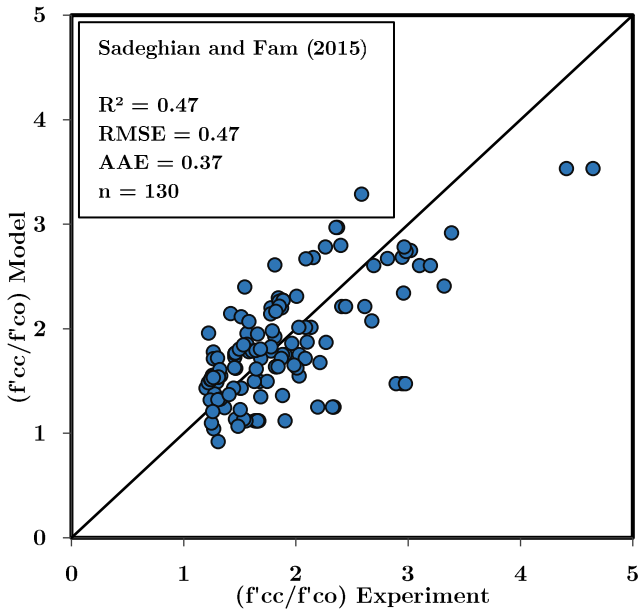

Figure 5.29 Performance of the strength model of Sadeghian and Fam (2015)

On the other hand, very low predictions were recorded for the strain model with $R^2 = 0.13$, RMSE = 4.71 and AAE = 3.38 and large scattered data (Fig. 5.29).

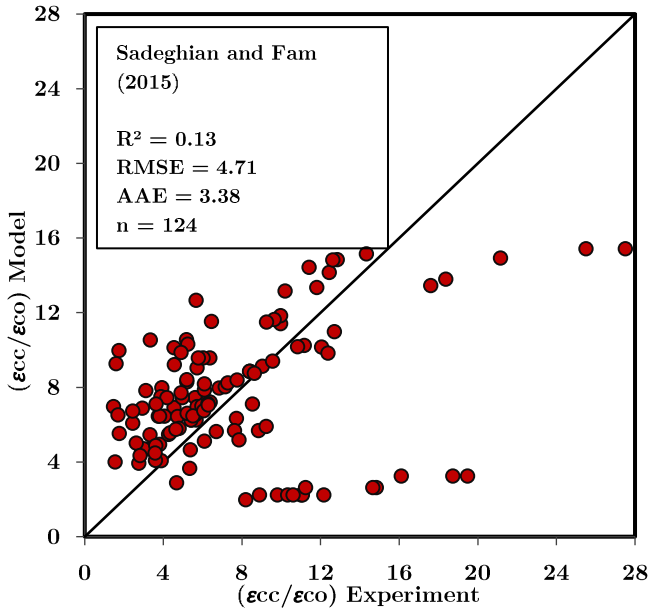

Figure 5.30 Performance of the strain model of Sadeghian and Fam (2015)

5.3.3.15 Touhari and Mitiche-Kettab (2016)

Touhari and Mitiche-Kettab (2016) conducted an experimental and analytical study to investigate the axial behaviour of FRP-confined concrete. The effects of different parameters such as type of FRP composite and number of FRP layers and unconfined concrete strength were examined.

Based on 27 test results on concrete cylinders wrapped with GFRP jackets tested under axial compression and using regression analysis, the authors calibrated strength and strain confinement models (Eq. (5.37) and (5.38)) based on the general form of the equation of Richart et al. (1929).

$$\frac{f'_{cc}}{f'_{co}} = 1 + 1.85\left(\frac{f_l}{f'_{co}}\right) \tag{5.37}$$

$$\frac{\varepsilon_{cc}}{\varepsilon_{co}} = 1.45 + 15\left(\frac{f_l}{f'_{co}}\right) \tag{5.38}$$

As shown in the results of the performance analysis of the strength model (Fig. 5.30), the data points are a little underestimated and a little scattered. The indices of performance indicate moderate predictions with $R^2 = 0.66$, RMSE = 0.48 and AAE = 0.36.

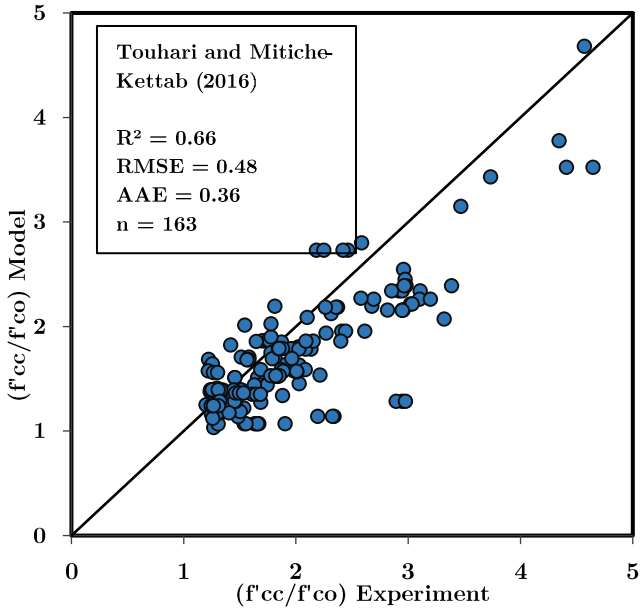

Figure 5.31 Performance of the strength model of Touhari and Mitiche-Kettab (2016)

The performance of the strain model is illustrated in Fig. 5.31 with $R^2 = 0.23$, RMSE = 4.49, and AAE = 3.26. The prediction is very poor, and the predicted points are very scattered. This may be due to the limited database used for the calibration of the models.

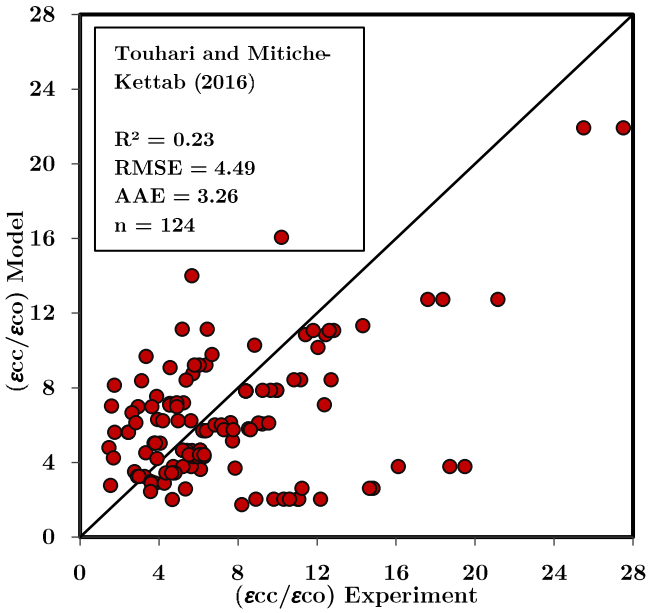

Figure 5.32 Performance of the strain model of Touhari and Mitiche-Kettab (2016)

5.3.3.16 Huang et al. (2016)

Huang et al. (2016) performed an assessment of existing 22 stress models and 13 strain models for ultimate conditions of axially loaded GFRP-confined concrete. A database of 212 compression tests on concrete cylinders confined with GFRP wraps and tubes was collected and analyzed by the authors to evaluate the performance of the stress and strain models.

The authors calibrated new strength and strain models (Eqs. (5.39) and (5.40)) basing on the general form of the equation of Richart et al. (1929), where the confinement effectiveness (f'_{cc}/f'_{co}) and the power of the confinement ratio ($f_{l,rup}/f'_{co}$) are linearly related.

$$\frac{f'_{cc}}{f'_{co}} = 1 + 1.69\left(\frac{f_{l,rup}}{f'_{co}}\right)^{0.63} \tag{5.39}$$

$$\frac{\varepsilon_{cc}}{\varepsilon_{co}} = 1 + 13.2\left(\frac{f_{l,rup}}{f'_{co}}\right)^{0.6} \tag{5.40}$$

Although the models are developed based on GFRP confined concrete data, they show poor performance. The strength model shows relatively lower performance compared to the models with the same equation form, such as Ciupala et al. (2007) and Youssef et al. (2007), with $R^2 = 0.52$, RMSE = 0.61 and AAE = 0.42 and underestimated data (Fig. 5.32).

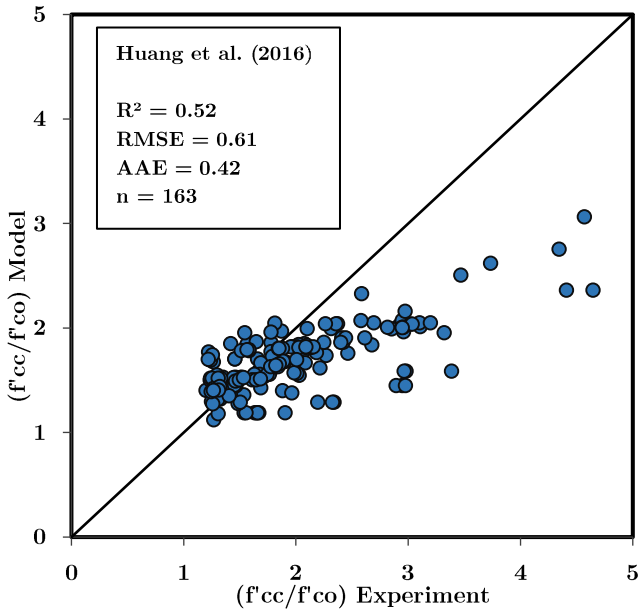

Figure 5.33 Performance of the strength model of Huang et al. (2016)

The indices of performance of the strain model and the data points shown in Fig. 5.33 show very poor performance and accuracy, where the majority of the data is underestimated.

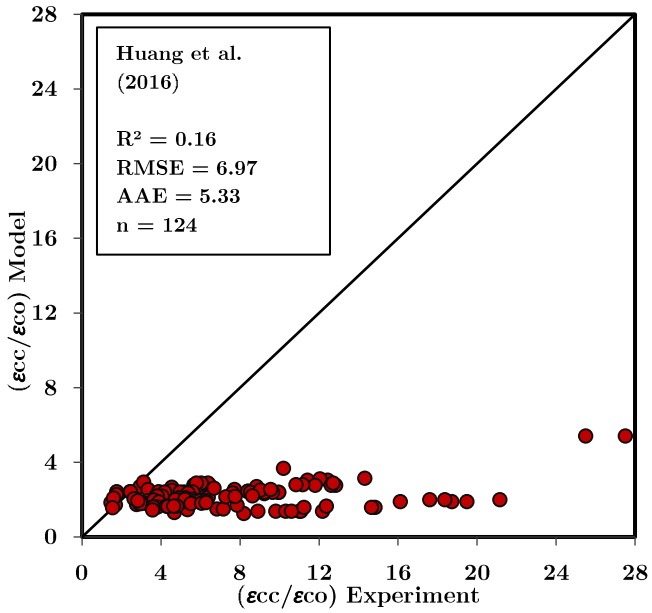

Figure 5.34 Performance of the strain model of Huang et al. (2016)

5.3.3.17 Baji et al. (2016)

Baji et al. (2016) derived design-oriented models for the ultimate strength and strain of FRP-confined concrete based on a probabilistic procedure. A database of

701 axial compression tests performed on circular concrete specimens confined with CFRP and GFRP was collected by the authors for calibrating the models.

The ultimate strength model (Eq. (5.41)) was expressed in a simple linear relationship between the (f'_{cc}/f'_{co}) and the confinement ratio ($f_{l,rup}/f'_{co}$). While the ultimate strain model (Eq. (5.42)) was written as a function of the strain ratio (ρ_ε) and the power of the lateral stiffness to the unconfined concrete strength ratio (E_l/f'_{co}).

$$\frac{f'_{cc}}{f'_{co}} = 1 + 3.29\left(\frac{f_{l,rup}}{f'_{co}}\right) \tag{5.41}$$

$$\frac{\varepsilon_{cc}}{\varepsilon_{co}} = 1 + 0.54\left[\left(\frac{1}{5.1}\right)\left(\frac{\varepsilon_{h,rup}}{\varepsilon_{co}}\right)\left(\frac{E_l}{f'_{co}}\right)^{0.56}\right] \tag{5.42}$$

The performance of the strength model is shown in Fig. 5.34, with $R^2 = 0.57$, RMSE = 0.49 and AAE = 0.35. The indices of performance and the figure show a poor prediction of the experimental data.

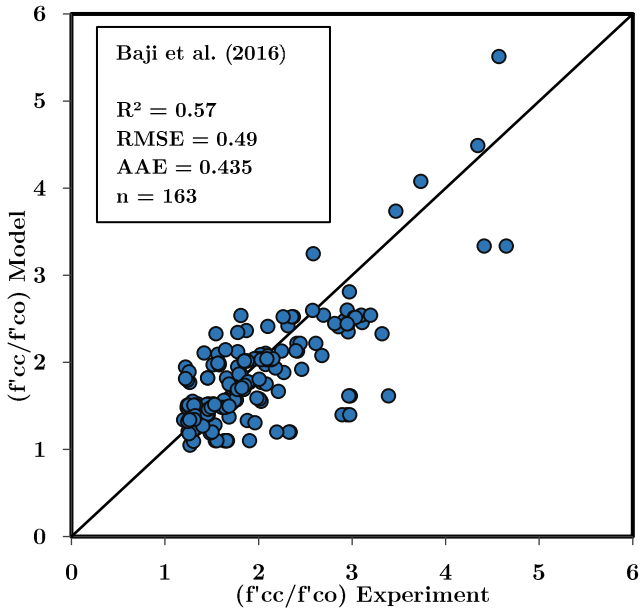

Figure 5.35 Performance of the strength model of Baji et al. (2016)

Very low accuracy is obtained for the predictions of the strain model with $R^2 = 0.13$, RMSE = 5.68, and AAE = 3.91 and highly scattered and underestimated data (Fig. 5.35).

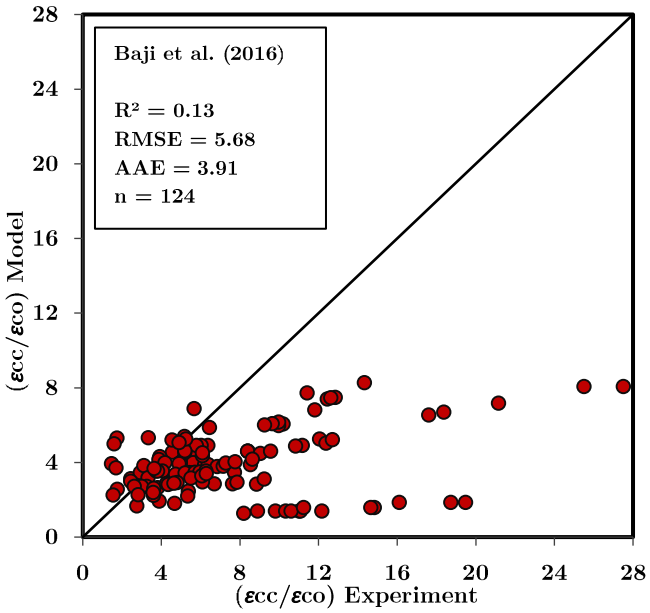

Figure 5.36 Performance of the strain model of Baji et al. (2016)

5.3.3.18 Lim et al. (2016)

Lim et al. (2016) developed confinement models to predict the ultimate conditions model for FRP-confined concrete using genetic programming. A large experimental database of 832 axial compression test results of concrete specimens confined with CFRP, GFRP, and AFRP wraps and tubes was assembled and used in the calibration of the models. Existing conventional and evolutionary algorithm models developed for FRP-confined concrete were then assessed and compared to the proposed models.

The genetic programming algorithm resulted in the equations below for the strength (Eq. (5.43)) and strain (Eq. (5.44)). The models involve multiple parameters such as the FRP rupture strain ($\varepsilon_{h,rup}$), the lateral stiffness of the FRP (E_l), and the unconfined concrete strain (ε_{co}).

$$\frac{f'_{cc}}{f'_{co}} = \frac{1 + E_l\varepsilon_{h,rup} + {E_l}^{1.5}{\varepsilon_{h,rup}}^2 + a}{f'_{co}} \quad a = \sqrt{E_l - \frac{f'_{co}}{\sqrt{\varepsilon_{h,rup}}}} \geq 0 \tag{5.43}$$

$$\frac{\varepsilon_{cc}}{\varepsilon_{co}} = \left(1 + \frac{b}{\varepsilon_{co}}\right)\left({\varepsilon_{co}}^c + \frac{E_l}{f'_{co}}(2\varepsilon_{co} + b)\right) \tag{5.44}$$

Where,

$$b = \varepsilon_{h,rup} - {\varepsilon_{h,rup}}^{\frac{E_l}{f'_{co}}} \tag{5.45}$$

$$c = f'_{co}(\varepsilon_{co} + \varepsilon_{h,rup} + e^{\varepsilon_{h,rup}})/E_l \tag{5.46}$$

$$\varepsilon_{h,rup} = \varepsilon_f / {f'_{co}}^{0.125} \tag{5.47}$$

$$\varepsilon_{co} = \left({f'_{co}}^{0.225}/1000\right)k_s k_a \tag{5.48}$$

$$k_s = (152/d)^{0.1} \tag{5.49}$$

$$k_a = (2d/h)^{0.13} \tag{5.50}$$

Using the database, the performance of the strength model is shown in Fig. 5.36. As shown in the figure, although the model was developed based on a large database and provides a good correlation with (R^2 = 0.73), it shows completely underestimated predictions with relatively high errors (RMSE = 1.07 and AAE = 1.00) compared to the other models.

The performance of the strain model is shown in Fig. 5.37 with (R^2 = 0.23, RMSE = 4.70, and AAE = 3.13). The figure and the indices of performance show low accuracy and high errors in predicting the ultimate strain.

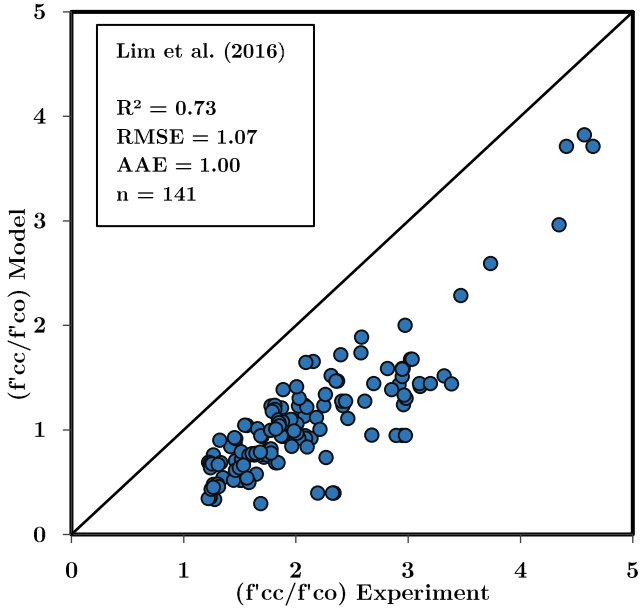

Figure 5.37 Performance of the strength model of Lim et al. (2016)

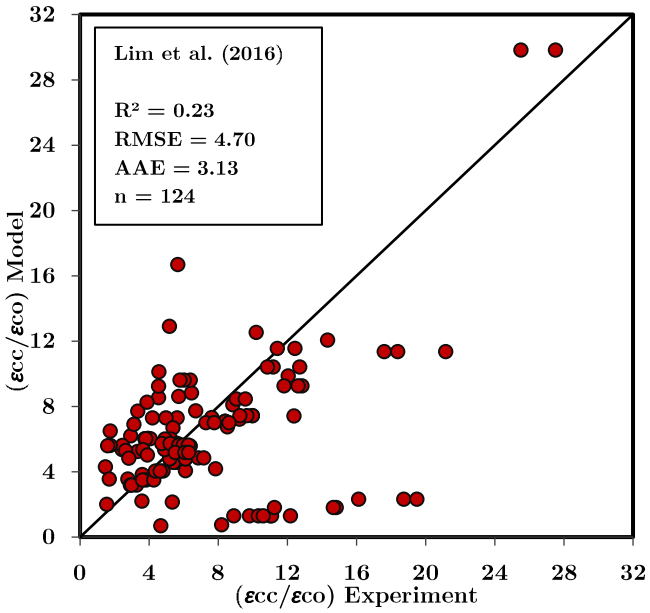

Figure 5.38 Performance of the strain model of Lim et al. (2016)

5.3.3.19 Keshtegar et al. (2017)

Keshtegar et al. (2017) calibrated nonlinear mathematical design-oriented confinement models using a dynamic harmony search (DHS) algorithm for the prediction of the ultimate conditions of FRP-confined concrete. The calibration is based on a database of FRP-confined concrete of 780 axial compression tests on normal and high-strength circular concrete specimens confined by CFRP, GFRP, and AFRP composites. The proposed strength and strain models (Eqs. (5.51) and (5.52)) were written in a function of three influential factors; the FRP area ratio (ρ_a) (Eq. (5.53)), the lateral confinement stiffness ratio (ρ_E) (Eq. (5.54)), and the strain ratio (ρ_ε). The proposed models were compared to existing models on the basis of the existing database.

$$\frac{f'_{cc}}{f'_{co}} = 1 + (0.85 + 1.40\rho_\varepsilon){\rho_a}^{0.82}{\rho_E}^{0.91} \tag{5.51}$$

$$\frac{\varepsilon_{cc}}{\varepsilon_{co}} = 1.5 + (-0.09 + 3.27{\rho_a}^{0.4}){\rho_E}^{0.6}{\rho_\varepsilon}^{1.04} \tag{5.52}$$

Where,

$$\rho_a = t_f/d \tag{5.53}$$

$$\rho_E = \frac{2E_f}{f'_{co}/\varepsilon_{co}} \tag{5.54}$$

The models were expressed in power functions of the influential parameters as the models of Sadeghian and Fam (2015). Fig. 5.38 shows the performance of the strength model with ($R^2 = 0.53$, RMSE = 0.45, and AAE = 0.33). The figure and the indices demonstrate a moderate accuracy with little scatter of the data around the perfect line.

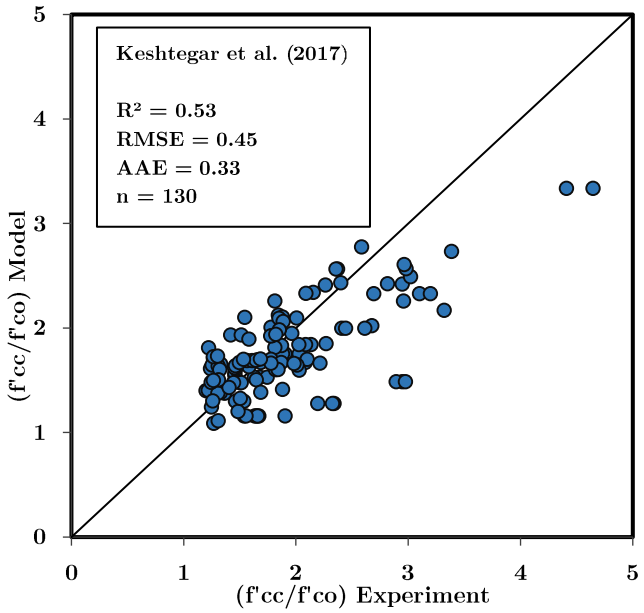

Figure 5.39 Performance of the strength model of Keshtegar et al. (2017)

On the other hand, the performance of the strain model is shown in Fig. 5.39 with (R^2 = 0.16, RMSE = 4.52, and AAE = 3.19). The figure and the indices of performance show very low accuracy and high spread of the data around the perfect line.

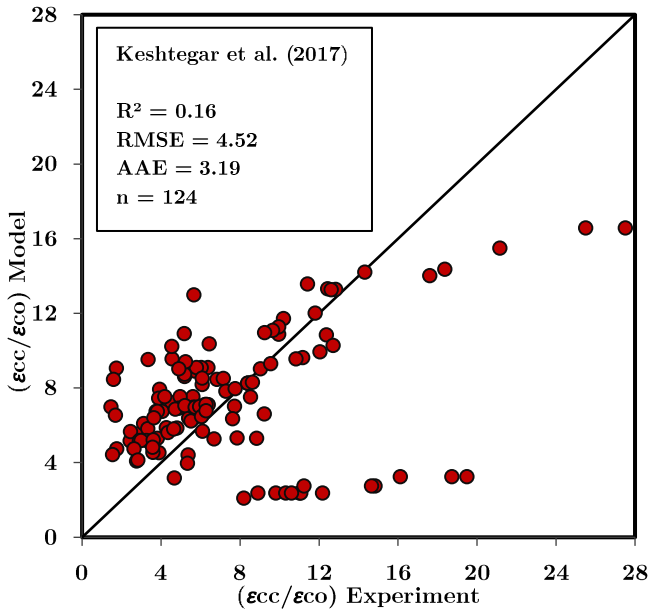

Figure 5.40 Performance of the strain model of Keshtegar et al. (2017)

5.3.3.20 Fallah Pour et al. (2018)

An experimental test database consisted of more than 800 datasets of FRP-confined normal- and high-strength concrete was compiled by the authors and used in the development of ultimate condition models for FRP-confined concrete. The proposed strength model (Eq. (5.55)) was based on the equation proposed by Richart et al. (1929), and the strain model was expressed in a nonlinear function of the lateral stiffness of the FRP (E_l), and the unconfined concrete strength (f'_{co}) (Eq. (5.56)). The proposed models were calibrated using regression analysis.

$$\frac{f'_{cc}}{f'_{co}} = 1 + \left(2.5 - 0.01 f'_{co}\right)\left(\frac{f_l}{f'_{co}}\right) \tag{5.55}$$

$$\frac{\varepsilon_{cc}}{\varepsilon_{co}} = 1.5 + (0.3 - 0.001 f'_{co})\left(\frac{E_l}{f'_{co}}\right)^{0.75} \frac{\varepsilon_f{}^{1.35}}{\varepsilon_{co}} \tag{5.56}$$

The performance of the strength model is shown in Fig. 5.40 where $R^2 = 0.67$, RMSE = 0.44, and AAE = 0.30. The figure and the indices of performance indicate medium accuracy with high dispersion of the data around the perfect line.

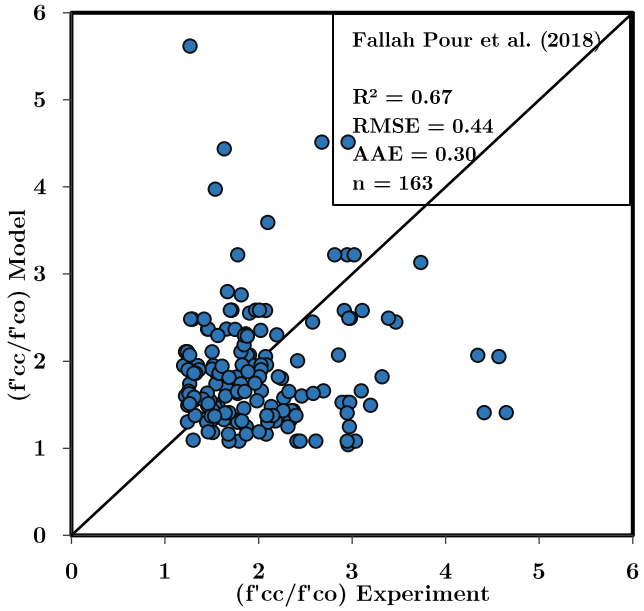

Figure 5.41 Performance of the strength model of Fallah Pour et al. (2018)

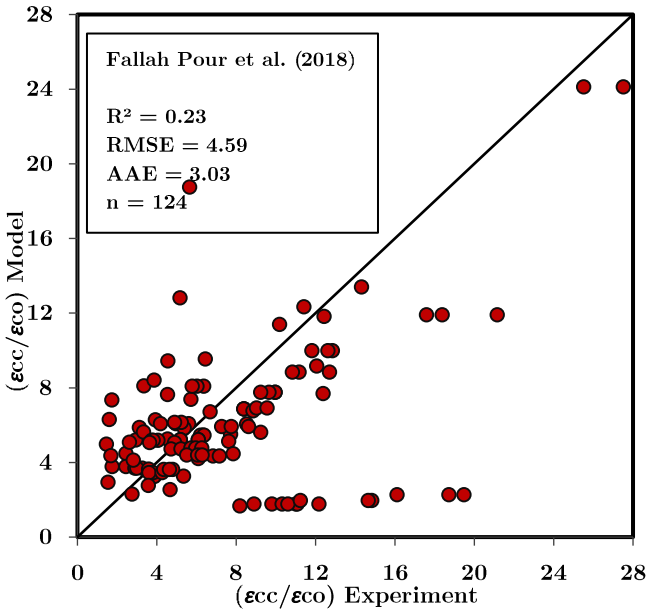

Figure 5.42 Performance of the strain model of Fallah Pour et al. (2018)

The indices of performance ($R^2 = 0.23$, RMSE = 4.59, and AAE = 3.03) and the figure 5.41 indicate low accuracy, high errors, and scattered predictions of the strain model.

5.3.3.21 Summary

The results of the performance analysis of the strength and strain models are summarized in Table 5.2.

Table 5.2 Performance of the selected strength and strain models

No.	Source	Strength model			Strain model		
		R^2	RMSE	AAE	R^2	RMSE	AAE
1	Saadatmanesh et al. (1994)	0.52	0.65	0.55	0.10	4.69	3.33
2	Karbhari and Gao (1997)	0.65	0.42	0.31	0.26	6.68	5.20
3	Toutanji (1999)	0.65	0.83	0.69	0.18	10.10	7.85
4	Moran and Pantelides (2002)	0.66	1.05	0.81	0.12	10.07	8.82
5	Xiao and Wu (2003)	0.69	0.99	0.65	0.23	5.00	3.42
6	Bisby et al. (2005)	0.69	0.40	0.28	0.26	6.24	4.78

7	Matthys et al. (2006)	0.55	0.50	0.38	0.07	6.53	4.89
8	Berthet et al. (2006)	0.63	0.53	0.35	0.31	4.07	3.12
9	Wu et al. (2006)	0.26	0.75	0.52	0.15	6.08	4.00
10	Ciupala et al. (2007)	0.64	0.81	0.69	0.65	3.13	2.30
11	Youssef et al. (2007)	0.67	0.49	0.37	0.23	5.12	3.57
12	Fahmy and Wu (2010)	0.72	0.47	0.34	0.09	5.12	3.65
13	Pham and Hadi (2014)	0.58	0.78	0.63	0.11	6.45	4.85
14	Sadeghian and Fam (2015)	0.47	0.47	0.37	0.13	4.71	3.38
15	Touhari and Mitiche-Kettab (2016)	0.66	0.48	0.36	0.23	4.49	3.26
16	Huang et al. (2016)	0.52	0.61	0.42	0.16	6.97	5.33
17	Baji et al. (2016)	0.57	0.49	0.35	0.13	5.68	3.91
18	Lim et al. (2016)	0.73	1.07	1.00	0.23	4.70	3.13
19	Keshtegar et al. (2017)	0.53	0.45	0.33	0.16	4.52	3.19
20	Fallah Pour et al. (2018)	0.67	0.44	0.30	0.23	4.59	3.03

From Tables 5.1 and 5.2, the following remarks can be drawn:

- The majority of the strength and strain models were expressed based on the general form of the well-known equation of Richart et al. (1929) (Eqs. (5.57) and (5.58)).

$$\frac{f'_{cc}}{f'_{co}} = c_1 + k_1\left(\frac{f_l}{f'_{co}}\right) \tag{5.57}$$

$$\frac{\varepsilon_{cc}}{\varepsilon_{co}} = c_2 + k_2\left(\frac{f_l}{f'_{co}}\right) \tag{5.58}$$

Where (c_1) and (c_2) are calibration constants, and (k_1) and (k_2) are strength and strain enhancement coefficients, and the confinement ratio could be in the forms ((f_l/f'_{co}), $(f_l/f'_{co})^a$, $((f_l)^a/(f'_{co})^b)$) adjusted to provide the best prediction.

- Most of the recent models have used the rupture strain of the FRP.
- The old and recent models calibrated based on large experimental data of FRP-confined concrete have shown low to moderate performance in predicting both the ultimate strength and strain.
- The models based on large or small test data of only GFRP-confined concrete have proved moderate predictions.
- The strain models have shown low predictions with an average of (R^2 = 0.20, RMSE = 5.75, and AAE = 4.25) compared to the strength models with (R^2 = 0.60, RMSE = 0.63, and AAE = 0.49).
- The best indices of performance for the strength models are recorded for the model of Lim et al. (2016) (R^2 = 0.73) and the model of Bisby et al. (2005) (RMSE=0.40, and AAE=0.28). However, the model of Lim et al. (2016) showed high errors and underestimated predictions, and the model of Bisby et al. (2005) showed relatively weak performance with (R^2=0.69).
- The best indices of performance for the strain models are recorded for the model of Ciupala et al. (2007), with the top (R^2 = 0.65) proving the best fit with the experimental data and the minimum values of the error indices (RMSE = 3.13) and (AAE = 2.3) indicating the highest accuracy comparing to the other 19 strain models. However, it shows high values of errors and low accuracy in predicting the experimental results, as illustrated by a large dispersion of the data around the reference line.
- Based on this analysis, there is no model with an accuracy reflecting a good performance in predicting the ultimate strength and strain, even the model of Touhari and Mitiche-Kettab (2016) that was based only on GFRP-wrapped concrete test results.

5.4 Proposed models for the ultimate condition of GFRP-wrapped concrete

After reviewing the selected models and showing their performance in predicting the ultimate condition of GFRP-wrapped concrete, improved design-oriented models are proposed in this section. The models were calibrated based on a regression analysis of the collected experimental database through consideration of various parameters.

The principal advantage of the regression analysis is the unlimited form of the equation and the unlimited parameters (Sedeghian and Fam 2015). However, this procedure can be heavy since it requires testing many cases and performing many iterations. To that end, the regression analysis was performed using an AI data analysis software called Eureqa® (Schmidt and Lipson, 2009).

5.4.1 Proposed ultimate stress model

After consideration of various parameters and testing a large number of cases, the parameters observed to have a strong influence on the strength of GFRP-wrapped concrete are the unconfined concrete strength (f'_{co}), the rupture confining pressure ($f_{l,rup}$), the strain ratio (ρ_ε), and the stiffness ratio (ρ_K). These parameters are inter-related as shown in Eq. (5.59):

$$\frac{f_{l,rup}}{f'_{co}} = \rho_K \rho_\varepsilon \tag{5.59}$$

The regression analysis resulted in the empirical relationship shown in Eq. (5.60).

$$\frac{f'_{cc}}{f'_{co}} = 0.775 + \frac{15.8}{f'_{co}} + \rho_K \left(4.34\,\rho_\varepsilon + \frac{24.5}{\rho_\varepsilon} - 16.4\right) \tag{5.60}$$

The relationship can be expressed as the general form of the equation of Richart et al. (1929), where (c_1) and (k_1) are expressed in function of (f'_{co} and ρ_ε) as shown in Eq. (5.61):

$$\frac{f'_{cc}}{f'_{co}} = \left(0.775 + \frac{15.8}{f'_{co}}\right) + \left(4.34 - \frac{16.4}{\rho_\varepsilon} + \frac{24.5}{{\rho_\varepsilon}^2}\right)\left(\frac{f_{l,rup}}{f'_{co}}\right) \tag{5.61}$$

5.4.2 Validation of the proposed strength model

The accuracy of the proposed model is assessed with the experimental results (Fig. 5.44) and compared with the selected strength models using the statistical indices (R^2, RMSE, and AAE) (Figs. 5.45-5.47).

It can be seen from Fig. 5.44 that predictions of the proposed strength model are in good agreement with the experimental data with a high coefficient of determination ($R^2 = 0.80$) and small indices of errors (RMSE = 0.28, and AAE = 0.21) that tend towards 0, indicating a good accuracy and well-concentrated data around the reference line.

Fig. 5.45 illustrates the values of the coefficient of determination (R^2) of the proposed model and the existing models. It can be seen that the proposed model outperformed the existing models with ($R^2 = 0.80$). It shows an increase of 7% in (R^2) compared to the best performing nonlinear models (Lim et al. 2016), an 8% increase compared to the best performing models that were based on the equation of Richart et al. (1929) (Fahmy and Wu, 2010), and a 14% increase compared to the model of Touhari and Mitiche-Kettab (2016) that was based only on GFRP-wrapped concrete test results.

Similarly, the proposed model shows the smallest value (RMSE = 0.28) compared to the other models (Fig. 5.46) with 12% better than the best performing models that were based on the equation of Richart et al. (1929) (Bisby et al. 2005), 17% better than the best performing nonlinear models (Keshtegar et al. 2017), and 20% better than the model of Touhari and Mitiche-Kettab (2016).

On the other hand, the best (AAE = 0.21) is recorded for the proposed model compared to the existing models (Fig. 5.47) with 7% better than the best performing models that were based on the equation of Richart et al. (1929) (Bisby et al. 2005), 12% better than the best performing nonlinear models (Keshtegar et al. 2017), and 15% better than the model of Touhari and Mitiche-Kettab (2016).

Therefore, it can be concluded that the proposed model is more effective in predicting the ultimate strength of GFRP-wrapped concrete.

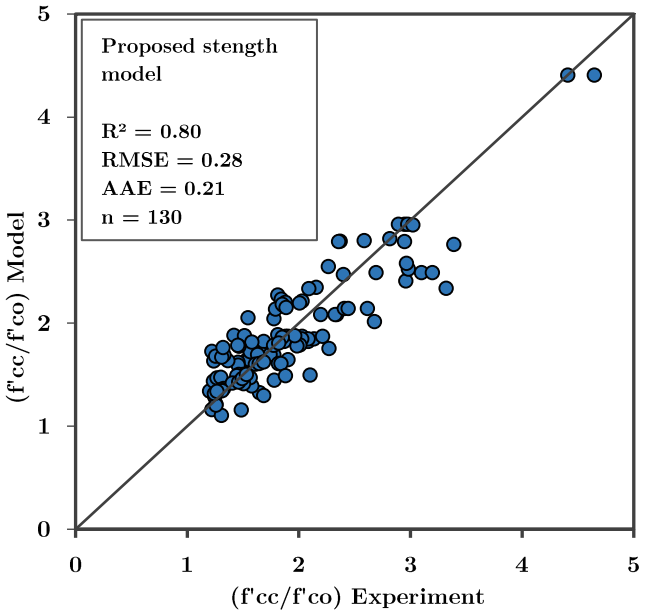

Figure 5.43 Performance of the proposed strength model

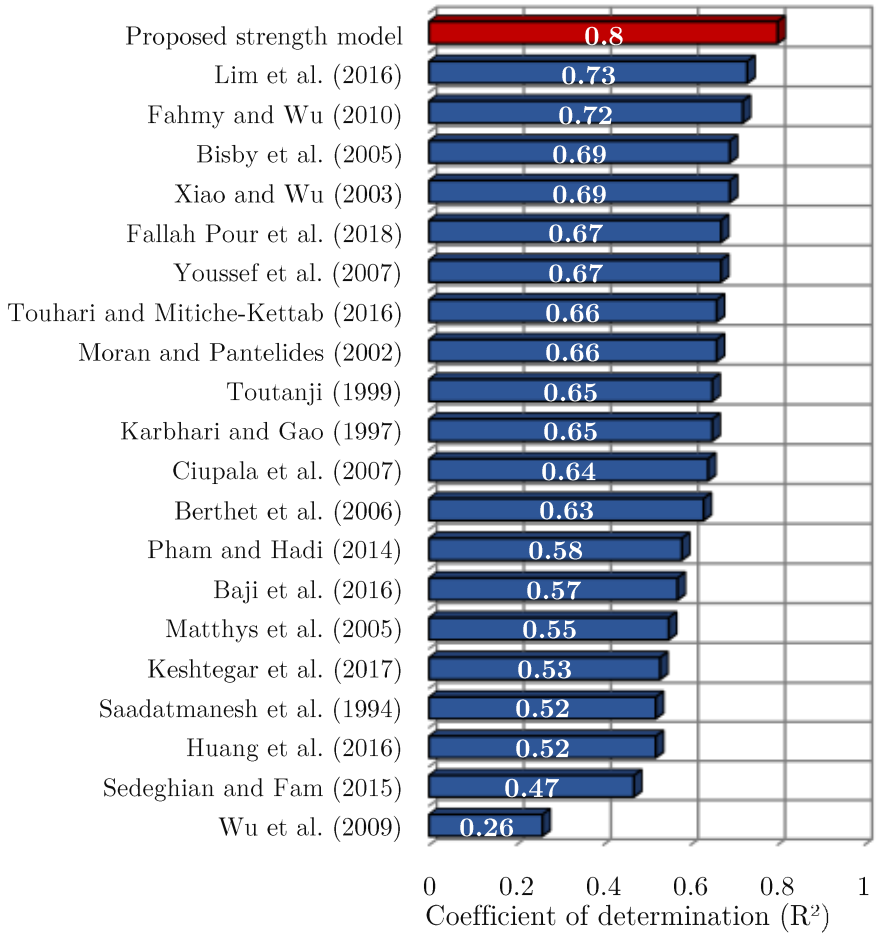

Figure 5.44 Coefficient of determination (R^2) of the proposed and existing strength models

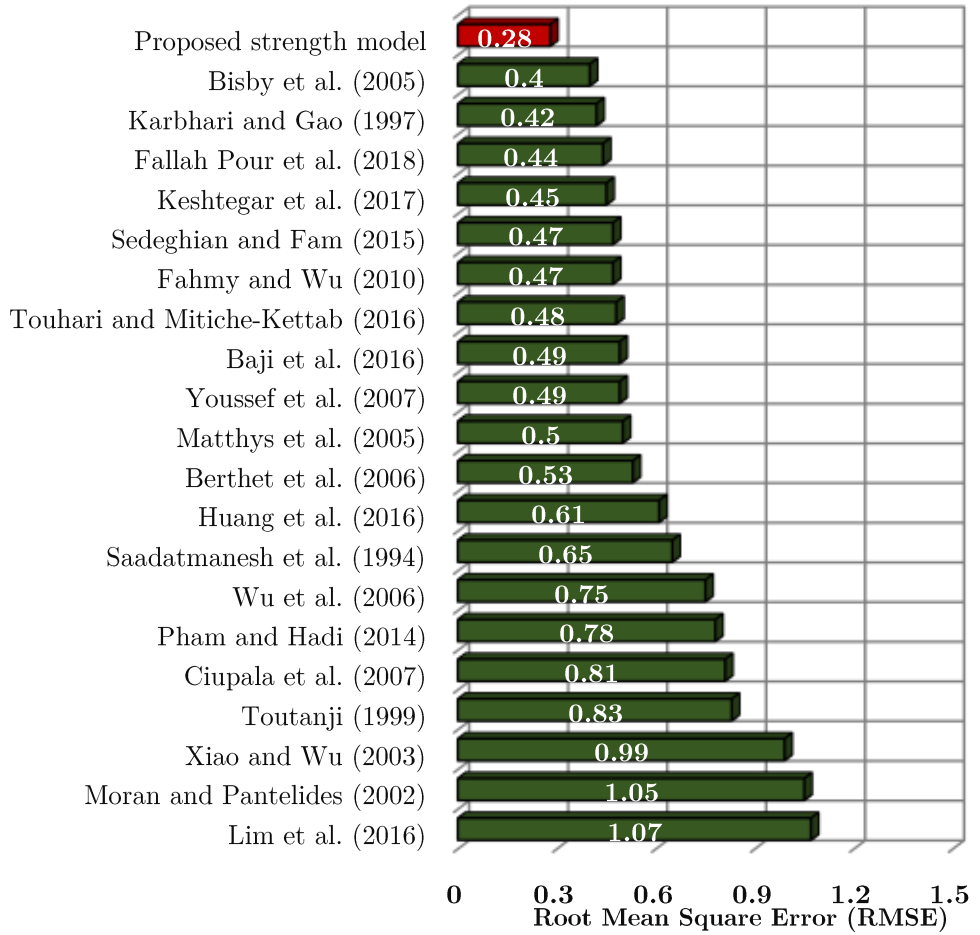

Figure 5.45 Root mean square error (RMSE) of the proposed and existing strength models

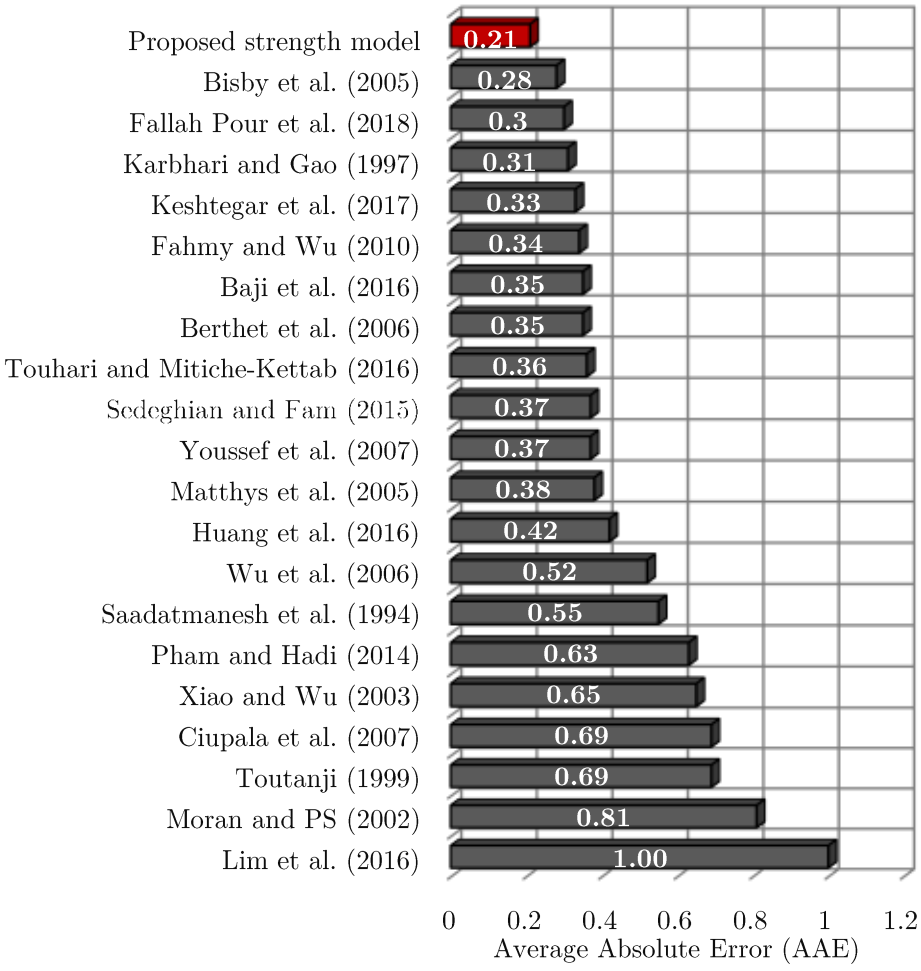

Figure 5.46 Average absolute error (AAE) of the proposed and existing strength models

5.4.3 Proposed ultimate strain model

Using the same procedure as in the proposed strength model, the rupture confining pressure ($f_{l,rup}$), the strain ratio (ρ_ε), the stiffness ratio (ρ_K), and the volumetric ratio of the FRP (ρ_f) are found to be the most influencing parameters on the ultimate strain of GFRP-wrapped concrete. The regression analysis resulted in the empirical relationship shown in Eq. (5.62).

$$\frac{\varepsilon_{cc}}{\varepsilon_{co}} = \frac{3.57\rho_K\rho_\varepsilon}{0.0842+\rho_f} + \frac{2.31}{0.31\,\rho_\varepsilon{}^2 - \rho_K} \tag{5.62}$$

As the strength model, the ultimate strain relationship can be expressed as the general form of the equation of Richart et al. (1929), where (c_2) and (k_2) are expressed in function of (ρ_ε, ρ_K, and ρ_f) as shown in Eq. (5.63):

$$\frac{\varepsilon_{cc}}{\varepsilon_{co}} = \left(\frac{2.31}{0.31\,\rho_\varepsilon{}^2 - \rho_K}\right) + \left(\frac{3.57}{0.0842+\rho_f}\right)\left(\frac{f_{l,rup}}{f'_{co}}\right) \tag{5.63}$$

5.4.4 Validation of the proposed strain model

The performance of the proposed strain model is illustrated in Fig. 5.48. Good fit of the experimental data is observed with (R^2 = 0.85), and small indices of errors (RMSE = 1.85, and AAE = 1.36) showing high accuracy and low scatter of the data around the reference line.

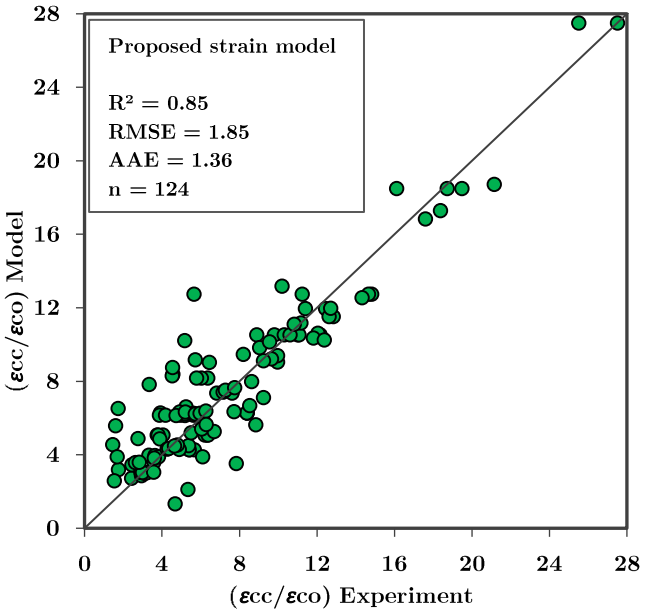

Figure 5.47 Performance of the proposed strain model

Figs. 49-51 illustrate comparisons of the statistical indices (R^2, RMSE, and AAE) of the proposed and existing strain models. As shown by the figures, the proposed model outperformed the assessed models by a significant margin.

It can be seen from Fig. 5.49 that the proposed model shows a better coefficient of determination (R^2 = 0.80) than the existing models. It shows an increase of 20% in (R^2) compared to the best performing nonlinear models (Ciupala et al., 2007), a 59% increase compared to the best performing models that were based on the equation of Richart et al. (1929) (Karbhari and Gao, 1997), and a 63% increase compared to the model of Touhari and Mitiche-Kettab (2016).

In Fig. 5.50, the proposed model shows the smallest value (RMSE = 1.85) compared to the other models with 128% better than the best performing nonlinear models (Ciupala et al. 2007) and 264% better than the model of Touhari and Mitiche-Kettab (2016) that was based on the equation of Richart et al. (1929).

In addition, the proposed model shows the best (AAE = 1.36) compared to the existing models (Fig. 5.47), with 94% better than the best performing nonlinear models (Ciupala et al. 2007) and 190% better than the model of Touhari and Mitiche-Kettab (2016) that was based on the equation of Richart et al. (1929).

Hence, it can be deduced that the proposed strain model is more efficient in predicting the ultimate strain of GFRP-wrapped concrete.

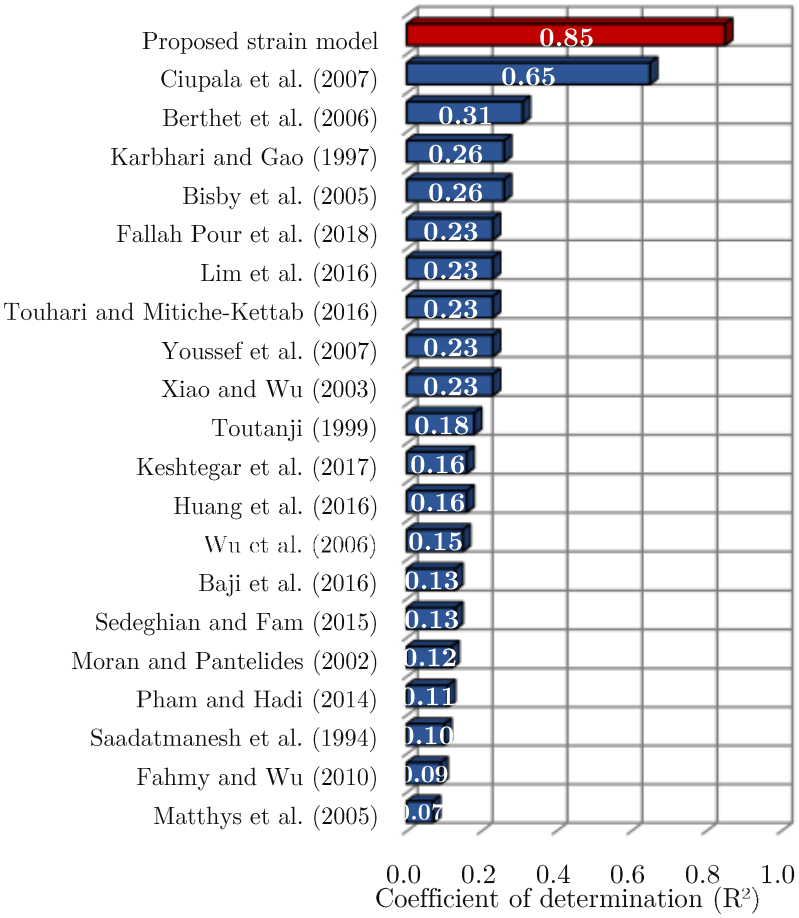

Figure 5.48 Coefficient of determination (R^2) of the proposed and existing strain models

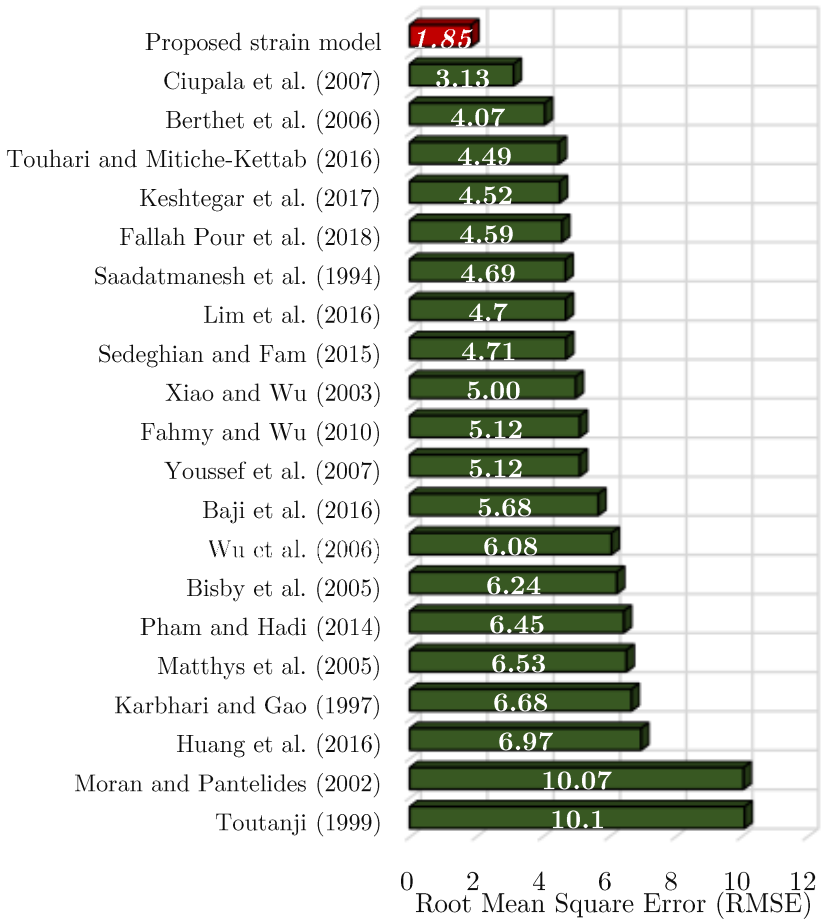

Figure 5.49 Root mean square error (RMSE) of the proposed and existing strain models

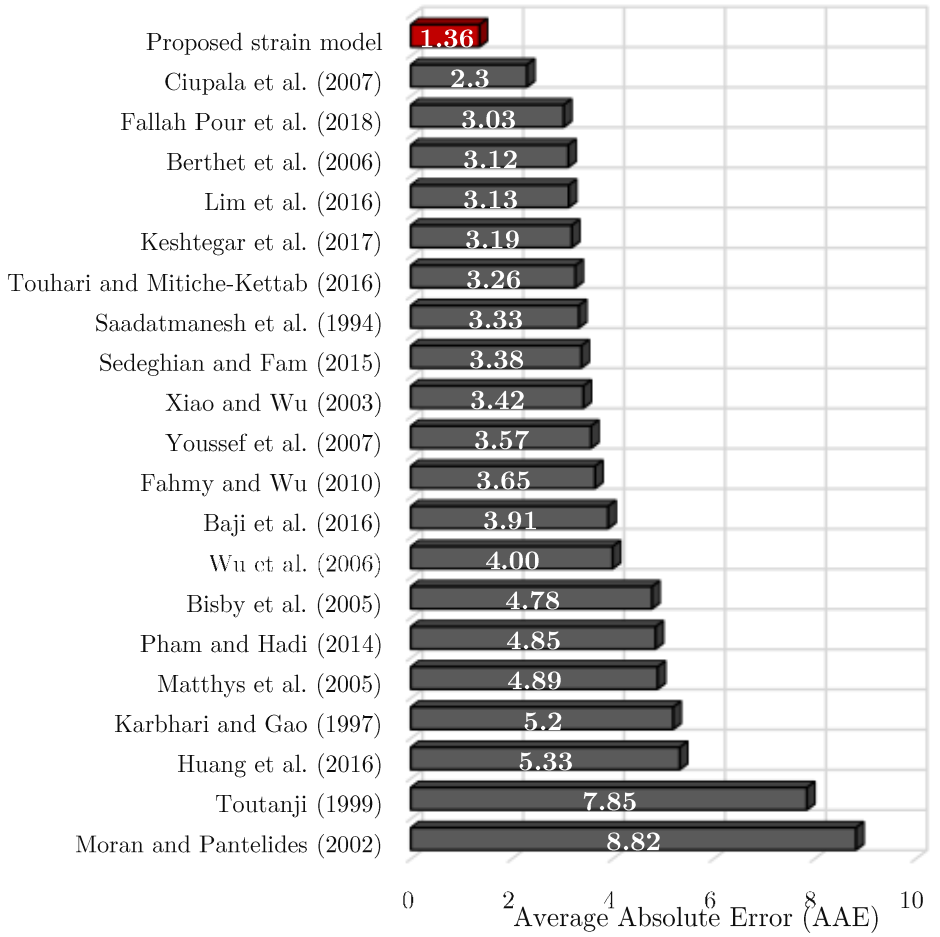

Figure 5.50 Average absolute error (AAE) of the proposed and existing strain models

5.5 Conclusion

In this chapter, twenty old and recent ultimate condition models of FRP-confined concrete were reviewed and assessed on the basis of the experimental database reported in Chapter 4 using three statistical indicators, namely: the coefficient of determination (R^2), the root mean square error (RMSE), and the average absolute error (AAE). Using regression analysis, new strength and strain models for GFRP-wrapped concrete were calibrated based on the experimental database using Eureqa® software. The following conclusions can be drawn:

- The predictions of the ultimate strain show much larger errors than the predictions of the ultimate stress. This can be attributed to the scatter in the measured experimental strains comparing to the experimental strengths.
- The models of Bisby et al. (2005), Fahmy and Wu (2010), and Fallah Pour et al. (2018) are the most accurate for the prediction of the ultimate strength. However, those of Berthet et al. (2006) and Ciupala et al. (2007) are the most accurate for the prediction of the ultimate strain.
- Although most of the existing models were developed from large experimental data, and most of the times are devoted to multiple kinds of FRP, and considering the fact that they use the rupture strain of the FRP instead of the ultimate strain provided by the manufacturer, which corresponds to the reality, they provide moderate accuracy, especially for the ultimate strain.
- The proposed models provide accurate predictions and show significantly better performance over the existing models, particularly for ultimate strains. Such improved models applied for concrete strengths up to 128 MPa can be considered as useful tools for future design applications

Chapter 6

Evaluation and proposition of stress-strain models for axially loaded GFRP-wrapped concrete

6.1 Introduction

This chapter provides an overview of the current state of the art on modeling the stress-strain relationship of FRP-confined concrete. Some previous design-oriented stress-strain models are reviewed and evaluated with existing experimental curves. A new stress-strain model for GFRP-wrapped concrete is proposed and verified with the existing models and the existing experimental curves.

6.2 Stress-strain models for FRP-confined concrete

For a rational and economical design of concrete structures retrofitted with FRP, a clear understanding of the behavior of FRP-confined concrete under axial and lateral loads is needed. In other words, the modeling of its complete stress-strain response (Parghi, 2016). The early studies have adopted the stress-strain relationships proposed for steel-confined concrete (Fardis & Khalili, 1981, 1982; Ahmad et al., 1991; Saadatmanesh et al., 1994). However, after realizing the distinct behavior of FRP-confined concrete, many researchers have studied the stress-strain response of FRP-confined concrete under concentric compression or axial and lateral loads of circular concrete columns and proposed descriptive models based on extensive experiments on FRP-confined concrete columns with different concrete strengths and FRP confining materials (Kwan et al., 2015).

The typical stress-strain curve of FRP-confined concrete under axial compression is shown in Fig. 6.1. At low axial strain, the FRP confining material is not activated, and the curve follows a similar pattern to that of unconfined concrete (Wu et al., 2006). With the increase of the axial load, the concrete follows two

different patterns depending on the confinement pressure provided by the FRP. When the confinement level is smaller than a certain confinement threshold, the concrete will not be effectively confined, and the axial stress gradually decreases after reaching its peak value until the rupture of the FRP. This response is known as strain-softening behavior. However, when the confinement level is higher than a certain confinement threshold, the concrete is effectively confined, and the stress continues to increase with a linear slope allowing to sustain additional compressive loads until failure of the FRP. This response is known as strain-hardening behavior (Ozbakkaloglu et al. (2013)).

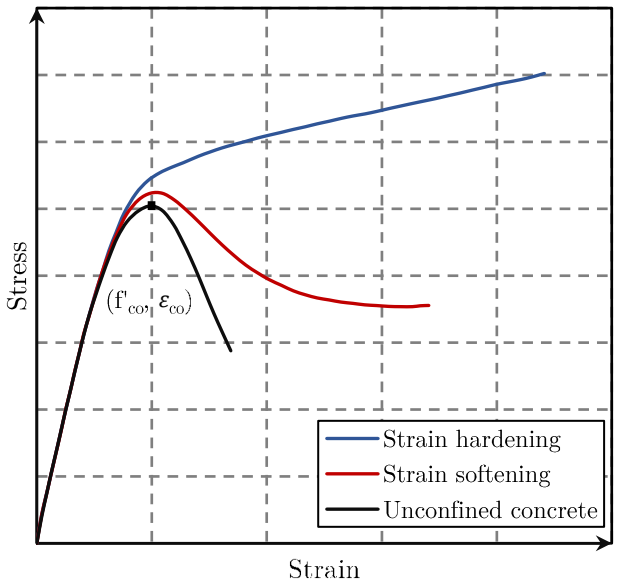

Figure 6.1 Typical stress-strain curve of FRP-confined concrete

Based on experimental observations, several researchers have suggested several criteria for the FRP confinement threshold. For instance, Mirmiran et al. (1997) suggested that enhancement in the compressive strength is expected if the confinement ratio is higher than 0.15 (i.e., $(f_l/f'_{co}) > 0.15$) for circular and rectangular concrete specimens. Spoelstra and Monti (1999) showed that a strain-softening behavior is expected when the (fl/f'co) is less than 0.07. Lam and Teng (2003) suggested that for $((f_{l,\ rup}/f'_{co}) \geq 0.07)$, the concrete can be considered sufficiently confined and exhibit an ascending second branch. Jiang and Teng (2007) differentiated between the sufficiently confined concrete with an ascending second branch, where they suggested that for $((f'_{cc}/f'_{co}) < 2)$ the concrete is considered moderately-confined, otherwise (i.e., $(f'_{cc}/f'_{co}) \geq 2$) it is considered heavily-confined concrete. Benzaid et al. (2010) reported that the concrete with $(f'_{co} \geq 50$ MPa) confined with FRP providing a confinement ratio $((f_l/f'_{co}) \leq 0.095)$ is considered insufficiently confined and exhibits a strain-softening response with reduced ductility. Ozbakkaloglu and Lim (2013) proposed a minimum threshold for the FRP stiffness to achieve a strain-hardening response $(E_l \geq f'^{1.65}_{co})$. Thereafter, Lim and Ozbakkaloglu (2014) established a new relationship for this

threshold using an exponential function of the unconfined concrete strength ($E_l \geq 73.7e^{0.027f'_{co}}$).

The majority of existing models can be classified as design-oriented models (DOMs) (Lam & Teng, 2003). In the following section, types of DOMs are presented.

6.2.1 Design-oriented stress-strain models

In DOMs, the stress-strain curve is described by simple closed-form equations derived based on regression analysis of the experimental data of FRP-confined concrete. The simplicity of the DOMs makes them suitable for direct use in design. However, the size, reliability, and parametric range of the test database highly affect their accuracy (Ozbakkaloglu et al., 2013). Most of the DOMs predict a strain-hardening response, whereas others (e.g., Xiao & Wu, 2000; Li et al., 2003; Binici, 2005; Teng et al., 2009; Wei and Wu, 2012; Kwan et al., 2015) can predict both strain-hardening and strain-softening response (Parghi, 2016).

A wide variety of DMOs were developed by researchers. After the early models that adopted the parabolic stress-strain curve of the steel or actively-confined concrete, bilinear stress-strain curves (Fig. 6.2) composed of two linear portions connected by a transition point (f'_{c1}, ε_{c1}) near the unconfined concrete have been adopted (e.g., Nanni & Bradford, 1995; Karbhari & Gao, 1997; 29Xiao & Wu, 2000). Where some models have simply defined (f'_{c1}, ε_{c1}) as the strength and strain of unconfined concrete (f'_{co}, ε_{co}).

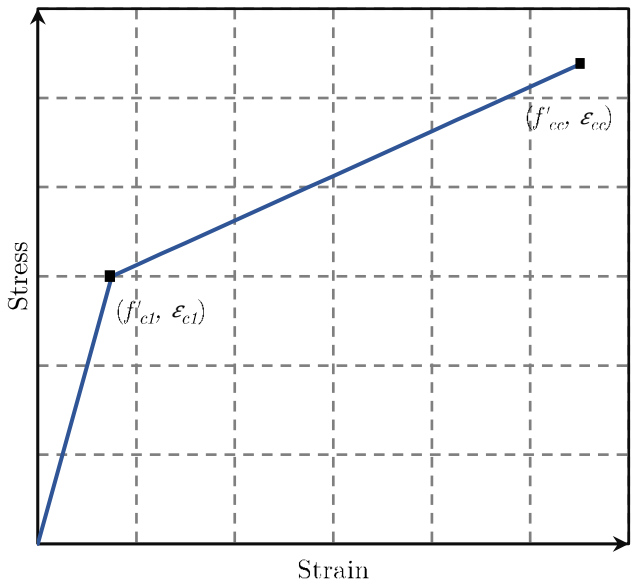

Figure 6.2 Bilinear stress-strain curve of FRP-confined concrete

Later, the bilinear model was improved by replacing the first linear portion with a parabolic one (Fig 6.3). Several researchers (e.g., Matthys et al., 2006; Youssef et al., 2007) have adopted Hognestad's parabola (1951) (Eq. (6.1)) to describe the

first branch of the stress-strain curve, while the second branch (Eq. (6.2)) remained linear up to the ultimate point (f'_{cc}, ε_{cc}).

$$f_c = f'_{c1}\left[2\left(\frac{\varepsilon_c}{\varepsilon_{c1}}\right) - \left(\frac{\varepsilon_c}{\varepsilon_{c1}}\right)^2\right] \quad if \ \ \varepsilon_c \le \varepsilon_{c1} \tag{6.1}$$

$$f_c = f'_{c1} + E_2(\varepsilon_c - \varepsilon_{c1}) \quad if \ \ \varepsilon_c > \varepsilon_{c1} \tag{6.2}$$

Where,

$$E_2 = \frac{f'_{cc} - f'_{c1}}{\varepsilon_{cc} - \varepsilon_{c1}} \tag{6.3}$$

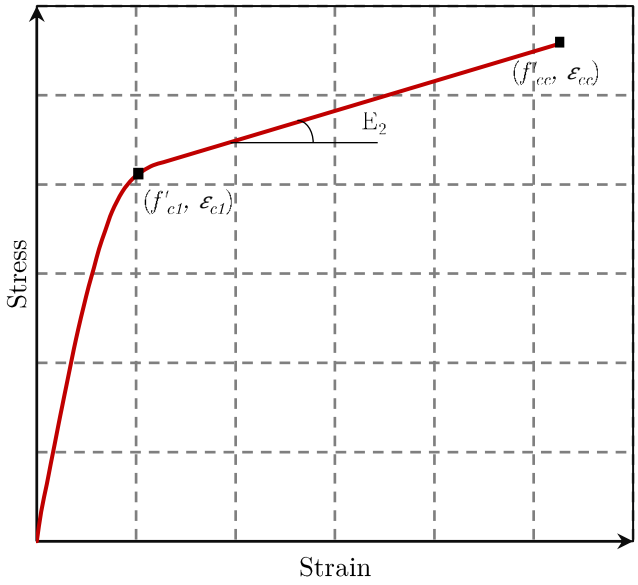

Figure 6.3 Parabolic-linear stress-strain curve of FRP-confined concrete

In addition, a wide range of studies have adopted for the two parts of the stress-strain relationship the equation proposed by Richard and Abbott (1975) (Eq. (6.4)) (e.g., Wu & Wang, 2010; Yu & Teng, 2011), while others have modified this equation to establish a new form of stress-strain model (e.g., Yan & Pantelides, 2007; Wu et al., 2009).

$$f_c = \frac{(E_1 - E_2)\varepsilon_c}{\left[1 + \left(\frac{(E_1 - E_2)\varepsilon_c}{f_o}\right)^n\right]^{\frac{1}{n}}} + E_2\varepsilon_c \tag{6.4}$$

Four parameters were used in this equation for the description of the stress-strain curve (Fig. 6.4). The elastic modulus (E_1), where most of the models have adopted the expression given by ACI 318-95 (Eq. (6.5)), the second branch slope (E_2), a shape parameter (n) to control the transition between the two portions of the curve (Eq. (6.6)), and the stress (f_o) corresponds to the intercept of the second portion of the curve with the stress axis (Eq. (6.7)).

$$E_1 = 4730\sqrt{f'_{co}} \tag{6.5}$$

$$n = 1 + \frac{1}{\frac{E_1}{E_2} - 1} - E_2\varepsilon_{cc} \tag{6.6}$$

$$f_o = f'_{cc} - E_2\varepsilon_{cc} \tag{6.7}$$

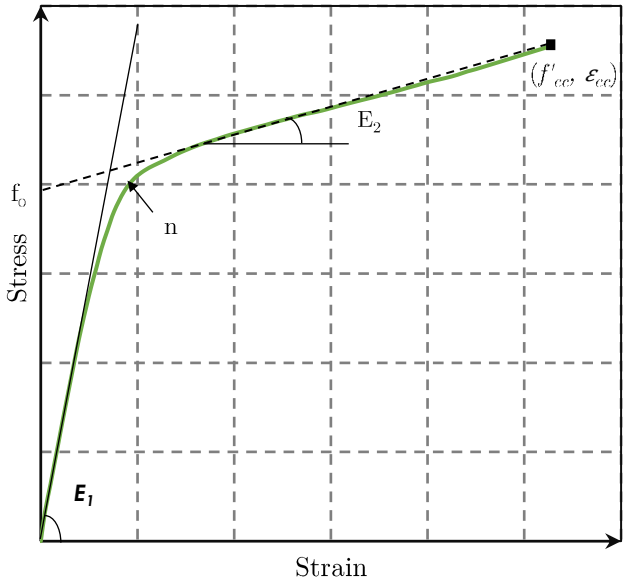

Figure 6.4 Stress-strain curve based on Richard and Abbott's (1975) equation

On the other hand, other models were adopted the stress-strain model developed by Toutanji (1999) (Eq. (6.8)), which takes its origin from expression developed by Sargin (1971) and then adopted by Ahmad and Shah (1982) for concrete confined by steel spirals (Fig. 6.5).

$$f_c = \frac{A\varepsilon_c}{1 + C\varepsilon_c + D{\varepsilon_c}^2} \tag{6.8}$$

Where,

$$A = E_1 \tag{6.9}$$

$$C = \frac{E_1}{{f'}_{c1}} - \frac{2}{\varepsilon_{c1}} + \frac{E_1E_2\varepsilon_{c1}}{{f'}_{c1}^{\,2}} \tag{6.10}$$

$$D = \frac{1}{{\varepsilon_{c1}}^2} - \frac{E_1E_2}{{f'}_{c1}^{\,2}} \tag{6.11}$$

E_1 = slope of the initial ascending branch;

E_2 = slope of the second branch taken immediately after the initial peak stress (f'_{c1}) is reached.

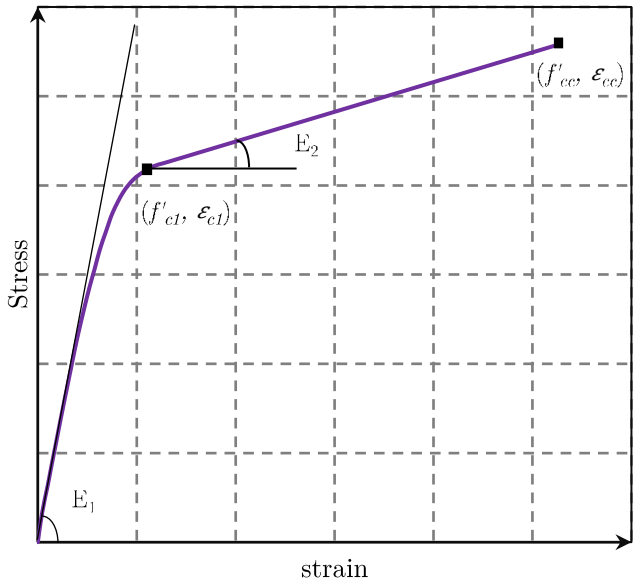

Figure 6.5 Stress-strain curve based on Toutanji's (1999) equation

6.3 Review of some design-oriented stress-strain models

In the following, old and recent existing (DOMs) of circular FRP-confined concrete exhibiting a strain-hardening behavior are reviewed.

6.3.1 Lam and Teng (2003)

Lam and Teng (2003) proposed a stress-strain equation to describe each portion of the stress-strain curve of FRP-confined concrete (Fig. 6.6). A parabolic equation and a linear equation were used for the first and second portions, respectively (Eqs. (6.12) and (6.13)).

$$f_c = E_1\varepsilon_c - \frac{(E_1 - E_2)^2}{4f_o}{\varepsilon_c}^2 \qquad if\ \ 0 \le \varepsilon_c \le \varepsilon_{c1} \tag{6.12}$$

$$f_c = f_o + E_2\varepsilon_c \qquad if\ \ \varepsilon_{c1} \le \varepsilon_c \le \varepsilon_{cc} \tag{6.13}$$

Where,

E_1 = the elastic modulus of the unconfined concrete, approximated as:

$$E_1 = 4730\sqrt{f'_{co}}\ \text{(GPa)} \tag{6.14}$$

E_2 = the slope of the linear portion, given by:

$$E_2 = (f'_{cc} - f'_{co})/\varepsilon_{cc}\ \ (GPa) \tag{6.15}$$

f_o = the stress at the intersection of the linear portion with the stress axis. For simplicity, it was suggested to be f'_{co} (MPa);

ε_{c1} = the axial strain at which the parabolic portion meets the linear portion.

$$\varepsilon_{c1} = 2f'_{co}/(E_1 - E_2) \tag{6.16}$$

Where for the ultimate condition, the following expressions were proposed:

$$\frac{f'_{cc}}{f'_{co}} = 1 + 3.3\left(\frac{f_{l,rup}}{f'_{co}}\right) \tag{6.17}$$

$$\frac{\varepsilon_{cc}}{\varepsilon_{co}} = 1.75 + 5.53\left(\frac{\varepsilon_{h,rup}}{\varepsilon_{co}}\right)^{0.45}\left(\frac{f_{l,rup}}{f'_{co}}\right) \tag{6.18}$$

Where,

$f_{l,rup}$ = the lateral confining pressure at the rupture of the FRP (MPa);

$\varepsilon_{h,rup}$ = the hoop strain at the rupture of the FRP;

ε_{co} = the axial strain corresponding to the unconfined concrete strength, suggested being: 0.002.

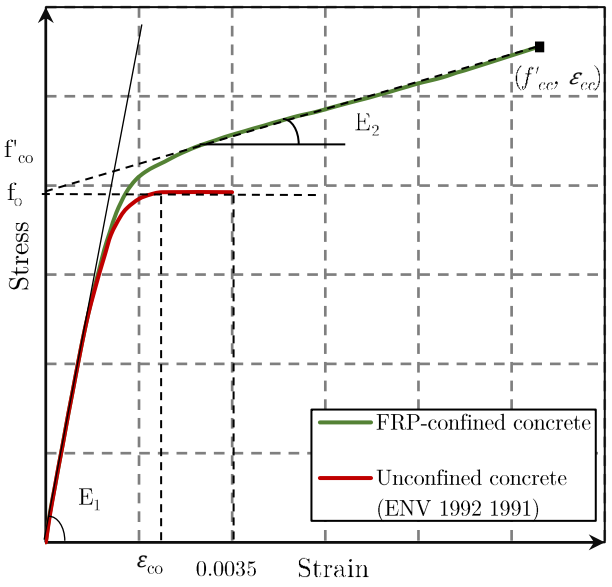

Figure 6.6 Stress-strain curve of FRP-confined concrete (Lam & Teng, 2003)

The model was developed based on normal strength concrete specimens with unconfined concrete strength ranges from 26.2 to 55.2 MPa, in which some specimens have an (h/d) ratio larger than 3.

6.3.2 Xiao and Wu (2003)

Xiao and Wu (2003) proposed a stress-strain equation for FRP-confined concrete based on the equation of Richard and Abbott (1975) (Eq. (6.19)). The model was

based on experimental data on concrete cylinders confined with CFRP and GFRP jackets having unconfined concrete strength ranging from 31.3 to 64.2 MPa.

$$f_c = \frac{(E_1 - E_2)\varepsilon_c}{\left[1 + \left(\frac{(E_1 - E_2)\varepsilon_c}{f_o}\right)^n\right]^{\frac{1}{n}}} + E_2\varepsilon_c \tag{6.19}$$

Where,

E_1 = the slope of the first branch of the curve, determined as:

$$E_1 = 4733\sqrt{f'_{co}}\,(GPa) \tag{6.20}$$

E_2 = the slope of the first branch of the curve, determined as:

$$E_2 = k_1 E_l \mu_{tu}\,(GPa) \tag{6.21}$$

Where (k_1) and (μ_{tu}) were determined based on regression analysis of the experimental data as:

$$k_1 = 4.1 - 0.45\left(\frac{E_l}{f'^{\,2}_{co}}\right)^{-1.4} \tag{6.22}$$

$$\mu_{tu} = 10\left(\frac{E_l}{f'_{co}}\right)^{-0.9} \tag{6.23}$$

E_l = the stiffness of the FRP in the hoop direction (MPa);

f_o = the stress at the intersection of the linear portion with the stress axis:

$$f_o = (1 + 4.8 \times 10^{-4} E_l) f'_{co}\,(MPa) \tag{6.24}$$

n = the curve factor suggested being 2.

The endpoint of the stress-strain curve was determined by the following equations (Eqs. (6.25) and (6.26)):

$$\frac{f'_{cc}}{f'_{co}} = 1 + \left(4.1 - 0.45\left(\frac{E_l}{f'^{\,2}_{co}}\right)^{-1.4}\right)\left(\frac{f_{l,rup}}{f'_{co}}\right) \tag{6.25}$$

$$\frac{\varepsilon_{cc}}{\varepsilon_{co}} = \frac{\varepsilon_{h,rup} - 0.00047}{10\varepsilon_{co}} \times \left(\frac{E_l}{f'_{co}}\right)^{0.9} \tag{6.26}$$

6.3.3 Matthys et al. (2006)

Matthys et al. (2005) proposed a stress-strain model for FRP-confined concrete based on experimental data. The equation of Hognestad (1951) (Eq. (6.27)) was used to model the first portion of the curve, which terminating at the point of compressive strength of unconfined concrete. While the second portion was approximated by a linear equation (Eq. (6.28)) ending with the ultimate stress and strain (Eqs. (6.32) and (6.33)).

$$f_c = f'_{c1}\left[2\left(\frac{\varepsilon_c}{\varepsilon_{c1}}\right) - \left(\frac{\varepsilon_c}{\varepsilon_{c1}}\right)^2\right] \qquad if\ \ \varepsilon_c \le \varepsilon_{c1} \tag{6.27}$$

$$f_c = f'_{c1} + E_2(\varepsilon_c - \varepsilon_{c1}) \qquad if\ \ \varepsilon_c > \varepsilon_{c1} \tag{6.28}$$

Where,

$$f'_{c1} = f'_{co} \tag{6.29}$$

$$\varepsilon_{c1} = \varepsilon_{co} \tag{6.30}$$

$$E_2 = \frac{f'_{cc} - f'_{c1}}{\varepsilon_{cc} - \varepsilon_{c1}} \tag{6.31}$$

$$\frac{f'_{cc}}{f'_{co}} = 1 + 3.5\left(\frac{f_{l,rup}}{f'_{co}}\right)^{0.85} \tag{6.32}$$

$$\frac{\varepsilon_{cc}}{\varepsilon_{co}} = 1 + (310.57\varepsilon_f + 1.9)\left(\frac{f'_{cc}}{f'_{co}} - 1\right) \tag{6.33}$$

6.3.4 Youssef et al. (2007)

Based on extensive experimental data, including large-scale circular, square, and rectangular short columns confined by CFRP and GFRP jackets under compression, Youssef et al. (2007) developed a stress-strain model for FRP-confined concrete. The authors used for modeling the first branch of the stress-strain curve a similar approach used by Hoshikuma et al. (1997) to develop a confinement model for concrete confined by transverse steel based on a polynomial function and a set of boundary conditions. The equation of the first portion of the curve is expressed in (Eq. (6.34)). While the second portion of the curve was modeled as a straight line up to failure (Eq. (6.35)) (Fig. 6.7).

$$f_c = E_1\varepsilon_c\left[1 - \frac{1}{n}\left(\frac{\varepsilon_c}{\varepsilon_{c1}}\right)^{n-1}\right] \qquad if\ \ 0 \le \varepsilon_c \le \varepsilon_{c1} \tag{6.34}$$

$$f_c = f_{c1} + E_2(\varepsilon_c - \varepsilon_{c1}) \qquad if\ \ \varepsilon_{c1} \le \varepsilon_c \le \varepsilon_{cc} \tag{6.35}$$

Where,

$$n = \frac{E_1\varepsilon_{c1}}{E_1\varepsilon_{c1} - f_{c1}} \tag{6.36}$$

The parameters of the model such as the first and second slope (E_1 and E_2), the transition point (f'_{c1}, ε_{c1}) between the first and second branch, and the ultimate stress and strain (f'_{cc}, ε_{cc}) were determined using regression analysis of the experimental data as shown in (Eqs. (6.37)-(6.42)):

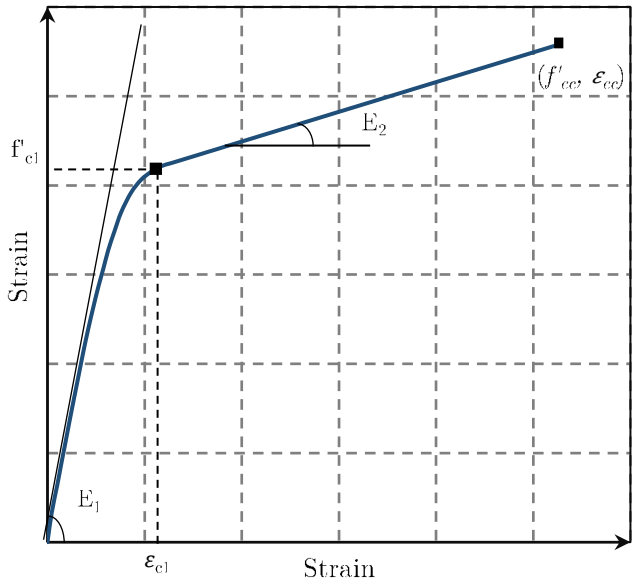

Figure 6.7 Stress-strain curve for FRP-confined concrete (Youssef et al. 2007)

$$E_1 = 4700\sqrt{f'_{co}} \tag{6.37}$$

$$E_2 = \frac{f'_{cc} - f'_{c1}}{\varepsilon_{cc} - \varepsilon_{c1}} \tag{6.38}$$

$$\frac{f'_{c1}}{f'_{co}} = 1 + 3\left(\frac{\rho_f E_f \varepsilon_f}{f'_{co}}\right) \tag{6.39}$$

$$\varepsilon_{c1} = 0.002748 + 0.1169\left(\frac{\rho_f E_f \varepsilon_f}{f'_{co}}\right)^{\frac{6}{7}}\left(\frac{f_f}{E_f}\right)^{\frac{1}{2}} \tag{6.40}$$

$$\frac{f'_{cc}}{f'_{co}} = 1 + 2.25\left(\frac{f_l}{f'_{co}}\right)^{1.25} \tag{6.41}$$

$$\frac{\varepsilon_{cc}}{\varepsilon_{co}} = \frac{0.003368}{\varepsilon_{co}} + \frac{0.2590}{\varepsilon_{co}}\left(\frac{f_f}{E_f}\right)^{\frac{1}{2}}\left(\frac{f_l}{f'_{co}}\right) \tag{6.42}$$

Where,

ρ_f = the volumetric ratio of the FRP;

E_f = the elasticity modulus of the FRP (GPa);

ε_f = the strain of the FRP in the hoop direction, taken as 0.002;

f_f = the tensile strength of the FRP (MPa);

f_l = the ultimate confining pressure (MPa).

6.3.5 Teng et al. (2009)

Teng et al. (2009) proposed a stress-strain model for FRP-confined concrete under compression by refining the stress-strain model initially proposed by Lam and Teng (2003) basing on larger experimental data. The first portion was modeled by a parabolic equation (Eq. (6.43)), while the second portion was modeled by a linear equation (Eq. (6.44)).

$$f_c = E_1\varepsilon_c - \frac{(E_1 - E_2)^2}{4f'_{co}}\varepsilon_c{}^2 \qquad if \;\; 0 \le \varepsilon_c \le \varepsilon_{c1} \tag{6.43}$$

$$f_c = f'_{co} + E_2\varepsilon_c \qquad if \;\; \varepsilon_{c1} < \varepsilon_c \le \varepsilon_{cc} \;\; and \;\; \rho_K \ge 0.01 \tag{6.44}$$

Where,

The slope of the parabola (E_1) at zero axial strain was taken as the elastic modulus of unconfined concrete given by ACI-318 (2005) (Eq. (6.45)), and the slope of the linear second portion (E_2) was given by (Eq. (6.46)):

$$E_1 = 4730\sqrt{f'_{co}} \tag{6.45}$$

$$E_2 = \frac{f'_{cc} - f'_{co}}{\varepsilon_{cc}} \tag{6.46}$$

The first portion and the second portion were related smoothly at (ε_{c1}) (Eq. (6.47)) and ended at the ultimate stress and ultimate strain (Eqs. (6.48) and (6.49)).

$$\varepsilon_{c1} = \frac{2f'_{co}}{E_1 - E_2} \tag{6.47}$$

$$\frac{f'_{cc}}{f'_{co}} = 1 + 3.5(\rho_K - 0.01)\rho_\varepsilon\,, \qquad if \;\; \rho_K \ge 0.01 \tag{6.48}$$

$$\frac{\varepsilon_{cc}}{\varepsilon_{co}} = 1.75 + 6.5\,\rho_K{}^{0.8} \times \rho_\varepsilon{}^{1.45} \tag{6.49}$$

Where,

ρ_K = the stiffness ratio of the FRP to the concrete;

ρ_ε = the strain ratio of the FRP to the concrete;

ε_{co} = the unconfined concrete strain (taken as 0.002).

6.3.6 Pellegrino and Modena (2010)

The model of Pellegrino and Modena 2010 was based on the four-parameters model of Richard and Abbott (1975) (Eq. (6.50)).

$$f_c = \frac{(E_1 - E_2)\varepsilon_c}{\left[1 + \left(\frac{(E_1 - E_2)\varepsilon_c}{f_o}\right)^n\right]^{\frac{1}{n}}} + E_2\varepsilon_c \tag{6.50}$$

Where,

The slope of the first and second branch (E_1, E_2) and the stress (f_o) were respectively shown in (Eqs. (6.51)-(6.53)):

$$E_1 = 4730\sqrt{f'_{co}} \tag{6.51}$$

$$E_2 = \frac{f'_{cc} - f'_{co}}{\varepsilon_{cc} - \varepsilon_{co}} \tag{6.52}$$

$$f_o = f'_{cc} - E_2\varepsilon_{cc} \tag{6.53}$$

The shape parameter (n) (Eq. (6.54)) was expressed as a function of the secant modulus (E_{co}) (Eq. (6.55)) that corresponds to the slope of the line passing from the origin and the point in which the slope of the curve changed.

$$n = 1 + \frac{1}{(E_1/E_{co}) - 1} \tag{6.54}$$

$$E_{co} = \frac{f'_{co}}{\varepsilon_{co}} \tag{6.55}$$

The ultimate stress and the ultimate strain were determined as shown in (Eqs. (6.56) and (6.57)).

$$\frac{f'_{cc}}{f'_{co}} = 1 + 3.55\left(\frac{f_{l,rup}}{f'_{co}}\right)^{0.85} \tag{6.56}$$

$$\frac{\varepsilon_{cc}}{\varepsilon_{co}} = 2 + 23\left(\frac{f_{l,rup}}{f'_{co}}\right) \tag{6.57}$$

6.3.7 Fahmy and Wu (2010)

An analytical model has been developed by Fahmy and Wu (2010) to predict the stress-strain response of FRP-confined concrete columns with strain hardening behavior. The model was based on experimental data of cylindrical concrete specimens confined with CFRP, GFRP, and AFRP composite material. The stress-strain response was described by two equations. The first was parabolic (Eq. (6.58)) taken from Lam and Teng's (2003) model, and the second was linear (Eq. (6.59)) with a slope (E_2) that intersects the stress axis at the unconfined concrete strength (f'_{co}).

$$f_c = E_1\varepsilon_c - \frac{(E_1 - E_2)^2}{4f'_{co}}\varepsilon_c{}^2 \qquad if\ \ 0 \le \varepsilon_c \le \varepsilon_{c1} \tag{6.58}$$

$$f_c = f_o + E_2\varepsilon_c \qquad if\ \ \varepsilon_{c1} < \varepsilon_c \le \varepsilon_{cc} \tag{6.59}$$

Where,

(E_1) defines the elastic modulus of unconfined concrete (Eq. (6.60)), and (E_2) (Eqs. (6.61) and (6.62)) is the slope of the second branch is described using both unconfined concrete strength (f'_{co}) and the confinement modulus of FRP (E_l).

$$E_1 = 4730\sqrt{f'_{co}} \tag{6.60}$$

$$E_2 = m_2\left(245.61{f'_{co}}^{m_1} + 0.6728E_l\right) \tag{6.61}$$

$$\begin{cases} m_1 = 0.5, \ m_2 = 0.83, & f'_{co} \le 40MPa \\ m_1 = 0.2, \ m_2 = 1.73, & f'_{co} > 40MPa \end{cases} \tag{6.62}$$

The stress (f_o) is the reference plastic stress taken as the compressive strength of unconfined concrete (f'_{co}).

(f'_{c1}) and (ε_{c1}) define the transition point, taken from Lam and Teng's (2003) model as shown in (Eqs. (6.63) and (6.64)):

$$f_{c1} = E_1\varepsilon_{c1} - \frac{(E_1 - E_2)^2}{4f'_{co}}{\varepsilon_{c1}}^2 \tag{6.63}$$

$$\varepsilon_{c1} = \frac{2f'_{co}}{E_1 - E_2} \tag{6.64}$$

The second ascending branch of the stress-strain curve terminates at the compressive strength of FRP-confined concrete (f'_{cc}) (Eqs. (6.65) and (6.66)) and its corresponding axial strain (ε_{cc}) (Eq. (6.67)).

$$\frac{f'_{cc}}{f'_{co}} = 1 + 4.5\left(\frac{{f_l}^{0.7}}{f'_{co}}\right) \qquad for\ f'_{co} \le 40MPa \tag{6.65}$$

$$\frac{f'_{cc}}{f'_{co}} = 1 + 3.75\left(\frac{{f_l}^{0.7}}{f'_{co}}\right) \qquad for\ f'_{co} > 40MPa \tag{6.66}$$

$$\frac{\varepsilon_{cc}}{\varepsilon_{co}} = \frac{f'_{cc} - f'_{co}}{E_2\varepsilon_{co}} \tag{6.67}$$

6.3.8 Kwan et al. (2015)

The model developed by Attard and Setunge (1996) shown in (Eq. (6.68)), which has been shown to be applicable to a wide range of concrete strength (from 20 to 130 MPa), was adopted by Kwan et al. (2015) for the modeling the stress-strain response of FRP-confined concrete. The accuracy of the model was verified with 174 FRP-confined concrete specimens test results available from the literature.

$$f_c = \left(\frac{A(\varepsilon_c/\varepsilon_{cc}) + B(\varepsilon_c/\varepsilon_{cc})^2}{1 + (A-2)(\varepsilon_c/\varepsilon_{cc}) + (B+1)(\varepsilon_c/\varepsilon_{cc})^2}\right)f'_{cc} \tag{6.68}$$

Where,

(A) and (B) are constants defining the shape of the stress-strain curve (Eqs. (6.69) and (6.70)):

$$A = \frac{E_c\varepsilon_{cc}}{f'_{cc}} \tag{6.69}$$

$$B = \frac{(A-1)^2}{0.55} - 1 \tag{6.70}$$

The authors claimed that the formulas derived by Xiao et al. (2010) for the ultimate axial stress (f'_{cc}) and its corresponding axial strain (ε_{cc}) (Eqs. (6.71) and (6.72)) based on the general form of the equations of Richart et al. (1929) provide accurate predictions comparing to the original formulas given by Attard and Setunge (1996), and hence they adopted these equations in their model.

$$\frac{f'_{cc}}{f'_{co}} = 1 + 3.24\left(\frac{f_l}{f'_{co}}\right)^{0.8} \tag{6.71}$$

$$\frac{\varepsilon_{cc}}{\varepsilon_{co}} = 1 + 17.4\left(\frac{f_l}{f'_{co}}\right)^{1.06} \tag{6.72}$$

6.3.9 Fallah Pour et al. (2018)

A model to predict the complete stress-strain curve of FRP-confined concrete was developed by Fallah Pour et al. (2018). The model used the expression given by Popovics (1973) for the first portion of the stress-strain curve (Eq. (6.73)) and a linear equation to model the second portion (Eq. (6.74)). The model is applicable to a wide range of concrete compressive strengths (f'_{co}) ranging from 10 to 120 MPa.

$$f_c = \frac{f'_{c1}\left(\frac{\varepsilon_c}{\varepsilon_{c1}}\right)n}{n - 1 + \left(\frac{\varepsilon_c}{\varepsilon_{c1}}\right)^n} \qquad if\ \ 0 \le \varepsilon_c \le \varepsilon_{c1} \tag{6.73}$$

$$f_c = f'_{c1} + E_2(\varepsilon_c - \varepsilon_{c1}) \qquad if\ \ \varepsilon_{c1} < \varepsilon_c \le \varepsilon_{cc} \tag{6.74}$$

Where,

n = a term used to define the concrete brittleness proposed by Carreira and Chu (1985) (Eq. (6.75)).

$$n = E_1 / \left(E_1 - \frac{f'_{c1}}{\varepsilon_{c1}}\right) \tag{6.75}$$

Where,

$$E_1 = 4400\sqrt{f'_{co}}\ (MPa) \tag{6.76}$$

E_2 = the slope of the second branch of the stress-strain curve (Eq. (6.77)).

$$E_2 = \frac{f'_{cc} - f'_{c1}}{\varepsilon_{cc} - \varepsilon_{c1}} \tag{6.77}$$

The transition point (f'_{c1}, ε_{c1}) between the first and second portion of the curve and the ultimate point (f'_{cc}, ε_{cc}) were derived based on large experimental data of CFRP, GFRP, and AFRP concrete specimens using regression analysis (Eqs. (6.78)-(6.81)).

$$f'_{c1} = f'_{co} + 0.007E_l \tag{6.78}$$

$$\varepsilon_{c1} = \varepsilon_{co}\left(1 + 0.024\frac{E_l}{f'_{co}}\right) \tag{6.79}$$

$$\frac{f'_{cc}}{f'_{co}} = 1 + \frac{(2.5 - 0.01f'_{co})E_l\varepsilon_f}{f'_{co}} \tag{6.80}$$

$$\frac{\varepsilon_{cc}}{\varepsilon_{co}} = 1.5 + (0.3 - 0.001f'_{co})\left(\frac{E_l}{f'_{co}}\right)^{0.75}\frac{{\varepsilon_f}^{1.35}}{\varepsilon_{co}} \tag{6.81}$$

6.4 Proposed stress-strain model for GFRP-wrapped concrete

In this section, a new design-oriented stress-strain model for concrete sufficiently confined by external GFRP wraps is proposed. The model is developed based on the behavior observed from several groups of GFRP-confined specimens available from the literature. The accuracy and the validity of the model are checked against available experimental data and compared to the old and recent existing models of FRP-confined concrete.

6.4.1 Mathematical equation

In this study, the stress-strain curve of FRP-confined concrete with a strain-hardening response is approximated by a parabolic-ascending linear shape (i.e., the first portion is modeled by a parabolic expression, and the second portion by a linear expression with a positive slope). The proposed model is based on the following assumptions:

(a) the initial slope of the parabola at ($\varepsilon_c = 0$) is not affected by the presence of the FRP, and it depends only on the properties of the concrete;
(b) the second linear portion of the stress-strain curve connects to the first portion smoothly with the same slope at a transition point (f'_{c1}, ε_{c1}) different from the unconfined concrete (f'_{co}, ε_{co});
(c) the transition point (f'_{c1}, ε_{c1}) is influenced by the presence of the FRP, and it is different from the unconfined concrete (f'_{co}, ε_{co});
(d) the linear second portion ends at the ultimate point (f'_{cc}, ε_{cc}) determined in Chapter 5 and intercepts the stress axis at the stress (f_o).

These assumptions can be interpreted as shown in the following relationships:

In the first portion:

- $For\ \ 0 \le \varepsilon_c \le \varepsilon_{c1}$

$$F_1 = f_c = a{\varepsilon_c}^2 + b\varepsilon_c + c \tag{6.82}$$

$$F_1 = 0 \qquad if\ \ \varepsilon_c = 0 \tag{6.83}$$

$$\frac{df_c}{d\varepsilon_c} = E_1 \quad if\ \ \varepsilon_c = 0 \tag{6.84}$$

$$\frac{df_c}{d\varepsilon_c} = E_2 \quad if\ \ \varepsilon_c = \varepsilon_{c1} \tag{6.85}$$

In the second portion:

- $For\ \ \varepsilon_{c1} \leq \varepsilon_c \leq \varepsilon_{cc}$

$$F_2 = f_c = a'\varepsilon_c + b' \tag{6.86}$$

$$a' > 0 \tag{6.87}$$

$$\frac{df_c}{d\varepsilon_c} = E_2 \qquad if\ \ \varepsilon_c = \varepsilon_{c1} \tag{6.88}$$

$$f_c = f_{cc} \qquad if\ \ \varepsilon_c = \varepsilon_{cc} \tag{6.89}$$

$$F_2 = f_c = f_o \qquad if\ \ \varepsilon_c = 0 \tag{6.90}$$

At the transition point:

$$F_1 = F_2 \qquad if\ \ \varepsilon_c = \varepsilon_{c1} \tag{6.91}$$

Based on these assumptions, the following relationships can be drawn:

Equation (6.83) implies:

$$c = 0 \tag{6.92}$$

Equation (6.84) implies:

$$b = E_1 \tag{6.93}$$

Equation (6.85) implies:

$$a = \frac{E_2 - E_1}{2\varepsilon_{c1}} \tag{6.94}$$

Equation (6.88) implies:

$$a' = E_2 \tag{6.95}$$

Equation (6.89) implies:

$$b' = f'_{cc} - E_2\varepsilon_{cc} \tag{6.96}$$

Equation (6.90) implies:

$$E_2 = \frac{f'_{cc} - f_o}{\varepsilon_{cc}} \tag{6.97}$$

Equation (6.91) implies:

$$\varepsilon_{c1} = \frac{2f_o}{E_1 - E_2} \tag{6.98}$$

Substituting Eq. (6.98) into Eq. (6.94):

$$a = -\frac{(E_1 - E_2)^2}{4f_o} \tag{6.99}$$

Therefore, the proposed stress-strain model can be expressed as follows (Eqs. (6.100) and (6.101)):

$$f_c = E_1\varepsilon_c - \frac{(E_1 - E_2)^2}{4f_o}{\varepsilon_c}^2 \qquad if\ \ 0 \le \varepsilon_c \le \varepsilon_{c1} \tag{6.100}$$

$$f_c = f'_{c1} + E_2(\varepsilon_c - \varepsilon_{c1}) \qquad if\ \ \varepsilon_{c1} \le \varepsilon_c \le \varepsilon_{cc} \tag{6.101}$$

Where the endpoint of the stress-strain curve is determined by the ultimate stress and the ultimate strain (Eqs. 87 and 88) proposed in Chapter 5.

$$\frac{f'_{cc}}{f'_{co}} = \left(0.775 + \frac{15.8}{f'_{co}}\right) + \left(4.34 - \frac{16.4}{\rho_\varepsilon} + \frac{24.5}{{\rho_\varepsilon}^2}\right)\left(\frac{f_{l,rup}}{f'_{co}}\right) \tag{6.102}$$

$$\frac{\varepsilon_{cc}}{\varepsilon_{co}} = \left(\frac{2.31}{0.31\,{\rho_\varepsilon}^2 - \rho_K}\right) + \left(\frac{3.57}{0.0842 + \rho_f}\right)\left(\frac{f_{l,rup}}{f'_{co}}\right) \tag{6.103}$$

The slope of the first portion of the curve (E_1) (Eq. (6.104)) and the stress (f_o) (Eq. (6.105)) were modeled by regression analysis of various existing experimental stress-strain curves of GFRP-wrapped concrete circular columns collected from the literature using Eureqa® software.

$$E_1 = 65.7 + \frac{1100}{64.8 - 3.37f'_{co}}\ \ (GPa) \tag{6.104}$$

$$f_o = f'_{co} + 1.87\left(f_{l,rup}\right)^{0.2}\ \ (MPa) \tag{6.105}$$

6.4.2 Validation of the proposed model

The accuracy of the proposed model is examined by comparison with existing experimental data and the stress-strain models reported above.

The experimental data include stress-strain curves of axial compression tests on GFRP-wrapped concrete circular specimens with a wide range of confinement levels and compressive strength from 7 experimental studies (Harries and Kharel (2002), Harries and Carey (2003), Au and Buyukozturk (2005), Almusallam (2007), Wu et al. (2008), Cui and Sheikh (2010), Touhari and Mitiche-Kettab (2016)). Details of these specimens are reported in Tables 6.1.

Table 6.1 Details of the specimens used in the validation of the proposed model

Source		Specimen dimensions			Unconfined concrete properties		GFRP properties				Properties of confined concrete		
		d (mm)	h (mm)	h/d	f'_{co} (MPa)	ε_{co} (%)	E_f (GPa)	f_f (MPa)	t_f (mm)	ε_f (%)	f'_{cc} (MPa)	ε_{cc} (%)	$\varepsilon_{h,rup}$ (%)
Harries and Kharel (2002)		152	305	2.01	32.1	0.28	4.9	75	9	1.531	46.7	0.680	1.110
Harries and Carey (2003)		152	305	2.01	32.1	0.39	4.9	75	9	1.600	53.2	0.950	1.438
Au and Buyukozturk (2005)		150	375	2.50	24.2	0.36	26.1	575	1.2	2.200	43.8	1.630	1.480
Almusallam (2007)		150	300	2.00	90.29	0.32	27	540	3.9	2.000	110	0.900	0.825
Wu et al. (2008)	(1)	150	300	2.00	22.7	0.31	73	1500	0.354	2.055	45	2.360	1.179
	(2)	150	300	2.00	23.1	0.27	73	1500	0.354	2.055	46.4	2.490	1.180
Cui and Sheikh (2010)		152	305	2.01	47.76	0.22	26.84	620	2.5	2.310	88	2.210	2.114
	(1)	160	320	2.00	26.2	0.27	26	325	2	1.900	49.4	2.410	1.450

Touhari and Mitiche-Kettab (2016)	(2)	160	320	2.00	42.6	0.29	26	325	1	1.900	59.8	1.230	1.630
	(3)	160	320	2.00	42.6	0.29	26	325	2	1.900	68.5	1.650	1.460
	(4)	160	320	2.00	42.6	0.29	26	325	3	1.900	75.5	2.100	1.400
	(5)	160	320	2.00	61.7	0.31	26	325	2	1.900	80.8	1.490	1.500

In the following, comparisons of the proposed model and the existing models in the predictions of the experimental stress-strain curves are presented.

6.4.2.1 Comparison with test results of Harries and Kharel (2002)

The experimental stress-strain curve of Harries and Kharel (2003) with the predictions of the proposed model and the existing models are shown in Figs. (6.8-6.11).

The proposed model provides the best prediction over the existing models. Good coincidence with the experimental curve is shown with a slight overestimation of the stresses. In addition, the ultimate condition is well predicted with perfect accuracy.

The models of Lam and Teng (2003) and Xiao and Wu (2003) show the closest agreement with the experimental curve compared to the other models but with an overestimation of the ultimate conditions. The rest of the models underestimate the stress in the plastic portion, show a discontinued slope at the transition zone (Matthys et al., (2006); Youssef et al., (2007); and Fallah Pour et al., (2018)), and overestimate the ultimate conditions.

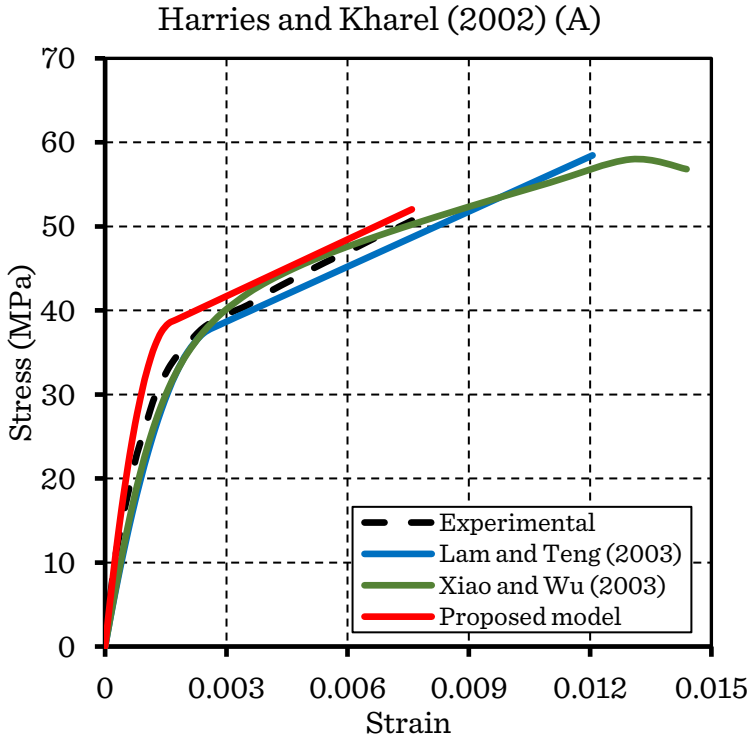

Figure 6.8 Comparison of experimental and predicted stress-strain curves of the proposed model and the existing models (A) (Specimen of Harries and Kharel (2002))

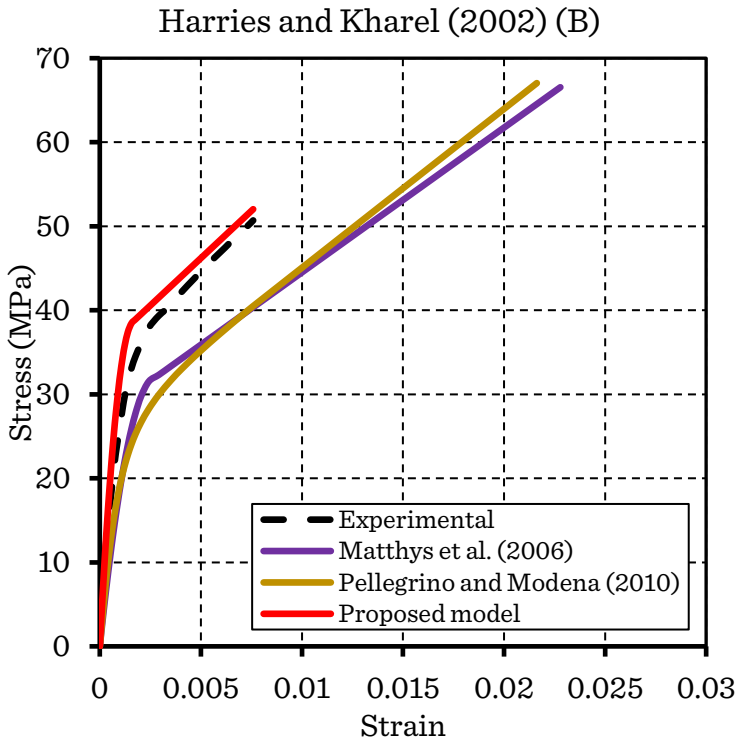

Figure 6.9 Comparison of experimental and predicted stress-strain curves of the proposed model and the existing models (B) (Specimen of Harries and Kharel (2002))

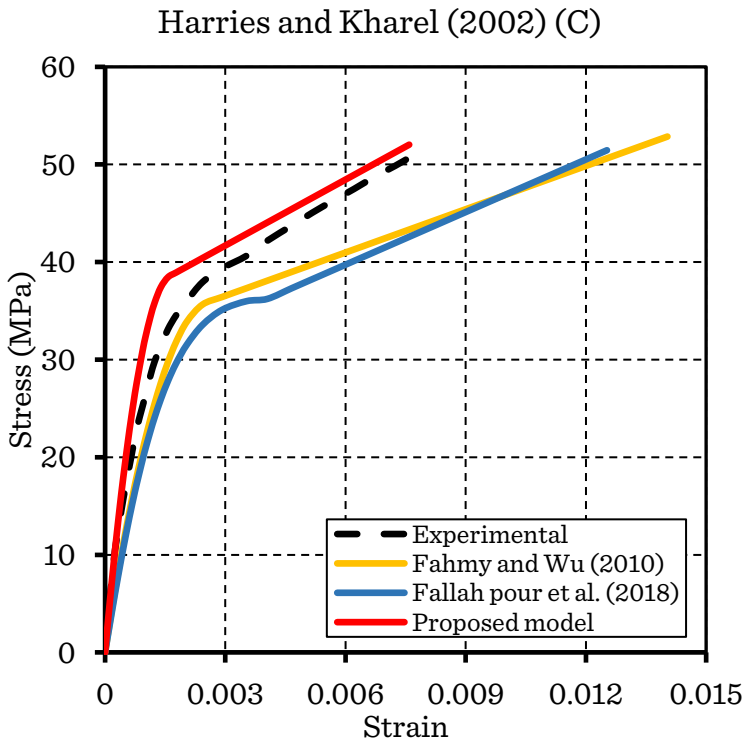

Figure 6.10 Comparison of experimental and predicted stress-strain curves of the proposed model and the existing models (C) (Specimen of Harries and Kharel (2002))

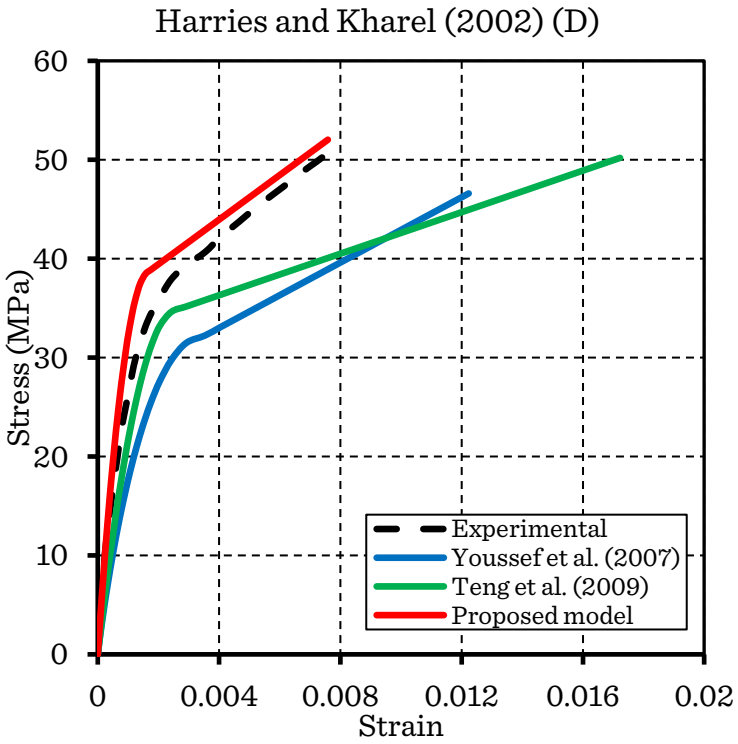

Figure 6.11 Comparison of experimental and predicted stress-strain curves of the proposed model and the existing models (D) (Specimen of Harries and Kharel (2002))

6.4.2.2 Comparison with test results of Harries and Carey (2003)

Figs. (6-12-6.15) illustrates the experimental stress-strain curve of Harries and Carey (2003) and predictions of the proposed and the existing stress-strain models.

The proposed model fits well the first branch of the experimental curve; however, it underestimates the stresses at the second branch. The ultimate strength is well predicted, but the ultimate strain is overestimated.

The model of Xiao and Wu (2003) show the best agreement with the experimental curve compared to the other models. However, it overestimates the ultimate strength and strain and shows a descending third branch (Fig. 6.12).

The rest of the models underestimate the stresses at the second branch compared to the experimental curve and overestimate the ultimate strain. The models of Youssef et al. (2007) and Fallah Pour et al. (2018) show a discontinued slope at the transition zone.

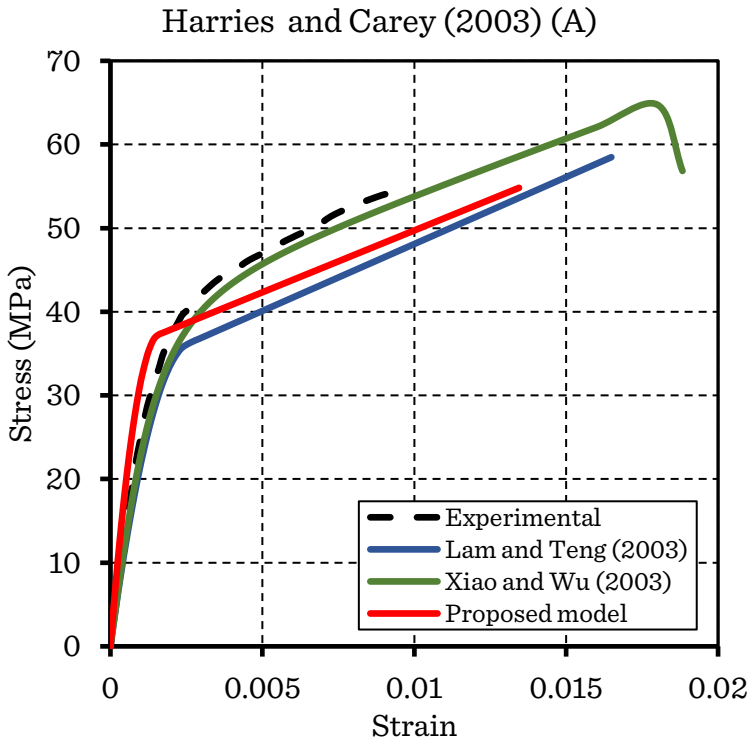

Figure 6.12 Comparison of experimental and predicted stress-strain curves of the proposed model and the existing models (A) (Specimen of Harries and Carey (2003))

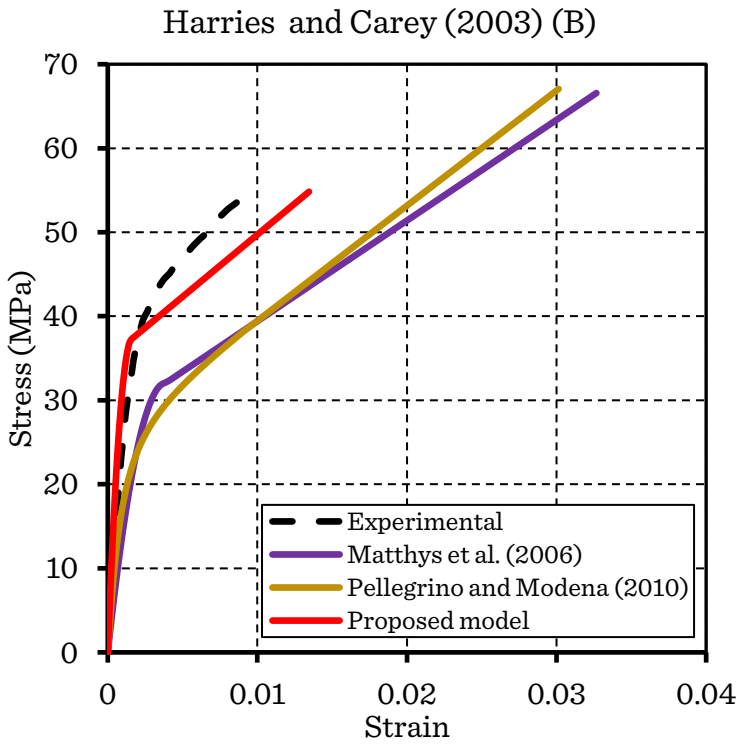

Figure 6.13 Comparison of experimental and predicted stress-strain curves of the proposed model and the existing models (B) (Specimen of Harries and Carey (2003))

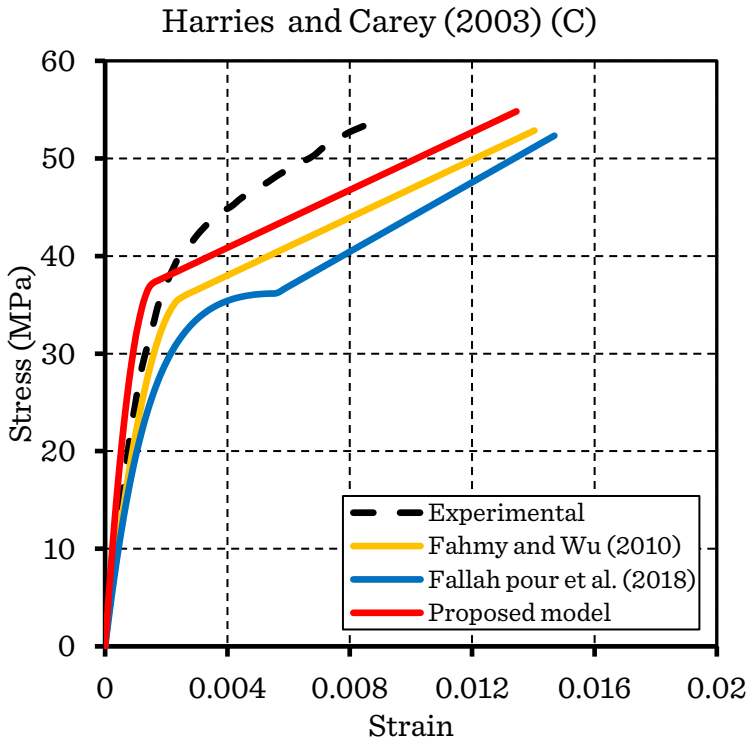

Figure 6.14 Comparison of experimental and predicted stress-strain curves of the proposed model and the existing models (C) (Specimen of Harries and Carey (2003))

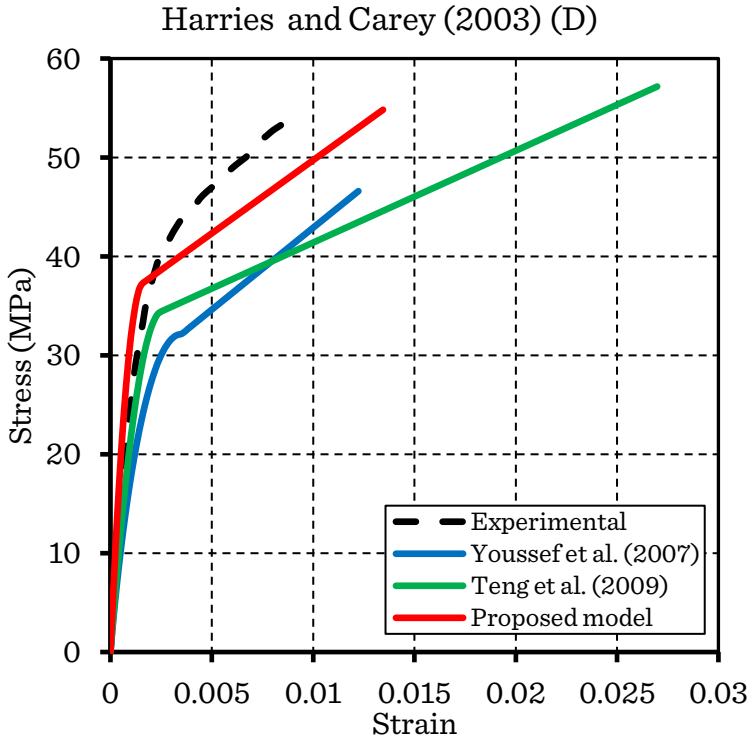

Figure 6.15 Comparison of experimental and predicted stress-strain curves of the proposed model and the existing models (D) (Specimen of Harries and Carey (2003))

6.4.2.3 Comparison with test results of Au and Buyukozturk (2005)

The first part of the stress-strain curve of Au and Buyukozturk (2005) (Figs. 6.16-6.19) is perfectly predicted by the proposed model. However, although it well predicts the ultimate strength, it underestimates the ultimate strain, making the second branch steep and (underestimation of the stresses at the second portion).

Compared to the other models, the models of Lam and Teng (2003) and Xiao and wu (2003) show the best prediction for both portions of the experimental curve (Fig. 6.16). However, the model of Xiao and Wu (2003) shows an overestimation of the ultimate condition with a third descending branch.

The rest of the models failed to predict the second branch of the curve (underestimation of the stresses), where the models of Youssef et al. (2007) and Fallah Pour et al. (2018) show a discontinued slope at the transition zone.

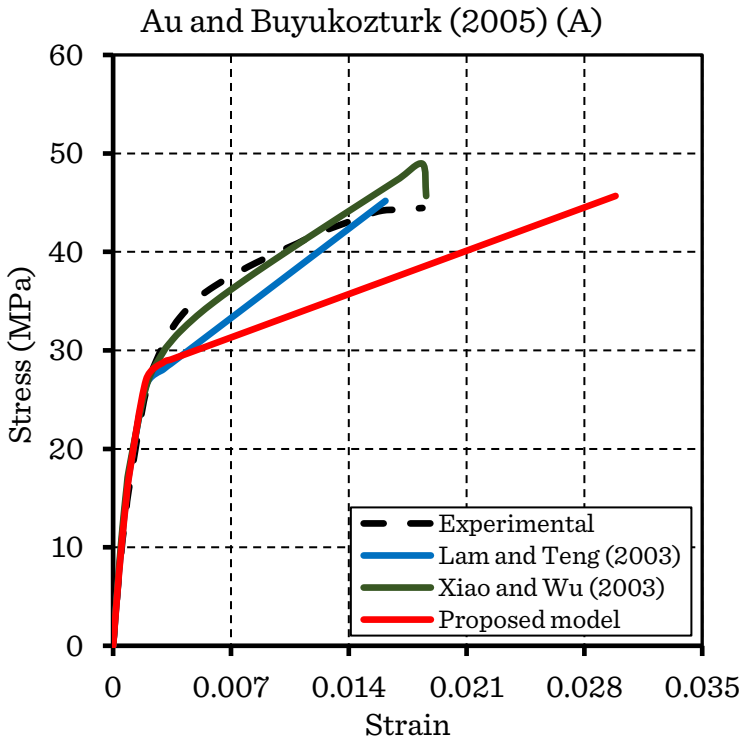

Figure 6.16 Comparison of experimental and predicted stress-strain curves of the proposed model and the existing models (A) (Specimen of Au and Buyukozturk (2005))

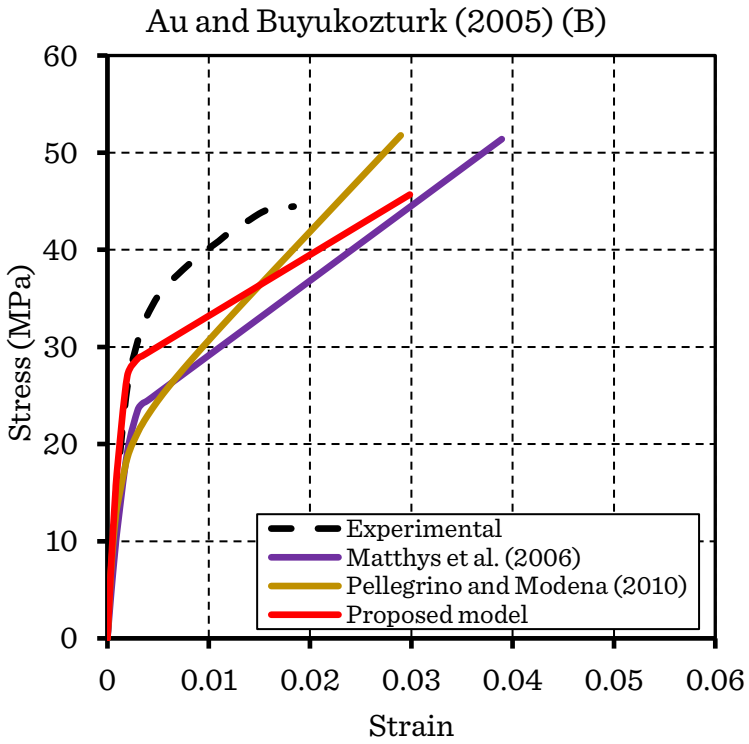

Figure 6.17 Comparison of experimental and predicted stress-strain curves of the proposed model and the existing models (B) (Specimen of Au and Buyukozturk (2005))

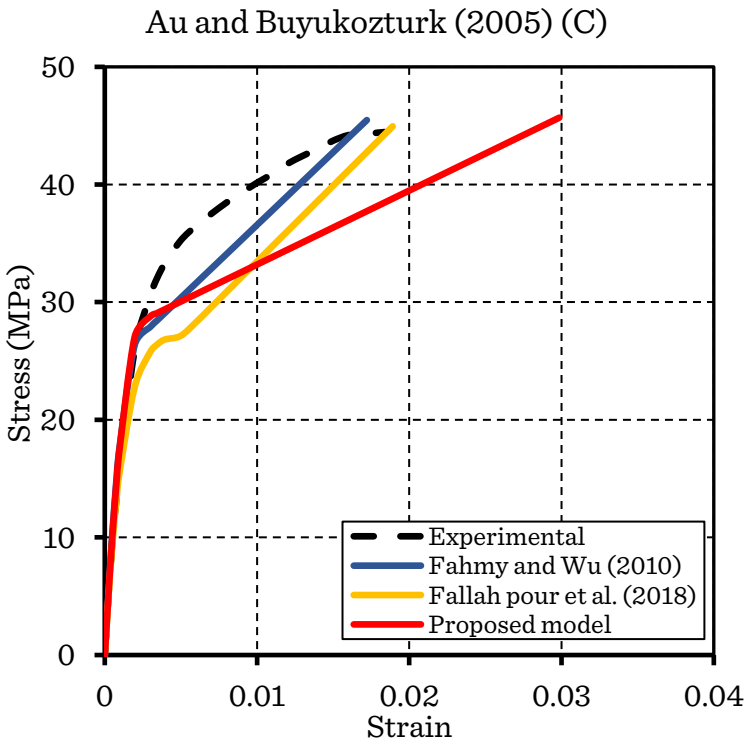

Figure 6.18 Comparison of experimental and predicted stress-strain curves of the proposed model and the existing models (C) (Specimen of Au and Buyukozturk (2005))

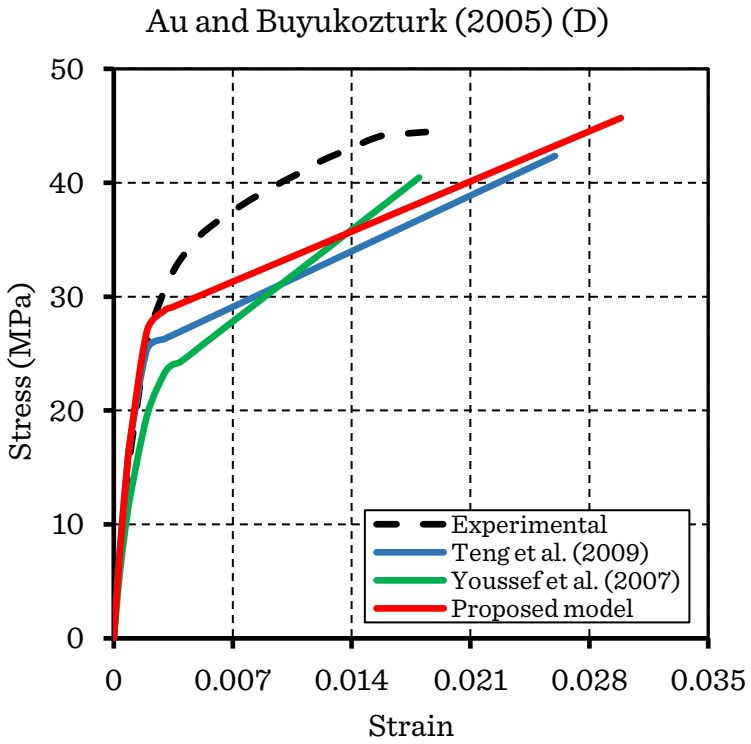

Figure 6.19 Comparison of experimental and predicted stress-strain curves of the proposed model and the existing models (D) (Specimen of Au and Buyukozturk (2005))

6.4.2.4 Comparison with test results of Almusallam (2007)

For the stress-strain curve of Almusallam (2007) (Figs. 6.20-6.23), the proposed model provides a reasonable agreement with the experimental result with a perfect match with the first ascending portion; however, the model slightly underestimates the stresses at the second branch and overestimate the ultimate strain.

The models of Fahmy and Wu (2010) and Teng et al. (2009) show the best fit with the experimental stress-strain curve (Figs. 6.22 and 6.23) where the model of Teng et al. (2009) overestimate the ultimate condition. The rest of the models predict well the first portion; however, they largely overestimate the strength and ductility, except the model of Xiao and Wu (2003) that shows a third descending branch (Fig. 6.20).

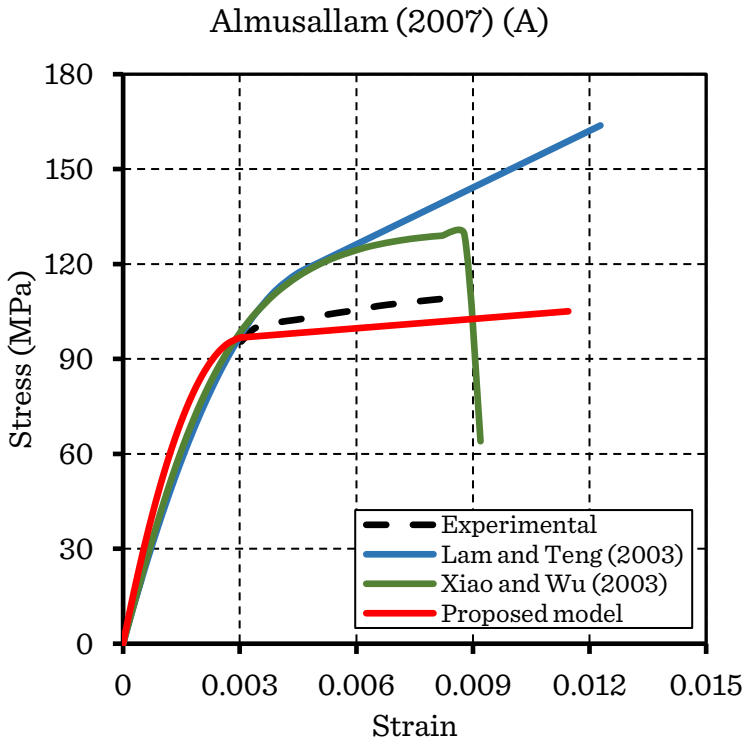

Figure 6.20 Comparison of experimental and predicted stress-strain curves of the proposed model and the existing models (A) (Specimen of Almusallam (2007))

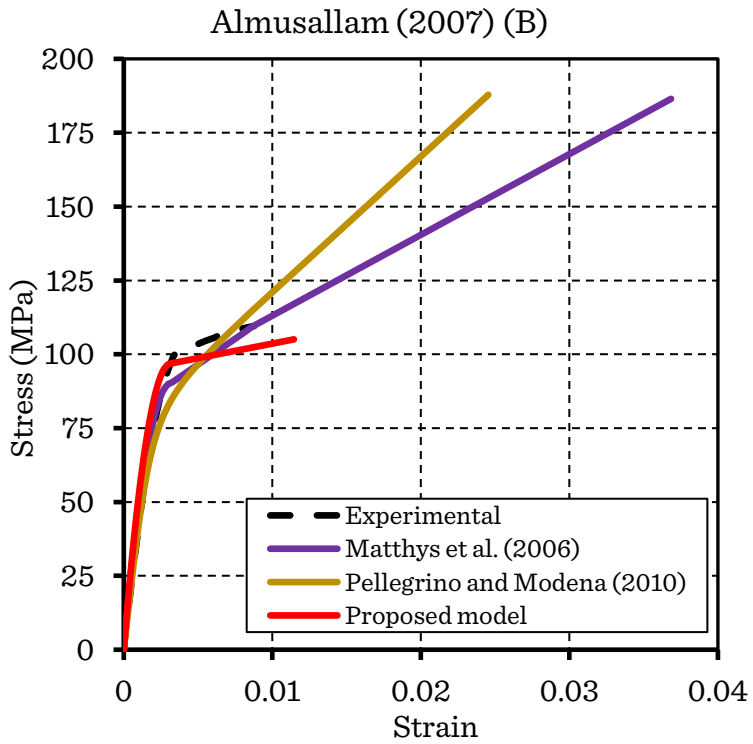

Figure 6.21 Comparison of experimental and predicted stress-strain curves of the proposed model and the existing models (B) (Specimen of Almusallam (2007))

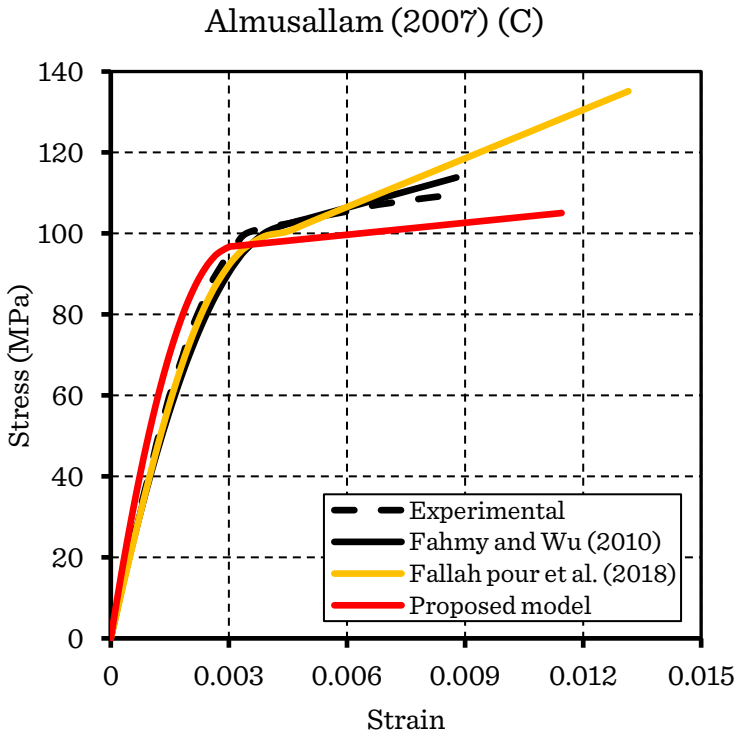

Figure 6.22 Comparison of experimental and predicted stress-strain curves of the proposed model and the existing models (C) (Specimen of Almusallam (2007))

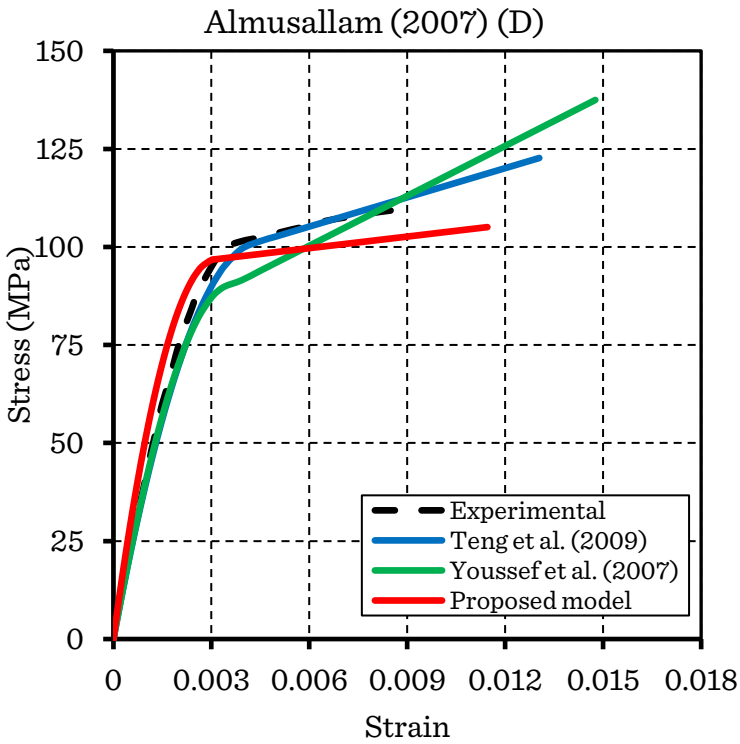

Figure 6.23 Comparison of experimental and predicted stress-strain curves of the proposed model and the existing models (D) (Specimen of Almusallam (2007))

6.4.2.5 Comparison with test results of Wu et al. (2008)

Figs. (6.24-6.27) shows the experimental stress-strain curve of the first specimen of Wu et al. (2008) with the predictions of the proposed and existing models.

The proposed model shows good agreement with the test results. A perfect coincidence with the first branch of the curve is achieved, while in the second branch, the confinement effectiveness is a little underestimated with very accurate ultimate strength and strain comparing to most of the models.

Most of the existing models overestimate the concrete stiffness at the early loading stage where the FRP confinement is not yet activated (Lam & Teng, (2003); Xiao & Wu, (2003); Fahmy & Wu, (2010); Fallah Pour et al., (2018); Teng et al., (2009)), and at the same time, they provide highly low ultimate strength and strain.

In addition, the models of Youssef et al. (2007) and Fallah Pour et al. (2018) show a discontinued slope at the transition zone, while the models of Xiao and Wu (2003) and Teng et al. (2009) show third descending and ascending branch respectively.

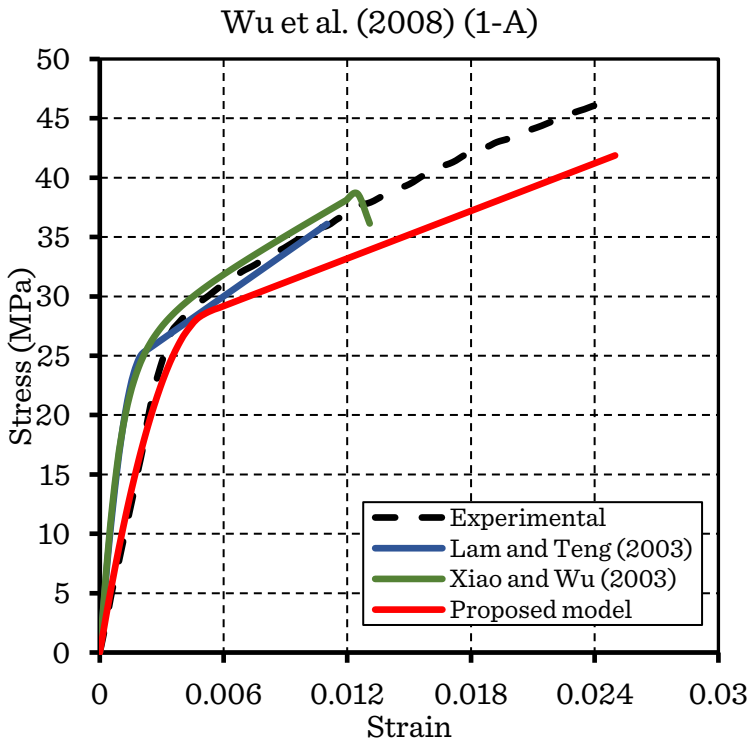

Figure 6.24 Comparison of experimental and predicted stress-strain curves of the proposed model and the existing models (A) (Specimen of Wu et al. (2008) (1))

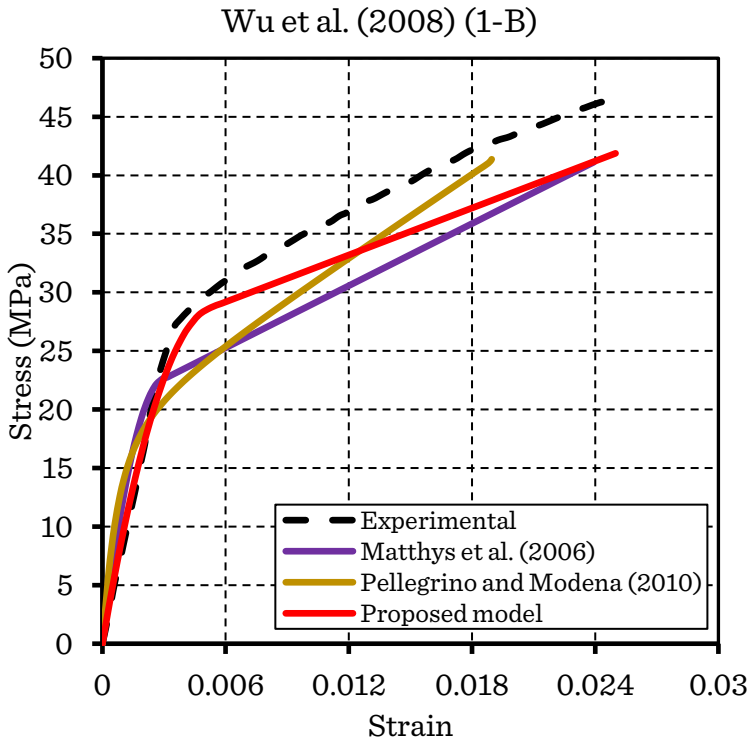

Figure 6.25 Comparison of experimental and predicted stress-strain curves of the proposed model and the existing models (B) (Specimen of Wu et al. (2008) (1))

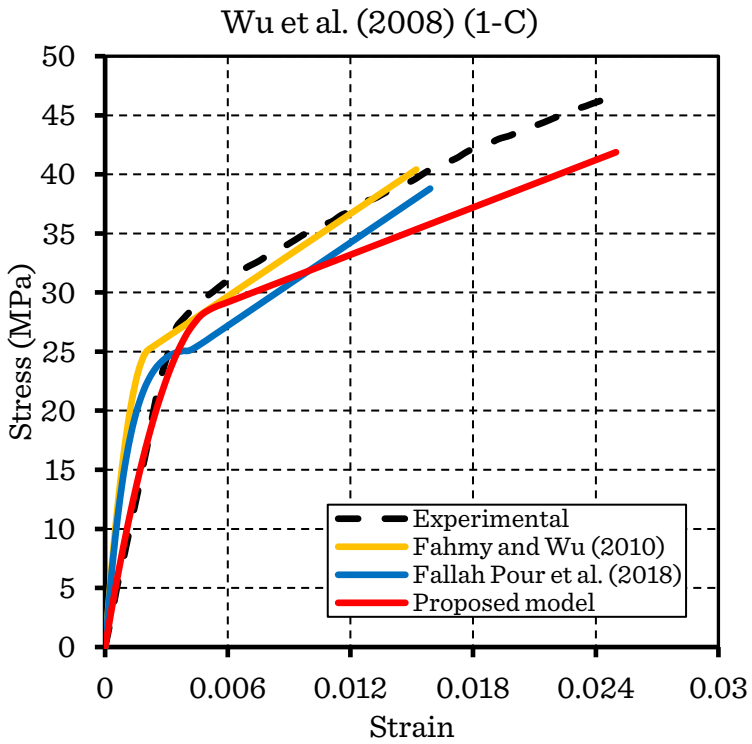

Figure 6.26 Comparison of experimental and predicted stress-strain curves of the proposed model and the existing models (C) (Specimen of Wu et al. (2008) (1))

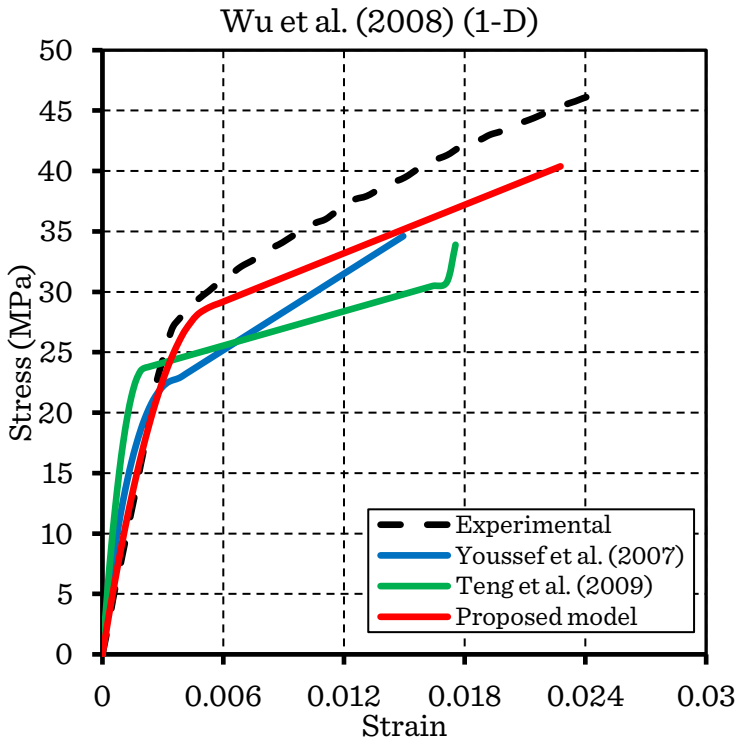

Figure 6.27 Comparison of experimental and predicted stress-strain curves of the proposed model and the existing models (D) (Specimen of Wu et al. (2008) (1))

In the second specimen of Wu et al. (200) (Figs. 6.28-6.31), the proposed model shows a perfect agreement with the experimental curve compared to the existing models with a slightly higher elasticity modulus and lower ultimate strength and strain.

Most of the existing models overestimate the first slope of the curve and underestimate the ultimate conditions; however, they provide generally accurate predictions, where the best performing model is that of Fahmy and Wu (2010). Discontinuity in the slope is also observed between the two parts of the curve for the models of Fallah Pour et al. (2018) (Fig. 6.30) and Teng et al. (2009) (Fig. 6.31), while the model of Xiao and Wu (2003) is terminated with a third descending branch.

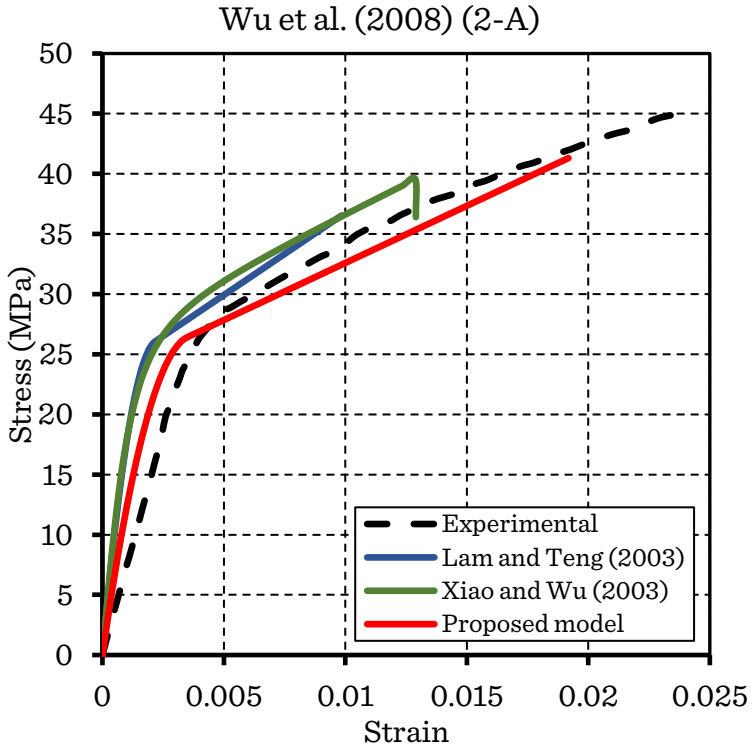

Figure 6.28 Comparison of experimental and predicted stress-strain curves of the proposed model and the existing models (A) (Specimen of Wu et al. (2008) (2))

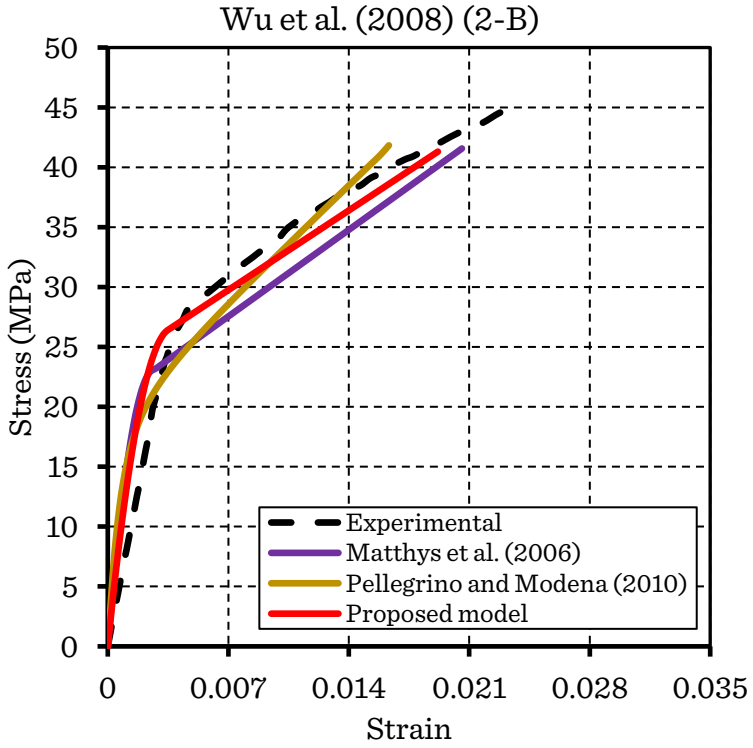

Figure 6.29 Comparison of experimental and predicted stress-strain curves of the proposed model and the existing models (B) (Specimen of Wu et al. (2008) (2))

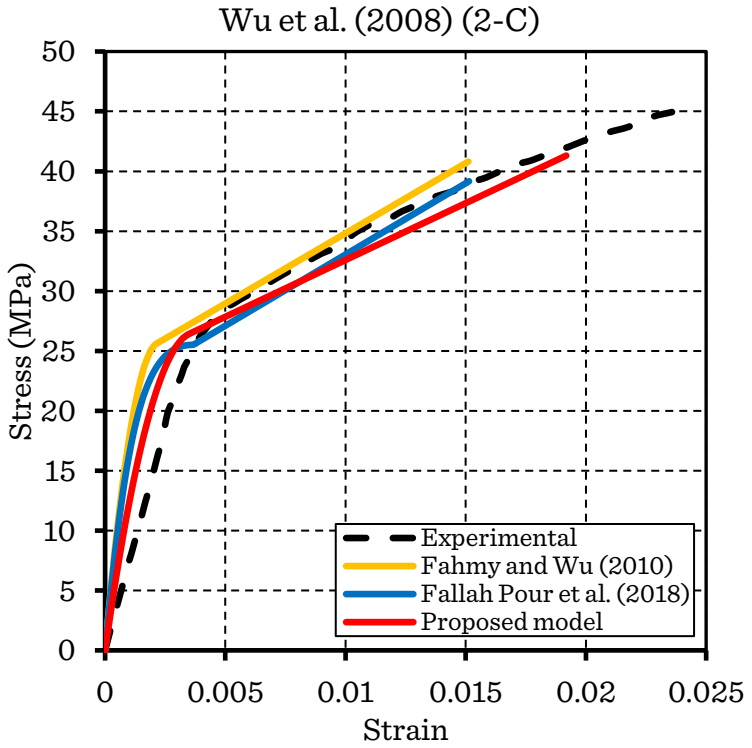

Figure 6.30 Comparison of experimental and predicted stress-strain curves of the proposed model and the existing models (C) (Specimen of Wu et al. (2008) (2))

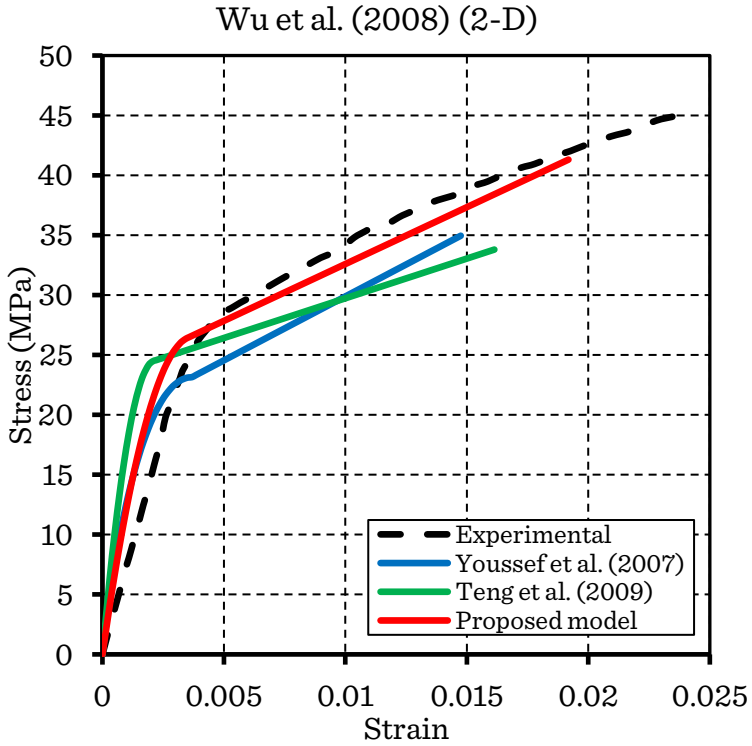

Figure 6.31 Comparison of experimental and predicted stress-strain curves of the proposed model and the existing models (D) (Specimen of Wu et al. (2008) (2))

6.4.2.6 Comparison with test results of Cui and Sheikh (2010)

For the specimen of Cui and Sheikh (2010) (Figs. 6.32-6.35), the proposed model provides accurate predictions with the experimental curve. The predictions coincide perfectly with the first portion and with a large part of the second portion of the experimental curve, where the ultimate strain is slightly underestimated.

Most of the existing models accurately predict the first branch of the curve. However, the models of Matthys et al. (2006) (Fig. 6.33), Fahmy and Wu (2010) (Fig. 6.34), Teng et al. (2009), and Youssef et al. (2007) (Fig. 6.35) underestimate the stresses in the second portion, while, the models of Lam and Teng (2003) and Xiao and Wu (2003) overestimate the stresses at the second portion (Fig. 6.35).

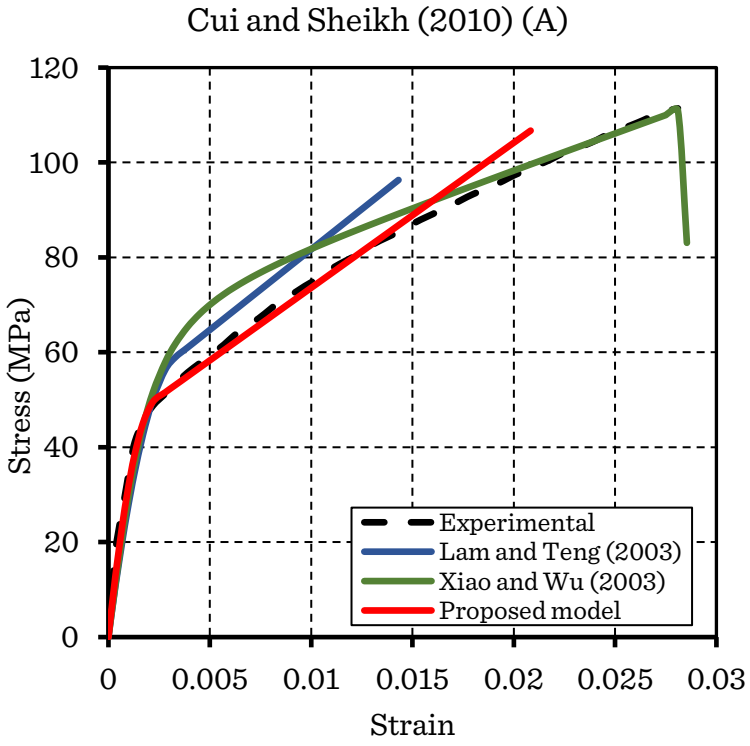

Figure 6.32 Comparison of experimental and predicted stress-strain curves of the proposed model and the existing models (A) (Specimen of Cui and Sheikh (2010))

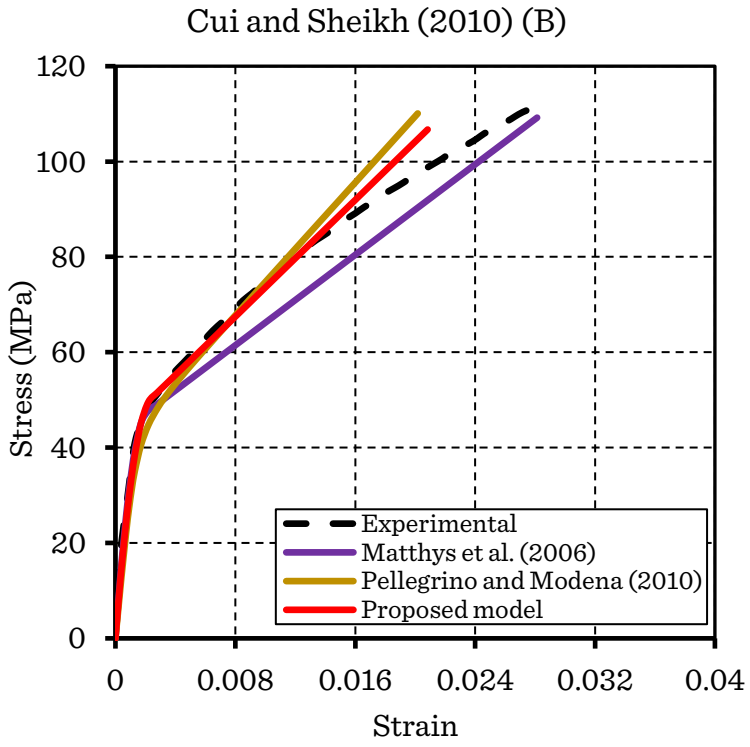

Figure 6.33 Comparison of experimental and predicted stress-strain curves of the proposed model and the existing models (B) (Specimen of Cui and Sheikh (2010))

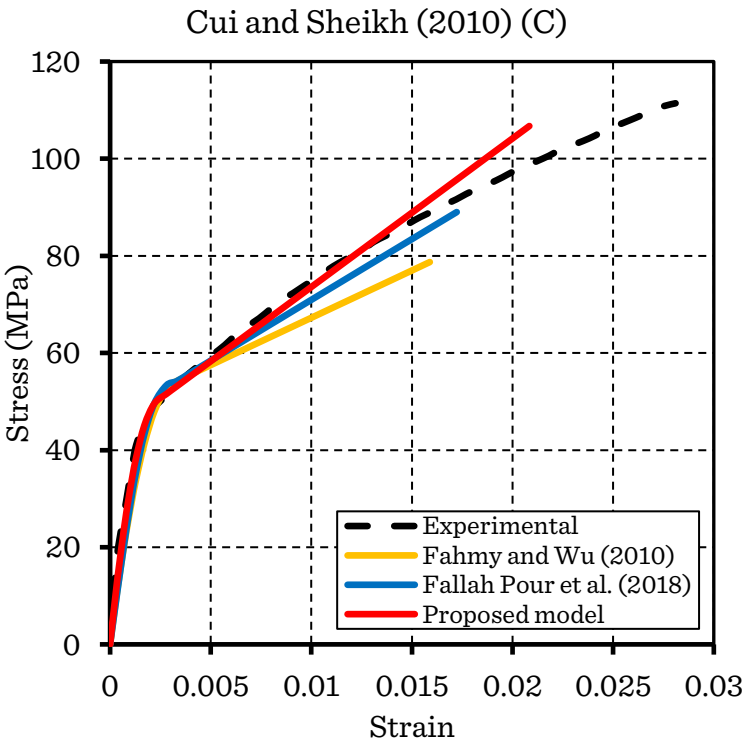

Figure 6.34 Comparison of experimental and predicted stress-strain curves of the proposed model and the existing models (C) (Specimen of Cui and Sheikh (2010))

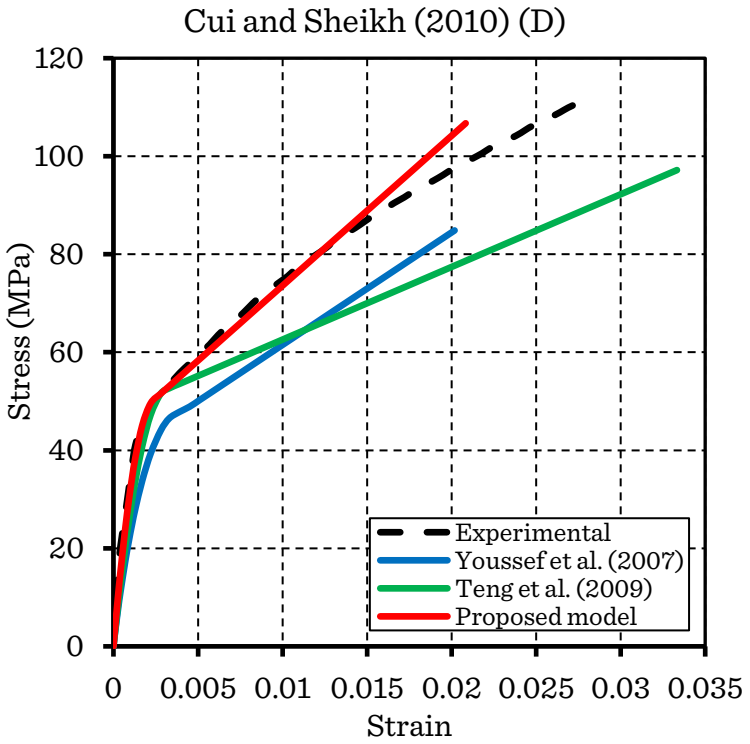

Figure 6.35 Comparison of experimental and predicted stress-strain curves of the proposed model and the existing models (D) (Specimen of Cui and Sheikh (2010))

6.4.2.7 Comparison with test results of Touhari and Mitiche-Kettab (2016)

In the first specimen of Touhari and Mitiche-Kettab (2016) (Figs. 6.36-6.39), the proposed model shows excellent agreement with the test results, with a slight overestimation of the ultimate point comparing to the existing models.

The model of Teng et al. (2009) provides the best predictions among the existing models with little underestimation of the stresses in the second portion and overestimation of the ultimate condition (Fig. 6.39), where most of the other models underestimate the first slope of the curve and the transition point.

As in the other specimens, the models of Fallah Pour et al. (2018) and Youssef et al. (2007) failed to provide a smooth transition between the two portions of the curve (Figs. 6.38 and 6.39). In addition, the model of Xiao and Wu (2003) provides an uncoherent curve at the ultimate point with a descending third portion (Fig. 6.36).

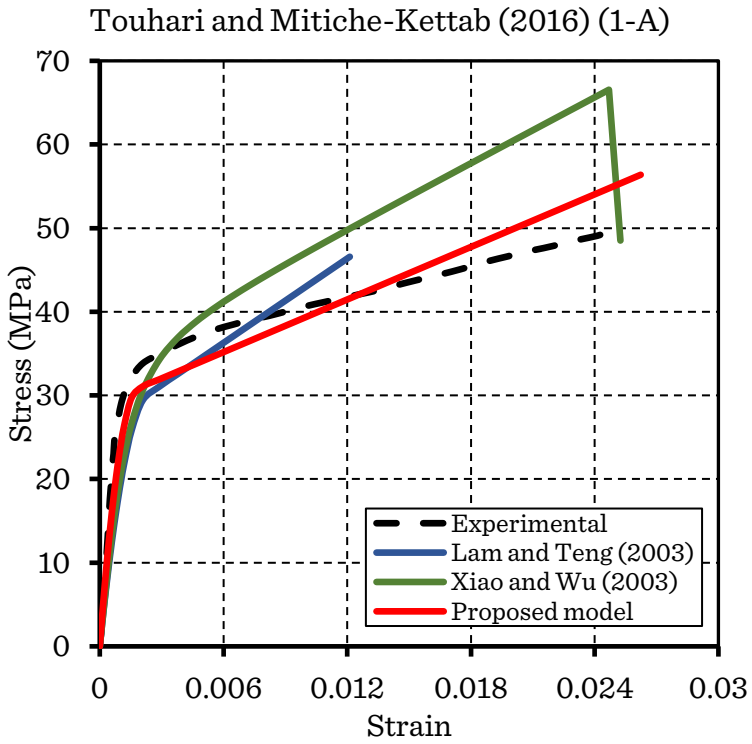

Figure 6.36 Comparison of experimental and predicted stress-strain curves of the proposed model and the existing models (A) (Specimen of Touhari and Mitiche-Kettab (2016) (1))

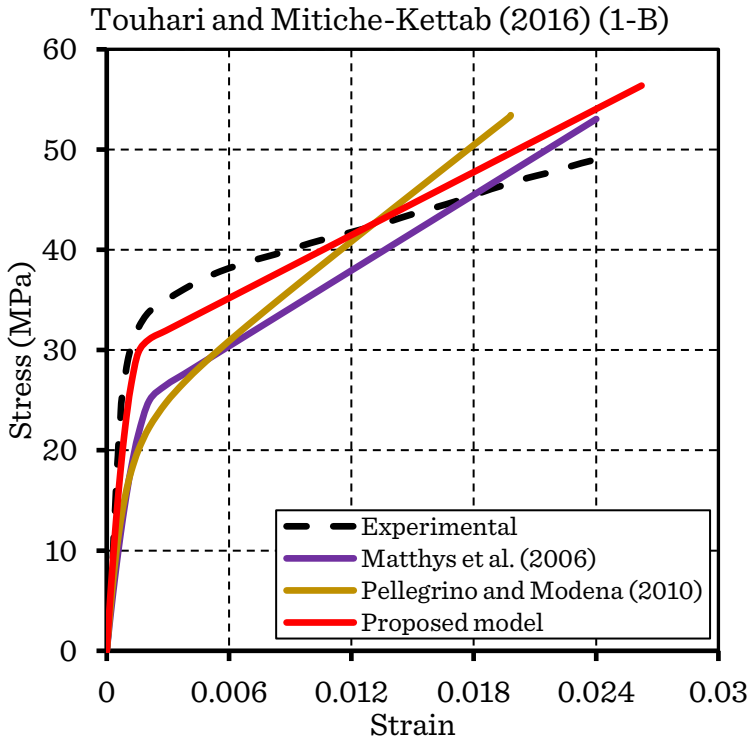

Figure 6.37 Comparison of experimental and predicted stress-strain curves of the proposed model and the existing models (B) (Specimen of Touhari and Mitiche-Kettab (2016) (1))

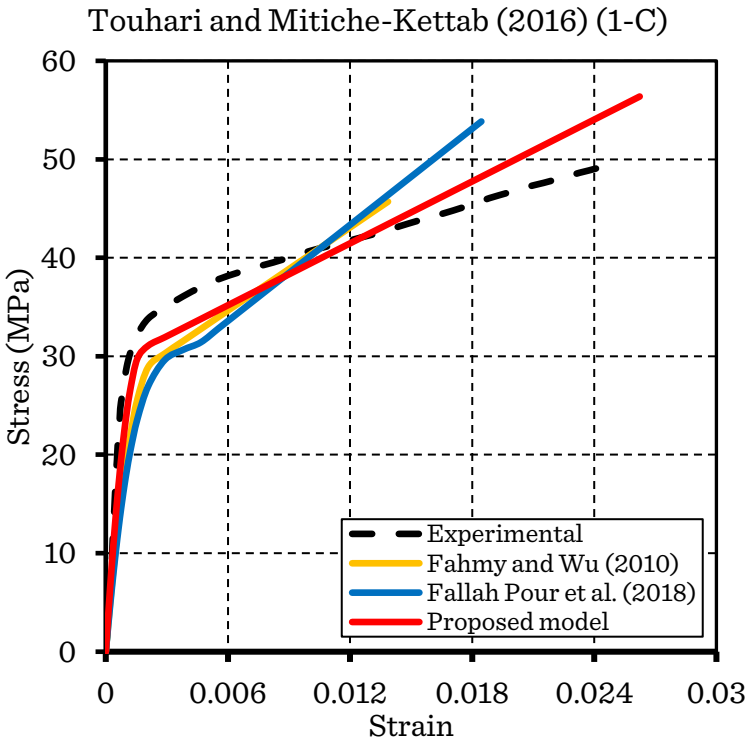

Figure 6.38 Comparison of experimental and predicted stress-strain curves of the proposed model and the existing models (C) (Specimen of Touhari and Mitiche-Kettab (2016) (1))

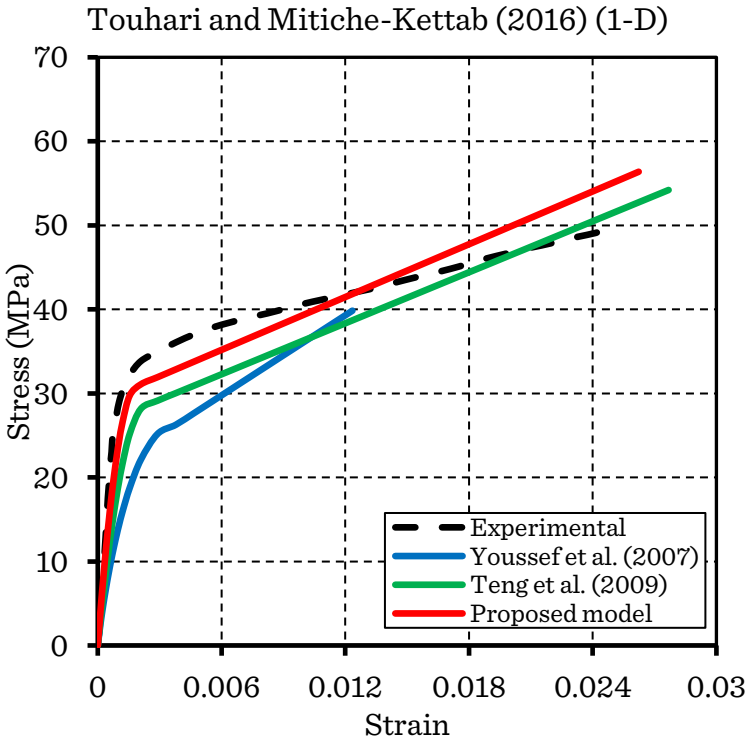

Figure 6.39 Comparison of experimental and predicted stress-strain curves of the proposed model and the existing models (D) (Specimen of Touhari and Mitiche-Kettab (2016) (1))

For the second specimen of Touhari and Mitiche-Kettab (2016) (Figs. 6.39-6.42), the prediction of the proposed model is perfect from all aspects. Total coincidence is obtained with the experimental curve. All the other models provide conservative results. They underestimate the elastic modulus of the concrete at the first branch and the stresses at the second branch, where the model of Xiao and Wu (2003) shows descending second and third branches (Fig. 6.41).

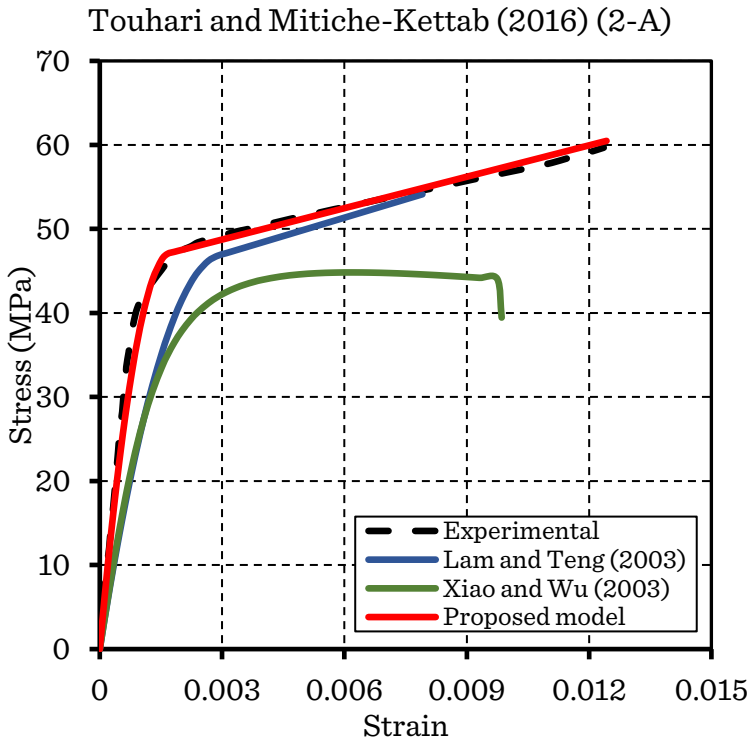

Figure 6.40 Comparison of experimental and predicted stress-strain curves of the proposed model and the existing models (A) (Specimen of Touhari and Mitiche-Kettab (2016) (2))

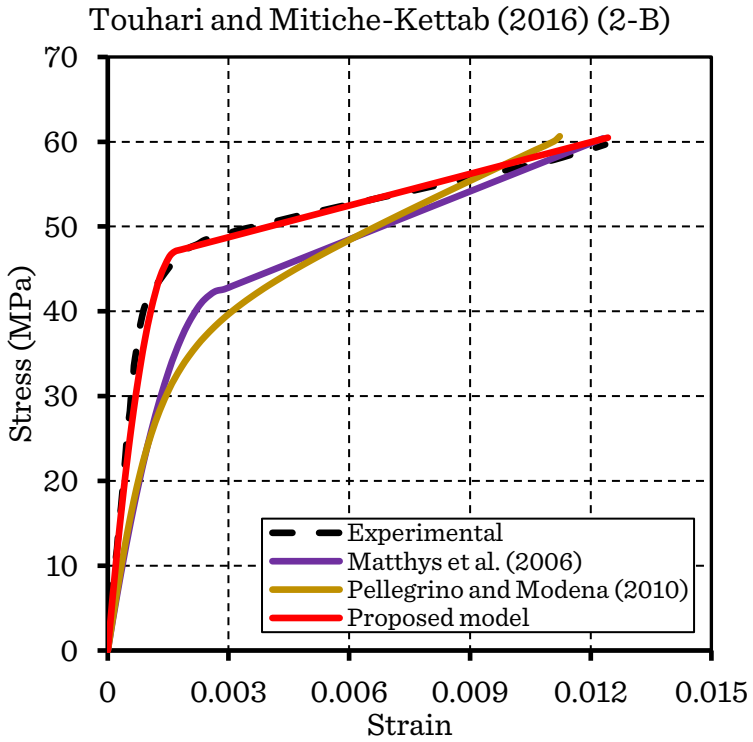

Figure 6.41 Comparison of experimental and predicted stress-strain curves of the proposed model and the existing models (B) (Specimen of Touhari and Mitiche-Kettab (2016) (2))

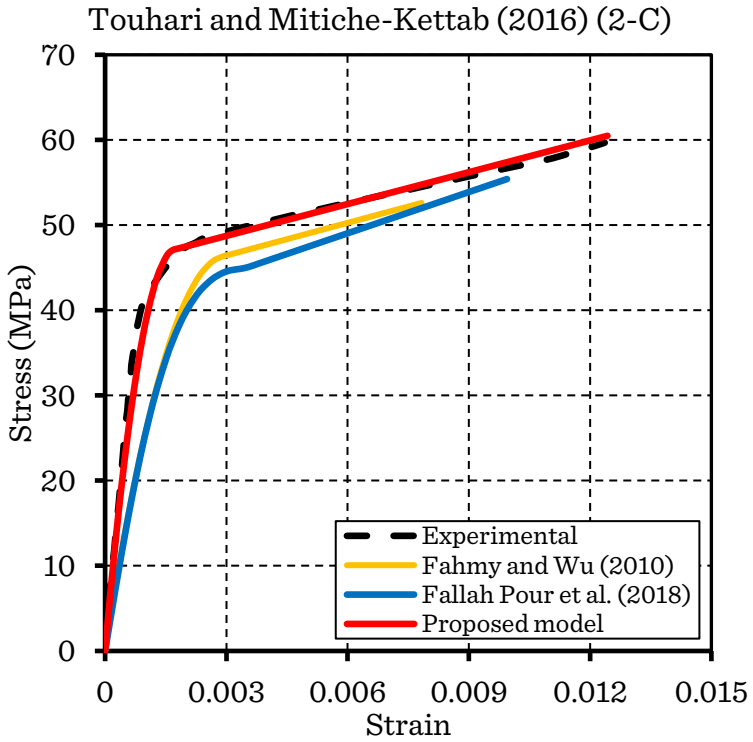

Figure 6.42 Comparison of experimental and predicted stress-strain curves of the proposed model and the existing models (C) (Specimen of Touhari and Mitiche-Kettab (2016) (2))

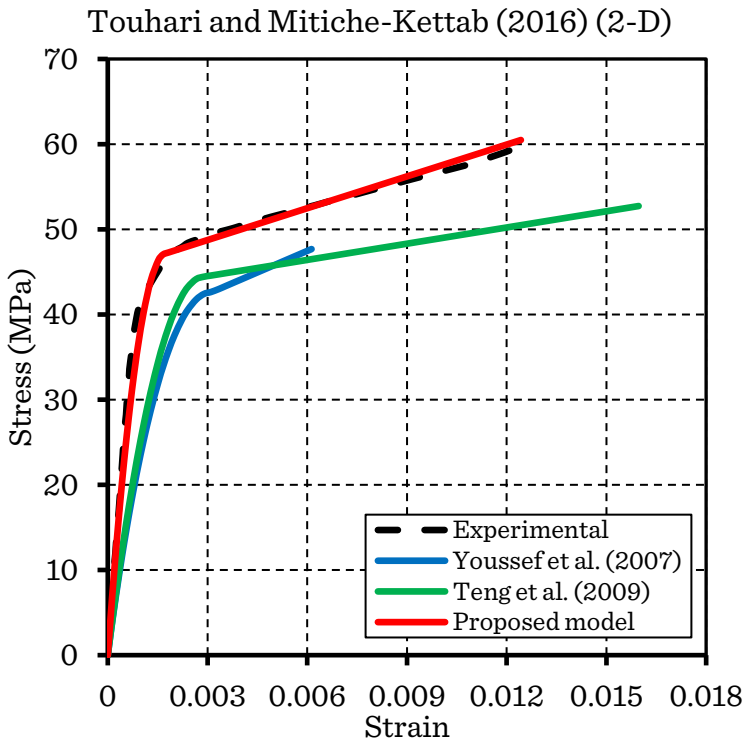

Figure 6.43 Comparison of experimental and predicted stress-strain curves of the proposed model and the existing models (D) (Specimen of Touhari and Mitiche-Kettab (2016) (2))

Similarly, for the third specimen of Touahri and Mitiche-Kettab (2016) (Figs. 6.43-6.46), the proposed model is the closest to the experimental curve without any comparison. The other models underestimate the elasticity modulus of the concrete and the stresses in the second branch except the model of Xiao and Wu (2003), which provides a descending third branch (Fig. 6.43). Also, the models of Fallah Pour et al. (2018) and Youssef et al. (2007) failed to provide a smooth transition between the two portions of the curve (Figs. 6.45 and 6.46).

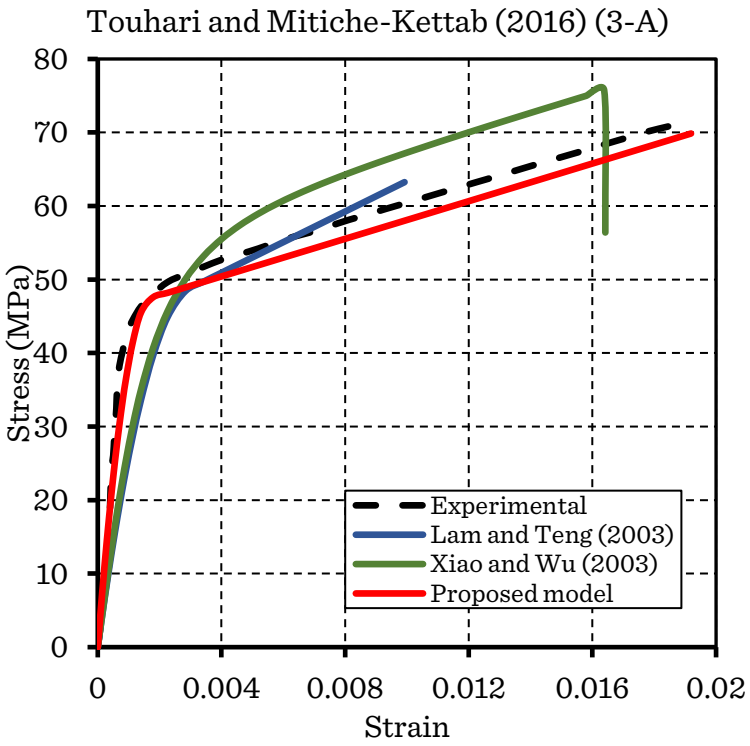

Figure 6.44 Comparison of experimental and predicted stress-strain curves of the proposed model and the existing models (A) (Specimen of Touhari and Mitiche-Kettab (2016) (3))

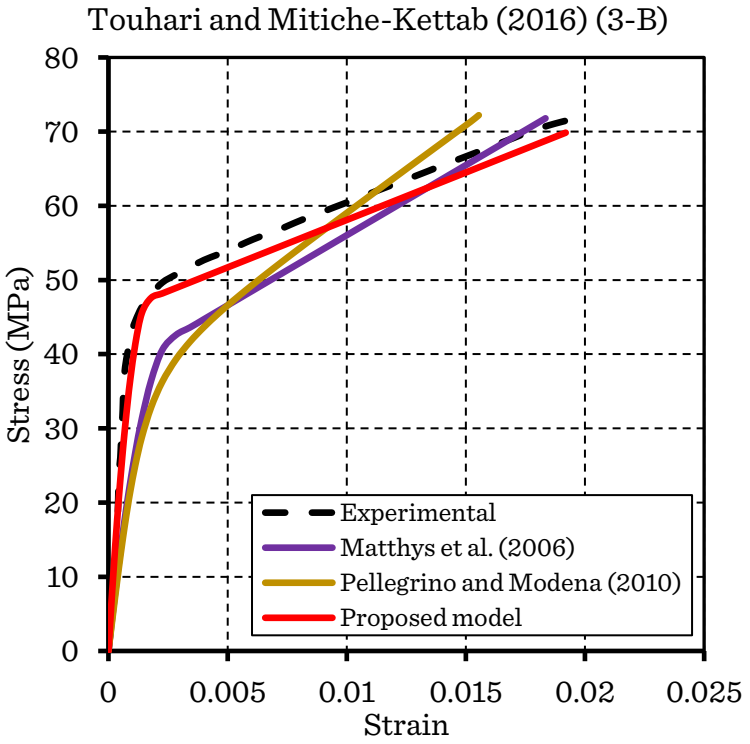

Figure 6.45 Comparison of experimental and predicted stress-strain curves of the proposed model and the existing models (B) (Specimen of Touhari and Mitiche-Kettab (2016) (3))

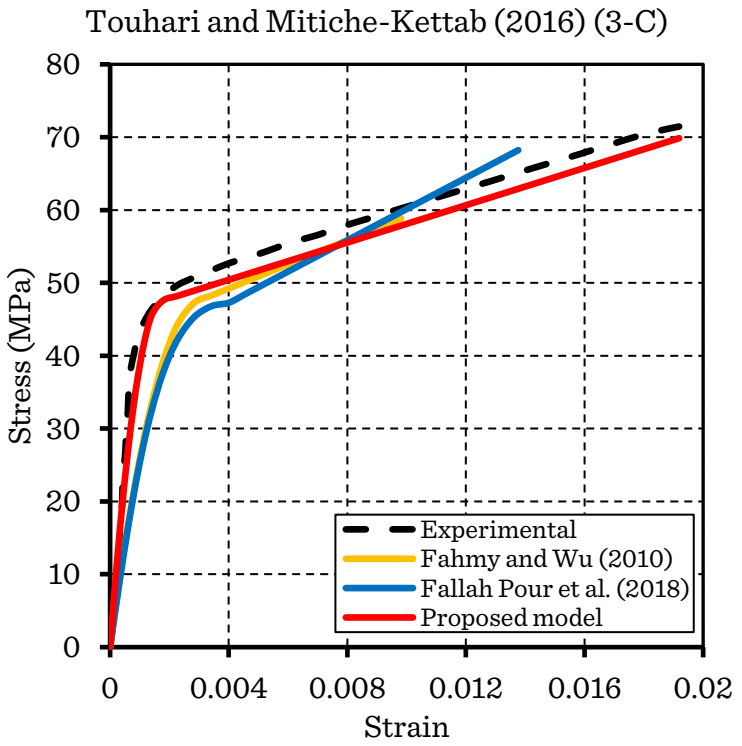

Figure 6.46 Comparison of experimental and predicted stress-strain curves of the proposed model and the existing models (C) (Specimen of Touhari and Mitiche-Kettab (2016) (3))

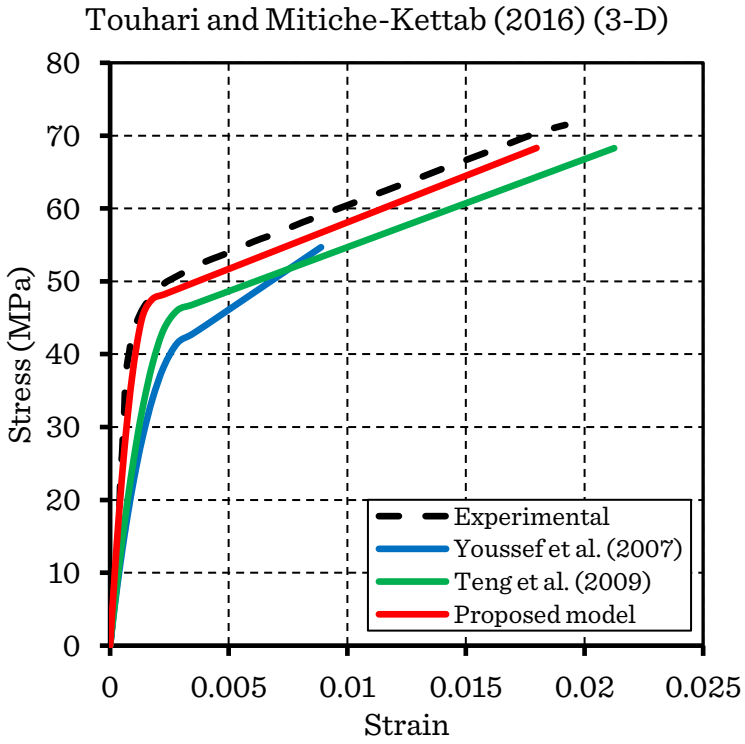

Figure 6.47 Comparison of experimental and predicted stress-strain curves of the proposed model and the existing models (D) (Specimen of Touhari and Mitiche-Kettab (2016) (3))

For the fourth specimen of Touahri and Mitiche-Kettab (2016) (Figs. 6.47-6.50), the proposed model provides accurate predictions compared to the other models with a perfect match with the first portion and slight underestimation of the stresses in the second portion. The ultimate condition is well predicted.

Similar to the other specimens of Touahri and Mitiche-Kettab (2016), the other models underestimate the elasticity modulus of the concrete and the stresses in the second branch. The models of Fallah Pour et al. (2018) and Youssef et al. (2007) show a discontinuous slope between the two portions of the curve (Figs. 6.49 and 6.50), while the model of Xiao and Wu (2003) shows a descending third branch (Fig. 6.47).

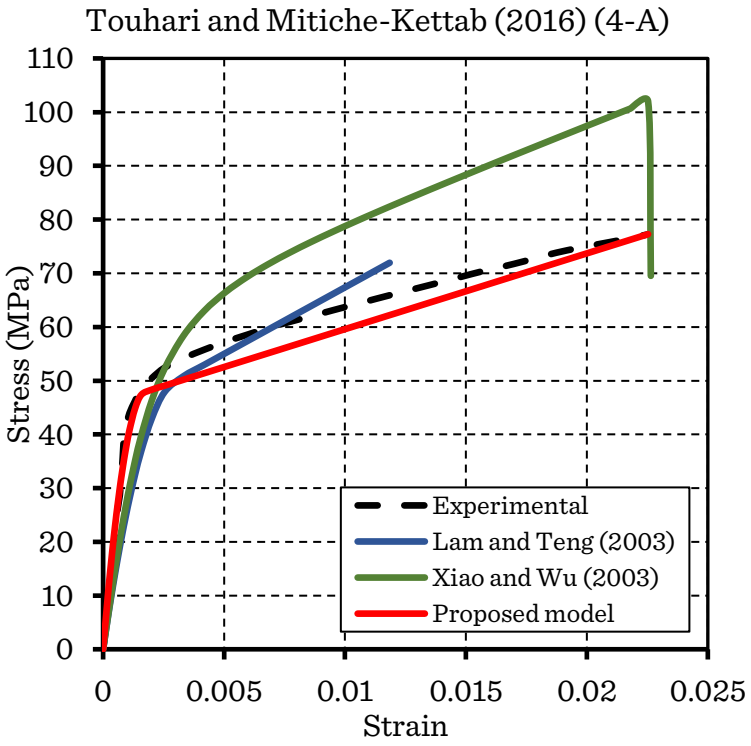

Figure 6.48 Comparison of experimental and predicted stress-strain curves of the proposed model and the existing models (A) (Specimen of Touhari and Mitiche-Kettab (2016) (4))

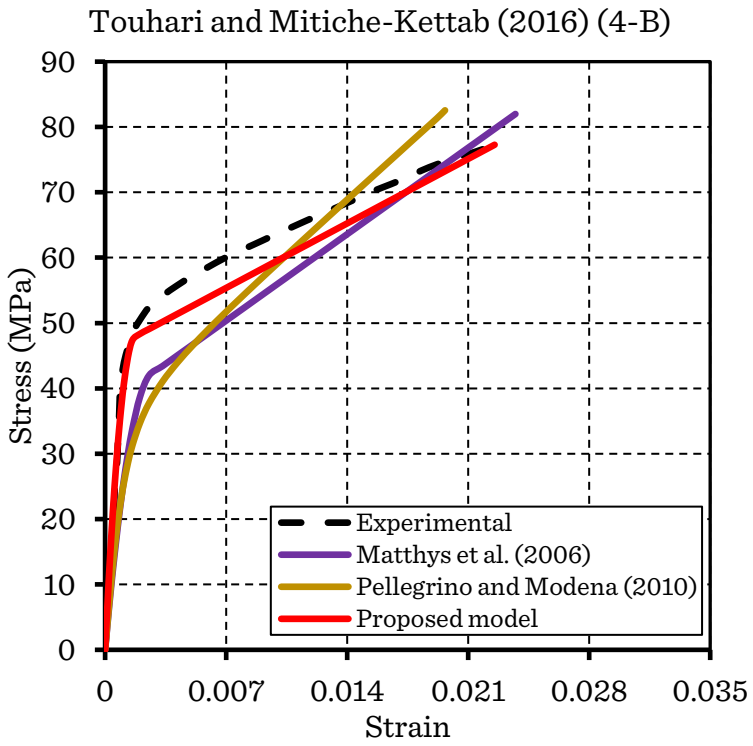

Figure 6.49 Comparison of experimental and predicted stress-strain curves of the proposed model and the existing models (B) (Specimen of Touhari and Mitiche-Kettab (2016) (4))

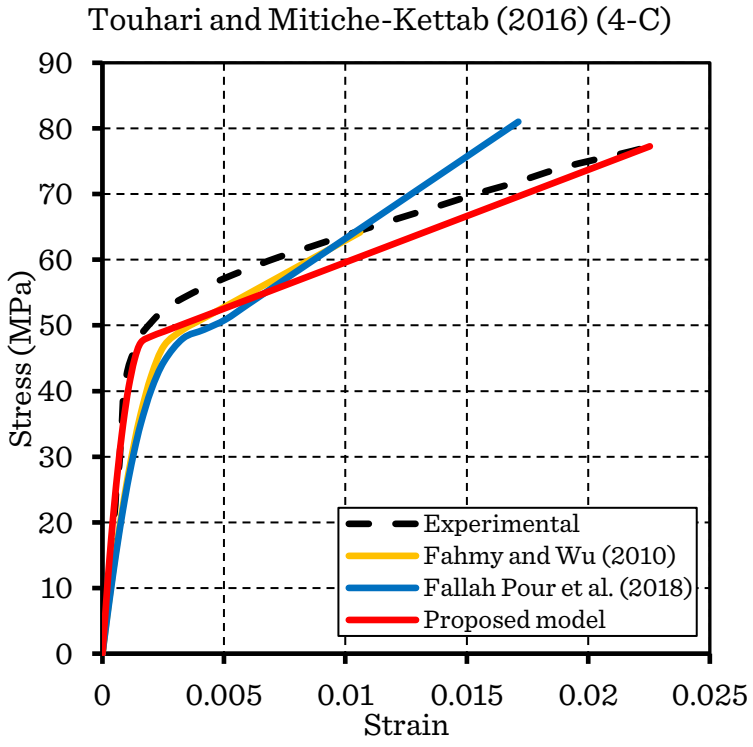

Figure 6.50 Comparison of experimental and predicted stress-strain curves of the proposed model and the existing models (C) (Specimen of Touhari and Mitiche-Kettab (2016) (4))

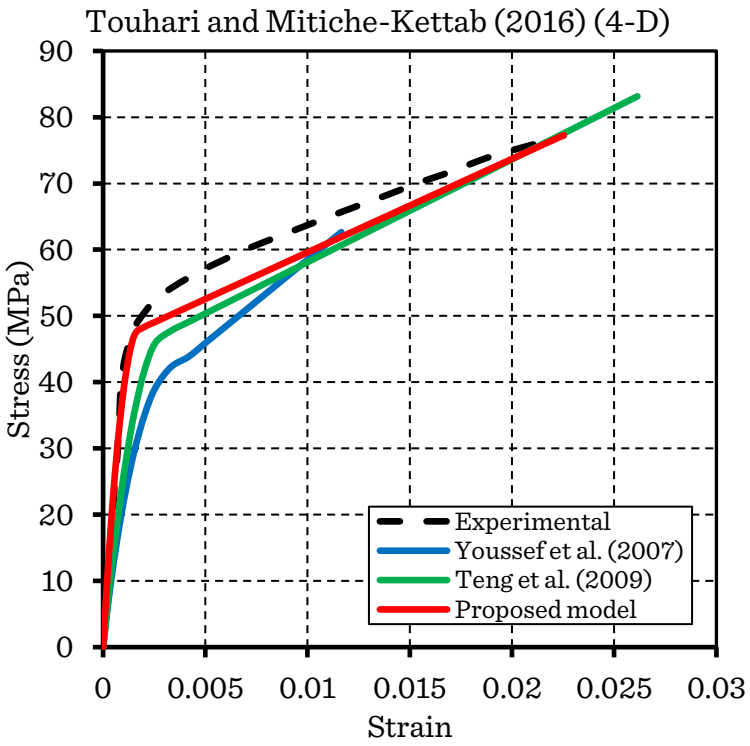

Figure 6.51 Comparison of experimental and predicted stress-strain curves of the proposed model and the existing models (D) (Specimen of Touhari and Mitiche-Kettab (2016) (4))

As shown in Figs. (6.51-6.54) of the last specimen of Touhari and Mitiche-Kettab (2016), the proposed model provides an accurate prediction of the first branch and overestimated stresses at the second branch with the best predicted ultimate condition.

The existing models underestimate the concrete stiffness at the first portion and overestimate the stresses at the second portion of the curve. The models of Fallah Pour et al. (2018) and Youssef et al. (2007), as in the previous specimens, show a discontinuous slope between the two portions of the curve (Figs. 6.53 and 6.54), while the model of Xiao and Wu (2003), shows a descending third branch (Fig. 6.47).

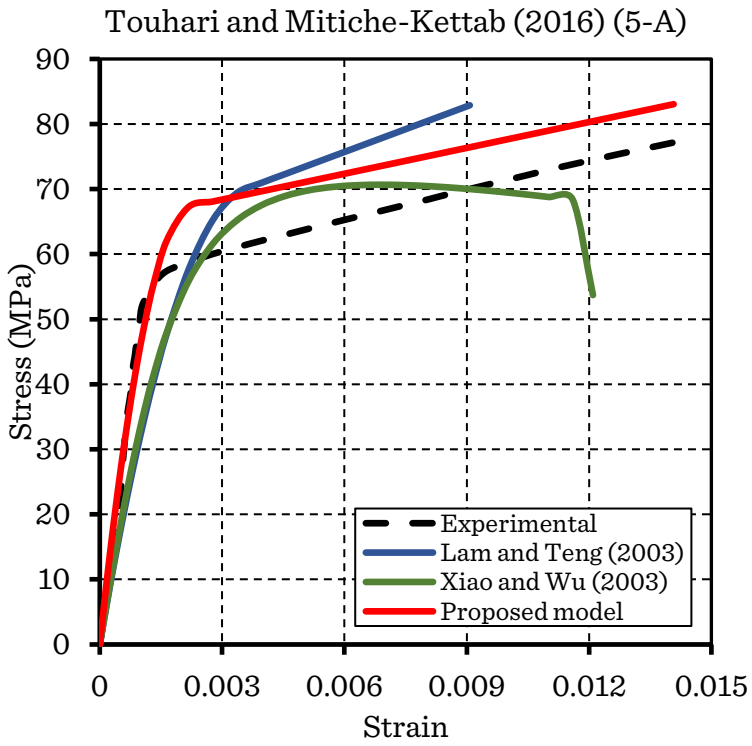

Figure 6.52 Comparison of experimental and predicted stress-strain curves of the proposed model and the existing models (A) (Specimen of Touhari and Mitiche-Kettab (2016) (5))

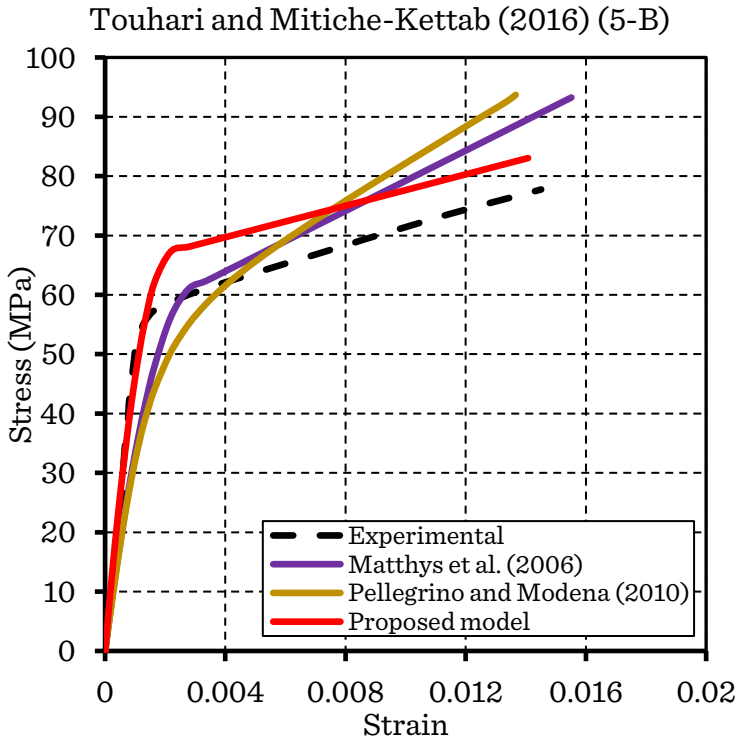

Figure 6.53 Comparison of experimental and predicted stress-strain curves of the proposed model and the existing models (B) (Specimen of Touhari and Mitiche-Kettab (2016) (5))

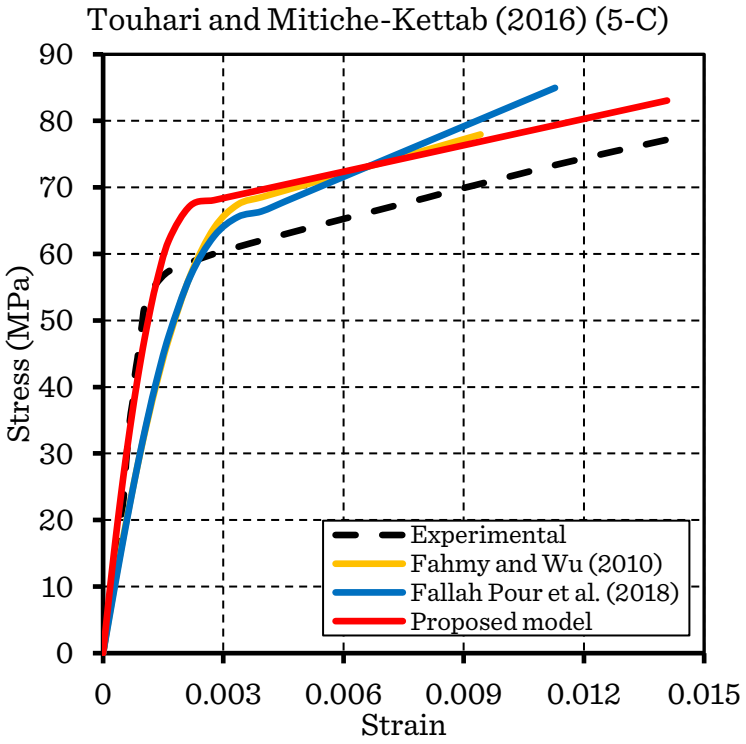

Figure 6.54 Comparison of experimental and predicted stress-strain curves of the proposed model and the existing models (C) (Specimen of Touhari and Mitiche-Kettab (2016) (5))

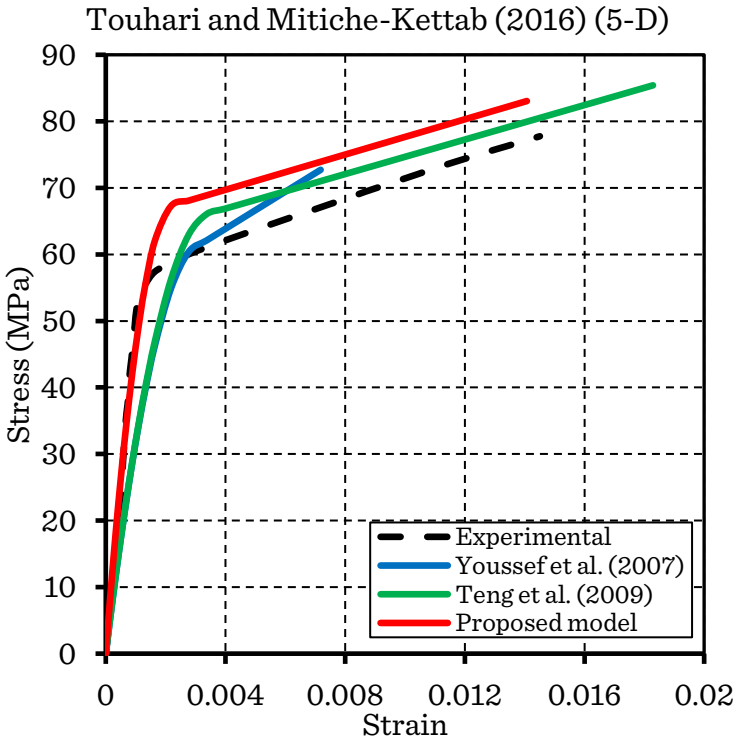

Figure 6.55 Comparison of experimental and predicted stress-strain curves of the proposed model and the existing models (D) (Specimen of Touhari and Mitiche-Kettab (2016) (5))

6.4.2.8 Summary of the performance of the models

After the comparison of the predictions of the proposed models and the existing models with the experimental results, the following observations can be drawn:

- Although the existing models were developed for concrete confined with different types of FRP, in most cases, they do not give satisfactory results for GFRP-confined concrete specimens.
- The model of Xiao and Wu (2003) failed to provide a coherent stress-strain curve. It shows a third descending portion due to the incompatibility of the ultimate condition equations with the stress-strain equation, and in other cases, it even provides a descending second portion.
- The model of Fallah Pour et al. (2018) and Youssef et al. (2007) failed to provide a smooth transition between the first and second portion of the stress-strain curve, which may be due to the incoherence in the slope of the first and second portions at the transition zone and the failure in the prediction of the transition point.
- The model of Kwan et al. (2015) failed to provide reasonable predictions of the stress-strain curve compared to the existing models. It was removed from the comparison due to the high deviation from the experimental curves.
- With simple equations, the proposed model can reasonably predict the axial stress-strain response of GFRP-wrapped concrete, including the ultimate point for a wide range of concrete strength and confinement levels, and outperforms the other existing models.
- The prediction of the second portion of the curve is highly dependent on the prediction of the ultimate conditions and the transition point.

6.5 Conclusion

In this chapter, a review of the available literature on modeling the stress-strain relationship of concrete confined with FRP was performed. Details on the different types of proposed equations were summarized. Nine old and recent stress-strain models for FRP-confined concrete were reviewed and evaluated based on several existing stress-strain curves from 7 experimental studies. A new stress-strain model for GFRP-wrapped concrete consisted of a parabolic equation for the first portion, and a linear equation for the second portion was proposed. The following conclusions can be drawn:

- The existing models showed moderate predictions of the axial behavior of GFRP-wrapped concrete.
- The models of Xiao and Wu (2003), Youssef et al. (2007), and Fallah Pour et al. (2018) showed deficiencies in the predictions of the ultimate point and the transition zone between the first and second portion of the curve.
- The proposed model provides reasonable agreement with the experimental curve and shows much better performance than the existing models.

Chapter 7

Influencing parameters on the behavior of GFRP-wrapped concrete under compression

7.1 Introduction

This chapter presents and discusses the effect of various parameters and their interactions on the axial response of GFRP-wrapped concrete. The parameters include the unconfined concrete strength, the FRP mechanical properties, and the specimen dimensions.

7.2 Strength and ductility parameters

As reported in Chapter 4, the characteristics of the stress-strain curve of FRP-confined concrete are dependent on several factors such as the confining material (i.e. type, amount, and characteristics of the FRP, the method of confinement, the concrete strength, and the interaction between the FRP and the concrete core) (Samaan et al., 1998). The essential characteristics of the stress-strain response include the slope of the first branch (E_1), the stress and the strain of the transition zone, the slope of the second branch (E_2) (the plastic stiffness), and the ultimate condition (f'_{cc}, ε_{cc}).

In this study, the investigation is based on the following parameters:

- The strength and strain enhancement effectiveness (Eq. (7.1) Eq. (7.2)) respectively.

$$\frac{f'_{cc}}{f'_{co}} = \left(0.775 + \frac{15.8}{f'_{co}}\right) + \left(4.34 - \frac{16.4}{\rho_\varepsilon} + \frac{24.5}{{\rho_\varepsilon}^2}\right)\left(\frac{f_{l,rup}}{f'_{co}}\right) \tag{7.1}$$

$$\frac{\varepsilon_{cc}}{\varepsilon_{co}} = \left(\frac{2.31}{0.31\,{\rho_\varepsilon}^2 - \rho_K}\right) + \left(\frac{3.57}{0.0842 + \rho_f}\right)\left(\frac{f_{l,rup}}{f'_{co}}\right) \tag{7.2}$$

- The energy absorption capacity, which is defined as the amount of energy per unit volume that a material can absorb before rupture (Eq. (7.3)) (Askeland et al., 2010). It is determined as the area under the confined concrete stress-strain curve up to ultimate stress (the blue area in Fig. 7.1).

$$U_T = \int_0^{\varepsilon_{cc}} \sigma d\varepsilon \qquad [N.m^{-2} = N.m.m^{-3} = J.m^{-3}] \tag{7.3}$$

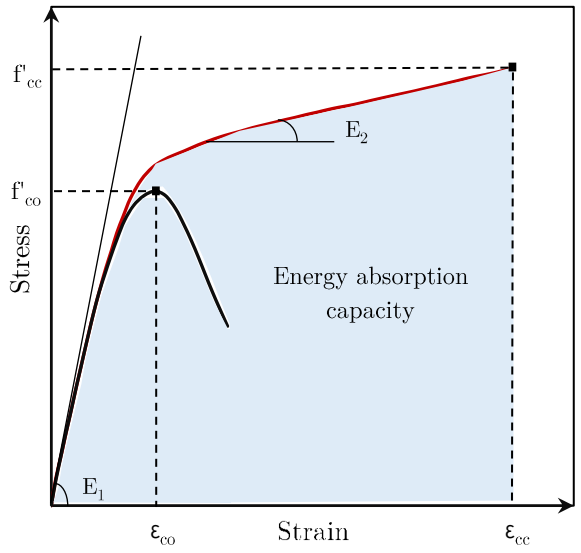

Figure 7.1 Parameters of the stress-strain curve of FRP-confined concrete

7.3 Influencing parameters on the stress-strain behavior of GFRP-wrapped concrete

In this study, the investigated variables are classified into two groups: 1) Those related to confinement material: amount, strength, and stiffness of the GFRP, and 2) Those related to the concrete: concrete strength and size of the concrete specimen (diameter).

7.3.1 Effect of FRP properties

7.3.1.1 Jacket thickness

The amount of FRP confinement has great importance in the performance and the economic effectiveness of FRP-confined concrete. In the present study, the effect of the amount of confinement is evaluated using five thicknesses (0.2, 0.5, 1, 2, and 3 mm). In order to provide a common base for the comparison, the same concrete strength ranging from low to high strength (30-120 MPa), the same

GFRP properties, and the same specimen dimensions (160, 320 mm) are used while changing the thickness of the jacket. For each of the concrete strengths and throughout the hole study, the unconfined concrete strain (ε_{co}) is calculated using the equation proposed by Lim and Ozbakkaloglu (2014) (Eq. (7.4)).

$$\varepsilon_{co} = \frac{f'^{\,0.225k_d}_{co}}{1000} k_s k_a \tag{7.4}$$

Where,

$$k_d = \left(\frac{2400}{\rho_{c,f}}\right)^{0.45} \tag{7.5}$$

$$k_s = \left(\frac{152}{d}\right)^{0.1} \tag{7.6}$$

$$k_a = \left(\frac{2d}{h}\right)^{0.1} \tag{7.7}$$

$\rho_{c,f}$ = the concrete density, taken as 2400 kg/m^3;

d = diameter of the cylinder;

h = height of the cylinder.

Table 7.1 shows the amount of GFRP with the volumetric ratios, the GFRP properties, and the concrete strength corresponding to each of the five considered cases.

Table 7.1 Variation of the thickness of the GFRP with the concrete strength

Specimen dimension (d, h) mm	GFRP properties		Concrete strength f'$_{co}$ (MPa)	ρ_ε (%)	0.5	1.25	2.5	5	7.5
	E_f (GPa)	f_f (MPa)							
(160, 320)	50	1000	30	t_f (mm)	0.2	0.5	1	2	3
			60		0.2	0.5	1	2	3
			90		0.2	0.5	1	2	3
			120		0.2	0.5	1	2	3

The effect of the thickness on the behavior of confined concrete for each of the concrete strengths is illustrated in Figs. 7.2-7.9, respectively. From these figures, it can be observed that:

- As noted in the assumptions of the proposed stress-strain model, the FRP confinement has no effect on the first branch of the curve. Hence, the elastic modulus of the confined concrete remains unchanged. Whereas the stress (f_o) improved as the amount of the GFRP increased for all concrete strengths due to the increase of the confining stress ($f_{l,rup}$) (Figs. 7.2, 7.4, 7.6, and 7.8).
- For the same concrete strength, as the thickness of the jacket increases, the slope of the second branch of the curve (the plastic stiffness of the confined concrete) improved, and it is more pronounced for high strength concretes. For instance, (E_2) improved from 1135 to 1769 MPa for 120 MPa when (t_f) increased from 2 to 3 mm (Fig. 9). Whereas for 30 MPa concrete, (E_2) improved only from 1102 to 1229 MPa (Fig. 7.3).
- For the same concrete strength, the strength enhancement ratio (f'_{cc}/f'_{co}) improved as the amount of confining FRP increased. This effect decreases for high strength concretes (need for more confinement (Figs. 7.6 and 7.8)). For instance, 120 MPa concrete confined with 2 mm of GFRP wraps shows only 16% of strength improvement (Fig. 7.9). However, for 30 MPa concrete wrapped with a smaller amount of FRP (i.e., t_f = 1 mm), the concrete strength improved by 75% (Fig. 7.3). These observations are confirmed by the results of Park et al. (2008) and Cui and Sheikh (2010).
- The strain enhancement ratio ($\varepsilon_{cc}/\varepsilon_{co}$) (axial ductility of the confined concrete) improved with the increase of the FRP thickness for the same concrete strength. However, with the increase of the concrete strength, this improvement decreases. For example, for 60 MPa concrete confined with 2 mm of GFRP wraps, the axial ductility ($\varepsilon_{cc}/\varepsilon_{co}$) improved seven times (Fig. 7.5), whereas, for 120 MPa confined with the same GFRP amount, this ratio has only improved by four times (Fig. 7.9). These results are confirmed by the results of Cui and Sheikh (2010).
- The effect of the amount of FRP on ductility is much more pronounced than that on strength. For instance, for 60 MPa concrete confined with 0.5 mm to 2 mm of GFRP, the strength increased from 15% to 50%, while the corresponding strain improved from 172% to 605% (Fig. 7.5).

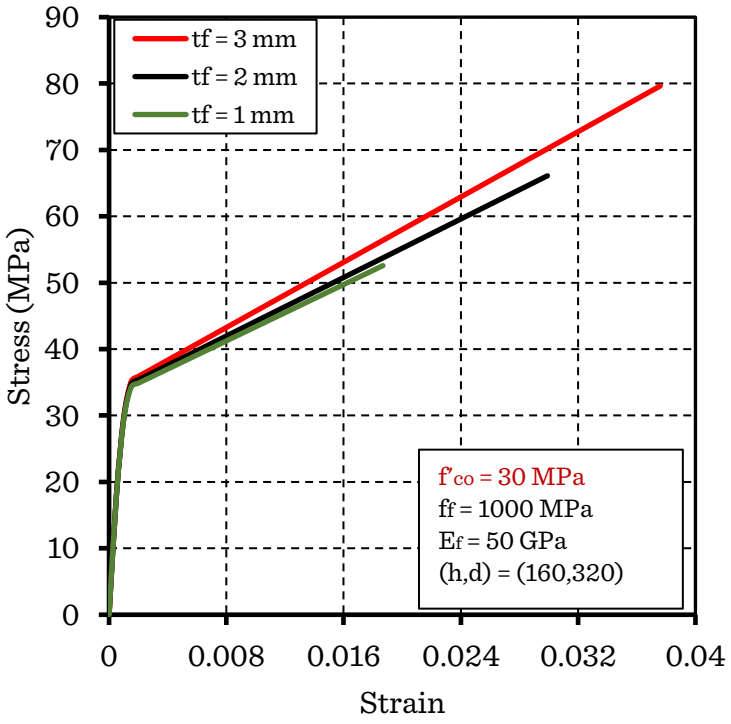

Figure 7.2 Influence of the FRP amount on the stress-strain behavior of GFRP-wrapped concrete (f'_{co} = 30 MPa)

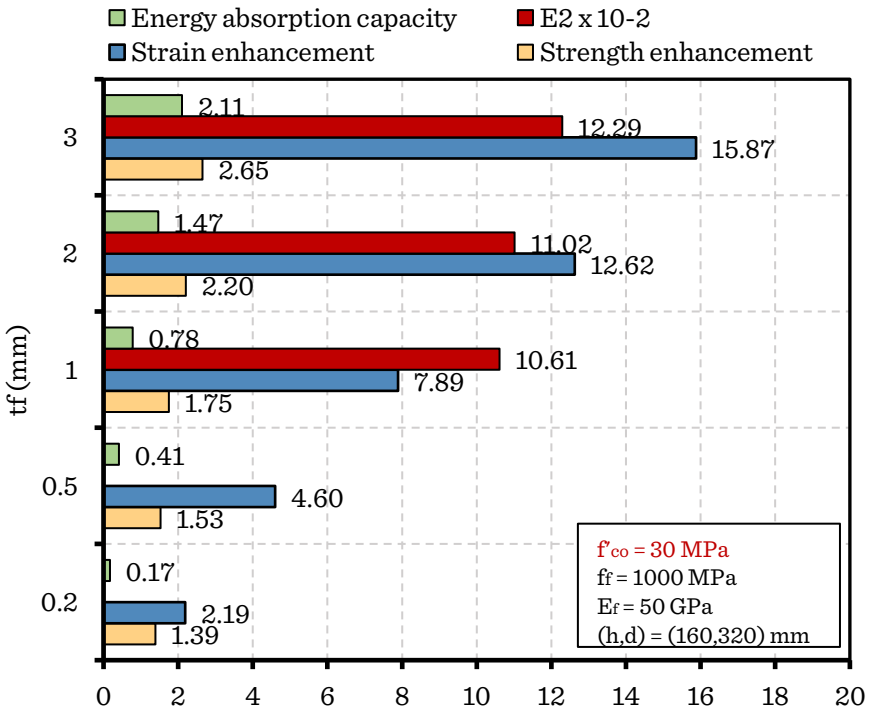

Figure 7.3 Variation of the confinement parameters with the amount of the GFRP (f'_{co} = 30 MPa)

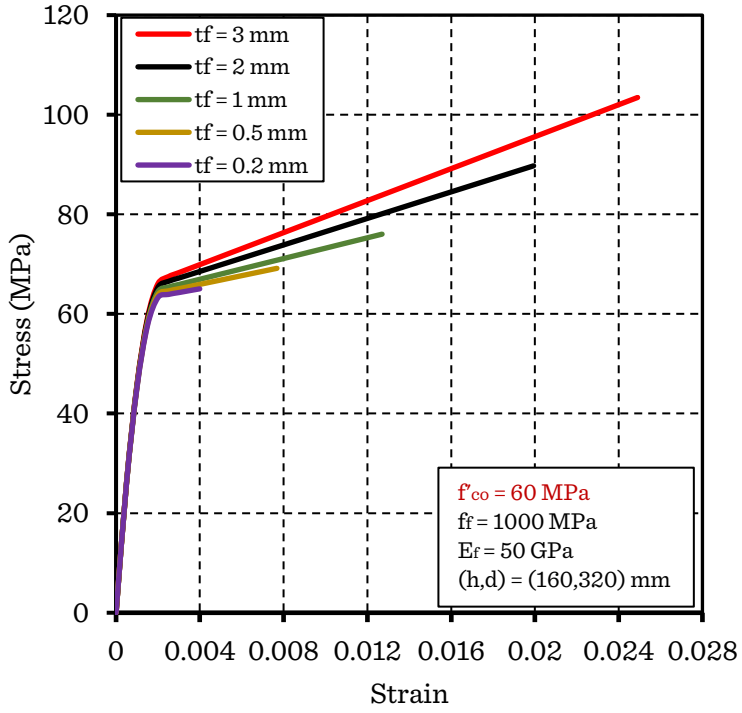

Figure 7.4 Influence of the GFRP amount on the stress-strain behavior of GFRP-wrapped concrete (f'_{co} = 60 MPa)

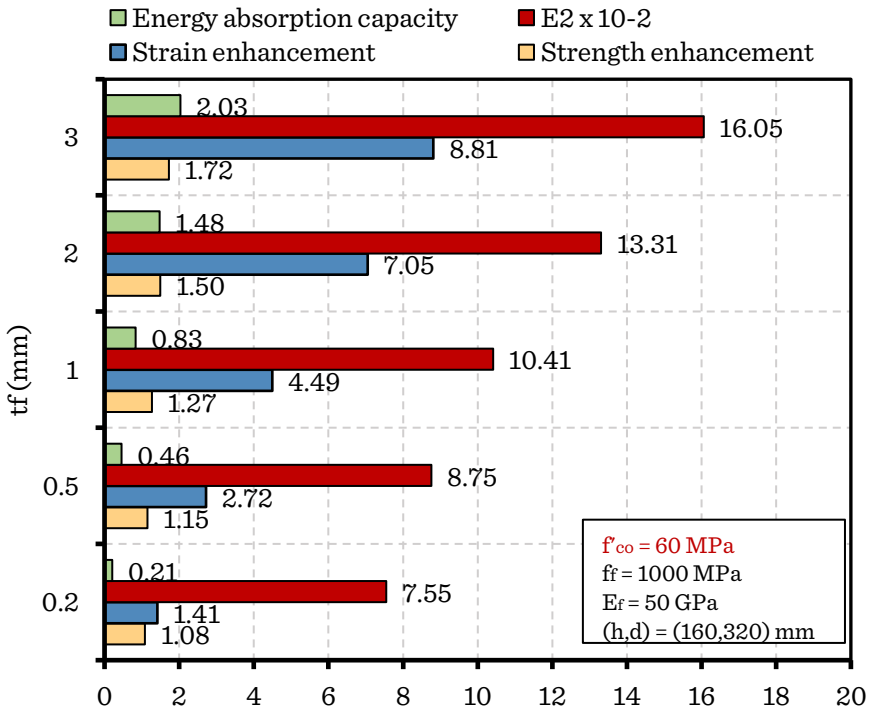

Figure 7.5 Variation of the confinement parameters with the amount of the GFRP (f'_{co} = 60 MPa)

- High-strength concretes require more confinement than LSCs. For instance, 0.2 mm and 0.5 mm of GFRP improved the strength by 39% and 53%, and the axial ductility with 119% and 360% for 30 MPa concrete, respectively (Fig. 7.3). However, for 90 MPa and 120 MPa concretes confined with the same amount of GFRP, the stress-strain curve exhibits a decreasing second branch indicating insufficient confinement (Figs. 7.7 and 7.9).
- The energy absorption capacity increases with the FRP amount. For instance, for 60 MPa concrete, increasing the thickness of the GFRP from 1 to 2 mm improved the energy absorption capacity from 0.83 to 1.48 J.m^{-3} (Fig. 5). It should be noted that HSCs absorb more energy than LSCs when confined with the same amount of FRP. For example, 30 MPa concrete wrapped with 2 and 3 mm of GFRP absorb 1.47 J.m^{-3} and 2.11 J.m^{-3} of energy (Fig. 7.3), whereas 120 MPa concrete absorb 1.72 J.m^{-3} and 2.31 J.m^{-3} of energy when confined with the same GFRP amount (Fig. 7.9).

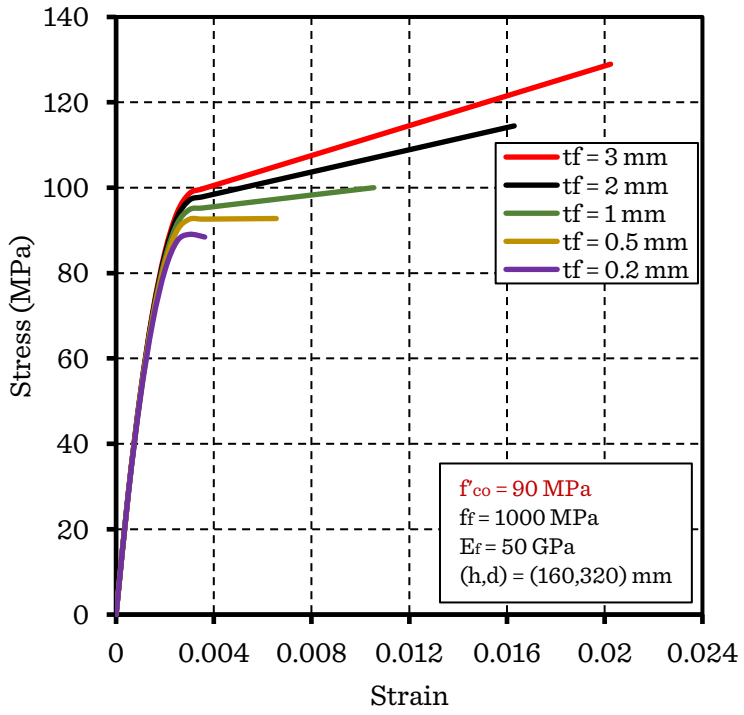

Figure 7.6 Influence of the FRP amount on the stress-strain behavior of GFRP-wrapped concrete (f'_{co} = 90 MPa)

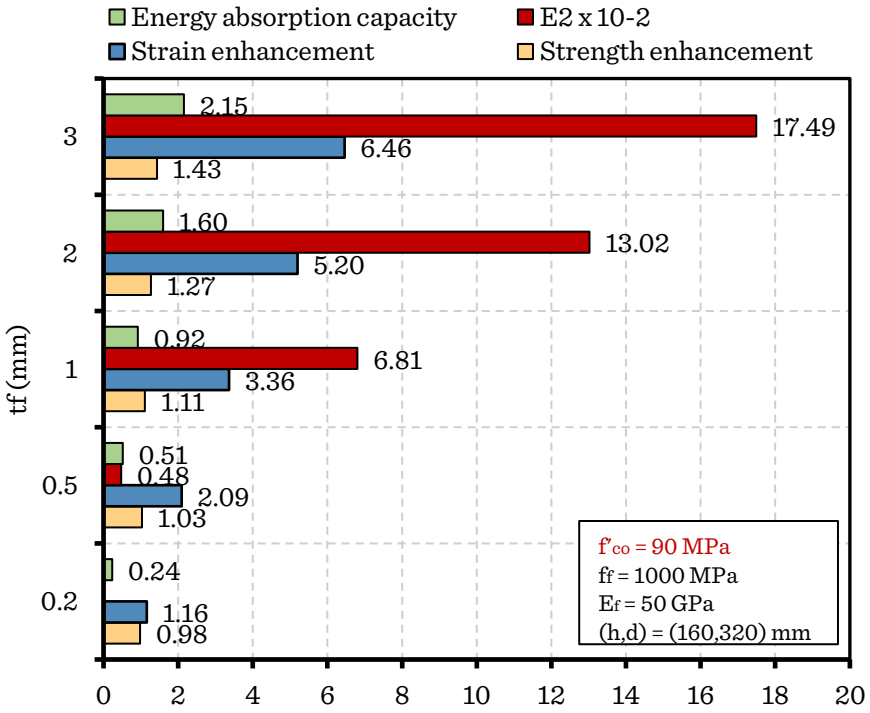

Figure 7.7 Variation of the confinement parameters with the amount of the GFRP (f'_{co} = 90MPa)

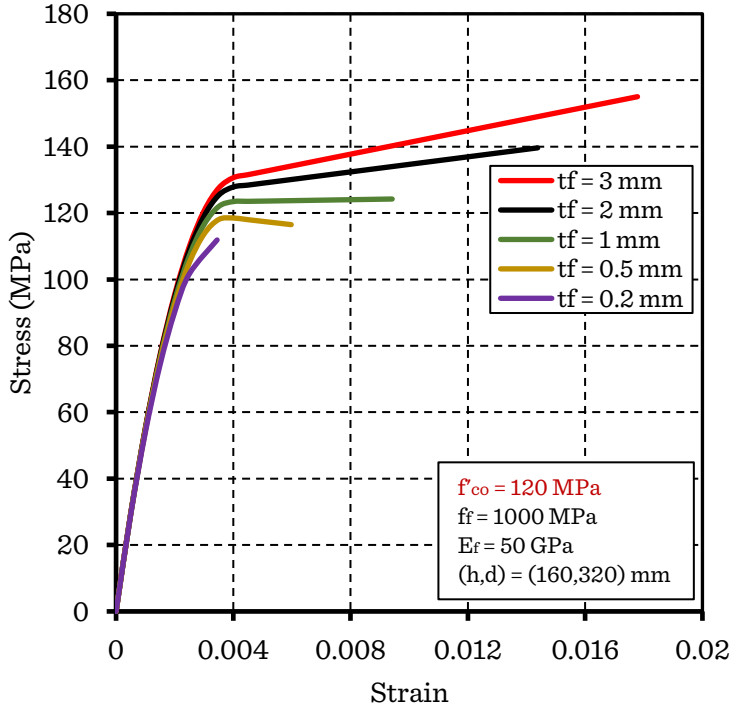

Figure 7.8 Influence of the FRP amount on the stress-strain behavior of GFRP-wrapped concrete (f'_{co} = 120 MPa)

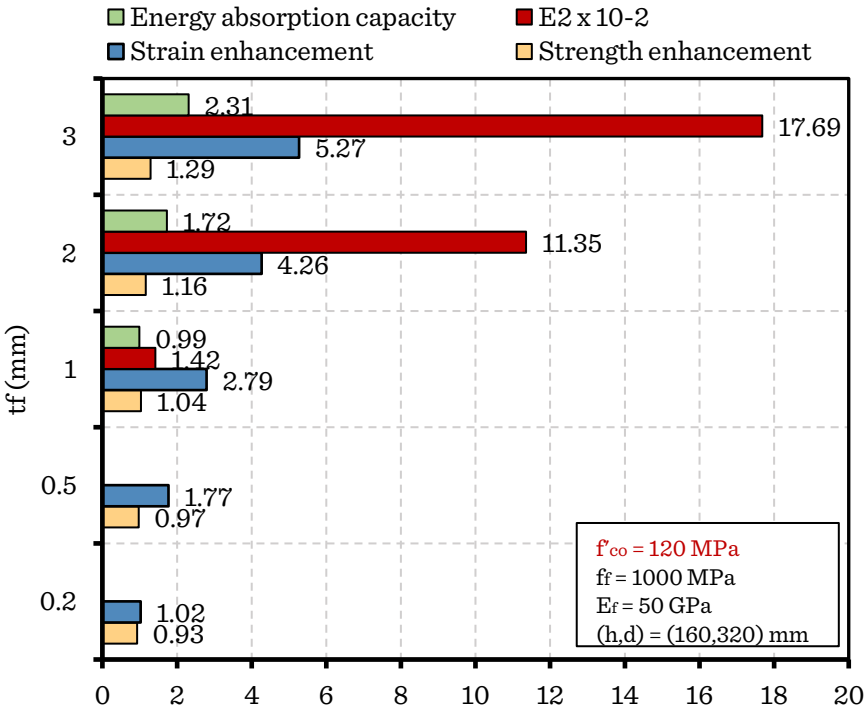

Figure 7.9 Variation of the confinement parameters with the amount of the GFRP (f'_{co} = 120 MPa)

7.3.1.2 Tensile strength

The effect of the tensile strength of GFRP on the stress-strain behavior of GFRP-confined concrete is evaluated using four values (400, 700, 1000, and 1400 MPa). In order to limit the study on the effect of the tensile strength, the same concrete strength ranging from low to high strength (30-120 MPa), the same GFRP properties (thickness and elastic modulus), and the same specimen dimensions (160, 320 mm) are used while varying the tensile strength of the jacket. All of these parameters are summarized in Table 7.2.

Table 7.2 Variation of the tensile strength of the GFRP with the concrete strength

Specimen dimension (d, h) mm	GFRP properties		Concrete strength f'_{co} (MPa)	Tensile strength f_f (MPa)			
	E_f (GPa)	t_f (mm)					
(160, 320)	50	2	30	400	700	1000	1400
			60	400	700	1000	1400
			90	400	700	1000	1400

	120	400	700	1000	1400

For each of the concrete strengths, the effect of the tensile strength on the stress-strain behavior of GFRP-confined concrete is illustrated in Figs. 7.10-7.17, respectively. From these figures, it can be observed that:

- The increase in the tensile strength of the FRP has no effect on the elastic modulus of the confined concrete, and the first branch remains unchanged. Similar findings can be observed for the stress (f_o), where no significant improvement has been reached.
- For low-strength concrete, increasing the tensile strength has no significant effect on the plastic stiffness (E_2) of the confined concrete (for (f_f) varying from 400 to 1400 MPa, (E_2) varied only from 1038 to 1112 MPa (Fig. 7.11)). However, for HSC (f'_{co} = 120 MPa), (E_2) improved as the tensile strength increased. For instance, when (f_f) increased from 700 to 1400 MPa, (E_2) improved from 586 to 1380 MPa (Fig. 7.17).
- For the same concrete strength, the strength enhancement ratio (f'_{cc}/f'_{co}) improved as the tensile strength of the FRP increased. This effect decreases for HSCs. For instance, for 30 MPa concrete, the concrete strength improved from 94% to 124% when (f_f) increased from 700 to 1400 MPa (Fig. 7.11). However, it is only improved from 18% to 31% for 90 MPa concrete (Fig. 7.15).
- The axial ductility ($\varepsilon_{cc}/\varepsilon_{co}$) of the confined concrete improved with the tensile strength increase for the same concrete strength. However, the improvement of the axial ductility decreases as the concrete strength increases. For instance, for 30 MPa concrete confined with GFRP of 1000 MPa of tensile strength, the axial ductility ($\varepsilon_{cc}/\varepsilon_{co}$) improved more than 12 times (Fig. 7.11), whereas, for 120 MPa, the ($\varepsilon_{cc}/\varepsilon_{co}$) has only improved with four times (Fig. 7.17).
- The effect of the tensile strength of FRP on ductility is much more pronounced than that on strength. For instance, for 60 MPa concrete confined with GFRP of tensile strength varying from 400 MPa to 1400 MPa, the strength increased from 29% to 53%, while the corresponding strain improved from 405% to 635% (Fig. 7.13).

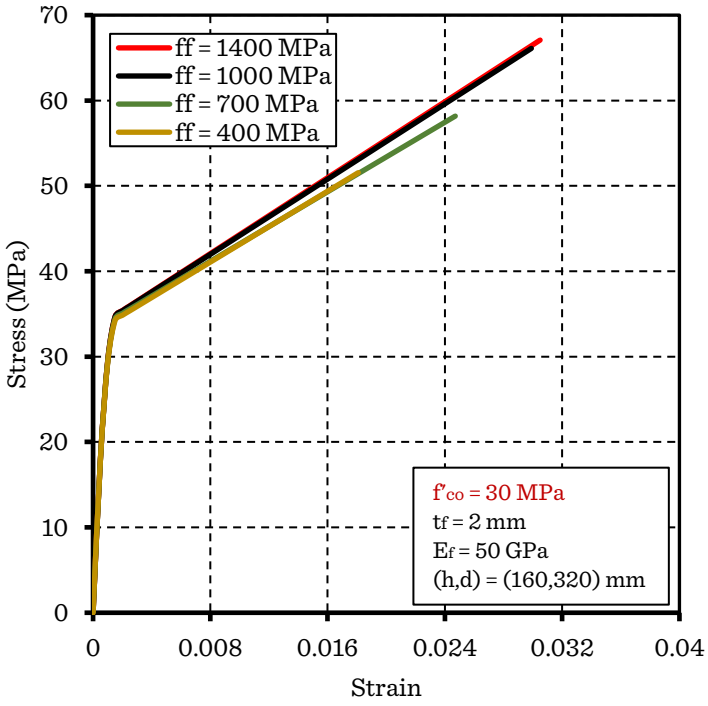

Figure 7.10 Influence of the FRP tensile strength on the stress-strain behavior of GFRP-wrapped concrete (f'_{co} = 30 MPa)

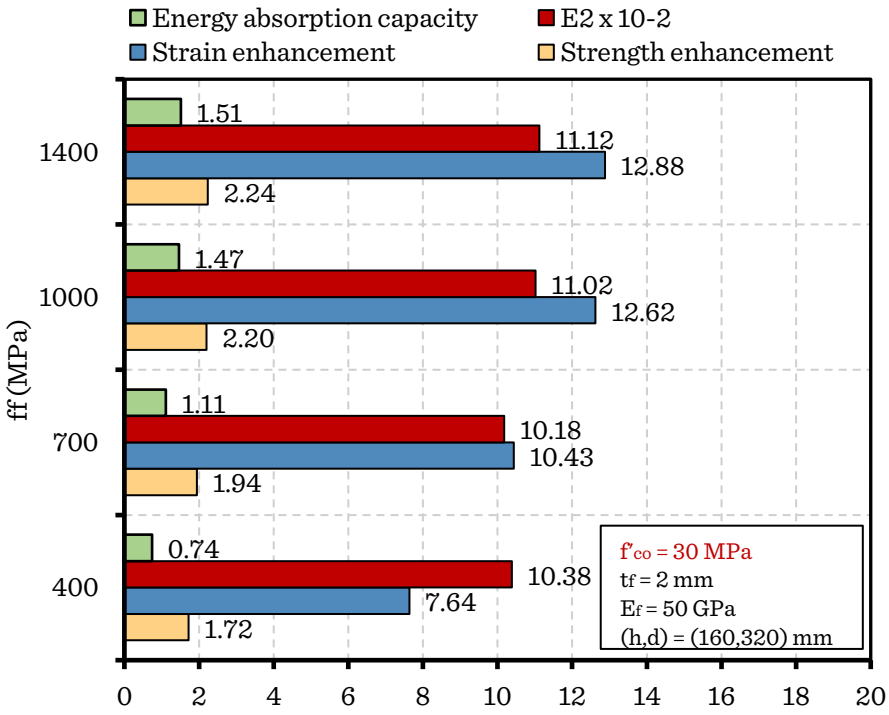

Figure 7.11 Variation of the confinement parameters with the tensile strength of the GFRP (f'_{co} = 30 MPa)

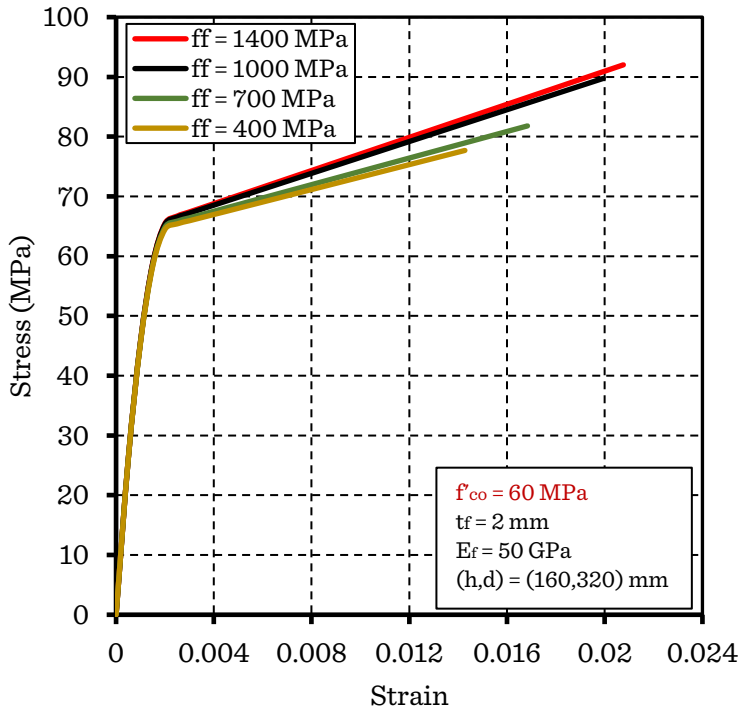

Figure 7.12 Influence of the GFRP tensile strength on the stress-strain behavior of GFRP-wrapped concrete (f'_{co} = 60 MPa)

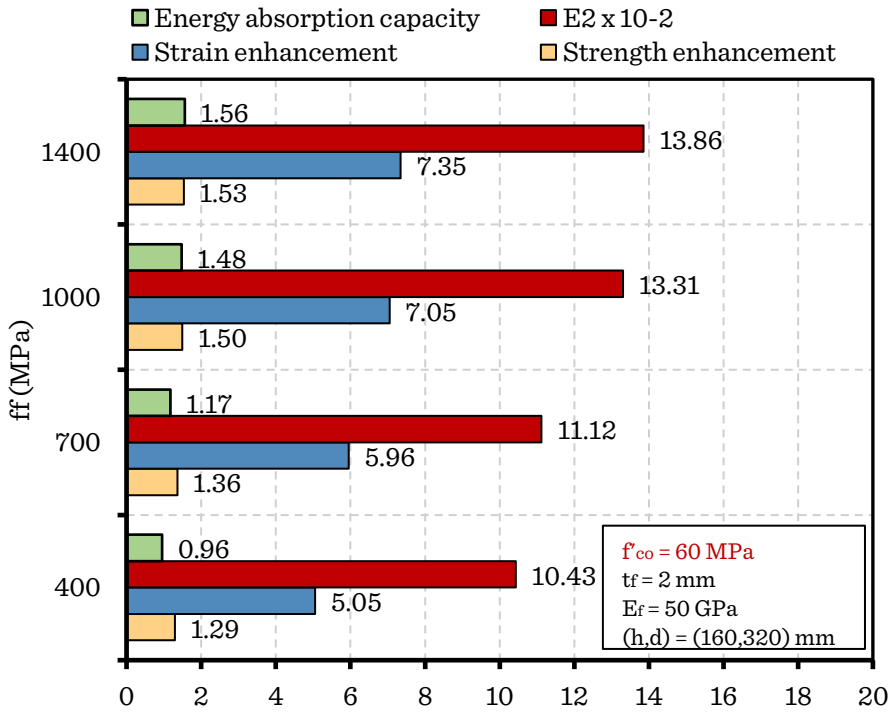

Figure 7.13 Variation of the confinement parameters with the tensile strength of the GFRP (f'_{co} = 60 MPa)

- HSCs require more confinement than LSCs (the need for higher tensile strength to achieve high confinement). For instance, GFRP with a tensile strength of 1000 MPa improved the strength by 120% and axial ductility by 1162% for 30 MPa, respectively (Fig. 7.11). However, for 120 MPa concretes confined with the same GFRP, the strength improved only by 16%, and the corresponding strain by 326% (Figs. 7.17).
- The energy absorption capacity increases as the tensile strength of the FRP increases. For instance, for 90 MPa concrete, increasing the tensile strength from 700 to 1400 MPa improved the energy absorption capacity from 1.30 to 1.72 $J.m^{-3}$ (Fig. 5.15). In addition, HSCs absorb more energy than LSCs when confined with the same GFRP (same tensile strength). For example, 30 MPa concrete wrapped with GFRP of tensile strength of 700 MPa absorbs 1.11 $J.m^{-3}$ of energy (Fig. 7.11), whereas 120 MPa concrete absorb 1.43 $J.m^{-3}$ of energy (Fig. 7.17).

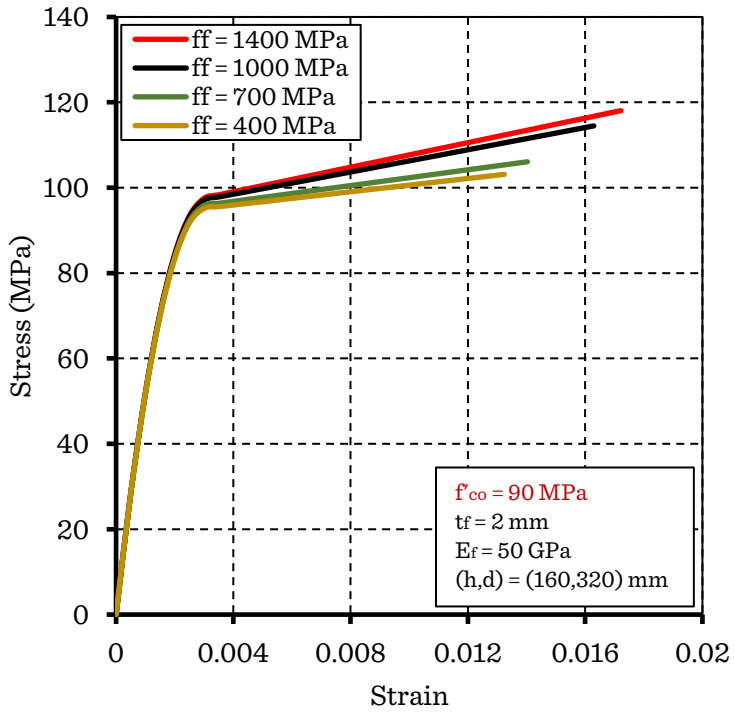

Figure 7.14 Influence of the FRP tensile strength on the stress-strain behavior of GFRP-wrapped concrete (f'_{co} = 90 MPa)

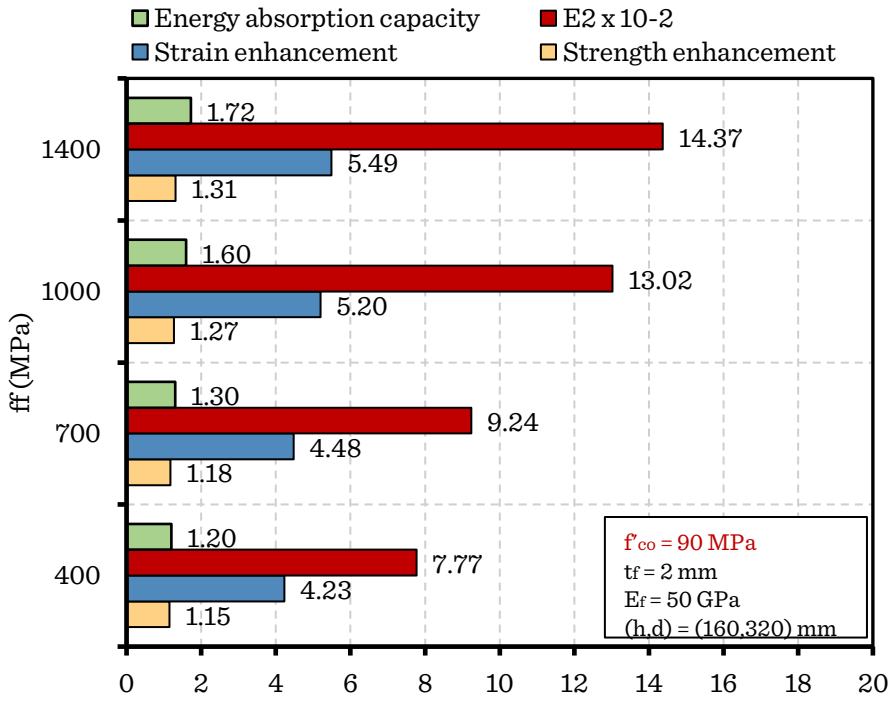

Figure 7.15 Variation of the confinement parameters with the tensile strength of the GFRP (f'_{co} = 90 MPa)

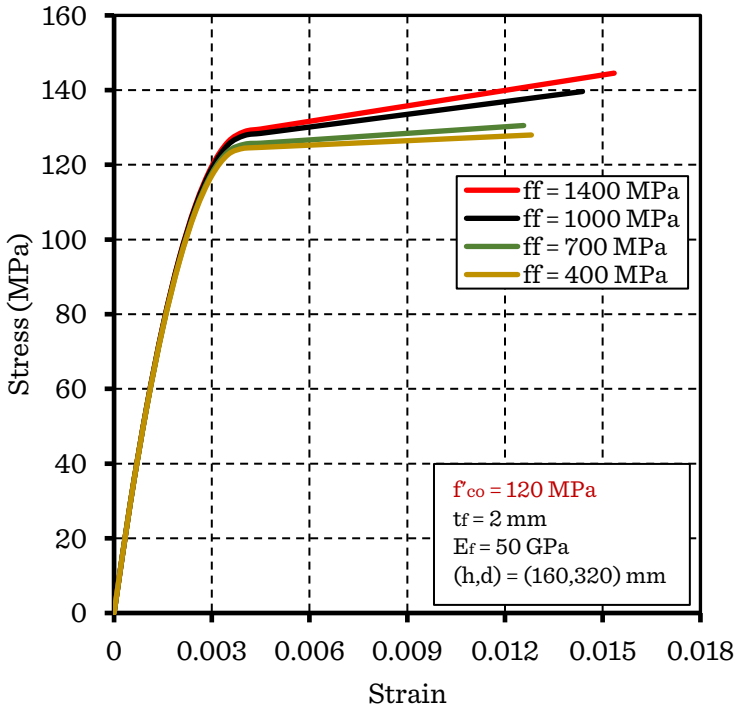

Figure 7.16 Influence of the FRP tensile strength on the stress-strain behavior of GFRP-wrapped concrete (f'_{co} = 120 MPa)

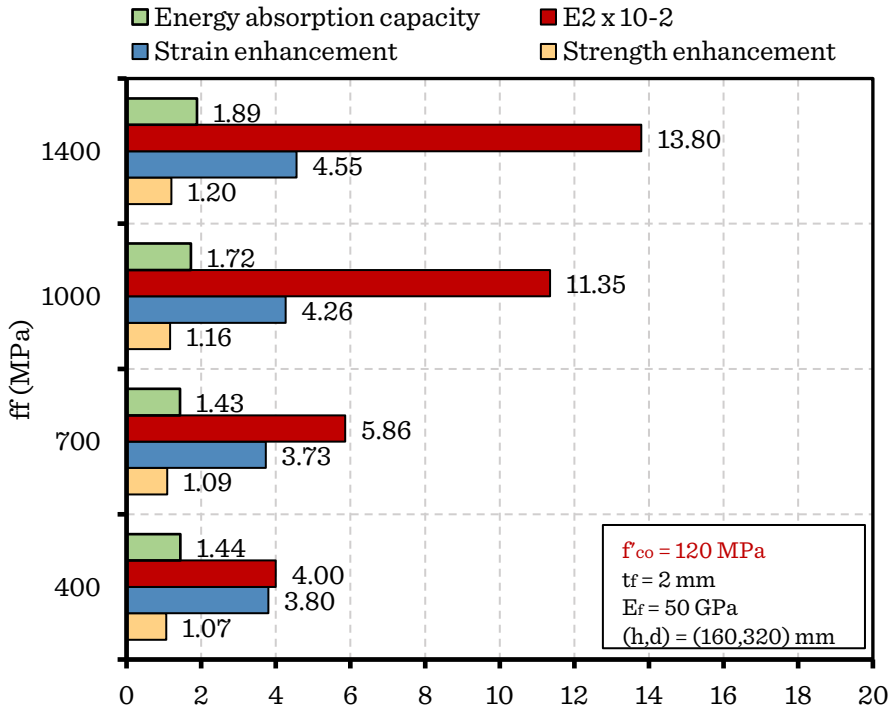

Figure 7.17 Variation of the confinement parameters with the tensile strength of the GFRP (f'_{co} = 120 MPa)

- When compared with the effect of the thickness of the GFRP, it can be observed that for the same concrete strength confined with the same GFRP, increasing the thickness of the GFRP is more efficient than increasing the tensile strength. For instance, for 30 MPa concrete confined with GFRP of (f_f = 1000 MPa, and E_f = 50 GPa), increasing the thickness from 2 mm to 3 mm improved the strength from 120% to 165%, the ductility from 1162% to 1487%, the plastic stiffness from 1102 to 1229 MPa, and the energy absorption capacity from 1.47 to 2.11 J.m^{-3} (Fig. 7.3). However, for the same concrete, increasing the strength from 1000 to 1400 MPa with (E_f = 50 GPa, and t_f = 2 mm), the strength only improved from 120% to 124%, the ductility from 1162% to 1288%, the plastic stiffness from 1102 to 1112 MPa, and the energy absorption capacity from 1.47 to 1.51 J.m^{-3} (Fig. 7.17). Similarly, for HSC (f'_{co} = 120 MPa), increasing the thickness from 2 mm to 3 mm (f_f = 1000 MPa and E_f = 50 GPa) improved the strength from 16% to 29%, the ductility from 326% to 427%, the plastic stiffness from 1135 to 1769 MPa, and the energy absorption capacity from 1.72 to 2.31 J.m^{-3} (Fig. 7.3). However, increasing the tensile strength from 1000 to 1400 MPa with (E_f = 50 GPa, and t_f = 2 mm), the strength only improved from 16% to 20%, the ductility from 326% to 355%, the plastic stiffness from 1135 to 1380 MPa, and the energy absorption capacity from 1.72 to 1.89 J.m^{-3} (Fig. 7.17).

7.3.1.3 Modulus of elasticity

The effect of the elasticity modulus of the GFRP on the stress-strain behavior of GFRP-confined concrete is evaluated using three values (25, 50, and 75 GPa). In order to isolate the effect of the (E_f), the same concrete strength ranging from low to high strength (30-120 MPa), the same GFRP properties (thickness and tensile strength), and the same specimen dimensions (160, 320 mm) are used while varying the elasticity modulus of the jacket. Table 7.3 summarizes the values of the parameters used in this study.

Table 7.3 Variation of the elasticity modulus of the GFRP with the concrete strength

Specimen dimension (d, h) mm	GFRP properties		Concrete strength f'_{co} (MPa)	Elasticity modulus (GPa)		
	f_f (MPa)	t_f (mm)				
(160, 320)	1000	2	30	25	50	75
			60	25	50	75
			90	25	50	75
			120	25	50	75

Figures 7.18-7.25 illustrate the results of the parametric study by varying the elasticity modulus for each of the concrete strengths. From these figures, it can be observed that:

- As found in the tensile strength, when increasing the elasticity modulus of the GFRP, the first branch of the confined concrete stress-strain curve (elastic modulus and the stress (f_o)) is unchanged.
- The increase in (E_f) of the GFRP leads to a decrease in the plastic slope of the confined concrete for all concrete strengths. For instance, (E_2) decreased from 1557 MPa to 905 MPa when (E_f) increased from 25 to 75 GPa for 30 MPa concrete (Fig. 7.19) and from 3295 to 1369 MPa for 120 MPa (Fig. 7.25). The same results are also found in Cui and Sheikh (2010).
- Similarly, increasing the (E_f) affects the compressive strength of the confined concrete for low and high concrete strengths. For (E_f) varying from 25 to 75 GPa, the strength enhancement decreased from 162% to 104 % for 30 MPa concrete (Fig. 7.19) and from 49% to 26% for 120 MPa concrete (Fig. 7.25).
- The strain enhancement ratio ($\varepsilon_{cc}/\varepsilon_{co}$) improved with a small amount as the (E_f) of the GFRP increased. For instance, for 60 MPa concrete, the

axial ductility improved from 6.74 to 7.60 when (E_f) increased from 25 to 75 GPa (Fig. 21) and from 4.93 to 5.86 for 120 MPa (Fig. 7.25).

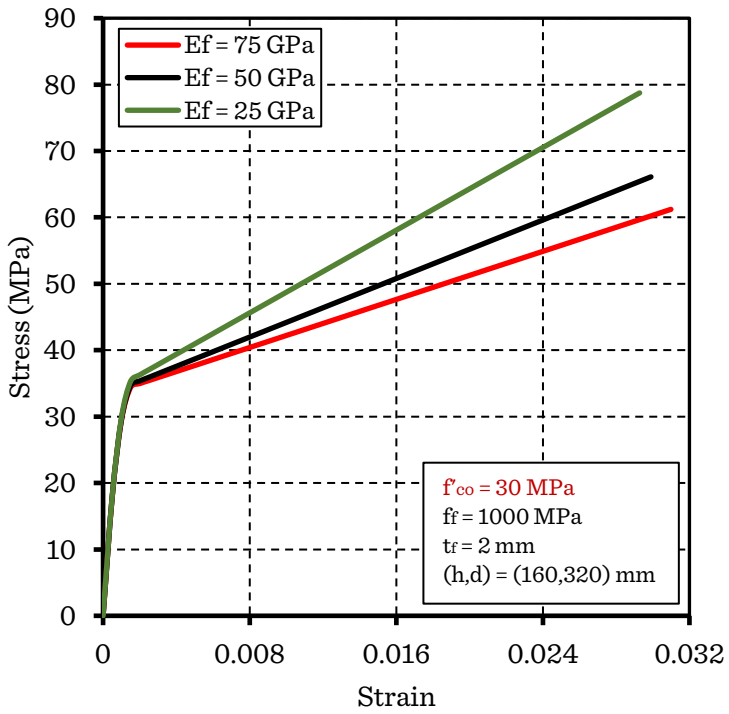

Figure 7.18 Influence of the modulus of elasticity of the GFRP on the stress-strain behavior of GFRP-wrapped concrete (f'_{co} = 30 MPa)

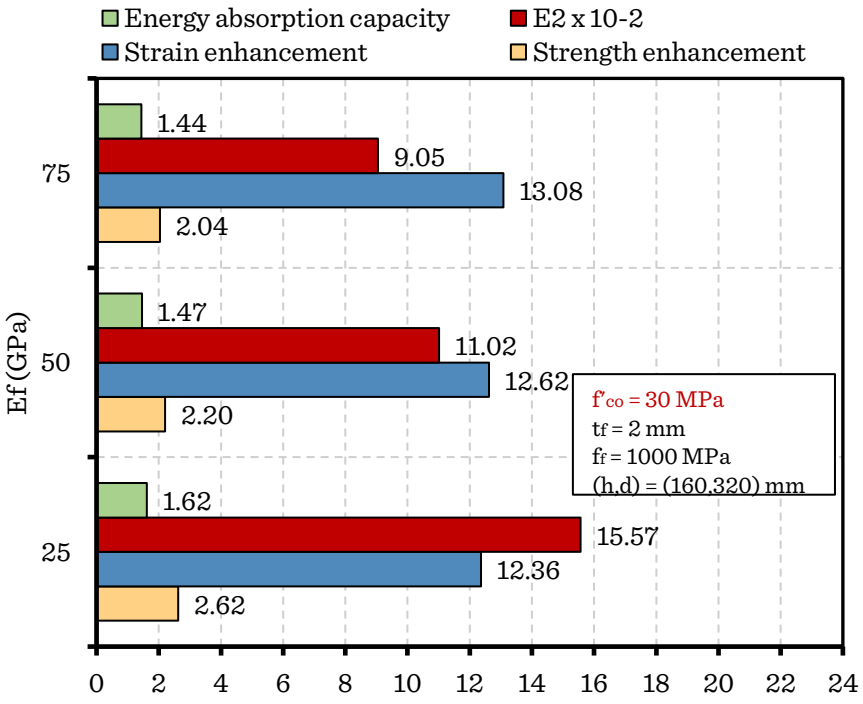

Figure 7.19 Variation of the confinement parameters with the modulus of elasticity of the GFRP (f'_{co} = 30 MPa)

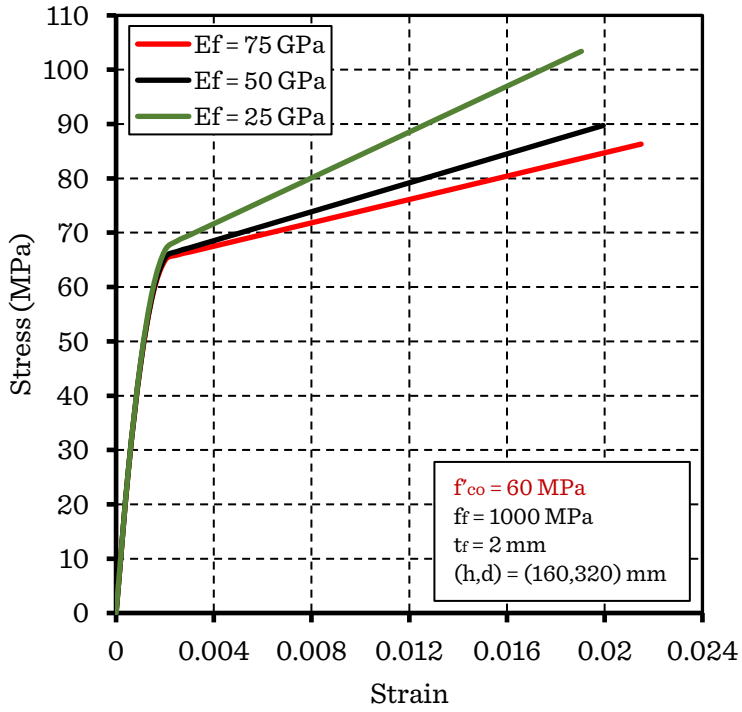

Figure 7.20 Influence of the modulus of elasticity of the GFRP on the stress-strain behavior of GFRP-wrapped concrete (f'_{co} = 60 MPa)

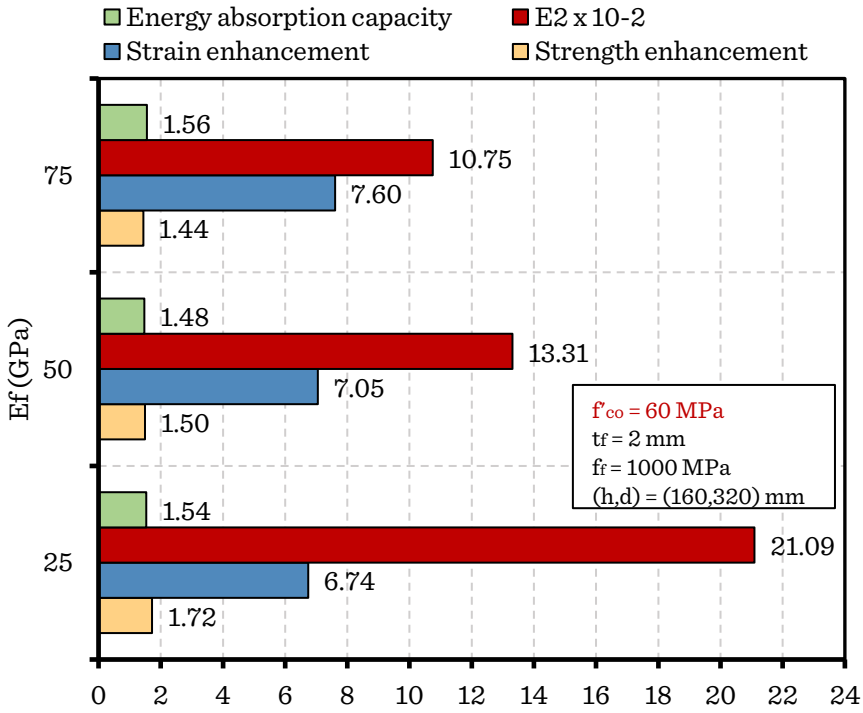

Figure 7.21 Variation of the confinement parameters with the modulus of elasticity of the GFRP (f'_{co} = 60 MPa)

- Due to the decrease of the plastic slope and the compressive strength of the confined concrete, and the increase in the axial ductility with the increase of the elasticity modulus of the FRP, the energy absorption capacity has no clear tendency (Figs. 7.21, 7.23, and 7.25) except for 30 MPa concrete in which it shows a decrease from 1.62 to 1.44 J.m^{-3} when (E_f) varied from 25 to 75 GPa (Fig. 7.19).

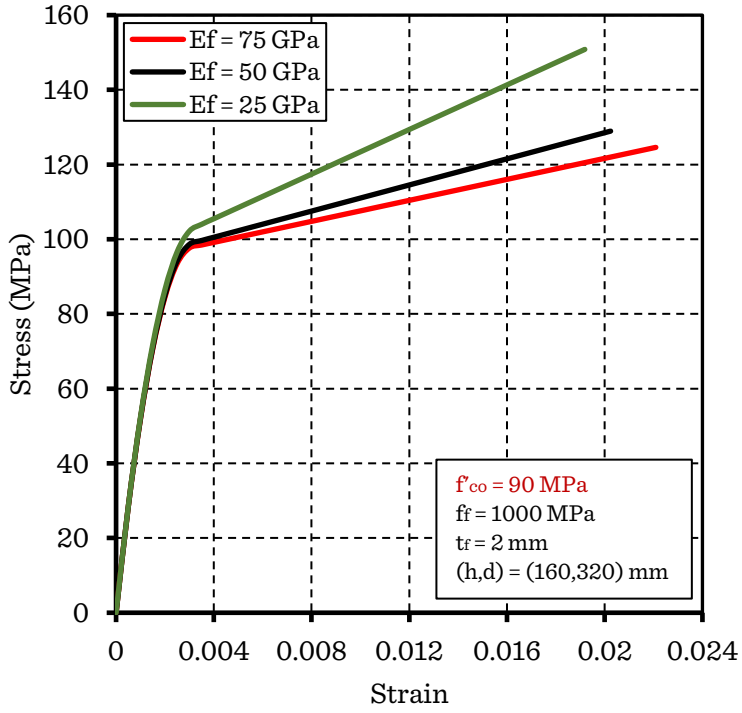

Figure 7.22 Influence of the modulus of elasticity of the GFRP on the stress-strain behavior of GFRP-wrapped concrete (f'_{co} = 90 MPa)

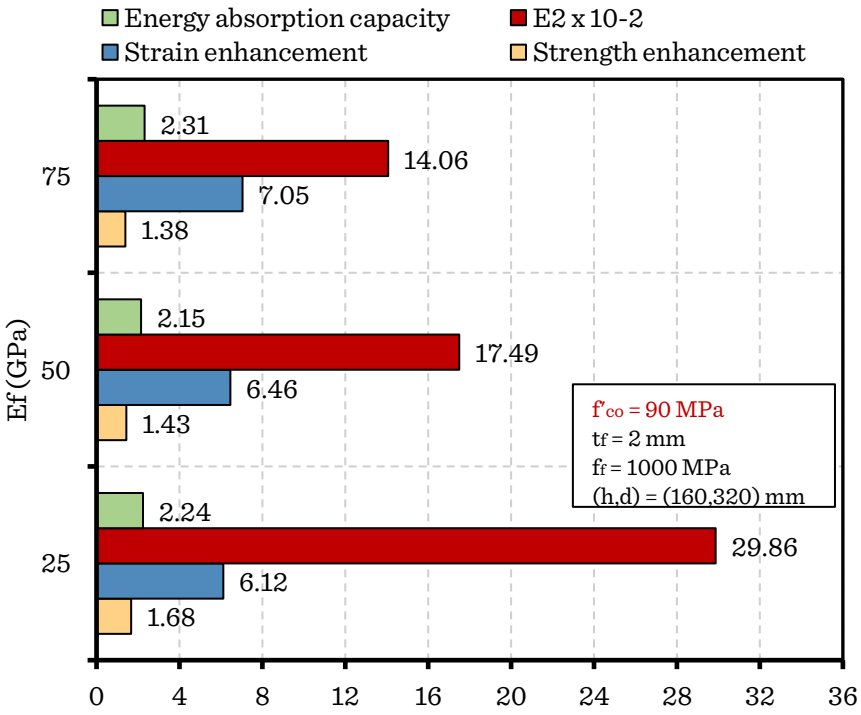

Figure 7.23 Variation of the confinement parameters with the modulus of elasticity of the GFRP (f'_{co} = 90 MPa)

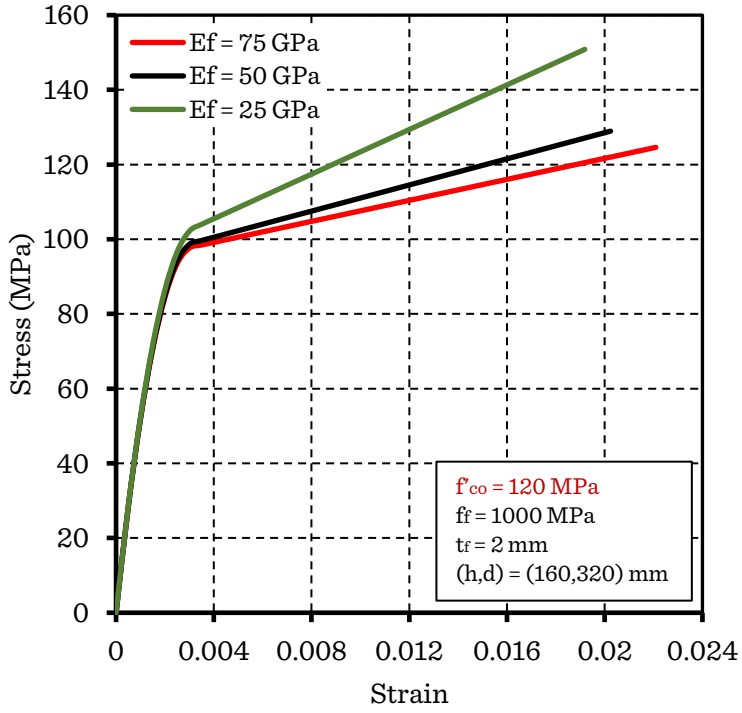

Figure 7.24 Influence of the modulus of elasticity of the GFRP on the stress-strain behavior of GFRP-wrapped concrete (f'_{co} = 120 MPa)

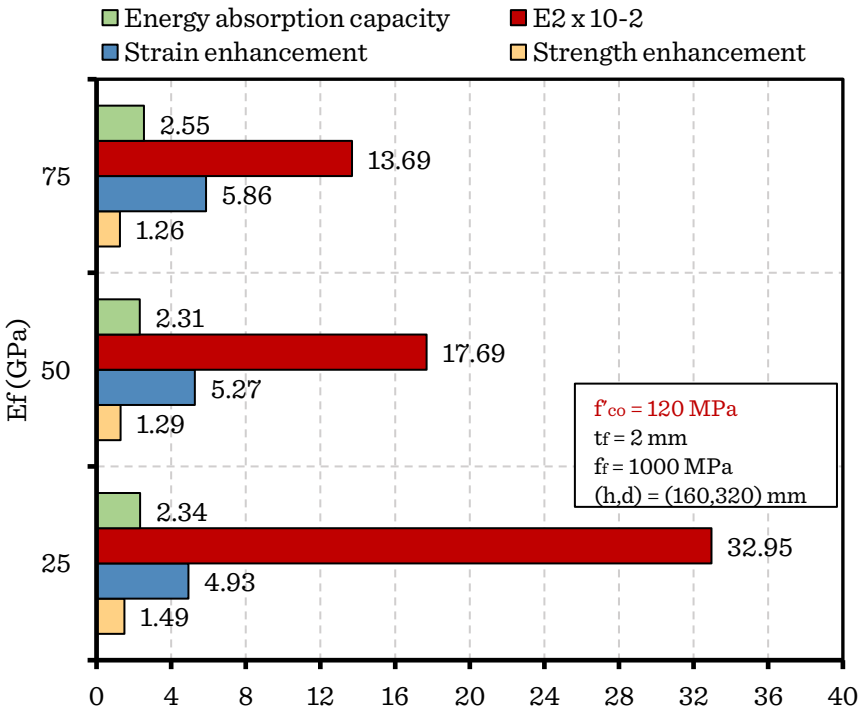

Figure 7.25 Variation of the confinement parameters with the modulus of elasticity of the GFRP (f'_{co} = 120 MPa)

7.3.2 Effect of concrete strength

The effect of the unconfined concrete strength on the stress-strain behavior of GFRP-wrapped concrete is studied by varying four concrete strengths (30, 60, 90, and 120 MPa) while fixing the same GFRP material and the same specimen geometry. Table 7.4 summarizes the parameters of the cylinders used in this study.

Table 7.4 Variation of the concrete strength with the GFRP properties

Specimen dimension (d, h) mm	GFRP properties			Concrete strength
	f_f (MPa)	E_f (GPa)	t_f (mm)	f'_{co} (MPa)
(160, 320)	1000	50	2	30
				60
				90
				120

In each case, the behavior of the confined concrete is compared with the unconfined concrete stress-strain curve. The stress-strain relationship of the unconfined concrete is drawn from the equations reported in the study of Lim and Ozbakkaloglu (2014) as shown in Table 7.5.

Table 7.5 Stress-strain relationship of unconfined concrete

Stress-Strain expression
$$f_c = \frac{f'_{co}(\varepsilon_c/\varepsilon_{co})r}{r-1+(\varepsilon_c/\varepsilon_{co})^r} \qquad if: 0 \le \varepsilon_c \le \varepsilon_{co}$$ $$f_c = f'_{co} - \frac{f'_{co} - f_{c,res}}{1+\left(\frac{\varepsilon_c-\varepsilon_{co}}{\varepsilon_{c,i}-\varepsilon_{co}}\right)^{-2}} \qquad if: \varepsilon_c > \varepsilon_{co}$$
Parameters
$$r = \frac{E_c}{E_c - f'_{co}/\varepsilon_{co}}$$ $$E_c = 4400\sqrt{f'_{co}}\left(\frac{\rho_{c,f}}{2400}\right)^{1.4}$$

$$\varepsilon_{c,i} = \left(2.8\varepsilon_{co}\left(\frac{f_{c,res}}{f'_{co}}\right)f'^{-0.12}_{co} + 10\varepsilon_{co}\left(1 - \frac{f_{c,res}}{f'_{co}}\right)f'^{-0.47}_{co}\right)\left(\frac{\rho_{c,f}}{2400}\right)^{0.4}$$

Axial strain adjustment according to specimen dimensions

$$\varepsilon_{c,h} = \varepsilon_c \qquad if: 0 \le \varepsilon_c \le \varepsilon_{co}$$

$$\varepsilon_{c,h} = \frac{(f_c - f'_{co})}{E_c}\left(1 - \frac{H_r}{h}\right) + \varepsilon_{co} + (\varepsilon_c - \varepsilon_{co})\frac{H_r}{h} + \varepsilon_d\frac{(H_d - H_r)}{h} \qquad if: \varepsilon_c > \varepsilon_{co}$$

$$H_d = 2d$$

$$\varepsilon_d = 0.02f'^{-0.5}_{co}\left(\frac{f'_{co} - f_c}{f'_{co}}\right)$$

Where,

$f_{c,res}$ = the residual stress, which equals 0 for unconfined concrete;

$\rho_{c,f}$ = the concrete density, taken as 2400 kg/m^3;

$\varepsilon_{c,h}$ = the axial strain of a specimen of height (h);

H_r = the reference specimen height (305 mm);

d = the diameter of the cylinder;

h = the height of the cylinder.

The results of the parametric study are depicted in Figs. 7.26-7.31. The observations from these figures are summarized in the following:

- As the unconfined concrete strength increases, the confinement with the GFRP becomes less effective (high demand of confinement with the increase in the concrete strength) (Figs. 7.26-7.29). For instance, when the concrete strength increased from 30 to 120 MPa, the strength improvement reduced from 120% to 16% (Fig. 7.30). This result is confirmed by the studies of Mandal et al. (2005), Cui and Sheikh (2010), and Micelli and Modarelli (2012).
- Similarly, the axial ductility ($\varepsilon_{cc}/\varepsilon_{co}$) exhibited a reduction as the unconfined concrete strength increased (Figs. 7.26-7.29). For an increase of (f'_{co}) from 30 to 120 MPa, the strain ratio decreased from 12.62 to 4.26.
- The slope of the second branch of the curve (E_2) is not largely influenced when the unconfined concrete strength increased (Fig. 7.31).
- The energy absorption capacity improved as the unconfined concrete strength increased. For instance, from (f'_{co}) varies from 30 to 120 MPa, the energy absorption capacity improved from 1.47 to 1.72 J.m^{-3} (Fig. 7.30).

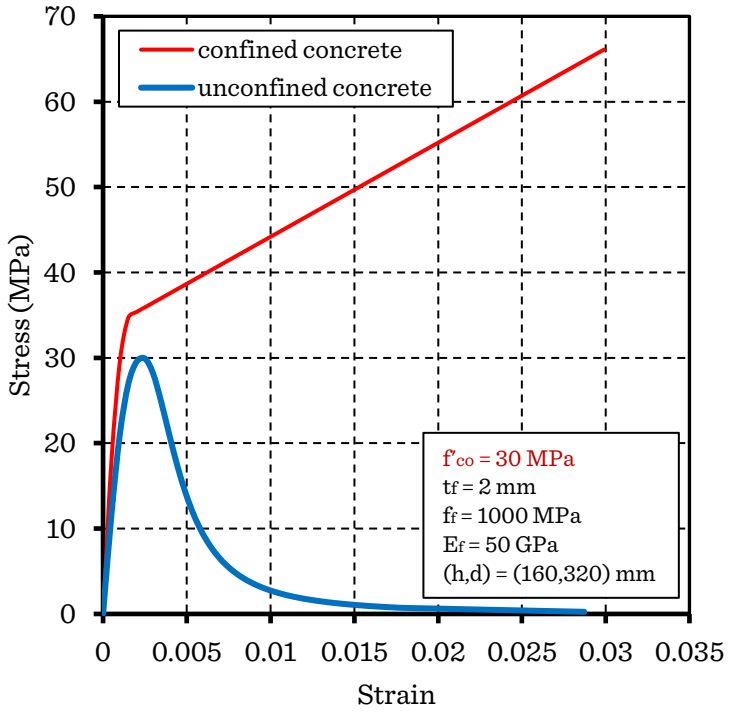

Figure 7.26 Influence of the unconfined concrete strength on the stress-strain behavior of GFRP-wrapped concrete (f'_{co} = 30 MPa)

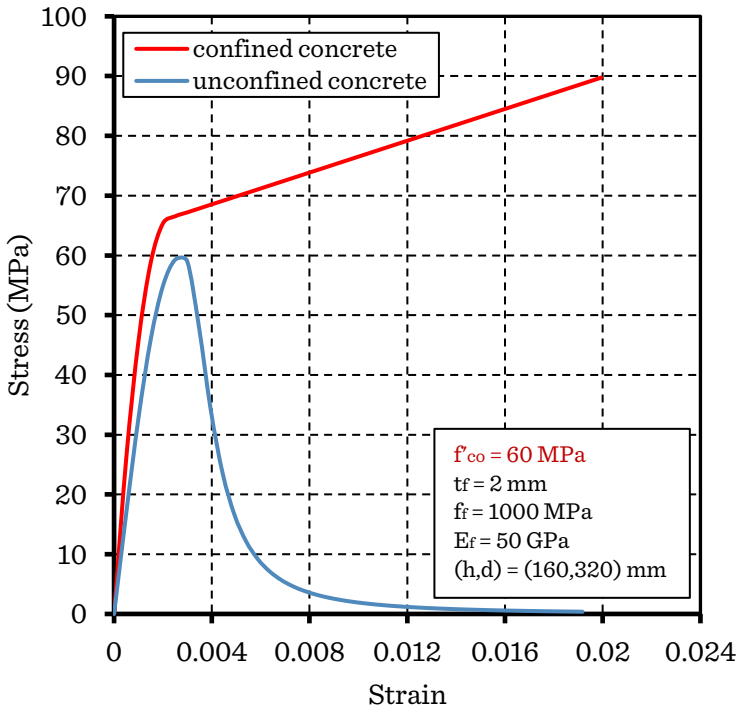

Figure 7.27 Influence of the unconfined concrete strength on the stress-strain behavior of GFRP-wrapped concrete (f'_{co} = 60 MPa)

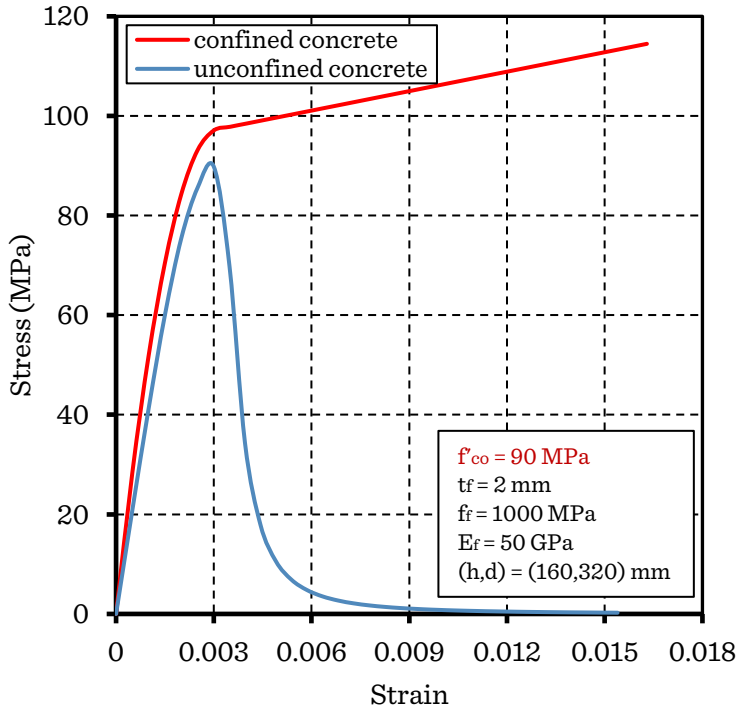

Figure 7.28 Influence of the unconfined concrete strength on the stress-strain behavior of GFRP-wrapped concrete (f'_{co} = 90 MPa)

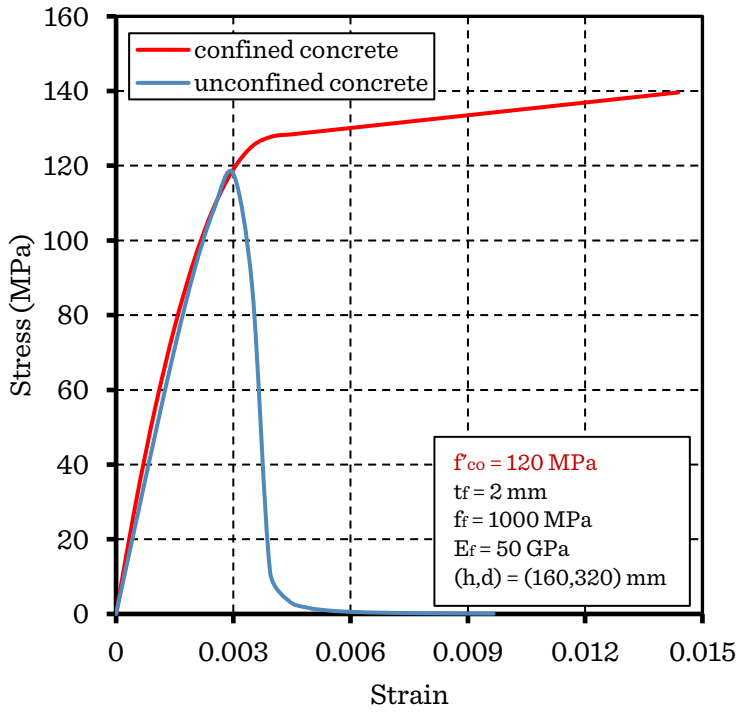

Figure 7.29 Influence of the unconfined concrete strength on the stress-strain behavior of GFRP-wrapped concrete (f'_{co} = 120 MPa)

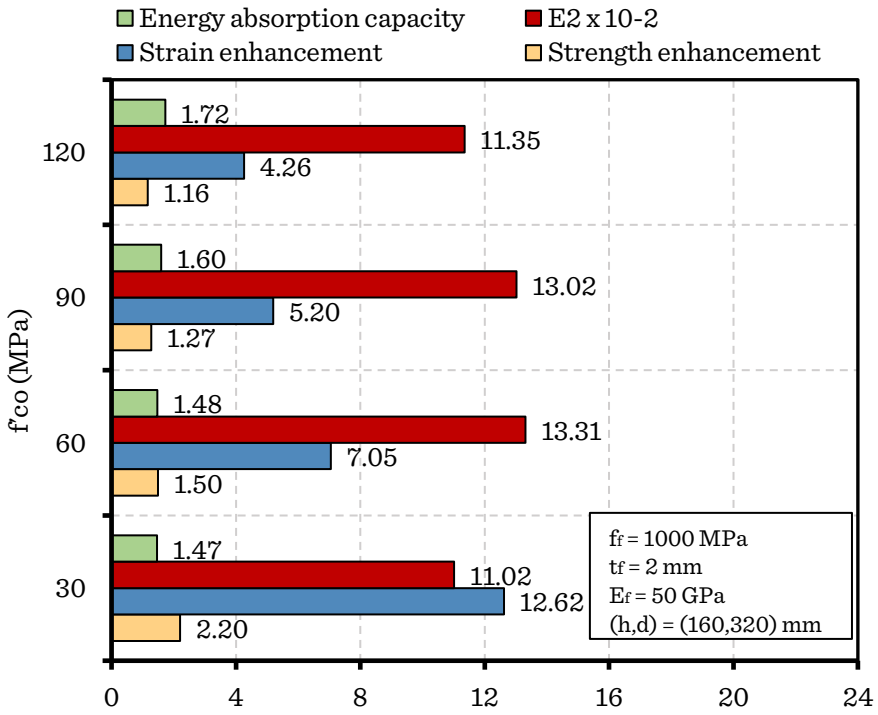

Figure 7.30 Variation of the confinement parameters with the unconfined concrete strength

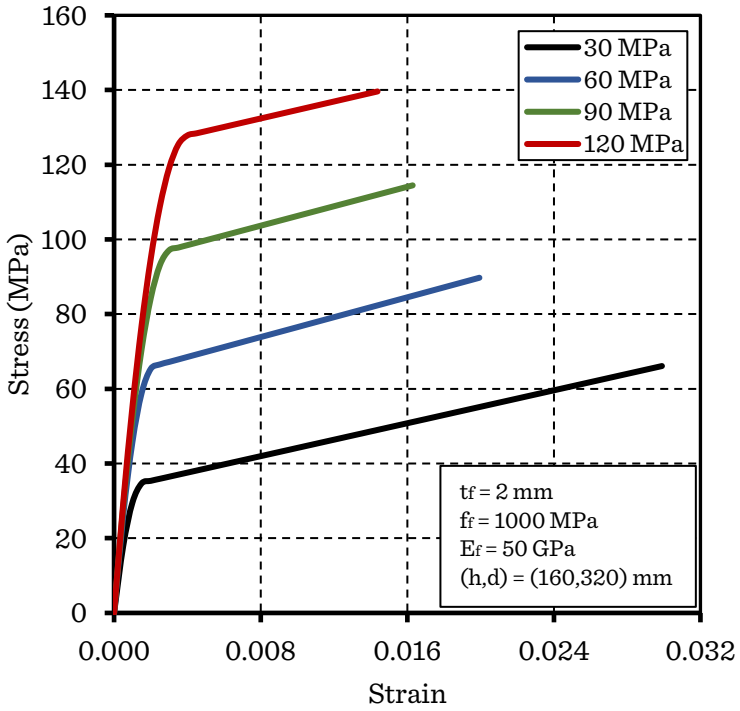

Figure 7.31 Effect of the unconfined concrete strength on the stress-strain behavior of GFRP-wrapped concrete

7.3.3 Effect of specimen diameter

The effect of the specimen dimension on the stress-strain behavior of GFRP-wrapped concrete is studied by fixing the GFRP properties (thickness, elasticity modulus, and tensile strength) and the concrete strength while varying the dimensions of the specimen (the diameter (d), and the corresponding height (h)), where the height-to-diameter ratio (h/d) is fixed to 2. Table 7.6 below reports the values of this parametric study.

Table 7.6 Variation of the specimen diameter with the concrete strength

GFRP properties			Concrete strength	Specimen dimension (d, h) mm				
f_f (MPa)	E_f (GPa)	t_f (mm)	f'_{co} (MPa)					
1000	50	2	30	(100,200)	(150,300)	(200,400)	(250,500)	(300,600)
			60	(100,200)	(150,300)	(200,400)	(250,500)	(300,600)
			90	(100,200)	(150,300)	(200,400)	(250,500)	(300,600)
			120	(100,200)	(150,300)	(200,400)	(250,500)	(300,600)

Figs. 7.32-7.39 illustrate the influence of the diameter of the specimen on the stress-strain behavior of concrete confined with the same GFRP wraps. From these figures, it can be observed that:

- Varying the specimen dimension has no effect on the first branch of the curve (the elastic modulus (E_1)), as well as the stress (f_o)).
- For low-strength concrete (30 MPa), the increase in the specimen diameter has no effect on the slope of the second branch of the curve (Fig. 7.32). However, for medium and higher concrete strength, the slope (E_2) becomes steeper (reduction in the plastic stiffness), and it is more pronounced for high strength concretes. For instance, (E_2) decreased from 1530 to 1191 MPa for 60 MPa when (d) increased from 100 to 300 mm (Fig. 35), and from 1711 to 329 MPa for 120 MPa concrete (Fig. 7.39).
- For the same concrete strength, the strength enhancement ratio (f'_{cc}/f'_{co}) decreased as the diameter of the specimen increased. For instance, for 30 MPa concrete, when (d) increased from 100 to 300 mm, the strength enhancement decreased from 170% to 80% (Fig. 7.33) and from 31% to 5% for 120 MPa (Fig. 7.39). This finding converges with the results of several researchers (e.g., Carey & Harries, 2005; Wang & Wu, 2011; Akogbe et al., 2011; Elsanadedy et al., 2012; Liang et al., 2012) which found that there is

a significant size effect for columns with constant wrap thickness, in which higher failure stresses were observed in smaller-diameter columns.

- The axial ductility ($\varepsilon_{cc}/\varepsilon_{co}$) decreased as the specimen diameter increased. For example, for 60 MPa concrete, ($\varepsilon_{cc}/\varepsilon_{co}$) decreased from 10.20 to 4.65 (Fig. 7.35), and from 5.48 to 2.56 for 120 MPa (Fig. 7.39) when the diameter (d) increased from 100 to 300 mm.
- The effect of the specimen diameter on ductility is much more pronounced than that on strength. For instance, for 90 MPa concrete, when (d) decreased from 100 to 300 mm, the strength decreased from 75% to 29%, while the corresponding strain corresponding reduced from 920% to 365% (Fig. 7.5).

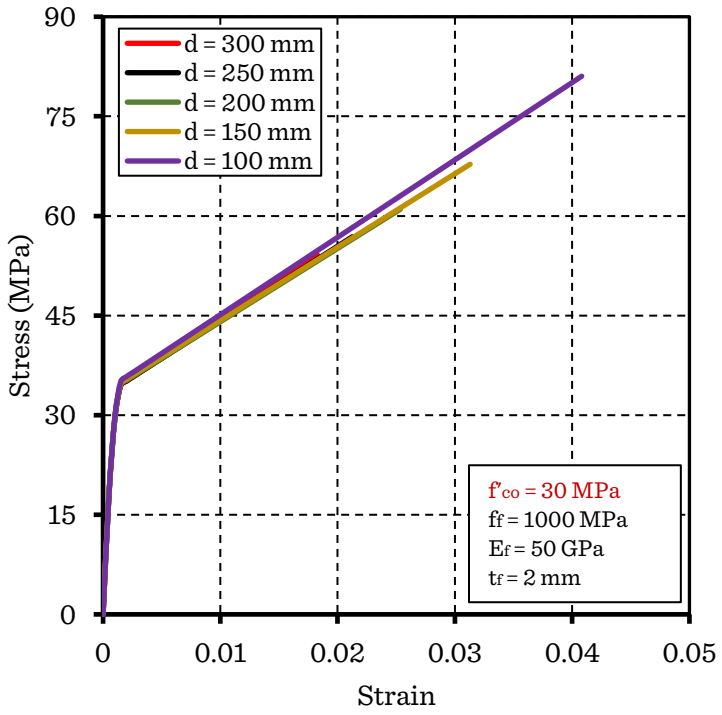

Figure 7.32 Influence of the diameter of the specimen on the stress-strain behavior of GFRP-wrapped concrete (f'_{co} = 30 MPa)

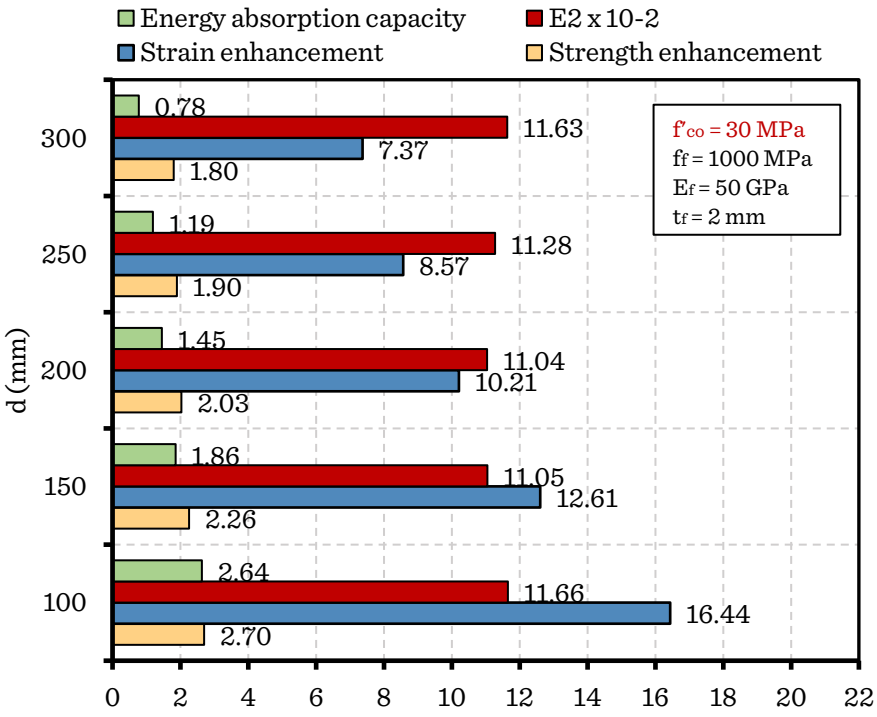

Figure 7.33 Variation of the confinement parameters with the diameter of the specimen (f'_{co} = 30 MPa)

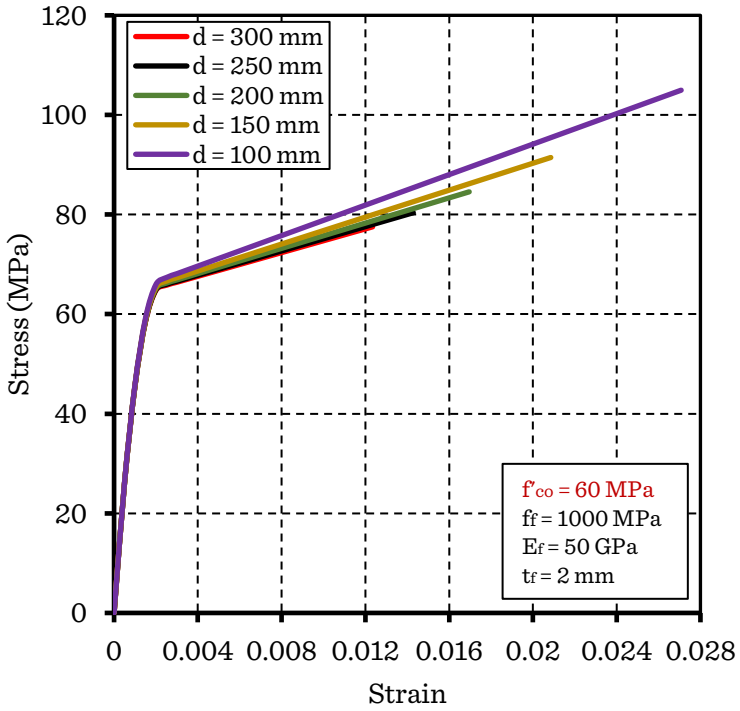

Figure 7.34 Influence of the diameter of the specimen on the stress-strain behavior of GFRP-wrapped concrete (f'_{co} = 60 MPa)

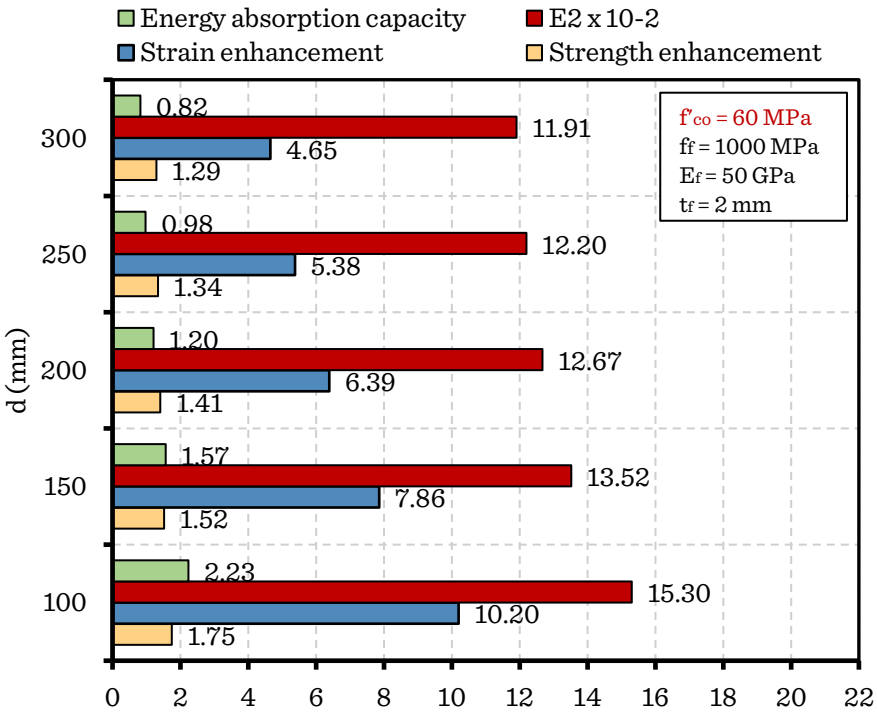

Figure 7.35 Variation of the confinement parameters with the diameter of the specimen (f'_{co} = 60 MPa)

- Specimens with large diameters require more confinement than the ones with small diameters. For example, for the specimen with (d = 100 mm) and unconfined concrete strength (f'_{co} = 90 MPa), the strength improved by 45% and the corresponding strain improved by 571%. However, for the specimen with (d = 300 mm) with the same concrete strength and confined with the same GFRP wrapping, the strength improvement is only 13%, and its corresponding strain is 210% (Fig. 5.37).
- As the compressive strength and the axial ductility decrease with the increase in the specimen diameter, the energy absorption capacity by its turn decreases as it is the area under the stress-strain curve. For instance, for 60 MPa concrete, increasing the diameter of the specimen from 100 to 300 mm decreased the energy absorption capacity from 2.23 to 0.82 $J.m^{-3}$ (Fig. 5.35).

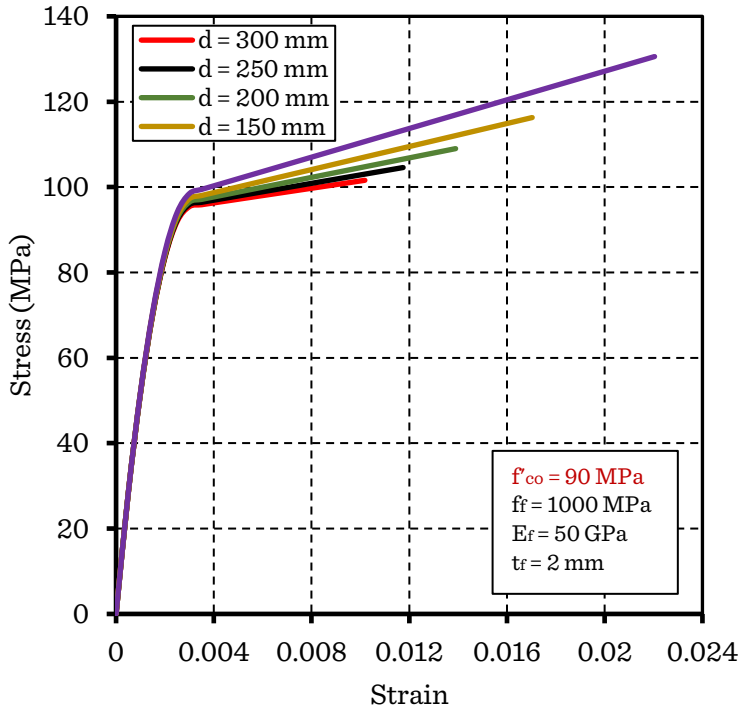

Figure 7.36 Influence of the diameter of the specimen on the stress-strain behavior of GFRP-wrapped concrete (f'_{co} = 90 MPa)

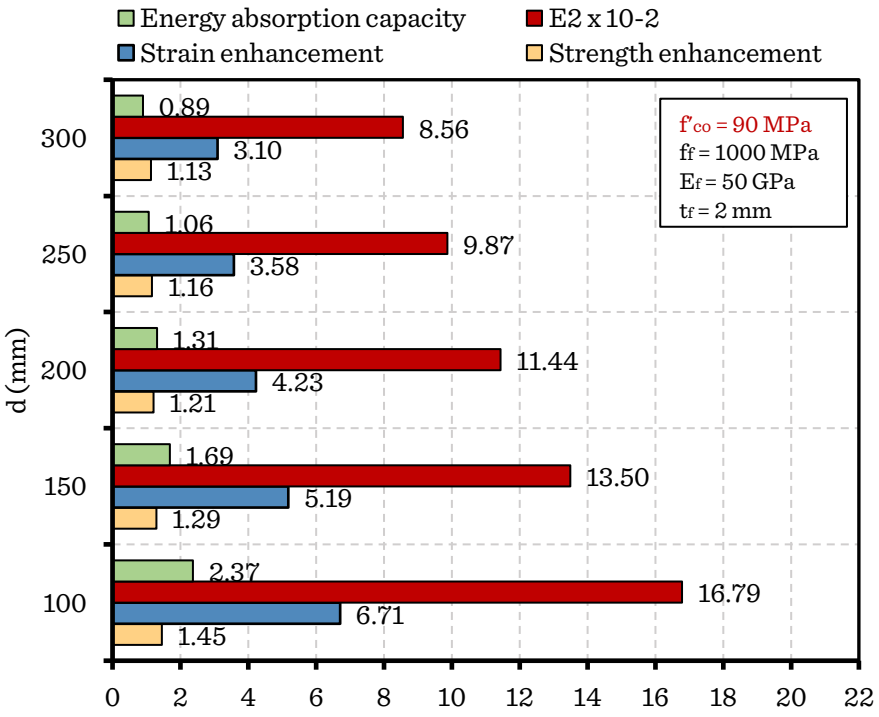

Figure 7.37 Variation of the confinement parameters with the diameter of the specimen (f'_{co} = 90 MPa)

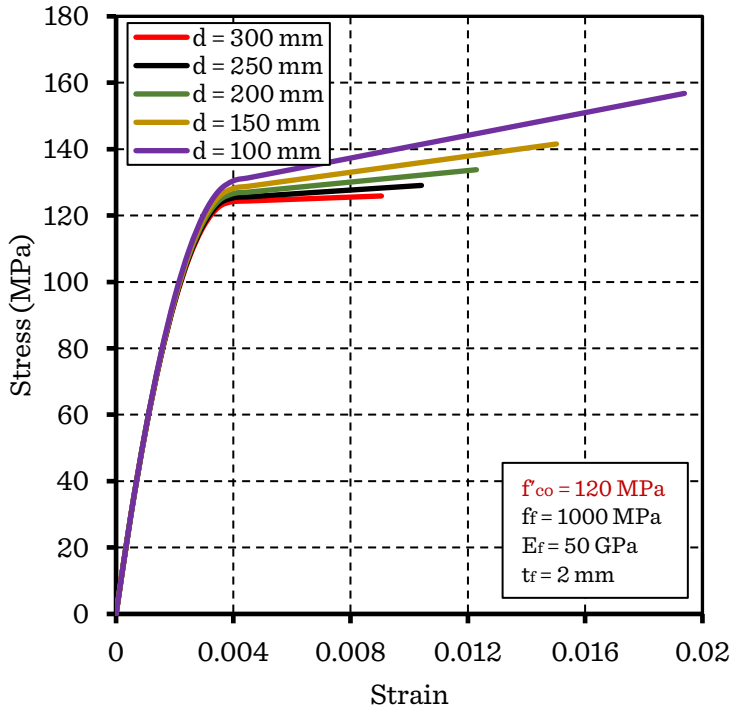

Figure 7.38 Influence of the diameter of the specimen on the stress-strain behavior of GFRP-wrapped concrete (f'_{co} = 120 MPa)

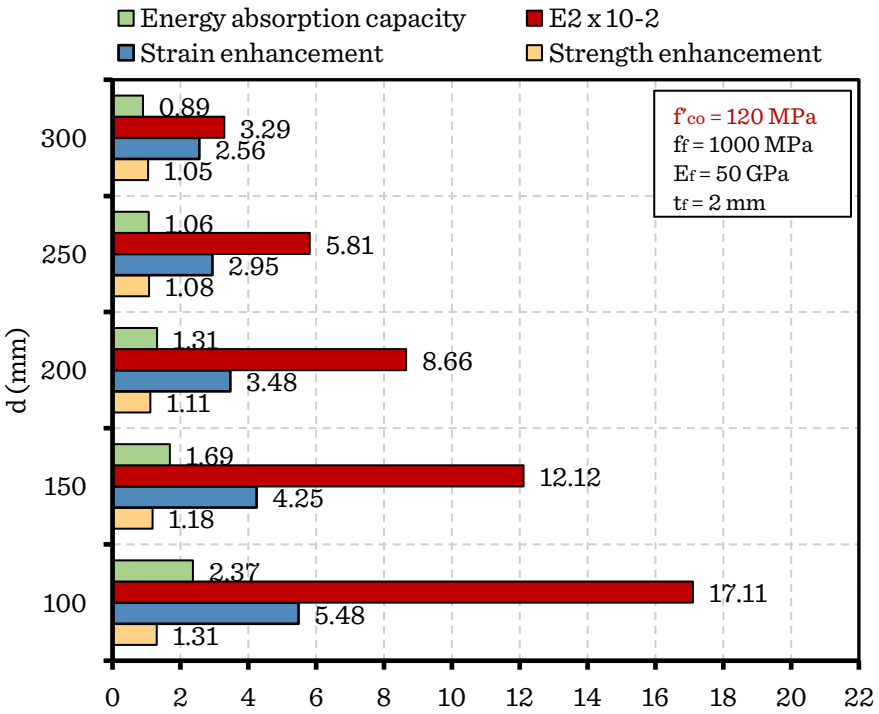

Figure 7.39 Variation of the confinement parameters with the diameter of the specimen (f'_{co} = 120 MPa)

7.4 Conclusion

In this chapter, the effects of different variables such as the concrete strength, the FRP properties, and the specimen dimensions on the axial behavior of GFRP-wrapped concrete have been evaluated. Form this study, the following conclusions can be drawn:

- The general shape of the stress-strain curve is remained unchanged (liner-elastic branch followed by linear plastic branch separated by a transition zone) for every variation of the studied parameters.
- The first branch of the curve (elastic stiffness (E_1) and the stress (f_o)) is not affected by any of the parameters, except by the thickness of the GFRP, which improves the stress (f_o) as it increases.
- The plastic stiffness (E_2) improves with the amount of the GFRP and decreases with the elasticity modulus of the GFRP for all concrete strengths (LSC to HSC).
- For LSC, the plastic stiffness (E_2) is independent of the tensile strength of the GFRP and the diameter of the specimen. Whereas, for MSC and HSC, (E_2) improves with the increase of the tensile strength of the GFRP and decreases with the increase of the diameter of the cylinder.
- The strength of confined concrete (f'_{cc}) improves with the amount and the tensile strength of the GFRP. However, it decreases with the elasticity modulus of the GFRP, the diameter of the specimen, and the unconfined concrete strength.
- The axial ductility ($\varepsilon_{cc}/\varepsilon_{co}$) of the confined concrete improves with the amount and tensile strength on the GFRP and with a small amount with the elasticity modulus of the GFRP. Whereas it decreases with the increase of the unconfined concrete strength and the diameter of the specimen.
- The axial ductility ($\varepsilon_{cc}/\varepsilon_{co}$) shows significantly more improvement with the thickness and the tensile strength of the GFRP than the strength enhancement ratio (f'_{cc}/f'_{co}).
- The energy absorption capacity of the specimens increased proportionally with the amount, the tensile strength of the GFRP, as well as with the concrete strength, and it is more pronounced for low strength concretes. However, it decreases with the diameter of the specimen.
- For more efficient confinement, the increase in the thickness of the GFRP is better than the increase in the tensile strength.
- High strength concrete requires more confinement than medium and low strength concrete.
- Large diameter specimens require more confinement than small diameter ones.
- High strength concrete and small diameter specimen display a higher energy absorption capacity compared to low strength concrete and large diameter specimens.

Conclusions and perspectives

Fiber-reinforced polymer (FRP) composites have gained popularity in the civil engineering community for their high appealing properties for rehabilitation and strengthening of concrete structures. These materials offer a fascinating solution for the rehabilitation of the Algerian national park of deteriorating bridges and important buildings. Numerous experimental studies have been carried out to understand the behavior of concrete confined with FRP under concentric loading, and numerous models have been developed for that purpose. Although GFRP composites are the most used in the industry due to their best cost-performance combination compared to the other FRP materials, few of the research work was devoted to these materials. The research work provided herein aimed to understand and model the axial behavior of concrete confined with GFRP wraps. It presents the mechanism of confinement of concrete with FRP materials and shows a comprehensive review of the experimental and analytical studies conducted on the axial behavior of GFRP-wrapped concrete. This research has ended with the following findings:

- Most of the investigated models can predict the strength and strain with moderate accuracy, where those of Bisby et al. (2005), Fahmy and Wu (2010), and Fallah Pour et al. (2018) are the most accurate for the prediction of the ultimate strength, and those of Berthet et al. (2006), and Ciupala et al. (2007) are the most accurate for the prediction of the ultimate strain.
- The predictions of the strain models show much larger errors than those of the ultimate stress, which can be due to the large variability in the recorded experimental strains.
- The development of new confinement models with higher accurarcy for the prediction of the ultimate stress and ultimate axial strain of GFRP-wrapped concrete based on an extensive database of test results on axially loaded GFRP-wrapped concrete columns.
- The development of a stress-strain model that can accurately describe the compressive behavior of axially loaded concrete confined with GFRP wraps.
- The investigation of the effect of various parameters such as the concrete strength, the FRP amount and properties, and diameter of the cylinder on the stress-strain behavior of GFRP-wrapped concrete. From this investigation, it was found that:
  - The increase in the GFRP amount or the tensile strength of the GFRP has a positive impact on the ultimate strength of the GFRP-wrapped concrete. Whereas the increase in the concrete strength, the specimen diameter, or the elasticity of the FRP has a negative one.

- The ultimate strain of the confined concrete improves the GFRP amount and the tensile strength of the GFRP. Whereas, it decreases with the increase of the unconfined concrete strength and the diameter of the specimen.
- The influence of the thickness and the tensile strength of the GFRP is more pronounced on the ultimate strain than on the ultimate strength.
- The GFRP amount, the tensile strength of the GFRP, and the concrete strength have a favorable effect on the energy absorption capacity of the specimens, while the increase of the diameter of the specimen has an adverse influence on it.
- High strength concrete and large diameter specimens require more confinement than medium and low strength concrete and small diameter specimens.

Based on this study, the following recommendations can be made for future research:

- The majority of the studies, including this one, are based on test results obtained from small scale specimens. Research on large-scale specimens is still limited, and hence, further research on this area needs to be performed.
- Most of the research available in the literature is performed on unreinforced concrete specimens. The inclusion of the internal steel reinforcement, especially in large scale specimens, needs more research.
- Most of the studies conducted on GFRP-confined concrete are made on low and moderate concrete strength specimens. It is recommended to perform more experimental studies on HSC specimens in order to improve the reliability of the proposed models.
- It is of great interest to perform an experimental study on large scale specimens under eccentric loadings with and without internal steel reinforcement.
- Establish a complete comparative economic study on the retrofit of concrete structures using GFRP especially vulnerable strategic buildings and bridges compared to the traditional retrofitting methods.

References

[Building collapsed due to soft story]. (n.d.). Retrofittingcalifornia. https://www.retrofittingcalifornia.com/soft-story-weinstein-retrofitting/

[Cypress street viaduct failure]. (n.d.). History. https://www.history.com/topics/natural-disasters-and-environment/1989-san-francisco-earthquake

[Fukae viaduct expressway failure]. (n.d.). Reddit. https://www.reddit.com/r/DestructionPorn/comments/5p26rb/collapsed_hanshin_expressway_kobe_earthquake/

A., Norris, M. S., & Bradford, N. M. (1993). Lateral confinement of concrete using FRP reinforcement. Special Issue, 138, 193-210.

Abbood, I. S., aldeen Odaa, S., Hasan, K. F., & Jasim, M. A. (2020). Properties evaluation of fiber reinforced polymers and their constituent materials used in structures–A review. Materials Today: Proceedings. https://doi.org/10.1016/j.matpr.2020.07.636

Abdelnaby, A. E., & Elnashai, A. S. (2014). Performance of degrading reinforced concrete frame systems under the Tohoku and Christchurch earthquake sequences. Journal of Earthquake Engineering, 18(7), 1009-1036. https://doi.org/10.1080/13632469.2014.923796

Aboutaha, R. S., Engelhardt, M. D., Jirsa, J. O., & Kreger, M. E. (1996). Retrofit of concrete columns with inadequate lap splices by the use of rectangular steel jackets. Earthquake Spectra, 12(4), 693-714. https://doi.org/10.1193/1.1585906

ACI 440.2R-08 Guide for the Design and Construction of Externally Bonded FRP Systems for Strengthening Concrete Structures

ACI Committee 318. (1995). Building code requirements for structural concrete: (ACI 318-95) and commentary (ACI 318R-95). Farmington Hills, MI: American Concrete Institute, 1995.

ACI Committee 318. (2005). Building code requirements for structural concrete (ACI 318-05) and commentary (ACI 318R-05). Farmington Hills, Mich.: American Concrete Institute, 2005.

ACMA (American Composite Manufacturers Association). (2016). Guidelines and recommended practices for fiber reinforced polymer (FRP) architectural products.

Ahmad, A., & Raza, A. (2020). Reliability analysis of strength models for CFRP-confined concrete cylinders. Composite Structures, 244, 112312. https://doi.org/10.1016/j.compstruct.2020.112312

Ahmad, S. H., & Shah, S. P. (1982). Complete Triaxial Stress-Strain Curves for Concrete. Journal of the Structural Division, 108(4), 728-742. https://doi.org/10.1061/jsdeag.0005921

Akogbe, R. K., Liang, M., & Wu, Z. M. (2011). Size Effect of Axial Compressive Strength of CFRP Confined Concrete Cylinders. International Journal of Concrete Structures and Materials, 5(1), 49-55. https://doi.org/10.4334/ijcsm.2011.5.1.049

Al Abadi, H., El-Naga, H. A., Shaia, H., & Paton-Cole, V. (2016). Refined approach for modelling strength enhancement of FRP-confined concrete. Construction and Building Materials, 119, 152-174. https://doi.org/10.1016/j.conbuildmat.2016.04.119

Almusallam, T. H. (2007). Behavior of normal and high-strength concrete cylinders confined with E-glass/epoxy composite laminates. Composites Part B: Engineering, 38(5-6), 629-639. https://doi.org/10.1016/j.compositesb.2006.06.021

Anagnostou, E., Rousakis, T. C., & Karabinis, A. I. (2019). Seismic retrofitting of damaged RC columns with lap-spliced bars using FRP sheets. Composites Part B: Engineering, 166, 598-612. https://doi.org/10.1016/j.compositesb.2019.02.018

Andrawes, B., Shin, M., & Wierschem, N. (2010). Active confinement of reinforced concrete bridge columns using shape memory alloys. Journal of Bridge Engineering, 15(1), 81-89. https://doi.org/10.1061/(ASCE)BE.1943-5592.0000038

Anggawidjaja, D., Ueda, T., Dai, J., & Nakai, H. (2006). Deformation capacity of RC piers wrapped by new fiber-reinforced polymer with large fracture strain. Cement and Concrete Composites, 28(10), 914-927. https://doi.org/10.1016/j.cemconcomp.2006.07.011

Arabshahi, A., Gharaei Moghaddam, N., & Tavakkolizadeh, M. (2020, March). Ultimate stress and strain models for AFRP confined concrete columns with inclined fiber orientation. In دوازدهمین کنگره ملی مهندسی عمران.

Arabshahi, A., Gharaei-Moghaddam, N., & Tavakkolizadeh, M. (2020, February). Development of applicable design models for concrete columns confined with aramid fiber reinforced polymer using Multi-Expression Programming. In Structures (Vol. 23, pp. 225-244). Elsevier. https://doi.org/10.1016/j.istruc.2019.09.019

Askeland, D. R., Fulay, P. P., & Wright, W. J. (2010). The Science and Engineering of Materials (6th ed.). CL Engineering.

Au, C., & Buyukozturk, O. (2005). Effect of Fiber Orientation and Ply Mix on Fiber Reinforced Polymer-Confined Concrete. Journal of Composites for Construction, 9(5), 397-407. https://doi.org/10.1061/(asce)1090-0268(2005)9:5(397)

Baciu, C., Murzea, P., & Cucu, V. (2015, June). The retrofitting of reinforced concrete columns. In International conference KNOWLEDGE-BASED ORGANIZATION (Vol. 21, No. 3, pp. 776-781). Sciendo. https://doi.org/10.1515/kbo-2015-0131

Baji, H., Ronagh, H. R., & Li, C. Q. (2016). Probabilistic Design Models for Ultimate Strength and Strain of FRP-Confined Concrete. Journal of Composites for Construction, 20(6), 04016051. https://doi.org/10.1061/(asce)cc.1943-5614.0000704

Ballinger, C., Maeda, T., & Hoshijima, T. (1993). Strengthening of reinforced concrete chimneys, columns and beams with carbon fiber reinforced plastics. Special Publication, 138, 233-248.

Barbero, E. J. 2011. Introduction to composite materials design. 2nd ed. Boca Raton, FL: CRC Press, Taylor & Francis Group.

Benzaid, R., Chikh, N. E., & Mesbah, H. (2009). Study of the compressive behavior of short concrete columns confined by fiber reinforced composite. Arabian Journal for Science and Engineering, 34(1B), 15-26.

Benzaid, R., Mesbah, H., & Chikh, N. E. (2010). FRP-confined concrete cylinders: axial compression experiments and strength model. Journal of Reinforced plastics and composites, 29(16), 2469-2488. https://doi.org/10.1177/0731684409355199

Berthet, J. F., Ferrier, E., & Hamelin, P. (2005). Compressive behavior of concrete externally confined by composite jackets. Part A: experimental study. Construction and building materials, 19(3), 223-232. https://doi.org/10.1016/j.conbuildmat.2004.05.012

Berthet, J. F., Ferrier, E., & Hamelin, P. (2006). Compressive behavior of concrete externally confined by composite jackets: Part B: Modeling. Construction and Building Materials, 20(5), 338-347. https://doi.org/10.1016/j.conbuildmat.2005.01.029

Bett, B. J., Klingner, R. E., & Jirsa, J. O. (1988). Lateral load response of strengthened and repaired reinforced concrete columns. Structural Journal, 85(5), 499-508. https://doi.org/10.14359/9226

Binici, B. (2005). An analytical model for stress-strain behavior of confined concrete. Engineering Structures, 27(7), 1040-1051. https://doi.org/10.1016/j.engstruct.2005.03.002

Bisby, L. A., Dent, A. J. S., & Green, M. F. (2005). Comparison of Confinement Models for Fiber-Reinforced Polymer-Wrapped Concrete. ACI Structural Journal, 102(1), 62-72. https://doi.org/10.14359/13531

Blaszak, G. (2018, April 25). Engineered Solutions: RenewWrapÂ®: Column Repair. Informed Infrastructure. https://informedinfrastructure.com/38111/engineered-solutions-renewwrap-column-repair/

Bousias, S. N., Triantafillou, T. C., Fardis, M. N., Spathis, L., & O'Regan, B. A. (2004). Fiber-reinforced polymer retrofitting of rectangular reinforced concrete columns with or without corrosion. Structural Journal, 101(4), 512-520. https://doi.org/10.14359/13337

Buckle, I. G., Friedland, I., Mander, J., Martin, G., Nutt, R., & Power, M. (2006). Seismic retrofitting manual for highway structures. Part 1, Bridges (No. FHWA-HRT-06-032). Turner-Fairbank Highway Research Center.

Carbon fiber reinforced polymer (CFRP) plate strengthening. (n.d.). Horseen. https://www.horseen.com/solution/Carbon-fiber-reinforced-polymer-CFRP-plate-strengthening?page=26

Carey, S. A., & Harries, K. A. (2005). Axial behavior and modeling of confined small-, medium-, and large-scale circular sections with carbon fiber-reinforced polymer jackets. ACI Structural Journal, 102(4), 596. https://doi.org/10.14359/14564

Carreira, D. J., & Chu, K.-H. (1985). Stress-Strain Relationship for Plain Concrete in Compression. ACI Journal Proceedings, 82(6). https://doi.org/10.14359/10390

Cascardi, A., Micelli, F., & Aiello, M. A. (2017). An Artificial Neural Networks model for the prediction of the compressive strength of FRP-confined concrete circular columns. Engineering Structures, 140, 199-208. https://doi.org/10.1016/j.engstruct.2017.02.047

ChaiI, Y. H., Priestley, M. N., & Seible, F. (1991). Seismic retrofit of circular bridge columns for enhanced flexural performance. Structural Journal, 88(5), 572-584. https://doi.org/10.14359/2759

Chajes, M. J., Januszka, T. F., Mertz, D. R., Thomson, T. A., & Finch, W. W. (1995). Shear strengthening of reinforced concrete beams using externally applied composite fabrics. Structural Journal, 92(3), 295-303. https://doi.org/10.14359/1130

Chandrakar, J., & Singh, A. K. (2017). Study of Various Local and Global Seismic Retrofitting Strategies-A review. Int. J. Eng. Res. Technol, 6, 824-831. https://doi.org/10.17577/IJERTV6IS060358

Chang, S. Y., Li, Y. F., & Loh, C. H. (2004). Experimental study of seismic behaviors of as-built and carbon fiber reinforced plastics repaired reinforced

concrete bridge columns. Journal of Bridge Engineering, 9(4), 391-402. https://doi.org/10.1061/(ASCE)1084-0702(2004)9:4(391)

Chen, J. (2005). Behavior of structural concrete members strengthened by composite fabrics (Ph.D. Thesis). New Jersey Institute of Technology. https://digitalcommons.njit.edu/dissertations/666

Choi, E., Kim, J. W., Rhee, I., & Kang, J. W. (2014). Behavior and modeling of confined concrete cylinders in axial compression using FRP rings. Composites Part B: Engineering, 58, 175-184. https://doi.org/10.1016/j.compositesb.2013.10.031

Ciupala, M. A., Pilakoutas, K., & Mortazavi, A. A. (2007, July). Effectiveness of FRP composites in confined concrete. In Proceedings of the 8th International Symposium on Fiber-Reinforced Polymer Reinforcement for Concrete Structures, FRPRCS-8, Patras, Greece, July (pp. 252-253).

Coffman, H. L., Marsh, M. L., & Brown, C. B. (1993). Seismic durability of retrofitted reinforced-concrete columns. Journal of Structural Engineering, 119(5), 1643-1661. https://doi.org/10.1061/(ASCE)0733-9445(1993)119:5(1643)

Comert, M., Goksu, C., & Ilki, A. (2009). Towards a tailored stress–strain behavior for FRP confined low strength concrete. In Proceedings of 9th international symposium on fiber reinforced polymer reinforcement for concrete structures, Sydney, Australia.

Considère, A. (1903). Experimental Research on Reinforced Concrete, Translated and Arranged by Leon S, Moisseiff, McGraw Publishing Co., New York

Cozmanciuc, Ciprian & Oltean, Ruxandra & Munteanu, Vlad. (2009). Strengthening Techniques of RC Columns Using Fibre Reinforced Polymeric Materials. Bulletin of the Polytechnic Institute of Jassy, CONSTRUCTIONS. ARCHITECTURE Section, Tomme LV (LIX), Fascicle 3, pages 85-92 (2009). 3.

Cui, C. (2009). Behaviour of Normal and High Strength Concrete Confined with Fibre Reinforced Polymers (FRP) (Ph.D. Dissertation). University of Toronto. http://hdl.handle.net/1807/17750

Cui, C., & Sheikh, S. A. (2010). Analytical model for circular normal-and high-strength concrete columns confined with FRP. Journal of Composites for Construction, 14(5), 562-572. https://doi.org/10.1061/(ASCE)CC.1943-5614.0000115

Dadvar, S. A., Mostofinejad, D., & Bahmani, H. (2020). Strengthening of RC columns by ultra-high performance fiber reinforced concrete (UHPFRC) jacketing. Construction and Building Materials, 235, 117485. https://doi.org/10.1016/j.conbuildmat.2019.117485

De Lorenzis, L., & Tepfers, R. (2003). Comparative study of models on confinement of concrete cylinders with fiber-reinforced polymer composites. Journal of Composites for Construction, 7(3), 219-237. https://doi.org/10.1061/(ASCE)1090-0268(2003)7:3(219)

Del Zoppo, M., Di Ludovico, M., Balsamo, A., Prota, A., & Manfredi, G. (2017). FRP for seismic strengthening of shear controlled RC columns: Experience from earthquakes and experimental analysis. Composites Part B: Engineering, 129, 47-57. https://doi.org/10.1016/j.compositesb.2017.07.028

Demers, M., & Neale, K. W. (1999). Confinement of reinforced concrete columns with fibre-reinforced composite sheets-an experimental study. Canadian Journal of Civil Engineering, 26(2), 226-241. https://doi.org/10.1139/l98-067

DesRoches, R., McCormick, J., & Delemont, M. (2004). Cyclic properties of superelastic shape memory alloy wires and bars. Journal of Structural Engineering, 130(1), 38-46. https://doi.org/10.1061/(ASCE)0733-9445(2004)130:1(38)

Di Ludovico, M., Nanni, A., Prota, A., & Cosenza, E. (2005). Repair of bridge girders with composites: Experimental and analytical validation. ACI Structural Journal, 102(5), 639. https://doi.org/10.14359/14659

Djafar-Henni, I., & Kassoul, A. (2018). Stress-strain model of confined concrete with Aramid FRP wraps. Construction and Building Materials, 186, 1016-1030. https://doi.org/10.1016/j.conbuildmat.2018.08.013

Dubčáková, R. (2010). Eureqa: software review. Genetic Programming and Evolvable Machines, 12(2), 173-178. https://doi.org/10.1007/s10710-010-9124-z

Dubey, R., & Kumar, P. (2016). Experimental study of the effectiveness of retrofitting RC cylindrical columns using self-compacting concrete jackets. Construction and Building Materials, 124, 104-117. https://doi.org/10.1016/j.conbuildmat.2016.07.079

Eid, R., & Paultre, P. (2007). Plasticity-based model for circular concrete columns confined with fibre-composite sheets. Engineering Structures, 29(12), 3301-3311. https://doi.org/10.1016/j.engstruct.2007.09.005

Eid, R., & Paultre, P. (2017). Compressive behavior of FRP-confined reinforced concrete columns. Engineering Structures, 132, 518-530. https://doi.org/10.1016/j.engstruct.2016.11.052

Eid, R., Dancygier, A. N., & Paultre, P. (2007). Elastoplastic confinement model for circular concrete columns. Journal of Structural Engineering, 133(12), 1821-1831. https://doi.org/10.1061/(ASCE)0733-9445(2007)133:12(1821)

Mohamed Elarbi, A. (2011). Durability performance of frp strenghtened concrete beams and columns exposed to hygrothermal environment (Ph.D. Dissertation). Wayne State University. https://digitalcommons.wayne.edu/oa_dissertations/307

Elsanadedy, H. M., & Haroun, M. A. (2005). Seismic design criteria for circular lap-spliced reinforced concrete bridge columns retrofitted with fiber-reinforced polymer jackets. ACI structural journal, 102(3), 354. https://doi.org/10.14359/14406

Elsanadedy, H. M., Abbas, H., Al-Salloum, Y. A., & Almusallam, T. H. (2014). Prediction of intermediate crack debonding strain of externally bonded FRP laminates in RC beams and one-way slabs. Journal of Composites for Construction, 18(5), 04014008. https://doi.org/10.1061/(ASCE)CC.1943-5614.0000462

Elsanadedy, H. M., Al-Salloum, Y. A., Alsayed, S. H., & Iqbal, R. A. (2012). Experimental and numerical investigation of size effects in FRP-wrapped concrete columns. Construction and Building Materials, 29, 56-72. https://doi.org/10.1016/j.conbuildmat.2011.10.025

Elwan, S. K., & Omar, M. A. (2014). Experimental behavior of eccentrically loaded RC slender columns strengthened using GFRP wrapping. Steel and Composite Structures, 17(3), 271-285. https://doi.org/10.12989/scs.2014.17.3.271

Emmons, P. H., Vaysburd, A. M., & Thomas, J. (1998). Strengthening concrete structures, Part II. Concrete International, 20(4), 56-60.

Facilitator, C. (2020, September 19). Retrofitting of structures - Design and Techniques. Constro Facilitator. https://www.constrofacilitator.com/retrofitting-of-structures-design-and-techniques/

Fahmy, M. F., & Wu, Z. (2010). Evaluating and proposing models of circular concrete columns confined with different FRP composites. Composites Part B: Engineering, 41(3), 199-213. https://doi.org/10.1016/j.compositesb.2009.12.001

Fakharifar, M. (2016). Composite confinement systems for RC column repair and construction under seismic loads: Concept, characterization and performance (Ph.D. Dissertation). Missouri University of Science and Technology. https://scholarsmine.mst.edu/doctoral_dissertations/2647

Fakharifar, M., Chen, G., Wu, C., Shamsabadi, A., ElGawady, M. A., & Dalvand, A. (2016). Rapid repair of earthquake-damaged RC columns with prestressed steel jackets. Journal of Bridge Engineering, 21(4), 04015075. https://doi.org/10.1061/(ASCE)BE.1943-5592.0000840

Fakharifar, M., Sharbatdar, M. K., Lin, Z., Dalvand, A., Sivandi-Pour, A., & Chen, G. (2014). Seismic performance and global ductility of RC frames

rehabilitated with retrofitted joints by CFRP laminates. Earthquake Engineering and Engineering Vibration, 13(1), 59-73. https://doi.org/10.1007/s11803-014-0212-6

Fallah Pour, A., Ozbakkaloglu, T., & Vincent, T. (2018). Simplified design-oriented axial stress-strain model for FRP-confined normal- and high-strength concrete. Engineering Structures, 175, 501-516. https://doi.org/10.1016/j.engstruct.2018.07.099

Fam, A. Z., & Rizkalla, S. H. (2001). Confinement model for axially loaded concrete confined by circular fiber-reinforced polymer tubes. Structural Journal, 98(4), 451-461. https://doi.org/10.14359/10288

Farahmandpour, C., Dartois, S., Quiertant, M., Berthaud, Y., & Dumontet, H. (2017). A concrete damage-plasticity model for FRP confined columns. Materials and Structures, 50(2), 1-17. https://doi.org/10.1617/s11527-017-1016-8

Fardis, M. N., & Khalili, H. (1981, November). Concrete encased in fiberglass-reinforced plastic. In Journal Proceedings (Vol. 78, No. 6, pp. 440-446). https://doi.org/10.14359/10527

Fardis, M. N., & Khalili, H. H. (1982). FRP-encased concrete as a structural material. Magazine of concrete research, 34(121), 191-202. https://doi.org/10.1680/macr.1982.34.121.191

Farrokh Ghatte, H., Comert, M., Demir, C., Akbaba, M., & Ilki, A. (2019). Seismic retrofit of full-scale substandard extended rectangular RC columns through CFRP jacketing: test results and design recommendations. Journal of Composites for Construction, 23(1), 04018071. https://doi.org/10.1061/(ASCE)CC.1943-5614.0000907

FRP Carbon Fibre Reinforcing Systems. (2020, November 12). Strong-Tie | Together We're Helping Build Safer Stronger Structures. https://strongtie.co.nz/products/frp-carbon-fibre-reinforcing-systems.

Fukuyama, H., Suzuki, H., & Nakamura, H. (1999). Seismic retrofit of reinforced concrete columns by fiber sheet wrapping without removal of finishing mortar and side wall concrete. Special Publication, 188, 205-216.

Gamble, W. L., Hawkins, N. M., & Kaspar, I. I. (1996). Seismic retrofitting experience and experiments in Illinois. In Proc., 5th National Workshop on Bridge Research in Progress (pp. 245-250). Buffalo, NY: National Center for Earthquake Engineering Research (NCEER), State Univ. of New York at Buffalo.

Gandomi, A. H., Alavi, A. H., & Sahab, M. G. (2010). New formulation for compressive strength of CFRP confined concrete cylinders using linear genetic programming. Materials and Structures, 43(7), 963-983. https://doi.org/10.1617/s11527-009-9559-y

Ghanem, S. (2016). Circular RC columns partially confined with FRP (Ph.D. Dissertation). University of Kentucky. https://uknowledge.uky.edu/ce_etds/38

Ghobarah, A., & Said, A. (2001). Seismic rehabilitation of beam-column joints using FRP laminates. Journal of earthquake engineering, 5(01), 113-129. https://doi.org/10.1142/S1363246901000297

Gibson, R. F. 1994. Principles of composite material mechanics. New York: McGraw Hill.

GÓRSKI, M., KRZYWOŃ, R., & Castro GOMES, J. (2016). HANDBOOK–Fibrous Composite Materials in Strengthening of Structures. Universidade da Beira Interior, C MADE - Centre of Materials and Building. https://www.researchgate.net/publication/293333100_Handbook___Fibrous_composite_materials_in_strengthening_of_structures

Guo, Y., Xie, J., Xie, Z., & Zhong, J. (2016). Experimental study on compressive behavior of damaged normal-and high-strength concrete confined with CFRP laminates. Construction and Building Materials, 107, 411-425. https://doi.org/10.1016/j.conbuildmat.2016.01.010

Han, Q., Wen, J., Du, X., & Jia, J. (2014). Experimental and numerical studies on seismic behavior of hollow bridge columns retrofitted with carbon fiber reinforced polymer. Journal of Reinforced Plastics and Composites, 33(24), 2214-2227. https://doi.org/10.1177/0731684414557716

Harajli, M. H., Hantouche, E., & Soudki, K. (2006). Stress-strain model for fiber-reinforced polymer jacketed concrete columns. Structural Journal, 103(5), 672-682. https://doi.org/10.14359/16919

Haroun, M. A., & Elsanadedy, H. M. (2005). Fiber-reinforced plastic jackets for ductility enhancement of reinforced concrete bridge columns with poor lap-splice detailing. Journal of Bridge Engineering, 10(6), 749-757. https://doi.org/10.1061/(ASCE)1084-0702(2005)10:6(749)

Harries, K. A., & Carey, S. A. (2003). Shape and "gap" effects on the behavior of variably confined concrete. Cement and Concrete Research, 33(6), 881-890. https://doi.org/10.1016/S0008-8846(02)01086-4

Harries, K. A., & Kharel, G. (2002). Behavior and Modeling of Concrete Subject to Variable Confining Pressure. ACI Materials Journal, 99(2). https://doi.org/10.14359/11711

Harries, K. A., Ricles, J. R., Pessiki, S., & Sause, R. (2006). Seismic retrofit of lap splices in nonductile square columns using carbon fiber-reinforced jackets. ACI Structural Journal, 103(6), 874. https://doi.org/10.14359/18242

He, R., Sneed, L. H., & Belarbi, A. (2013). Rapid repair of severely damaged RC columns with different damage conditions: An experimental study.

International Journal of Concrete Structures and Materials, 7(1), 35-50. https://doi.org/10.1007/s40069-013-0030-7

Hognestad, E. (1951). A study of combined bending and axial load in reinforced concrete members. University of Illinois at Urbana Champaign, College of Engineering. Engineering Experiment Station. http://hdl.handle.net/2142/4360

Hollaway, L. C., & Teng, J. G. (Eds.). (2008). Strengthening and rehabilitation of civil infrastructures using fibre-reinforced polymer (FRP) composites. Elsevier. https://doi.org/10.1533/9781845694890

Hou, D., Wu, Z., Zheng, J., & Cui, Y. (2015). Seismic rehabilitation of substandard RC columns with partially deteriorated concrete using CFRP composites. Computers and Concrete, 15(1), 1-20. https://doi.org/10.12989/cac.2015.15.1.001

Huang, L., Gao, C., Yan, L., Kasal, B., Ma, G., & Tan, H. (2016). Confinement models of GFRP-confined concrete: Statistical analysis and unified stress-strain models. Journal of Reinforced Plastics and Composites, 35(11), 867-891. https://doi.org/10.1177/0731684416630609

Hui, W. (2007). Constitutive model of concrete confined by advanced fiber composite materials and applications in seismic retrofitting (Ph.D. Dissertation). University of Southern California. http://digitallibrary.usc.edu/cdm/ref/collection/p15799coll127/id/551376

Hyer, M. W. 1998. Stress analysis of fiber reinforced composite materials. New York: WCB/ McGraw Hill

Ilki, A., Kumbasar, N., & Koc, V. (2004). Low strength concrete members externally confined with FRP sheets. Structural Engineering and Mechanics, 18(2), 167-194. https://doi.org/10.12989/sem.2004.18.2.167

Itani, R. (2003). Effects of retrofitting applications on reinforced concrete bridges (No. WA-RD 570.1).

Jiang, K., Han, Q., Bai, Y., & Du, X. (2020). Data-driven ultimate conditions prediction and stress-strain model for FRP-confined concrete. Composite Structures, 242, 112094. https://doi.org/10.1016/j.compstruct.2020.112094

Jiang, T., & Teng, J. G. (2007). Analysis-oriented stress-strain models for FRP-confined concrete. Engineering Structures, 29(11), 2968-2986. https://doi.org/10.1016/j.engstruct.2007.01.010

Karabinis, A. I., & Rousakis, T. C. (2002). Concrete confined by FRP material: a plasticity approach. Engineering structures, 24(7), 923-932. https://doi.org/10.1016/S0141-0296(02)00011-1

Karayannis, C. G., Chalioris, C. E., & Sirkelis, G. M. (2008). Local retrofit of exterior RC beam-column joints using thin RC jackets-An experimental

study. Earthquake Engineering & Structural Dynamics, 37(5), 727-746. https://doi.org/10.1002/eqe.783

Karbhari, V. M., & Gao, Y. (1997). Composite jacketed concrete under uniaxial compression-Verification of simple design equations. Journal of materials in civil engineering, 9(4), 185-193. https://doi.org/10.1061/(ASCE)0899-1561(1997)9:4(185)

Karbhari, V. M., Eckel, D. A., & Tunis III, G. C. (1993). Strengthening of concrete column stubs through resin infused composite wraps. Journal of Thermoplastic Composite Materials, 6(2), 92-107. https://doi.org/10.1177/089270579300600201

Kawashima, K. (1990). "Seismic design, seismic strengthening and seismic repair of highway bridges in Japan." 1st US-Japan workshop on seismic retrofit of bridges, Tsukuba science city, Japan

Keshtegar, B., Sadeghian, P., Gholampour, A., & Ozbakkaloglu, T. (2017). Nonlinear modeling of ultimate strength and strain of FRP-confined concrete using chaos control method. Composite Structures, 163, 423-431. https://doi.org/10.1016/j.compstruct.2016.12.023

Khaloo, A., Tabatabaeian, M., & Khaloo, H. (2020, October). The axial and lateral behavior of low strength concrete confined by GFRP wraps: An experimental investigation. In Structures (Vol. 27, pp. 747-766). Elsevier. https://doi.org/10.1016/j.istruc.2020.06.008

Kharal, Z. (2019). Towards Understanding the Seismic Behaviour of GFRP Confined Concrete Columns (Ph.D. dissertation). University of Toronto. https://hdl.handle.net/1807/95853

Kissman, V., & Sundar, L. (2020). An experimental study on strengthening of RC column with GFRP. Materials Today: Proceedings, 21, 278-285. https://doi.org/10.1016/j.matpr.2019.05.430

Kumutha, R., Vaidyanathan, R., & Palanichamy, M. S. (2007). Behaviour of reinforced concrete rectangular columns strengthened using GFRP. Cement and concrete composites, 29(8), 609-615. https://doi.org/10.1016/j.cemconcomp.2007.03.009

Kurt, C. E. (1978). Concrete filled structural plastic columns. Journal of the Structural Division, 104(1), 55-63. https://doi.org/10.1061/JSDEAG.0004849

Labossiere, P., Neale, K. W., Demers, M., & Picher, F. (1992). Repair of reinforced concrete columns with advanced composite materials confinement. Repair and Rehabilitation of the Infrastructure of the Americas, 153-165.

Lam, L., & Teng, J. G. (2003). Design-oriented stress-strain model for FRP-confined concrete. Construction and building materials, 17(6-7), 471-489. https://doi.org/10.1016/S0950-0618(03)00045-X

Lam, L., & Teng, J. G. (2004). Ultimate condition of fiber reinforced polymer-confined concrete. Journal of Composites for Construction, 8(6), 539-548. https://doi.org/10.1061/(ASCE)1090-0268(2004)8:6(539)

Lavergne S and Labossiere P. (1997) "Experimental Study of Concrete Columns Confined by a Composite Jacket under Combined Axial and Flexural Loads.' Proceedings CSCE Annual Conference, Sherbrook, Quevec, 6, 11-20.

Li, Y. F., Hwang, J. S., Chen, S. H., & Hsieh, Y. M. (2005). A study of reinforced concrete bridge columns retrofitted by steel jackets. Journal of the Chinese Institute of Engineers, 28(2), 319-328. https://doi.org/10.1080/02533839.2005.9670997

Liang, M., Wu, Z. M., Ueda, T., Zheng, J. J., & Akogbe, R. (2012). Experiment and modeling on axial behavior of carbon fiber reinforced polymer confined concrete cylinders with different sizes. Journal of Reinforced Plastics and Composites, 31(6), 389-403. https://doi.org/10.1177/0731684412439347

Lim, J. C., & Ozbakkaloglu, T. (2014). Confinement Model for FRP-Confined High-Strength Concrete. Journal of Composites for Construction, 18(4), 04013058. https://doi.org/10.1061/(asce)cc.1943-5614.0000376

Lim, J. C., & Ozbakkaloglu, T. (2014b). Design model for FRP-confined normal- and high-strength concrete square and rectangular columns. Magazine of Concrete Research, 66(20), 1020-1035. https://doi.org/10.1680/macr.14.00059

Lim, J. C., & Ozbakkaloglu, T. (2014c). Stress-strain model for normal- and light-weight concretes under uniaxial and triaxial compression. Construction and Building Materials, 71, 492-509. https://doi.org/10.1016/j.conbuildmat.2014.08.050

Lim, J. C., & Ozbakkaloglu, T. (2015). Investigation of the influence of the application path of confining pressure: Tests on actively confined and FRP-confined concretes. Journal of Structural Engineering, 141(8), 04014203. https://doi.org/10.1061/(ASCE)ST.1943-541X.0001177

Lim, J. C., Karakus, M., & Ozbakkaloglu, T. (2016). Evaluation of ultimate conditions of FRP-confined concrete columns using genetic programming. Computers & Structures, 162, 28-37. https://doi.org/10.1016/j.compstruc.2015.09.005

Lin, H. J., & Chen, C. T. (2001). Strength of concrete cylinder confined by composite materials. Journal of reinforced plastics and composites, 20(18), 1577-1600. https://doi.org/10.1177/073168401772679066

Lin, H. J., & Liao, C. I. (2004). Compressive strength of reinforced concrete column confined by composite material. Composite Structures, 65(2), 239-250. https://doi.org/10.1016/j.compstruct.2003.11.001

Lin, Y., Gamble, W. L., & Hawkins, N. M. (1994). Report to ILLDOT for Testing of Bridge Piers, Poplar Street Bridge Approaches. Internal Report, Department of Civil Engineering, University of Illinois at Urbana-Champaign.

Lin, Z., Fakharifar, M., Wu, C. B., Chen, G., Bevans, W. J., Gunasekaran, A. V. K., & Sedigh, S. (2013). Design, construction and load testing of the Pat Daly Road Bridge in Washington County, MO, with internal glass fiber reinforced polymers reinforcement.

Lobo, P. S., Faustino, P., Jesus, M., & Marreiros, R. (2018). Design model of concrete for circular columns confined with AFRP. Composite Structures, 200, 69-78. https://doi.org/10.1016/j.compstruct.2018.05.094

Lopez, A., Galati, N., Alkhrdaji, T., & Nanni, A. (2007). Strengthening of a reinforced concrete bridge with externally bonded steel reinforced polymer (SRP). Composites Part B: Engineering, 38(4), 429-436. https://doi.org/10.1016/j.compositesb.2006.09.003

Ma, C. K., Apandi, N. M., Sofrie, C. S. Y., Ng, J. H., Lo, W. H., Awang, A. Z., & Omar, W. (2017). Repair and rehabilitation of concrete structures using confinement: A review. Construction and Building Materials, 133, 502-515. https://doi.org/10.1016/j.conbuildmat.2016.12.100

Maekawa, K., & An, X. (2000). Shear failure and ductility of RC columns after yielding of main reinforcement. Engineering Fracture Mechanics, 65(2-3), 335-368. https://doi.org/10.1016/S0013-7944(99)00119-8

Mallick, P. K. (2007). Fiber-reinforced composites: materials, manufacturing, and design. CRC press. https://doi.org/10.1201/9781420005981

Mander, J. B., Priestley, M. J., & Park, R. (1988). Theoretical stress-strain model for confined concrete. Journal of structural engineering, 114(8), 1804-1826. https://doi.org/10.1061/(ASCE)0733-9445(1988)114:8(1804)

Marques, S. P. C., Marques, D. C. D. S. C., Lins da Silva, J., & Cavalcante, M. A. A. (2004). Model for analysis of short columns of concrete confined by fiber-reinforced polymer. Journal of Composites for Construction, 8(4), 332-340. https://doi.org/10.1061/(ASCE)1090-0268(2004)8:4(332)

Martinola, G., Meda, A., Plizzari, G. A., & Rinaldi, Z. (2010). Strengthening and repair of RC beams with fiber reinforced concrete. Cement and concrete composites, 32(9), 731-739. https://doi.org/10.1016/j.cemconcomp.2010.07.001

Matthys, S., Toutanji, H., Audenaert, K., & Taerwe, L. (2005). Axial load behavior of large-scale columns confined with fiber-reinforced polymer composites. ACI Structural Journal, 102(2), 258. https://doi.org/10.14359/14277

Mertz, D. R., & Gillespie Jr, J. W. (1996). Rehabilitation of steel bridge girders through the application of advanced composite materials (No. NCHRP-IDEA Project 011).

Mesbah, H. A., & Benzaid, R. (2017). Damage-based stress-strain model of RC cylinders wrapped with CFRP composites. Advances in concrete construction, 5(5), 539. https://doi.org/10.12989/acc.2017.5.5.539

Micelli, F., & Modarelli, R. (2013). Experimental and analytical study on properties affecting the behaviour of FRP-confined concrete. Composites Part B: Engineering, 45(1), 1420-1431. https://doi.org/10.1016/j.compositesb.2012.09.055

Micelli, F., Angiuli, R., Corvaglia, P., & Aiello, M. A. (2014). Passive and SMA-activated confinement of circular masonry columns with basalt and glass fibers composites. Composites Part B: Engineering, 67, 348-362. https://doi.org/10.1016/j.compositesb.2014.06.034

Miller, R. A. (2004). Connection of simple-span precast concrete girders for continuity (Vol. 519). Transportation Research Board.

Mirmiran, A., & Shahawy, M. (1997). Behavior of concrete columns confined by fiber composites. Journal of structural engineering, 123(5), 583-590. https://doi.org/10.1061/(ASCE)0733-9445(1997)123:5(583)

Mirmiran, A., Kargahi, M., Samaan, M., & Shahawy, M. (1996, January). Composite FRP-concrete column with bi-directional external reinforcement. In First International Conference on Composites in Infrastructure National Science Foundation National Sicence Foundation.

Mirmiran, A., Zagers, K., & Yuan, W. (2000). Nonlinear finite element modeling of concrete confined by fiber composites. Finite elements in analysis and design, 35(1), 79-96. https://doi.org/10.1016/S0168-874X(99)00056-6

Miyauchi, K., Nishibayashi, S., & Inoue, S. (1997). Estimation of Strengthening Effects with Carbon Fiber Sheet for Concrete Column. In Proc Third International Symp Non-Metallic FRP Concr Struct Japan (Vol. 224).

Mo, Y. L., Yeh, Y. K., & Hsieh, D. M. (2004). Seismic retrofit of hollow rectangular bridge columns. Journal of Composites for Construction, 8(1), 43-51. https://doi.org/10.1061/(ASCE)1090-0268(2004)8:1(43)

Moran, D. A., & Pantelides, C. P. (2002). Variable Strain Ductility Ratio for Fiber-Reinforced Polymer-Confined Concrete. Journal of Composites for Construction, 6(4), 224-232. https://doi.org/10.1061/(asce)1090-0268(2002)6:4(224)

Moran, D. A., & Pantelides, C. P. (2005). Damage-based stress-strain model for fiber-reinforced polymer-confined concrete. ACI structural journal, 102(1), 54. https://doi.org/10.14359/13530

Munteanu V., Îmbunătăţirea performanţelor structurale ale stâlpilor din beton armat

Nanni, A. (2000, March). FRP reinforcement for bridge structures. In Proceedings, Structural Engineering Conference, The University of Kansas, Lawrence, KS (Vol. 5).

Nanni, A., & Bradford, N. M. (1995). FRP jacketed concrete under uniaxial compression. Construction and Building Materials, 9(2), 115-124. https://doi.org/10.1016/0950-0618(95)00004-Y

Nanni, A., 2004. Strengthening of impact-damaged PC girder. Concr. Repair Bull. 17 (3), 16-20.

Nanni, A., Norris, M. S., & Bradford, N. M. (1993). Lateral confinement of concrete using FRP reinforcement. Special Report, 138, 193-210.

Narule, G. N., & Bambole, A. N. (2021). An experimental study on axial behavior of CFRP-strengthened RC rectangular columns with variable slenderness ratio. Asian Journal of Civil Engineering, 22(2), 263-275. https://doi.org/10.1007/s42107-020-00312-5

Nesheli, K. N., & Meguro, K. (2006, April). Seismic retrofitting of earthquake-damaged concrete columns by lateral pre-tensioning of FRP belts. In Proceedings of the Eighth US National Conference on Earthquake Engineering.

Newman, K., & Newman, J. B. (1971). Failure theories and design criteria for plain concrete. Structure, solid mechanics and engineering design, 963-995.

Norris, T., Saadatmanesh, H., & Ehsani, M. R. (1997). Shear and flexural strengthening of R/C beams with carbon fiber sheets. Journal of structural engineering, 123(7), 903-911. https://doi.org/10.1061/(ASCE)0733-9445(1997)123:7(903)

Ohtaki, T., Benzoni, G., Priestley, M. J. N., & Seible, F. (1997). Seismic performance of a full scale bridge column-as built and as repaired. In Second National Seismic Conference on Bridges and Highways California Department of Transportation; and Federal Highway Administration.

Oliveira, D. S., Raiz, V., & Carrazedo, R. (2019). Experimental study on normal-strength, high-strength and ultrahigh-strength concrete confined by carbon and glass FRP laminates. Journal of Composites for Construction, 23(1), 04018072. https://doi.org/10.1061/(ASCE)CC.1943-5614.0000912

Otsuka, K., & Wayman, C. M. (Eds.). (1999). Shape memory materials. Cambridge university press.

Ouyang, L. J., Gao, W. Y., Zhen, B., & Lu, Z. D. (2017). Seismic retrofit of square reinforced concrete columns using basalt and carbon fiber-reinforced polymer sheets: A comparative study. Composite Structures, 162, 294-307. https://doi.org/10.1016/j.compstruct.2016.12.016

Ozbakkaloglu, T., & Akin, E. (2012). Behavior of FRP-confined normal-and high-strength concrete under cyclic axial compression. Journal of Composites for Construction, 16(4), 451-463. https://doi.org/10.1061/(ASCE)CC.1943-5614.0000273

Ozbakkaloglu, T., & Lim, J. C. (2013). Axial compressive behavior of FRP-confined concrete: Experimental test database and a new design-oriented model. Composites Part B: Engineering, 55, 607-634. https://doi.org/10.1016/j.compositesb.2013.07.025

Ozbakkaloglu, T., & Saatcioglu, M. (2006). Seismic behavior of high-strength concrete columns confined by fiber-reinforced polymer tubes. Journal of Composites for Construction, 10(6), 538-549. https://doi.org/10.1061/(ASCE)1090-0268(2006)10:6(538)

Ozbakkaloglu, T., & Saatcioglu, M. (2007). Seismic performance of square high-strength concrete columns in FRP stay-in-place formwork. Journal of Structural Engineering, 133(1), 44-56. https://doi.org/10.1061/(ASCE)0733-9445(2007)133:1(44)

Ozbakkaloglu, T., Gholampour, A., & Lim, J. C. (2016). Damage-plasticity model for FRP-confined normal-strength and high-strength concrete. Journal of composites for construction, 20(6), 04016053. https://doi.org/10.1061/(ASCE)CC.1943-5614.0000712

Ozbakkaloglu, T., Lim, J. C., & Vincent, T. (2013). FRP-confined concrete in circular sections: Review and assessment of stress-strain models. Engineering Structures, 49, 1068-1088. https://doi.org/10.1016/j.engstruct.2012.06.010

Ozcan, O., Binici, B., & Ozcebe, G. (2010). Seismic strengthening of rectangular reinforced concrete columns using fiber reinforced polymers. Engineering Structures, 32(4), 964-973. https://doi.org/10.1016/j.engstruct.2009.12.021

Pan, Y., Guo, R., Li, H., Tang, H., & Huang, J. (2017). Analysis-oriented stress-strain model for FRP-confined concrete with preload. Composite Structures, 166, 57-67. https://doi.org/10.1016/j.compstruct.2017.01.007

Pantelides, C. P., Gergely, J., & Reaveley, L. D. (2001). In-situ verification of rehabilitation and repair of reinforced concrete bridge bents under simulated seismic loads. Earthquake Spectra, 17(3), 507-530. https://doi.org/10.1193/1.1586186

Pantelides, C. P., Gergely, J., Reaveley, L. D., & Volnyy, V. A. (1999). Retrofit of RC bridge pier with CFRP advanced composites. Journal of Structural Engineering, 125(10), 1094-1099. https://doi.org/10.1061/(ASCE)0733-9445(1999)125:10(1094)

Pantelides, C. P., Gergely, J., Reaveley, L. D., & Volnyy, V. A. (2000). Seismic strengthening of reinforced concrete bridge pier with FRP composites. In

Proceedings of the 12th World Conference on Earthquake Engineering, New Zealand (Vol. 127).

Parghi, A. M. (2016). Seismic performance evaluation of circular reinforced concrete bridge piers retrofitted with fibre reinforced polymer (Ph.D. dissertation), University of British Columbia. https://doi.org/10.2749/vancouver.2017.2141

Parghi, A., & Alam, M. S. (2017). Seismic collapse assessment of non-seismically designed circular RC bridge piers retrofitted with FRP composites. Composite Structures, 160, 901-916. https://doi.org/10.1016/j.compstruct.2016.10.094

Park, T. W., Na, U. J., Chung, L., & Feng, M. Q. (2008). Compressive behavior of concrete cylinders confined by narrow strips of CFRP with spacing. Composites Part B: Engineering, 39(7-8), 1093-1103. https://doi.org/10.1016/j.compositesb.2008.05.002

Pellegrino, C., & Modena, C. (2010). Analytical model for FRP confinement of concrete columns with and without internal steel reinforcement. Journal of Composites for Construction, 14(6), 693-705. https://doi.org/10.1061/(ASCE)CC.1943-5614.0000127

Pessiki, S., Harries, K. A., Kestner, J. T., Sause, R., & Ricles, J. M. (2001). Axial behavior of reinforced concrete columns confined with FRP jackets. Journal of composites for Construction, 5(4), 237-245. https://doi.org/10.1061/(ASCE)1090-0268(2001)5:4(237)

Pham, T. M., & Hadi, M. N. (2014). Confinement model for FRP confined normal- and high-strength concrete circular columns. Construction and Building Materials, 69, 83-90. https://doi.org/10.1016/j.conbuildmat.2014.06.036

Popovics, S. (1973). A numerical approach to the complete stress-strain curve of concrete. Cement and Concrete Research, 3(5), 583-599. https://doi.org/10.1016/0008-8846(73)90096-3

Pour, A. F., Ozbakkaloglu, T., & Vincent, T. (2018). Simplified design-oriented axial stress-strain model for FRP-confined normal-and high-strength concrete. Engineering Structures, 175, 501-516. https://doi.org/10.1016/j.engstruct.2018.07.099

Priestley, M. J. N., & Seible, F. (1995). Design of seismic retrofit measures for concrete and masonry structures. Construction and Building Materials, 9(6), 365-377. https://doi.org/10.1016/0950-0618(95)00049-6

Priestley, M. J. N., Seible, F., Xiao, Y., & Verma, R. (1994). Steel jacket retrofit of squat RC bridge columns for enhanced shear strength-Part 2-Experimental results. ACI Struct. J, 91(5), 537-551.

Priestley, M. N., Seible, F., & Calvi, G. M. (1996). Seismic design and retrofit of bridges. John Wiley & Sons. https://doi.org/10.1002/9780470172858

Priestley, M. N., Seible, F., Xiao, Y., & Verma, R. (1994). Steel jacket retrofitting of reinforced concrete bridge columns for enhanced shear strength-part 1: Theoretical considerations and test design. Structural Journal, 91(4), 394-405. https://doi.org/10.14359/9885

Rasheed, H. A. (2014). Strengthening design of reinforced concrete with FRP. CRC Press. https://doi.org/10.1201/b17968

Rasouli, M., & Broujerdian, V. (2019). 3D finite element modeling of FRP-confined rectangular short columns considering variation of Poisson's ratio. Iranian Journal of Science and Technology, Transactions of Civil Engineering, 1-13. https://doi.org/10.1007/s40996-019-00276-w

Raza, A., Khan, Q. U. Z., & Ahmad, A. (2020). Prediction of axial compressive strength for FRP-confined concrete compression members. KSCE Journal of Civil Engineering, 24, 2099-2109. https://doi.org/10.1007/s12205-020-1682-x

Raza, S., Khan, M. K., Menegon, S. J., Tsang, H. H., & Wilson, J. L. (2019). Strengthening and repair of reinforced concrete columns by jacketing: State-of-the-art review. Sustainability, 11(11), 3208. https://doi.org/10.3390/su11113208

Realfonzo, R., & Napoli, A. (2011). Concrete confined by FRP systems: confinement efficiency and design strength models. Composites Part B: Engineering, 42(4), 736-755. https://doi.org/10.1016/j.compositesb.2011.01.028

Retrofitting of Concrete Structures by Externally Bonded FRPS, with Emphasis on Seismic Applications. Technical Report, Fédération Internationale du Béton, fib TG 9.3, Lausanne, 2006.

Richard, R. M., & Abbott, B. J. (1975). Versatile Elastic-Plastic Stress-Strain Formula. Journal of the Engineering Mechanics Division, 101(4), 511-515. https://doi.org/10.1061/jmcea3.0002047

Richart, F. E., Brandtzæg, A., & Brown, R. L. (1928). A study of the failure of concrete under combined compressive stresses. University of Illinois at Urbana Champaign, College of Engineering. Engineering Experiment Station.

Richart, F. E., Brandtzæg, A., & Brown, R. L. (1929). Failure of plain and spirally reinforced concrete in compression. University of Illinois at Urbana Champaign, College of Engineering. Engineering Experiment Station.

Rizkalla, S., Dawood, M., & Schnerch, D. (2008). Development of a carbon fiber reinforced polymer system for strengthening steel structures. Composites Part A: Applied Science and Manufacturing, 39(2), 388-397. https://doi.org/10.1016/j.compositesa.2007.10.009

Rocca, S. (2007). Experimental and analytical evaluation of FRP-confined large size reinforced concrete columns (Ph.D. dissertation). University of Missouri--Rolla. https://scholarsmine.mst.edu/doctoral_dissertations/1997

Rochette, P., & Labossiére, P. (1996, August). A plasticity approach for concrete columns confined with composite materials. In Second International Conference on Advanced Composite Materials in Bridges and Structures, Montreal.

Rodriguez, M., & Park, R. (1994). Seismic load tests on reinforced concrete columns strengthened by jacketing. Structural Journal, 91(2), 150-159. https://doi.org/10.14359/4593

Rousakis, T. C., & Tourtouras, I. S. (2014). RC columns of square section-passive and active confinement with composite ropes. Composites Part B: Engineering, 58, 573-581. https://doi.org/10.1016/j.compositesb.2013.11.011

Rousakis, T. C., Karabinis, A. I., Kiousis, P. D., & Tepfers, R. (2008). Analytical modelling of plastic behaviour of uniformly FRP confined concrete members. Composites Part B: Engineering, 39(7-8), 1104-1113. https://doi.org/10.1016/j.compositesb.2008.05.001

Rousakis, T. C., Kouravelou, K. B., & Karachalios, T. K. (2014). Effects of carbon nanotube enrichment of epoxy resins on hybrid FRP-FR confinement of concrete. Composites Part B: Engineering, 57, 210-218. https://doi.org/10.1016/j.compositesb.2013.09.044

Ruano, G., Isla, F., Pedraza, R. I., Sfer, D., & Luccioni, B. (2014). Shear retrofitting of reinforced concrete beams with steel fiber reinforced concrete. Construction and Building Materials, 54, 646-658. https://doi.org/10.1016/j.conbuildmat.2013.12.092

Sá, M. F., Gomes, A. M., Correia, J. R., & Silvestre, N. (2011). Creep behavior of pultruded GFRP elements-Part 1: Literature review and experimental study. Composite Structures, 93(10), 2450-2459. https://doi.org/10.1016/j.compstruct.2011.04.013

Saadatmanesh, H., Ehsani, M. R., & Jin, L. (1996). Seismic strengthening of circular bridge pier models with fiber composites. ACI Structural Journal, 93(6), 639-738. https://doi.org/10.14359/510

Saadatmanesh, H., Ehsani, M. R., & Jin, L. (1997). Repair of earthquake-damaged RC columns with FRP wraps. ACI structural Journal, 94, 206-215. https://doi.org/10.14359/474

Saadatmanesh, H., Ehsani, M. R., & Li, M. W. (1994). Strength and ductility of concrete columns externally reinforced with fiber composite straps. Structural Journal, 91(4), 434-447. https://doi.org/10.14359/4151

Saafi, M., Toutanji, H., & Li, Z. (1999). Behavior of concrete columns confined with fiber reinforced polymer tubes. Materials Journal, 96(4), 500-509. https://doi.org/10.14359/652

Saatcioglu, M., & Yalcin, C. (2003). External prestressing concrete columns for improved seismic shear resistance. Journal of Structural Engineering, 129(8), 1057-1070. https://doi.org/10.1061/(ASCE)0733-9445(2003)129:8(1057)

Saatcioglu, M., Chakrabarti, S., Selby, R., & Mes, D. (2002). Improving Ductility and Shear Capacity of Reinforced Concrete Columns with the Retro-Belt Retrofitting System. In Proceedings of the 7th US National Conference on Earthquake Engineering, Earthquake Engineering Research Institute.

Sadeghian, P., & Fam, A. (2015). Improved design-oriented confinement models for FRP-wrapped concrete cylinders based on statistical analyses. Engineering Structures, 87, 162-182. https://doi.org/10.1016/j.engstruct.2015.01.024

Samaan, M., Mirmiran, A., & Shahawy, M. (1998). Model of concrete confined by fiber composites. Journal of structural engineering, 124(9), 1025-1031. https://doi.org/10.1061/(ASCE)0733-9445(1998)124:9(1025)

Sargin, M. (1971). Stress-strain relationships for concrete and the analysis of structural concrete sections. Solid Mechanics Division, University of Waterloo.

Sarker, P., Begum, M., & Nasrin, S. (2011). Fiber reinforced polymers for structural retrofitting: a review. J Civil Eng, 39(1), 49-57.

Seible, F., Burgueno, R., Abdallah, M. G., & Nuismer, R. (1995, December). Advanced composite carbon shell systems for bridge columns under seismic loads. In Proceedings of the National Seismic Conference on Bridges and Highways (p. 16). San Diego, California.

Seible, F., Innamorato, D., Baumgartner, J., Karbhari, V., & Sheng, L. H. (1999). Seismic retrofit of flexural bridge spandrel columns using fiber reinforced polymer composite jackets. Special Publication, 188, 919-932.

Seible, F., Priestley, M. N., Hegemier, G. A., & Innamorato, D. (1997). Seismic retrofit of RC columns with continuous carbon fiber jackets. Journal of composites for construction, 1(2), 52-62. https://doi.org/10.1061/(ASCE)1090-0268(1997)1:2(52)

Shahawy, M., Mirmiran, A., & Beitelman, T. (2000). Tests and modeling of carbon-wrapped concrete columns. Composites Part B: Engineering, 31(6-7), 471-480. https://doi.org/10.1016/S1359-8368(00)00021-4

Shehata, I. A., Carneiro, L. A., & Shehata, L. C. (2002). Strength of short concrete columns confined with CFRP sheets. Materials and Structures, 35(1), 50-58. https://doi.org/10.1007/BF02482090

Sheikh, S. A., Jaffry, S. A., & Cui, C. (2007). Investigation of glass-fibre-reinforced-polymer shells as formwork and reinforcement for concrete columns. Canadian Journal of Civil Engineering, 34(3), 389-402. https://doi.org/10.1139/l06-110

Shimomura, T., & Phong, N. H. (2007). Structural performance of concrete members reinforced with continuous fiber rope. FRPRCS-8 Conference: Fiber-Reinforced Polymer Reinforcement for Concrete Structures, July, 16-18.

Shin, M. (2012). Seismic retrofit and repair of reinforced concrete bridge columns using shape memory alloy spirals (Ph.D. dissertation), University of Illinois at Urbana-Champaign. http://hdl.handle.net/2142/30991

Shin, M., & Andrawes, B. (2010). Experimental investigation of actively confined concrete using shape memory alloys. Engineering Structures, 32(3), 656-664. https://doi.org/10.1016/j.engstruct.2009.11.012

Siddiqui, N. A., Alsayed, S. H., Al-Salloum, Y. A., Iqbal, R. A., & Abbas, H. (2014). Experimental investigation of slender circular RC columns strengthened with FRP composites. Construction and Building Materials, 69, 323-334. https://doi.org/10.1016/j.conbuildmat.2014.07.053

Sonnenschein, R., Gajdosova, K., & Holly, I. (2016). FRP composites and their using in the construction of bridges. Procedia engineering, 161, 477-482. https://doi.org/10.1016/j.proeng.2016.08.665

Spoelstra, M. R., & Monti, G. (1999). FRP-confined concrete model. Journal of composites for construction, 3(3), 143-150. https://doi.org/10.1061/(ASCE)1090-0268(1999)3:3(143)

Staton, J. F., & Knauff, J. (2007). Performance of Michigan's concrete barriers (Vol. 1498). Michigan. Dept. of Transportation. Construction and Technology Division.

Stress-Strain Relationship of Confined and Unconfined Concrete. (1996). ACI Materials Journal, 93(5). https://doi.org/10.14359/9847

Sun, L., Wei, M., & Zhang, N. (2017). Experimental study on the behavior of GFRP reinforced concrete columns under eccentric axial load. Construction and Building Materials, 152, 214-225. https://doi.org/10.1016/j.conbuildmat.2017.06.159

Tadaki, T., Otsuka, K., & Shimizu, K. (1988). Shape memory alloys. Annual Review of Materials Science, 18(1), 25-45. https://doi.org/10.1146/annurev.ms.18.080188.000325

Täljsten, B. (1997). Strengthening of beams by plate bonding. Journal of materials in civil engineering, 9(4), 206-212. https://doi.org/10.1061/(ASCE)0899-1561(1997)9:4(206)

Tasdemir, M. A., Tasdemir, C., Akyüz, S., Jefferson, A. D., Lydon, F. D., & Barr, B. I. G. (1998). Evaluation of strains at peak stresses in concrete: a three-phase composite model approach. Cement and concrete composites, 20(4), 301-318. https://doi.org/10.1016/S0958-9465(98)00012-2

Tavakkolizadeh, M., & Saadatmanesh, H. (2003). Repair of damaged steel-concrete composite girders using carbon fiber-reinforced polymer sheets. Journal of Composites for Construction, 7(4), 311-322. https://doi.org/10.1061/(ASCE)1090-0268(2003)7:4(311)

Teng, J. G., & Lam, L. (2004). Behavior and modeling of fiber reinforced polymer-confined concrete. Journal of structural engineering, 130(11), 1713-1723. https://doi.org/10.1061/(ASCE)0733-9445(2004)130:11(1713)

Teng, J. G., Chen, J. F., Smith, S. T., & Lam, L. (2003). Behaviour and strength of FRP-strengthened RC structures: a state-of-the-art review. Proceedings of the institution of civil engineers-structures and buildings, 156(1), 51-62. https://doi.org/10.1680/stbu.2003.156.1.51

Teng, J. G., Jiang, T., Lam, L., & Luo, Y. Z. (2009). Refinement of a Design-Oriented Stress-Strain Model for FRP-Confined Concrete. Journal of Composites for Construction, 13(4), 269-278. https://doi.org/10.1061/(ASCE)CC.1943-5614.0000012

Thériault, M., Neale, K. W., & Claude, S. (2004). Fiber-reinforced polymer-confined circular concrete columns: Investigation of size and slenderness effects. Journal of composites for construction, 8(4), 323-331. https://doi.org/10.1061/(ASCE)1090-0268(2004)8:4(323)

Tobias, D. H., Anderson, R. E., Hodel, C. E., Kramer, W. M., Wahab, R. M., & Chaput, R. J. (2008). Overview of earthquake resisting system design and retrofit strategy for bridges in Illinois. Practice Periodical on Structural Design and Construction, 13(3), 147-158. https://doi.org/10.1061/(ASCE)1084-0680(2008)13:3(147)

Tongo, R. B. (n.d.). [Total collapse due to first story columns' failure]. Abcnews. https://abcnews.go.com/International/rescuers-scramble-find-dozens-people-trapped-earthquake-kills/story?id=52901523

Toshimi Kabeyasawa, "Recent Development of Seismic Retrofit Methods in Japan", Japan Building Disaster Prevention Association, January, 2005.

Touhari, M., & Mitiche-Kettab, R. (2016). Behaviour of FRP confined concrete cylinders: Experimental investigation and strength model. Periodica Polytechnica Civil Engineering, 60(4), 647-660. https://doi.org/10.3311/PPci.8759

Toutanji, H. (1999). Stress-strain characteristics of concrete columns externally confined with advanced fiber composite sheets. Materials Journal, 96(3), 397-404. https://doi.org/10.14359/639

Toutanji, H., & Saafi, M. (2001). Durability studies on concrete columns encased in PVC-FRP composite tubes. Composite structures, 54(1), 27-35. https://doi.org/10.1016/S0263-8223(01)00067-8

Tu, J., Gao, K., He, L., & Li, X. (2019). Experimental study on the axial compression performance of GFRP-reinforced concrete square columns. Advances in Structural Engineering, 22(7), 1554-1565. https://doi.org/10.1177/1369433218817988

Turgay, T., Köksal, H. O., Polat, Z., & Karakoc, C. (2009). Stress-strain model for concrete confined with CFRP jackets. Materials & Design, 30(8), 3243-3251. https://doi.org/10.1016/j.matdes.2008.11.022

Vincent, T., & Ozbakkaloglu, T. (2013). Influence of concrete strength and confinement method on axial compressive behavior of FRP confined high- and ultra high-strength concrete. Composites Part B: Engineering, 50, 413-428. https://doi.org/10.1016/j.compositesb.2013.02.017

Walker, R. A., & Karbhari, V. M. (2007). Durability based design of FRP jackets for seismic retrofit. Composite structures, 80(4), 553-568. https://doi.org/10.1016/j.compstruct.2006.07.003

Walkup, S. L. (1998). Rehabilitation of non-ductile reinforced concrete building columns using fiber reinforced polymer jackets.

Wang, J., & Yang, Q. (2010). Experimental study on mechanical properties of concrete confined with plastic pipe. ACI Materials Journal, 107(2), 132. https://doi.org/10.14359/51663576

Wang, Y. F., & Wu, H. L. (2011). Size effect of concrete short columns confined with aramid FRP jackets. Journal of Composites for Construction, 15(4), 535-544. https://doi.org/10.1061/(ASCE)CC.1943-5614.0000178

Wei, Y. Y., & Wu, Y. F. (2012). Unified stress-strain model of concrete for FRP-confined columns. Construction and Building Materials, 26(1), 381-392. https://doi.org/10.1016/j.conbuildmat.2011.06.037

Wu, G., Lü, Z. T., & Wu, Z. S. (2006). Strength and ductility of concrete cylinders confined with FRP composites. Construction and building materials, 20(3), 134-148. https://doi.org/10.1016/j.conbuildmat.2005.01.022

Wu, G., Wu, Z. S., Lu, Z. T., & Ando, Y. B. (2008). Structural performance of concrete confined with hybrid FRP composites. Journal of reinforced plastics and composites, 27(12), 1323-1348. https://doi.org/10.1177/0731684407084989

Wu, H. C., & Eamon, C. D. (2017). Strengthening of concrete structures using fiber reinforced polymers (FRP): design, construction and practical applications. https://doi.org/10.1016/B978-0-08-100636-8.00002-8

Wu, H. L., & Wang, Y. F. (2010). Experimental study on reinforced high-strength concrete short columns confined with AFRP sheets. Steel and Composite Structures, 10(6), 501-516. https://doi.org/10.12989/scs.2010.10.6.501

Wu, H. L., Wang, Y. F., Yu, L., & Li, X. R. (2009). Experimental and computational studies on high-strength concrete circular columns confined by aramid fiber-reinforced polymer sheets. Journal of Composites for Construction, 13(2), 125-134. https://doi.org/10.1061/(ASCE)1090-0268(2009)13:2(125)

Wu, Z., Wu, Y., & Fahmy, M. F. (2020). Structures Strengthened with Bonded Composites. Woodhead Publishing.

Xiao, J., Yang, J., Huang, Y., & Wang, Z. (2011). Experimental study on recycled concrete confined by steel tube under axial compression. Jianzhu Jiegou Xuebao (Journal of Building Structures), 32(6), 92-98.

Xiao, Q. G., Teng, J. G., & Yu, T. (2010). Behavior and modeling of confined high-strength concrete. Journal of Composites for Construction, 14(3), 249-259. https://doi.org/10.1061/(ASCE)CC.1943-5614.0000070

Xiao, Y., & Ma, R. (1997). Seismic retrofit of RC circular columns using prefabricated composite jacketing. Journal of structural engineering, 123(10), 1357-1364. https://doi.org/10.1061/(ASCE)0733-9445(1997)123:10(1357)

Xiao, Y., & Wu, H. (2000). Compressive behavior of concrete confined by carbon fiber composite jackets. Journal of materials in civil engineering, 12(2), 139-146. https://doi.org/10.1061/(ASCE)0899-1561(2000)12:2(139)

Xiao, Y., & Wu, H. (2003). Retrofit of reinforced concrete columns using partially stiffened steel jackets. Journal of Structural Engineering, 129(6), 725-732. https://doi.org/10.1061/(ASCE)0733-9445(2003)129:6(725)

Xiao, Y., He, W., & Choi, K. K. (2005). Confined concrete-filled tubular columns. Journal of structural engineering, 131(3), 488-497. https://doi.org/10.1061/(ASCE)0733-9445(2005)131:3(488)

Xie, J., Fu, Q., & Yan, J. B. (2019). Compressive behaviour of stub concrete column strengthened with ultra-high performance concrete jacket. Construction and Building Materials, 204, 643-658. https://doi.org/10.1016/j.conbuildmat.2019.01.220

Yan, Z., & Pantelides, C. P. (2007). Design-oriented model for concrete columns confined with bonded FRP jackets or post-tensioned FRP shells. In Proceedings of the 8th International Symposium on Fiber Reinforced Polymer Reinforcement for Concrete Structures. University of Patras.

Yan, Z., Pantelides, C. P., & Reaveley, L. D. (2007). Posttensioned FRP composite shells for concrete confinement. Journal of Composites for Construction, 11(1), 81-90. https://doi.org/10.1061/(ASCE)1090-0268(2007)11:1(81)

Yang, J. Q., & Feng, P. (2020). Analysis-oriented models for FRP-confined concrete: 3D interpretation and general methodology. Engineering Structures, 216, 110749. https://doi.org/10.1016/j.engstruct.2020.110749

Yoshimura, K., Kikuchi, K., Kuroki, M., Wang, J., & Ichinose, K. (2004, August). Seismic Strengthening of Rectangular R/C Columns Confined by Circular Steel-and CF-Jackets. In 13th World Conference on Earthquake Engineering, Vancouver, BC Canada, Paper (No. 2036).

Youssef, M. N., Feng, M. Q., & Mosallam, A. S. (2007). Stress-strain model for concrete confined by FRP composites. Composites Part B: Engineering, 38(5-6), 614-628. https://doi.org/10.1016/j.compositesb.2006.07.020

Youssf, O., ElGawady, M. A., Mills, J. E., & Ma, X. (2014). Finite element modelling and dilation of FRP-confined concrete columns. Engineering Structures, 79, 70-85. https://doi.org/10.1016/j.engstruct.2014.07.045

Yu, T. T. J. G., Teng, J. G., Wong, Y. L., & Dong, S. L. (2010). Finite element modeling of confined concrete-I: Drucker-Prager type plasticity model. Engineering structures, 32(3), 665-679. https://doi.org/10.1016/j.engstruct.2009.11.013

Zaghi, A. E., Saiidi, M. S., & Mirmiran, A. (2012). Shake table response and analysis of a concrete-filled FRP tube bridge column. Composite structures, 94(5), 1564-1574. https://doi.org/10.1016/j.compstruct.2011.12.018

Zeng, J. J., Lin, G., Teng, J. G., & Li, L. J. (2018). Behavior of large-scale FRP-confined rectangular RC columns under axial compression. Engineering Structures, 174, 629-645. https://doi.org/10.1016/j.engstruct.2018.07.086

Zong-Cai, D., Daud, J. R., & Hui, L. (2014). Seismic behavior of short concrete columns with prestressing steel wires. Advances in Materials Science and Engineering, 2014. https://doi.org/10.1155/2014/180193

Zureick, A., & Scott, D. (1997). Short-term behavior and design of fiber-reinforced polymeric slender members under axial compression. Journal of Composites for Construction, 1(4), 140-149. https://doi.org/10.1061/(ASCE)1090-0268(1997)1:4(140)